UNIVERSITY OF CANTERBURY
Te Whare Wānanga o Waitaha
CHRISTCHURCH NEW ZEALAND

BOND AND SHEAR MECHANICS WITHIN REINFORCED CONCRETE BEAM-COLUMN JOINTS INCORPORATING THE SLOTTED BEAM DETAIL

A THESIS
SUBMITTED IN PARTIAL FULFULMENT OF
THE REQUIREMENTS FOR THE DEGREE OF
MASTER OF ENGINEERING
AT THE UNIVERSITY OF CANTERBURY

Joseph D. R. Byrne
December 2012

Supervisor:
Professor Des Bull

Department of Civil and Natural Resources Engineering
University of Canterbury,
Christchurch, New Zealand

To my parents

Abstract

The recent earthquakes in Christchurch have made it clear that issues exist with current RC frame design in New Zealand. In particular, beam elongation in RC frame buildings was widespread and resulted in numerous buildings being rendered irreparable. Design solutions to overcome this problem are clearly needed, and the slotted beam is one such solution. This system has a distinct advantage over other damage avoidance design systems in that it can be constructed using current industry techniques and conventional reinforcing steel. As the name suggests, the slotted beam incorporates a vertical slot along part of the beam depth at the beam-column interface. Geometric beam elongation is accommodated via opening and closing of these slots during seismically induced rotations, while the top concrete hinge is heavily reinforced to prevent material inelastic elongation.

Past research on slotted beams has shown that the bond demand on the bottom longitudinal reinforcement is increased compared with equivalent monolithic systems. Satisfying this increased bond demand through conventional means may yield impractical and economically less viable column dimensions. The same research also indicated that the joint shear mechanism was different to that observed within monolithic joints and that additional horizontal reinforcement was required as a result.

Through a combination of theoretical investigation, forensic analysis, and database study, this research addresses the above issues and develops design guidelines. The use of supplementary vertical joint stirrups was investigated as a means of improving bond performance without the need for non-standard reinforcing steel or other hardware. These design guidelines were then validated experimentally with the testing of two 80% scale beam-column sub-assemblies. The revised provisions for bond within the bottom longitudinal reinforcement were found to be adequate while the top longitudinal reinforcement remained nominally elastic throughout both tests. An alternate mechanism was found to govern joint shear behaviour, removing the need for additional horizontal joint reinforcement. Current NZS3101:2006 joint shear reinforcement provisions were found to be more than adequate given the typically larger column depths required rendering the strut mechanism more effective.

The test results were then used to further refine design recommendations for practicing engineers. Finally, conclusions and future research requirements were outlined.

Acknowledgements

This research would not have been possible without the direction and guidance of Professor Des Bull. For this, I am extremely grateful and offer my sincere thanks. I would also like to thank Des for facilitating funding of this project and associated financial assistance through the Foundation for Research in Science and Technology. I must also acknowledge Professor Richard Fenwick for his assistance during the early stages of my research.

Big thanks to all the Structures Laboratory technicians for their hard work throughout the experimental phase of this project. While every technician gave me a hand at one point or another, particular thanks go to Tim Perigo for his dedication and skill throughout the project. I would also like to thank Mohammad Soleymani Ashtiani – a fellow post-graduate student – for his help with construction and testing of the specimens. James MacKechnie at Allied Concrete also deserves a mention here for his assistance with the concrete mix design

Cheers to all the other civil post-grads, many of whom have become good mates. The E342 lads get a special mention here – Anton "I don't really have a go to nickname" Kivell, Joe Good, Mark "Mork" Hannah, and Chris Lai – you're all top blokes. Cheers to anyone else who attended the many BYOs over the years – Anthony "Stubbzy" Stubbs, Andrew "Stretch" Baird, Josh "Mr. Hockey" Bird, and Craig Muir – to name a few.

The most important thanks are reserved for my family – my parents, Vince and Sue, and my siblings, Hamish and Julia. Your love and support over the years has done more than I can possibly express here in words. Of course, special thanks go to my partner, Megan, for putting up with all the late nights and weekends spent in the office. I don't know how I would have coped without you.

Finally, this work is dedicated to all those who lost their lives in the Canterbury earthquake on February 22nd 2011 in the hope that it goes some small way to ensuring the safety of buildings in the future.

Table of Contents

List of Figures

List of Tables

Chapter 1 - INTRODUCTION

1.1 Context

Reinforced concrete framed structures have been widely used over the past 60 years both in New Zealand and around the world in a variety of applications. Initially, these structures were entirely cast on site using scaffolding, formwork, and large amounts of manual labour. Then, in the early 1960's, the use of precast concrete began to emerge in the industry. This method of construction allowed components to be cast off site thus ensuring better quality control and reducing the amount of work carried out on site. Several decades later, the 1980's saw an explosion in the use of precast flooring units in New Zealand largely due to the rapid installation time and greater achievable spans compared with reinforced concrete floor slabs. The use of Hollowcore flooring units was particularly popular during this period and was subsequently the focus of significant research at the University of Canterbury.

Meanwhile, research was changing the way structures were designed for seismic regions, culminating in the development of capacity design (Park & Paulay, 1975). Capacity design accepts that inelastic behaviour will occur during large seismic events and aims to ensure formation of a desirable mechanism by allocating element capacities accordingly. Extended by Paulay and Priestley (1992), the desired beam sway inelastic mechanism involving yielding in plastic hinges near the column bases and beam ends is still used in current design practice. However, failure to allocate the correct strength hierarchy can result in formation of a column sway mechanism in which columns yield locally, resulting in formation of a soft storey. The difference between these two inelastic mechanisms is illustrated in Figure 1-1.

Research into plastic hinge regions has shown that beam elongation on the order of 2 – 5% of the beam depth per plastic hinge occurs during seismic excitation (Lau, 2001; Fenwick & Megget, 1993; Blakeley, Megget & Priestley, 1975). Additionally, research at the University of Canterbury by Lindsay (2004) and Matthews (2004) showed that beam elongation within framed structures can lead to a loss of both gravity support and diaphragm action within floors; failures of this sort were observed in parking structures during the Northridge earthquake (Hall, 1994). Later, research by Lau, Fenwick, and Davidson (2007) showed that beam elongation induces significant axial compression within the beam due to restraint provided by the attached floor. This increases the resulting beam overstrength moment and can lead to formation of a soft storey if the adjacent columns are not detailed sufficiently to cope with this increased moment demand. Peng (2009), found that this elongation can extend

into the floor diaphragm thus further increasing the column overstrength demand and the potential for formation of a soft storey mechanism.

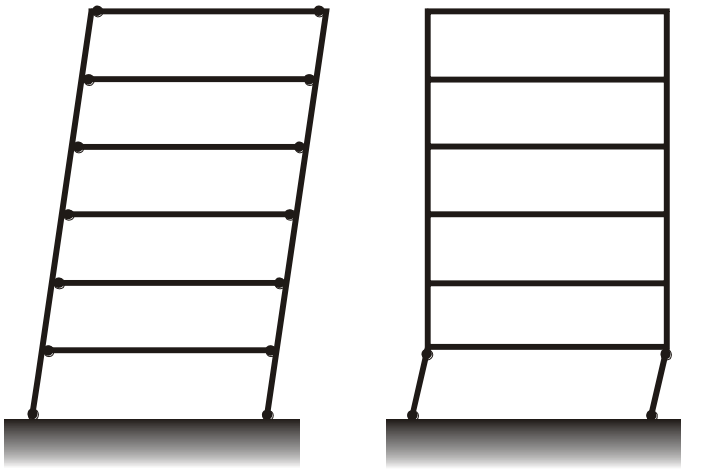

(a) Beam sway mechanism (b) Soft-storey mechanism

Figure 1-1: *Beam sway and soft storey failure mechanisms*

The above research and observations from previous earthquakes shows that improvements to current design practices are needed due to the potential that exists for severe loss of life in a large seismic event. A new structural system is required that addresses these issues without compromising constructability or budget. Extensive research has been carried out on post-tensioned rocking systems for use in seismic areas, but these do not, however, eliminate beam elongation and its associated problematic issues. The lower stiffness of these systems also results in large interstorey drifts; these can severely damage non-structural elements such as ceilings and infill walls. Additionally, they are relatively expensive and time consuming to install as they require special construction techniques; consequently, they have seen little use in the New Zealand construction industry. This research will instead focus on the relatively less familiar, but nonetheless promising, slotted beam system and look to develop on recent work by Au (2010) and Leslie (2010) at the University of Canterbury.

1.2 The Slotted Beam Concept

Slotted beams were first investigated by Ohkubo, Matsuoka, Yoshioka, and Anderson in 1999 and were found to reduce plastic hinge damage and cracking while achieving similar moment capacity compared with monolithic reinforced concrete beams. Further research by Ohkubo and Hamamoto (2004) including floor units showed that beam elongation and floor diaphragm activation – where reinforcement within the topping slab is activated as it attempts to restrain elongation within the adjacent beam – were also reduced. In terms of

constructability, the main difference between slotted and monolithic beams is the presence of a slot along approximately three quarters of the beam depth where it connects to the column, as shown in Figure 1-2. Due to this similarity, slotted beams can be constructed using the same precast techniques currently used in the industry. This gives them a significant advantage over other damage reducing structural systems such as post-tensioned rocking systems which, as discussed previously, require specialist construction methods thus making them relatively expensive and time consuming to produce.

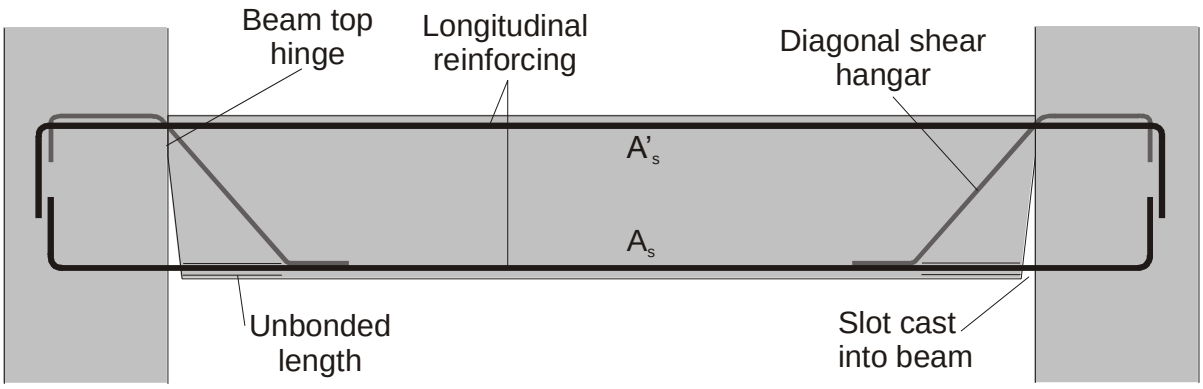

Figure 1-2: *Diagram of slotted reinforced concrete beam*

The primary aim of slotted beam systems is to reduce beam elongation, floor diaphragm activation, and damage due to formation of plastic hinges. Beam elongation is caused by two mechanisms - geometric and material elongation - and the slotted beam addresses both of these. Geometric elongation occurs in monolithic frames due to seismic induced beam rotation about the beam neutral axis as it moves either above or below the beam mid-depth. Because the beam is cast directly up against the column, additional room is therefore required to accommodate the rotation thus effectively elongating the beam. However, in a slotted beam, these rotations are accommodated via gap opening and closing as shown in Figure 1-3, thus significantly reducing geometric elongation. Material elongation in monolithic beams is caused by yielding of reinforcement and floor diaphragm activation. Because rotation in a slotted beam occurs about the top concrete hinge, the neutral axis is contained within this area. This significantly reduces yielding of the top reinforcement, shear hangers, and activation of the floor slab reinforcement by minimising the strain levels in each of these. Reduction in deformation at the floor slab level also helps to reduce cracking and damage to this area which is commonly observed in monolithic structures (Au, 2010; Matthews, 2004). Additionally, top reinforcement strength is detailed to be approximately twice the strength of the bottom such that moment capacity is governed by yielding of the bottom reinforcement. Overstrength moments can therefore be equilibrated by the top reinforcement without significant yielding and floor slab activation is further reduced (Au, 2010; Leslie, 2010).

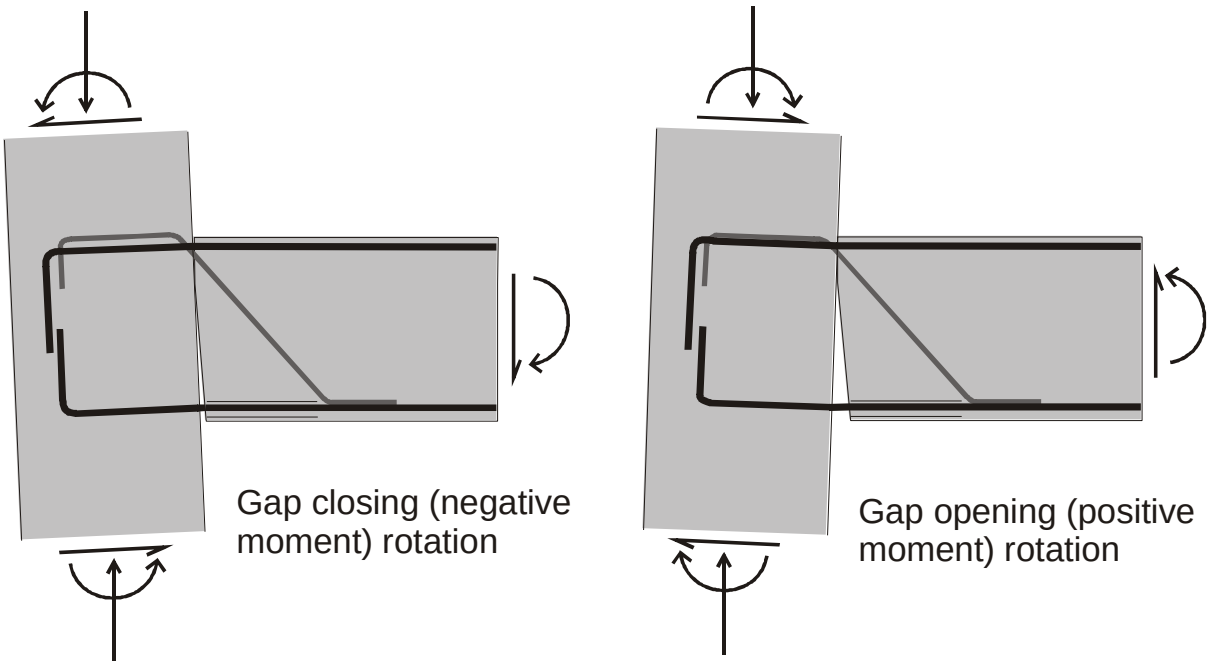

(a) Gap closing rotation (negative moment) (b) Gap opening rotation (positive moment)

Figure 1-3: *Accommodation of geometric rotation via slot*

However, the presence of the slot does introduce several complications in the design of these systems. Firstly, local strains in the bottom longitudinal reinforcement produced by gap opening and closing are very large due to the small distance the strains develop over. To reduce the magnitude of these strains, this reinforcement is unbonded over a short length by casting steel tubes into the beam and passing the reinforcement through these. Tests by Ohkubo et al (1999) found that inclusion of this unbonded length can lead to formation of a diagonal 'S-crack' extending from the end of the unbonded length diagonally up the beam. This cracking was due to the concrete being required to act in tension across the end of the unbonding tube as discussed in Section 2.2.1. Secondly, the significant reduction in concrete cross section at the beam-column interface means the shear transfer mechanism is compromised; this was confirmed in initial tests by Ohkubo et al (1999) in which shear cracks extending from the top of the slot to the top of the beam were observed. However, further tests by Ohkubo and Hamamoto (2004) showed that inclusion of diagonal shear hangers in the form of deformed reinforcement can significantly limit the formation of both aforementioned crack types. It is imperative that this shear reinforcement be well anchored both within the beam-column joint and beyond the extent of the unbonded beam reinforcement to ensure successful transfer of load such that cracking is reduced.

Following on from the aforementioned work, Au (2010) confirmed solutions to the shear cracking issues and developed recommendations for prevention of reinforcement buckling within the unbonded length. However, this research highlighted further issues relating to bond

of bottom longitudinal beam reinforcement in interior beam-column joints. Due to the lack of concrete compression at the beam soffit against the column face, the entire force from the moment couple must be transferred by the longitudinal reinforcement into the beam-column joint via bond. Additionally, the absence of lateral confinement from adjacent beams causes concrete along the beam-column interface to exhibit poor bond performance. This has caused concrete cones to form and become dislodged from the joint in past testing by Au (2010). The combination of these issues can yield columns that are 20 – 40% deeper (Au, 2010) and increase frame widths by 60 – 75 mm. Initial reaction from the construction industry was that such dimensions may be unattractive, particularly in the Auckland commercial building market. Clearly, the required column depth for prevention of bar slip failure needs to be established such that column sizes are no larger than necessary. Moreover, techniques to improve the bond performance – such as provision of supplementary vertical joint reinforcement – need to be investigated.

The correct joint shear transfer mechanism must also be determined as the method proposed by the Au (2010) was based on a test in which the specimen failed due to bar slip of the bottom longitudinal beam reinforcement. According to Au (2010), there is an apparent need for supplementary horizontal joint shear reinforcement when slotted beams are used. The validity of this requirement needs to be tested when bar slip failure is prevented as the joint shear mechanism may change when this does not occur. Finally, Au (2010) assumed that top reinforcement behaved in a nominally elastic manner and, therefore, bond requirements seldom governed. The validity of this assumption needs to be confirmed as inelastic behaviour in these bars could potentially lead to bond issues similar to those currently observed in the bottom reinforcement. Desktop and experimental investigation of these issues resulting in design solutions and recommendations will form the basis of this thesis

1.3 Research Objectives

The primary aim of this research is to quantify the required column depth for prevention of bar slip failure when the slotted beam detail is used. A secondary objective – and one likely to emerge when the primary aim is satisfied – is to determine the governing joint shear mechanism.

The key areas of investigation are as follows:

- Determine the required column depth for prevention of bar slip failure in bottom longitudinal beam reinforcement when traditional reinforcement is used.

- Investigate effect of supplementary vertical stirrups on bond enhancement within the beam-column joint and the resulting required column depth when these techniques are employed.
- Determine which shear transfer mechanism governs the behaviour of the beam-column joint when slotted beams are used.
- Determine whether or not additional horizontal joint shear reinforcement is required when bar slip failure is not the method of failure.
- Confirm or otherwise longitudinal beam reinforcement requirements suggested by recent research (Au, 2010).
- Confirm or otherwise if current New Zealand Concrete Structures Design Standard bond requirements for nominally elastic reinforcement are applicable for the top longitudinal reinforcement (Standards Association of New Zealand, 2006). If outside of the Standard, prepare recommendations for slotted beam application.
- Confirm adequacy of other details unique to slotted beams including unbonding tubes along the bottom longitudinal reinforcement and beam shear hangers
- Confirm significant reduction of beam elongation when slotted beams are used.
- Refine design recommendations for bond of bottom longitudinal reinforcement and joint shear reinforcement.
- Outline further research required based on findings.

1.4 Overview of Thesis

This thesis is organised into 7 chapters. A summary of each chapter is given in this section along with an overview of how the individual chapters relate to one another. Chapter One includes a brief historical background of reinforced concrete design focussing on the New Zealand construction industry and the advent of capacity design. An introduction to the slotted beam concept is given in which the differences and similarities between slotted and monolithic reinforced concrete beams are discussed. The research objectives are then presented to give the reader an idea of the scope of this project.

Chapter Two gives an overview of current industry practice and the research from which this was developed. Deficiencies of current practice are presented along with a summary on the performance of modern concrete framed structures in several recent earthquakes. The merits of various recently developed structural systems are briefly discussed. Finally, several previous experimental studies on slotted beam systems are analysed.

Chapter Three covers bond mechanics and the various stages leading to bond failure for both well and poorly confined specimens under monolithic and cyclic loading. The major factors influencing bond performance are discussed in detail as a precursor to the bond modification factors and bond improvement techniques discussed in Chapter Four. A summary of several extensive experimental programmes on bond mechanics is also presented to reinforce the theory developed throughout the chapter.

Chapter Four examines the mechanics of both slotted and monolithic interior beam-column joints in detail. The results of a database study on monolithic specimens are presented as a basis for determining slotted beam bond parameters. Bond demand and associated modification factors are developed using material from Chapter Three. Supplementary vertical joint stirrups are investigated as a means of bond improvement. Shear demand and resistance mechanisms are discussed for both monolithic and slotted joints. Monolithic joint behaviour is taken from theory and reinforced using the findings of previous experimental studies, while slotted beam behaviour is derived from Au (2010) recommendations and first principles. A parametric study is carried out to determine the applicability of current NZS3101:2006 joint reinforcement provisions to slotted beams. Finally, experimental results from Chapter Five are used to refine design recommendations for bond of longitudinal reinforcement and joint shear reinforcement.

Chapter Five details the design, instrumentation, and testing procedure for two 80% scale slotted beam specimens. Visual observations during testing are reported and linked to the observed response. Strain profiles for each type of reinforcement within the specimens are presented and discussed. The bond performance of both the top and bottom longitudinal beam reinforcement is analysed and design parameters are extracted from this. Evidence is presented that supports a revised joint shear mechanism heavily dominated by the strut mechanism. The experimental results are compared with those found by Au (2010) where applicable.

Chapter Six summarises the research undertaken and recommends aspects requiring further investigation. References are listed in Chapter Seven. Database specimen summaries are given in Appendix A.

Chapter 2 - BACKGROUND RESEARCH

2.1 Precast Concrete History

2.1.1 Precast Construction in New Zealand

Current design practice within New Zealand is focussed on the use of precast construction techniques. Precast concrete systems are popular due to the increased quality control and reductions in site labour they allow compared with monolithic reinforced concrete construction. While precast concrete has been around since the 1960's, it was not until the 1980's that it began to see significant use in the New Zealand construction industry. During this period, the use of precast units for flooring and seismic resistance elements including walls and moment frames increased dramatically as a result of innovation from industry.

However, the then current New Zealand Concrete Structures Design Standard was lacking in regard to seismic performance of precast concrete systems. As such, behaviour of these was commonly assumed from extrapolation of monolithic test data, and their design was based on emulation of monolithic structures. In order to bridge this gap between industry progress and code documents, a group including representatives from the New Zealand Concrete Society, the New Zealand National Society for Earthquake Engineering, and the Centre for Advanced Engineering was formed to produce a set of guidelines for use in the precast construction industry. First published in 1991, these guidelines became recognised in industry and later formed the basis of the revised 1995 Concrete Structures Standard in relation to precast construction (CAE, 1991). The group's – hereinafter referred to as the CAE report – findings are briefly outlined below.

The CAE report recognised that capacity design methods posed significant challenges for precast moment frames. While relatively easy to achieve in monolithic structures, correct strength hierarchies were more difficult to produce in precast structures with element connections and plastic hinges of particular concern. Beam elements were generally connected outside plastic hinge zones and incorporated 'wet' joints with spliced or plate welded bars, while column elements were often placed over longitudinal bars protruding from the previous unit and grouted into place. Attention was also given to precast flooring units and the CAE report recommended details to address issues such as moment continuity at supports, floor seating lengths, and construction tolerances; however, the report also stressed the need for further research in these areas (CAE, 1991). Subsequently, the CAE report was revised in 1999 to incorporate findings from recent research, lessons learnt from the Northridge and

Kobe earthquakes, and to better reflect some technical aspects of the current New Zealand Concrete Structures Design Standard. Still popular in current industry practice, several precast construction techniques are illustrated in Figure 2-1 below.

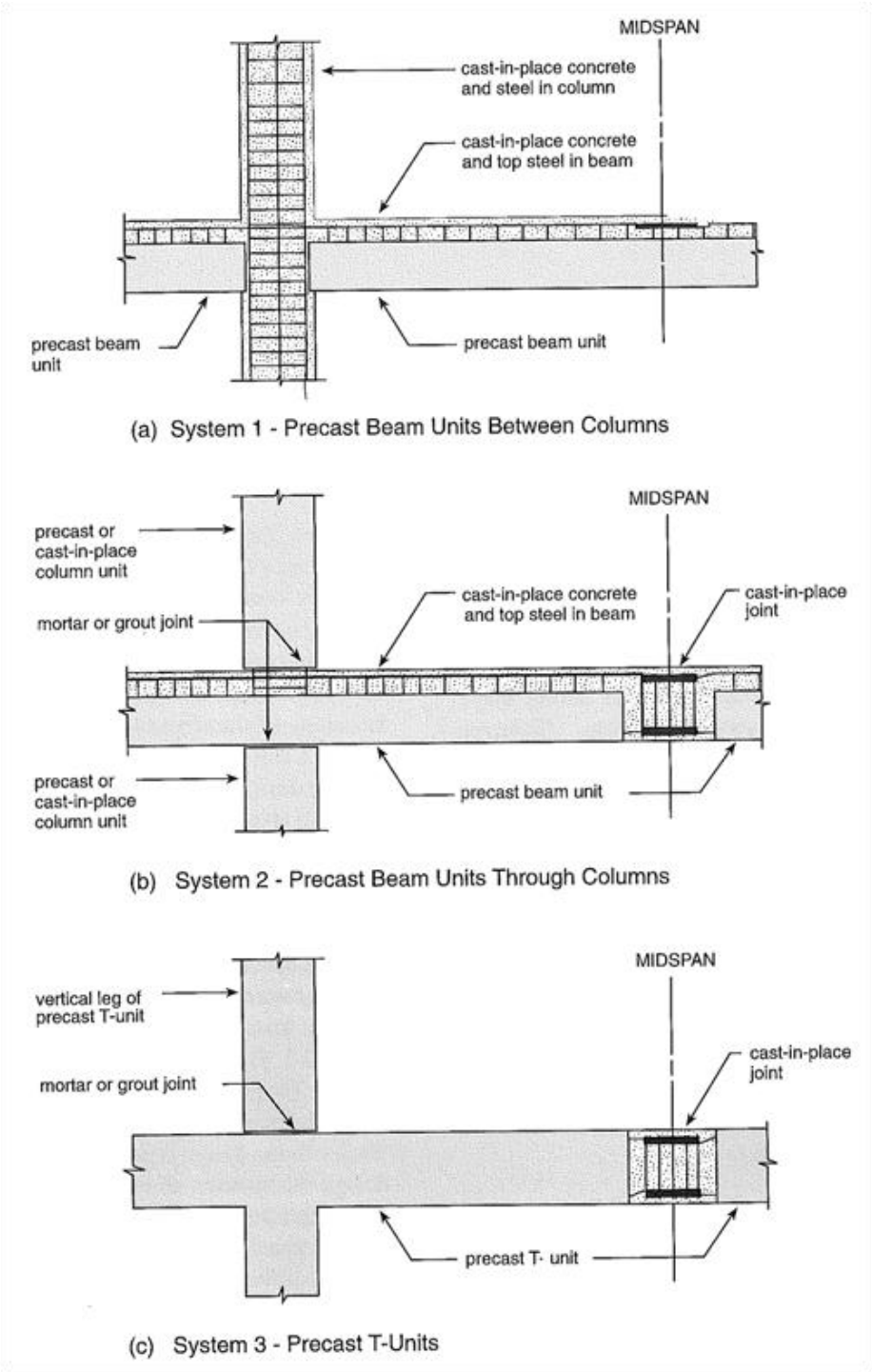

Figure 2-1: *Precast construction techniques for frames (CAE, 1999)*

2.1.2 Earthquake Performance of Concrete Structures

During the last few decades there have been a number of significant earthquakes in countries which employ a high standard of building design and construction practices, similar to New Zealand. Although few post-1976 reinforced concrete frame structures failed to the extent of

being irreparable in the 1994 Northridge earthquake, floor diaphragm activation and significant damage to beam ends was observed and attributed to the formation of plastic hinges in these regions (Holmes & Somers, 1995; Norton, King, Bull, Chapman, McVerry, Larkin & Spring, 1994). Because capacity design relies on such damage to dissipate earthquake energy, subsequent rehabilitation after an earthquake is often very expensive and not always possible. This presents one of the main shortcomings of the capacity design method which was once again observed following the Christchurch earthquake in February 2011.

While the majority of modern concrete structures performed satisfactorily in these earthquakes, some did fail catastrophically. Several collapses in the Northridge earthquake occurred due to inadequate detailing of columns which consequently behaved in a non-ductile manner forming localised soft storey mechanisms (Holmes & Somers, 1995). Similar failures were observed during the 1995 Kobe earthquake with a number of soft storey mechanisms occurring, again, due to inadequate detailing of columns which were consequently unable to cope with larger than expected beam overstrength moments (Mitchell, DeVall, Kobayashi, Tinawi & Tso, 1996). A number of collapses also occurred due to a loss of seating in precast flooring units as shown in Figure 2-2.

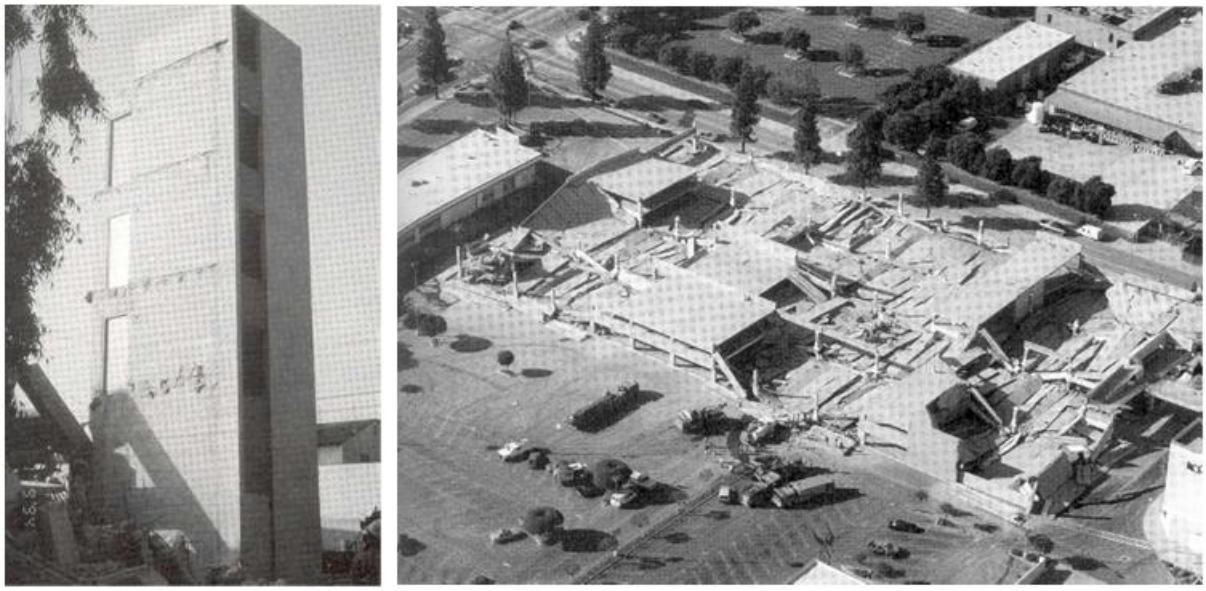

Figure 2-2: *Collapsed parking structures following the 1994 Northridge Earthquake (Holmes & Somers, 1995)*

2.1.3 Recent Developments

In response to the shortcomings of existing structures observed during previous earthquakes, a number of innovative structural systems have been developed in recent times. One of the first research projects in this area was the PRESSS – Precast Seismic Structural Systems –

research programme, jointly undertaken by researchers in the United States and Japan. Beginning in 1991, the goal of this project was to develop and test precast systems for adoption by building codes (Priestley, 1991). This project culminated in the testing of a 60% scale, 5 storey structure with post-tensioned walls and frames in either direction. As illustrated in Figure 2-3, one of the frame details tested incorporated a gap at the beam-column interface and energy dissipation via tension/compression yielding of mild reinforcing steel. Both lateral systems were found to possess a high degree of energy dissipation and self-centring ability. However, vertical sliding at the beam-column interface and associated damage was observed, highlighting issues with the clamping together of components via post-tensioning (Priestley, Sritharan, Conley & Pampanin, 1999). The issue of beam vertical sliding was later addressed by Pampanin, Pagani, and Zambelli (2004) through the use of shear keys embedded within the column.

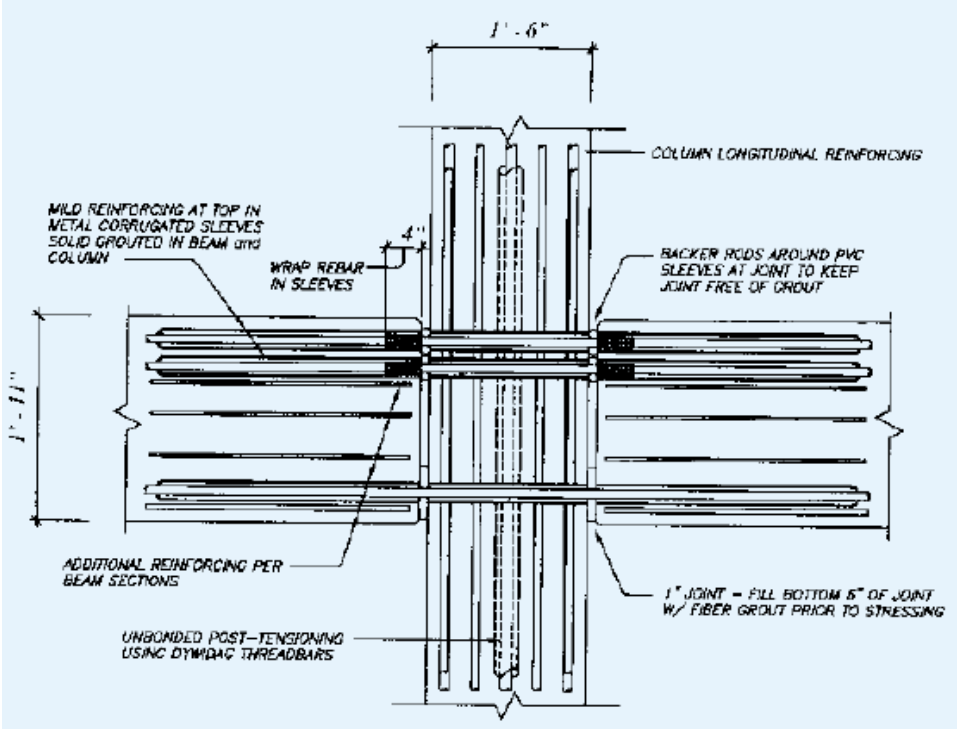

Figure 2-3: *TCY-gap connection from PRESSS programme (Priestley et al, 1999)*

Thus far, such connections had generally used mild steel within the beam or wall for energy dissipation. Recognising the impracticality with replacing this reinforcement after a severe seismic event, Amaris, Pampanin, Bull, and Carr (2008) tested frames with external mild steel dissipaters as shown in Figure 2-4(b) designed to prevent beam elongation and associated floor damage. Non-tearing floor connections were further developed by Leslie (2010) who conducted tests incorporating floor slabs with a number of different hinge details. The connections were found to perform well with significantly reduced floor damage compared with traditional monolithic systems.

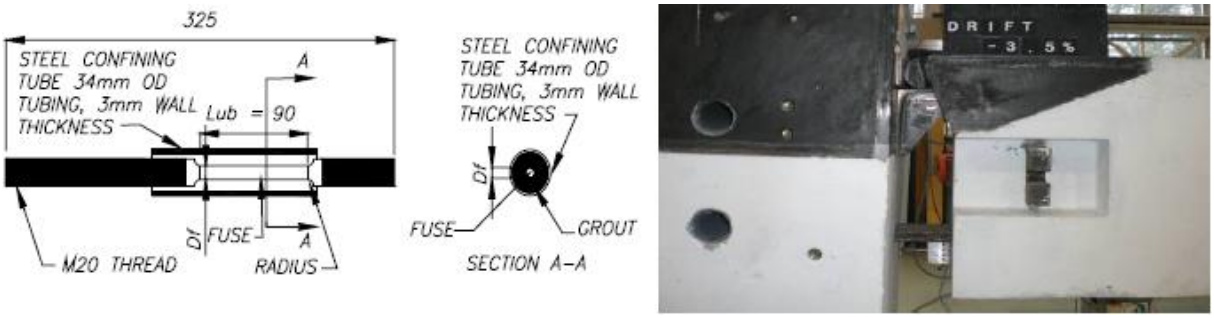

(a) External mild steel dissipaters (b) Steel top beam hinge

Figure 2-4: *Mild steel dissipaters and non-tearing hinge details (Amaris et al, 2008)*

2.2 Past Testing of Slotted Beams

From initial tests in which their ability to achieve similar moment capacity to conventional beams was realised (Ohkubo et al, 1999), slotted beams have improved significantly. Subsequent experimental work by Ohkubo and Hamamoto (2004) and Au (2010) has gone a long way to proving the advantages of slotted beam systems including reductions in beam elongation and damage within the beam plastic hinge zones, and damage to adjacent floors. Several critical issues including shear transfer from the beam into the column and buckling of bottom longitudinal beam reinforcement were also addressed by these researchers. This section outlines the findings of these researchers and the issues that must be addressed before slotted beams can be integrated into current industry practice.

2.2.1 Ohkubo et al (1999)

As outlined in Section 1.2, Ohkubo et al (1999) were the first to test slotted beams in reinforced concrete frames. These researchers recognised the need for an unbonded length over part of the bottom reinforcement to reduce local strains, and that top longitudinal reinforcement should be sized larger than the bottom such that material elongation in the top hinge is limited. Subsequently, the unbonded length was detailed to be 180 mm, or 45% of the beam depth, while the mechanical reinforcement ratio, A'_s/A_s, between the top and bottom longitudinal layers was approximately 1.34; both significantly less than values used by Au (2010) in later testing. The specimens used for this testing were cantilever beams connected to a column at the slotted end and loaded at the free end over 12 cycles up to a maximum drift of 4%. Unlike all later tests, no additional shear reinforcement across the beam-column interface was provided in the initial test. Subsequently, one of the major issues encountered during the first two tests was formation of a shear crack – termed an ‘S-crack’ – extending from the end of the unbonded bottom reinforcement diagonally up the beam as illustrated in Figure 2-5.

This cracking was unexpected as it occurred when the beam soffit was in compression at approximately 2% drift in the first specimen (RCSB-1). The crack formed because, unlike in a monolithic beam, the compression struts set up in the concrete as part of the beam shear transfer mechanism were unable to be resisted by compression from the column face. Instead, the struts had to be tied back into the beam through the steel unbonding tubes surrounding the reinforcement. At the ends of the tubes, the tension force was required to move through the concrete in order to be taken up by the bottom beam reinforcement; this tension demand in the concrete caused the crack to initiate.

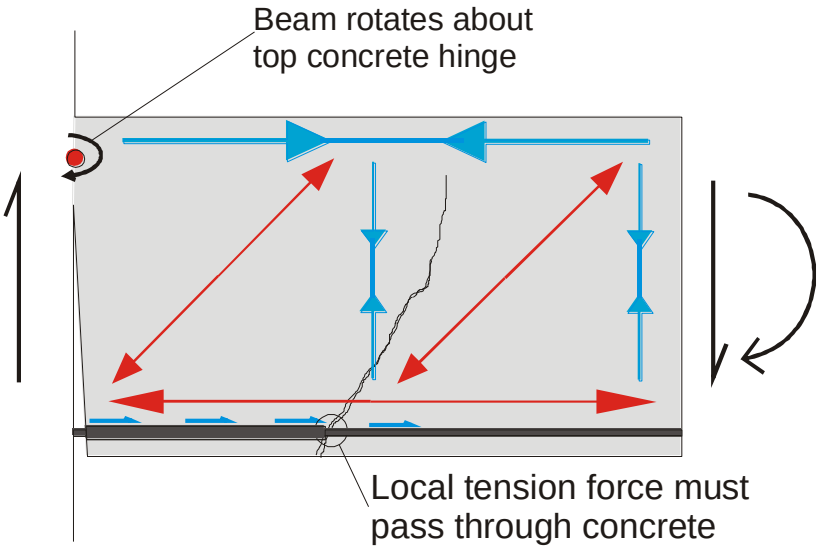

Figure 2-5: *Formation of 'S-crack' during initial slotted beam testing*

The crack propagation is also easily explained. Due to the downwards shear from applied loading and the corresponding upwards shear at the column face, the beam has a tendency to rotate about the top concrete hinge. This induces a tension demand in the concrete perpendicular to the compression struts thus causing the crack to propagate diagonally up the beam. Due to the greater distance from the centre of rotation, the crack was found to be larger at the beam soffit. As a result of this cracking, the first test exhibited a poor hysteretic response with significant pinching (Ohkubo et al, 1999).

Otherwise identical to the first, the second specimen, RCSB-2, included additional shear reinforcement in the form of inclined, high-strength stirrups, or 'U-bars'. Shown in Figure 2-6 below, these were included in an attempt to prevent formation of the 'S-crack' that formed in specimen RCSB-1 as discussed above.

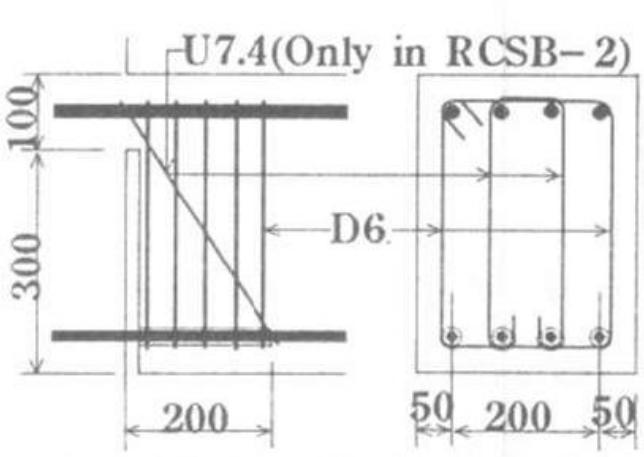

Figure 2-6: *Specimen RCSB-3 showing 'U-bar' shear reinforcement across the hinge*

However, unlike later testing by Ohkubo and Hamamoto (2004) and Au (2010), this reinforcement was not extended past the end of the unbonded length. Due to this poor detailing, the S-crack appeared earlier than in the initial test at a drift of 0.5% and even before yielding of the bottom reinforcement. Ohkubo et al (1999) proposed that, due to the lack of anchorage along the beam soffit, tension in the U-bars acted on concrete near the end of the unbonded length thus increasing its tendency to crack. Again, the hysteretic response was poor and comparable with that of the first test.

Ohkubo et al (1999) then conducted three further tests in an attempt to prevent the severe cracking observed in the initial tests and achieve a satisfactory hysteretic response. One of these tests, RCSB-3, included the now standard diagonal shear reinforcement extending adjacent to the bottom longitudinal reinforcement. However, high-strength stirrups were again used as opposed to deformed bars in later testing by Ohkubo and Hamamoto (1999) and Au (2010). This configuration was found to significantly delay formation of the S-crack until approximately 4% drift and resulted in a satisfactory hysteretic response as shown in Figure 2-7. At around the same drift, the specimen failed due to buckling of the bottom reinforcement within the unbonded length despite the use of a steel unbonding tube and a stirrup spacing of around $2.5d_b$. This buckling occurred within the steel tube, most likely due to excessive clearance between the longitudinal bar and tube wall.

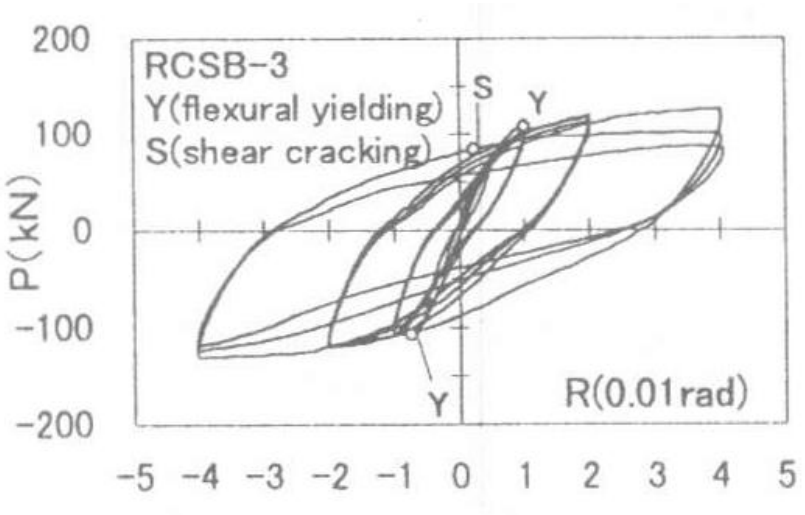

Figure 2-7: *Hysteretic response of RSCB-3 (Ohkubo et al, 1999)*

In addition to the previously discussed S-crack, relatively large cracks are visible in Figure 2-8 extending diagonally from the top of the slot to the top of the beam; these also occurred on the other specimens. These cracks initiated at a relatively low drift, likely due to slipping of the undeformed U-bars. This slipping in turn caused the beam to move downwards with the associated shear force and thus induce a tensile stress in the concrete. Due to the reduced concrete section within the hinge region, the magnitude of stress induced was higher and sufficient to initiate cracking. However, Ohkubo et al (1999) found that dowel action of reinforcement crossing the crack was effective at transferring the shear over the slot and, as such, the crack was not critical to the beams performance. This is evidenced by the satisfactory hysteretic response achieved in RCSB-3 and other subsequent tests incorporating U-bars for shear transfer.

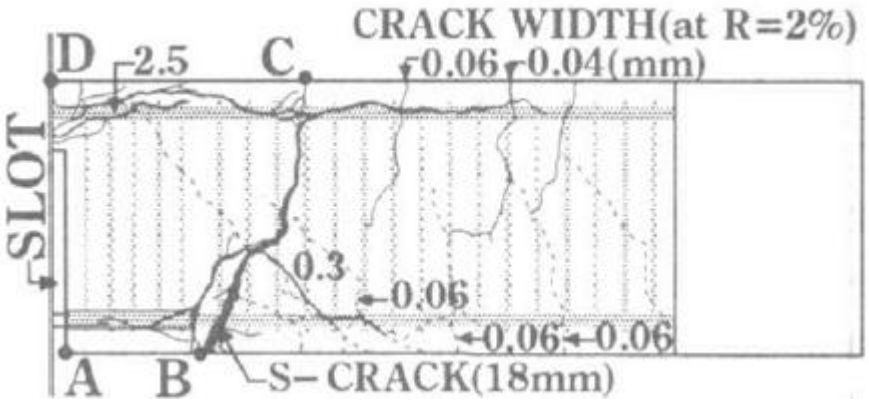

Figure 2-8: *Cracking pattern of RCSB-1 (Ohkubo et al, 1999)*

2.2.2 Ohkubo & Hamamoto (2004)

Ohkubo and Hamamoto (2004) extended the research on slotted beams to determine the behaviour when floor slabs were included. Both slotted beam specimens tested were interior sub-assemblies with floor slabs on either side. Deformed bars were used for diagonal shear

reinforcement as opposed to high-strength stirrups in order to reduce bar slip and associated shear cracking observed in previous tests. Unbonded length and mechanical reinforcement ratio were the same as those used by Ohkubo et al (1999). However, the loading protocol was less severe with a maximum drift of only 3% being reached after 8 cycles. Hysteretic responses were again satisfactory with similar moment capacity achieved compared with the benchmark monolithic specimen; the small deficit due to the lack of floor slab contribution in the slotted specimens. Energy dissipation was found to be higher than the monolithic specimen above 1% drift; likely due to the bottom steel yielding in both tension and compression during each cycle.

More importantly, damage to both the floor and frame was reduced in the slotted beam specimens. Figure 2-9 illustrates the comparison in cracking between the slotted beam specimen and monolithic specimens. While shear cracking extending from the top of the slot to the top of the beam is still evident to a reduced extent, the S-crack observed by Ohkubo et al (1999) is clearly not present. However, a small crack occurred running diagonally across the beam-column joint; possibly due to congestion of the joint. Nonetheless, the damage is significantly reduced to both the frame and floor of the slotted beam specimen, and this is reflected by the significantly reduced beam elongation shown in Figure 2-10.

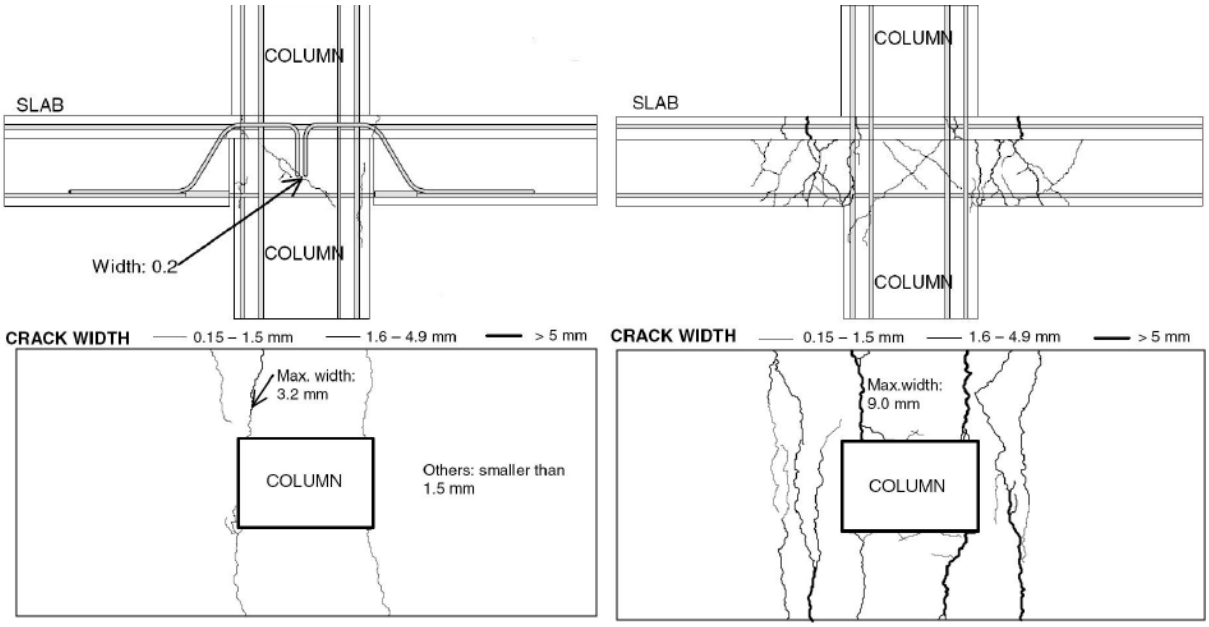

(a) Slotted beam specimen (b) Monolithic specimen

Figure 2-9: *Cracking patterns for slotted and monolithic specimens (Ohkubo & Hamamoto, 2004)*

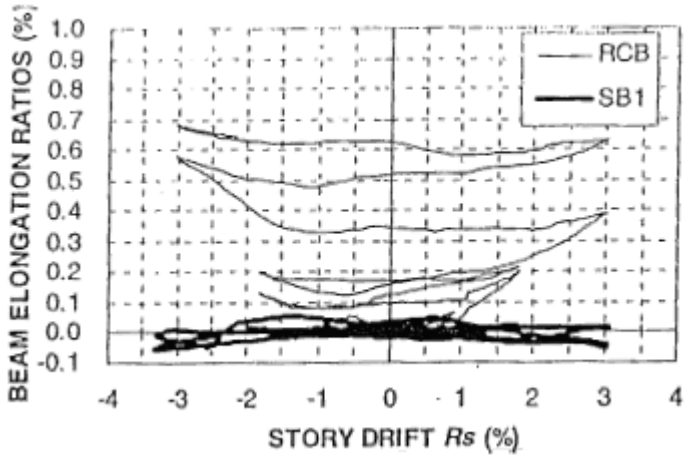

Figure 2-10: *Beam elongation for slotted beam and monolithic specimens (Ohkubo & Hamamoto, 2004)*

2.2.3 Au (2010)

Working out of the University of Canterbury, Au (2010) recently conducted several reduced scale experiments on interior slotted beam sub-assemblies. Unlike previous researchers, he used the more demanding ACI loading protocol (ACI Committee 374, 2005) which involves approximately 35 cycles up to a maximum drift of 4.5%. He also increased the unbonded length to between 65 and 70% of the beam depth to limit the effects of low cycle fatigue. Mechanical reinforcement ratio was set at around 2 in an attempt to reduce yielding of the top reinforcement.

This research confirmed reductions in beam elongation/damage and floor diaphragm activation observed by Ohkubo et al (1999) and Ohkubo and Hamamoto (2004). The effectiveness of deformed diagonal shear reinforcement – from here on in referred to as 'shear hangers' – as a means of transferring shear from the beam into the column was also confirmed. Au (2010) also recognised the importance of terminating the unbonding tube before the shear hanger bend; if this detailing is not adhered to, the surrounding concrete will be required to act in tension to transfer the horizontal shear hanger reaction. This can result in similar cracking to the S-crack discussed in Section 2.2.1. Further buckling failures were observed with remedial techniques proposed and low cycle fatigue was investigated as a potential failure mechanism. The previously unrealised failure mechanism of concrete cone pullout failure within an interior beam-column joint also occurred in one of the tests. This was prevented in a subsequent test through the use of a relatively large column depth compared with that typical of conventional frames.

Beam elongation and hinge damage were investigated for both Grade 300 and 500 reinforcement in specimens SB2 and SB3, respectively. Note that 'Grade' refers to the lower

characteristic yield strength of the reinforcement; this shorthand is adopted throughout the thesis. Figure 2-11 shows that beam elongation is negligible regardless of reinforcement grade with both specimens experiencing peak elongation of around 0.5% of the beam depth. Comparison of crack widths between specimens shows the reinforcement grade has minimal influence on these also.

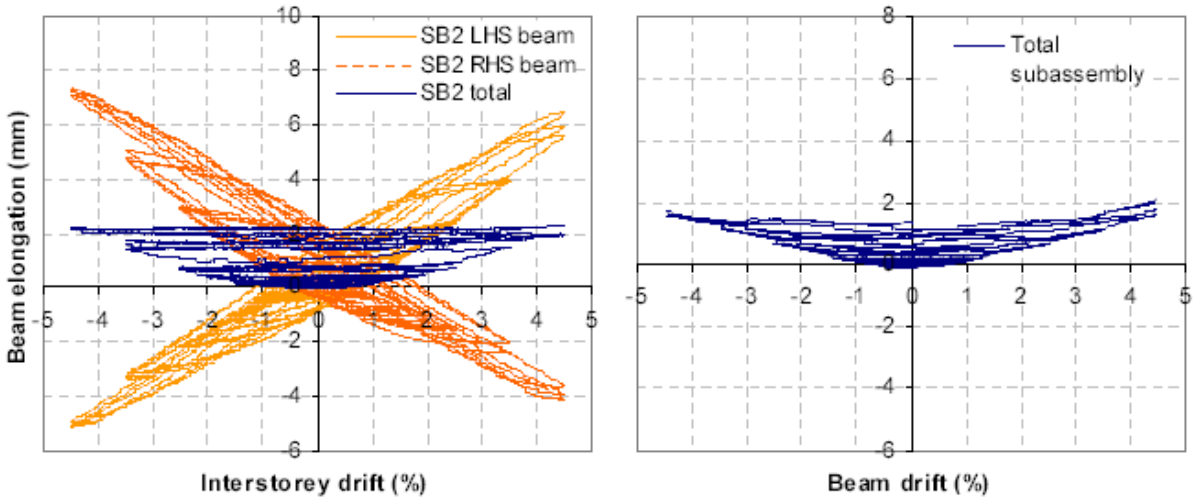

(a) SB2 (b) SB3

Figure 2-11: *Measured beam elongation in interior joint specimens (Au, 2010)*

Bar buckling can occur in the bottom longitudinal reinforcement within slotted beams due to the presence of the slot and unbonded length. Because the bottom reinforcement governs the moment capacity of the system, it is critical that it not be compromised by this phenomenon. When the beam is subject to downwards vertical shear, it will move downwards relative to the column. This will induce a slight eccentricity between the bar at the column face and where it enters the unbonded length as shown in Figure 2-12(a). As the slot closes during seismic loading, this eccentricity will increase until buckling results, leading to spalling of the cover concrete as shown in Figure 2-12(b). As illustrated in Figure 2-13(a), this method of failure was observed by Au (2010) on an exterior joint specimen, SB1, at -3.5% drift. In this test, the stirrups were spaced at $6d_b$ and a PVC unbonding tube was used as opposed to the now standard steel tube. This buckling resulted in a slight loss of strength as illustrated in Figure 2-14 and major cracking of the beam soffit. However, as discussed below, it may also have contributed to the ultimate failure of this specimen through fracture.

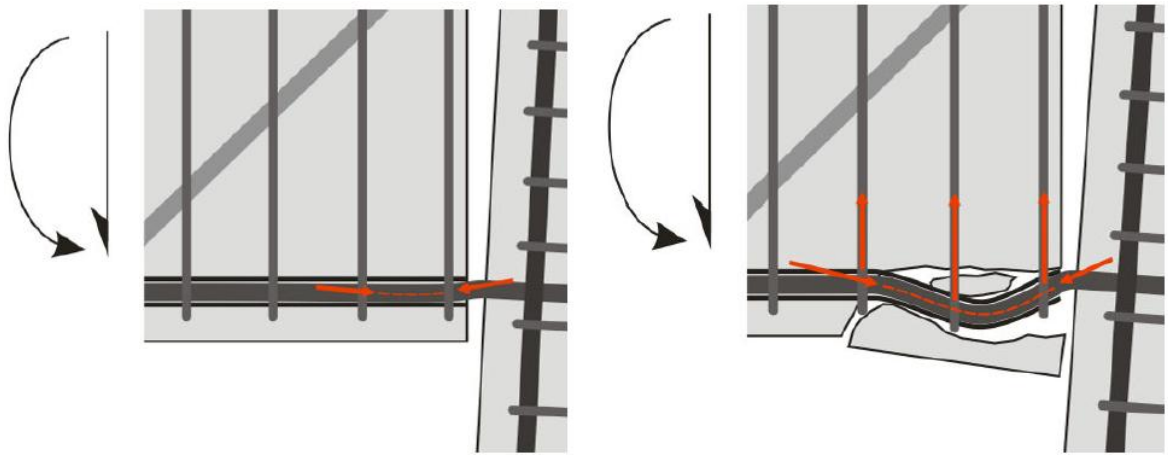

(a) Induced eccentricity (b) Buckling causes spalling

Figure 2-12: *Buckling in bottom reinforcement (Au, 2010)*

In a subsequent test, SB3, Au (2010) found that reducing the stirrup spacing to $4d_b$ and using a steel unbonding tube could prevent the aforementioned mode of failure. Note that the stirrup spacing limit alone is insufficient because the bars could still buckle at a higher mode between the stirrups in the absence of a steel unbonding tube. The steel tube itself must also be thick enough to prevent buckling and the clearance to the bar small enough such that buckling can actually be restrained. Au (2010) initially used grout filled tubes but found that tape wrapped around the bars to reduce the clearance was sufficient. Furthermore, the use of grouted tubes can lead to differential responses in compression and tension due to bearing of the bars on the grout. As such, the specimens constructed as part of this research project will use bars wrapped in tape and enclosed within steel tubes.

(a) Buckling at -3.5 % drift (b) Fracture at 4.5 % drift

Figure 2-13: *Buckling and fracture observed in specimen SB1 (Au, 2010)*

Bottom reinforcement within slotted beams is especially vulnerable to low cycle fatigue. This is because, unlike in a monolithic system, the reinforcement within a slotted beam yields in both tension and compression every cycle. Accumulation of this plastic strain over multiple cycles can lead to fracture of the reinforcement. This generally results in a sudden and substantial loss of strength to the system as shown in Figure 2-14 where all bars fractured in

rapid succession; it is therefore imperative that this mode of failure be prevented. Au (2010) observed bar fracturing in all three slotted beam specimens and proposed that fracture susceptibility was related to previous buckling in the bar – buckling induces high strains in the extreme fibres of the bar which are then prone to fracture when the bar is put into tension during subsequent cycles. This was true of the first specimen in which all bars buckled during the first cycle to -3.5% drift; these bars all went on to fracture during the first cycle to 4.5% drift as shown in Figure 2-13(b). However, fracturing of single bars in further tests at between 3.5 and 4.5% drift did not always follow earlier buckling.

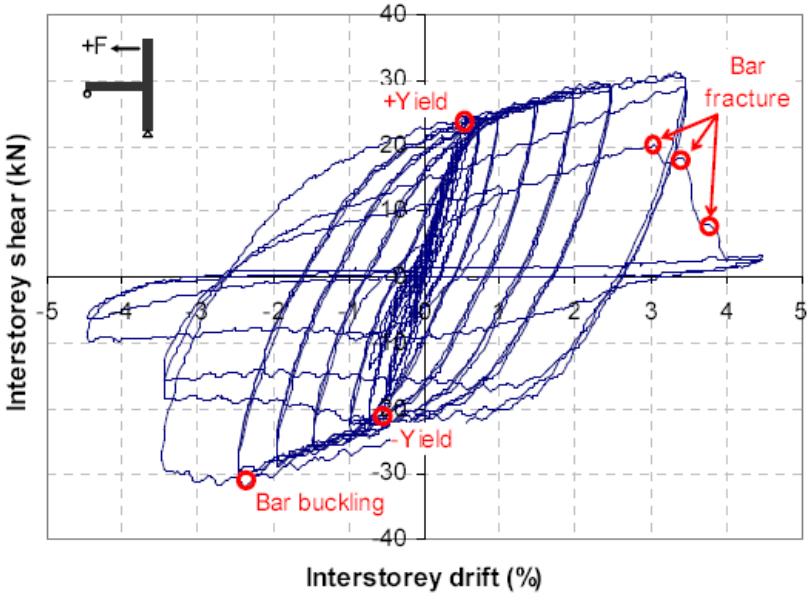

Figure 2-14: *Ram force vs. drift for specimen SB1 (Au, 2010)*

Au (2010) identified unbonded length and reinforcement ratio of the bottom longitudinal reinforcement as the key variables in relation to strain accumulation. Increasing unbonded length reduces the strain magnitude and thus the number of cycles until the accumulated strain reaches critical levels. Similarly, increasing reinforcement ratio allows use of shallower beams such that strains are lower due to decreased distance from the neutral axis. However, these two mechanisms are interdependent as unbonded length is generally detailed as a function of beam depth and, therefore, reinforcement ratio. In practice, the strain magnitude and thus the strain accumulation rate is therefore proportional to the reinforcement ratio alone. Au (2010) recommends a minimum reinforcement ratio for the bottom longitudinal reinforcement between 0.006 and 0.008.

Bar slip and concrete cone pullout failure were observed by Au (2010) in the first test, SB2, on an interior beam-column joint incorporating slotted beams. The bar slip failure was due to an insufficient column depth which was subsequently found to be inadequate to resist the increased bond demands found in slotted beam-column joints; the reasons for this increased

bond demand are discussed in Section 4.2.1. The resulting decrease in stiffness of the specimen's response is clearly evident in Figure 2-15 where the response becomes flatter after bar slip failure has occurred. Required column depth for the prevention of bar slip failure is discussed further in Section 4.2.2.

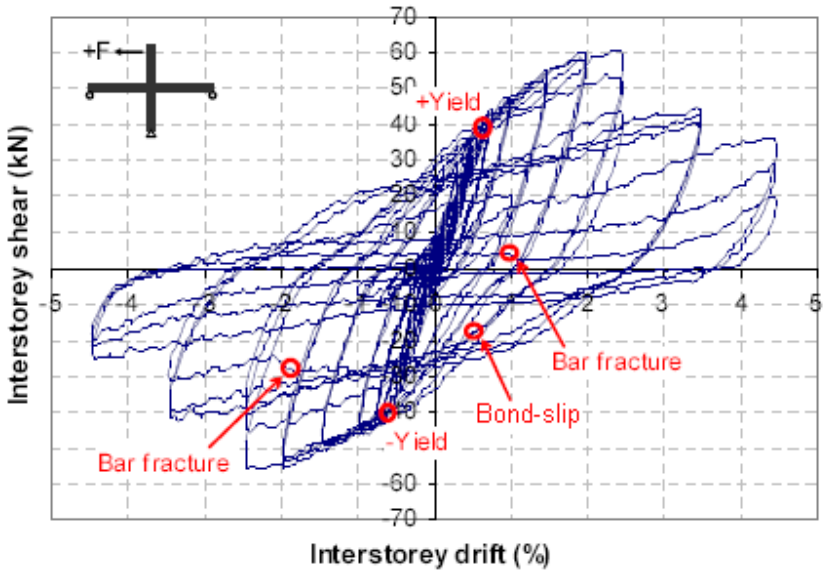

Figure 2-15: *Ram force vs. drift for specimen SB2 (Au, 2010)*

The cone pullout, shown in Figure 2-16, is an indicator of significant inelastic behaviour in the reinforcement rather than a failure mode itself. Severe strain levels in the bottom longitudinal reinforcement confirm this cone formed due to strain penetration into the beam-column joint. Combined with a lack of confinement from the adjacent beam, the cone was allowed to come away from the joint face. Considered alone, it contributes minimal strength loss to the system because it is generally confined to the weaker concrete cover as discussed in Section 3.4.2.

Figure 2-16: *Concrete cone pullout on face of beam-column joint specimen SB2 (Au, 2010)*

In order to prevent bar slip failure from occurring again, Au (2010) increased the concrete strength from 30 to 40 MPa and used a larger column depth in a subsequent test, SB3. While successful at preventing another bar slip failure, this column depth was possibly excessive to the point that horizontal joint reinforcement was not activated until a drift of 3.5%. Given architectural and economic restraints, such a column depth could be unacceptable in current industry practice. This gives rise to the primary research objective as stated in Section 1.3 of determining the required column depth for prevention of bar slip failure when a slotted beam detail is used. Figure 2-17 shows that, regardless of bar slip failure being prevented, a concrete cone still formed and detached from the specimen, albeit to a lesser extent.

Figure 2-17: *Reduced concrete cone pullout damage in specimen SB3 (Au, 2010)*

Examination of strain profiles in Figure 2-18 at 2.5% drift, corresponding to cone formation, reveals that the bottom longitudinal reinforcement is within the inelastic range at the column face. This is further evidence that cone formation is due to inelastic behaviour in the steel as opposed to bar slip failure. Observations by Viwathanatepa, Popov, and Bertero (1979) in which cone formation was consistently detected at between 74 – 92% of nominal yield strength reinforce this statement.

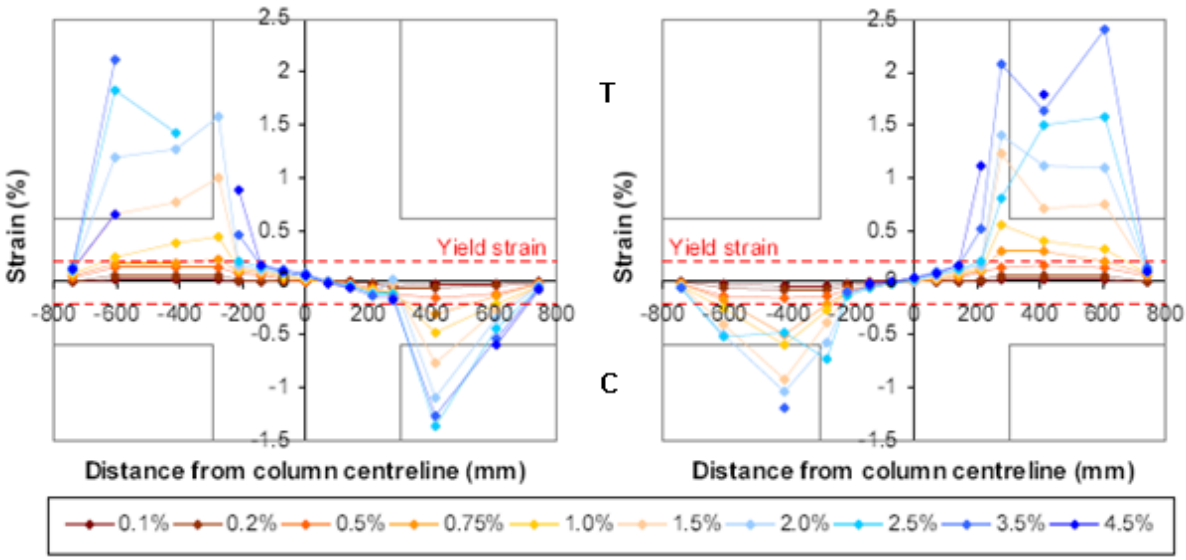

(a) Positive drifts (b) Negative drifts

Figure 2-18: *Bottom reinforcement strain profile for specimen SB3. Adapted from Au (2010)*

Chapter 3 - BOND MECHANICS

3.1 Mechanisms of Bond

3.1.1 Introduction

In terms of reinforced concrete, bond refers to the mechanism by which forces within reinforcement bars are transferred into the surrounding concrete. Similarly, bond stress refers to the stresses along the bar-concrete interface which modify the steel stresses along the bar through the process of bond (Federation internationale du beton, 2000). Given a force, $C + T$, is to be transferred via bond, the resulting average local bond stress, τ, is given by Equation 3-1 (Park & Paulay, 1975; ACI Committee 408, 1992; Esfahani & Rangan, 1998; Tastani & Pantazopoulou, 2010). While this equation is only valid for short embedment lengths where the bond stress distribution can be approximated as uniform, as shown in Figure 3-1(a), it is often used to express the average bond stress over larger embedment lengths, u_a, where the distribution, as shown in Figure 3-1(b), is not uniform. The latter is true for the majority of design situations, thus why the equation is commonly used to provide a comparison even though it is not technically correct.

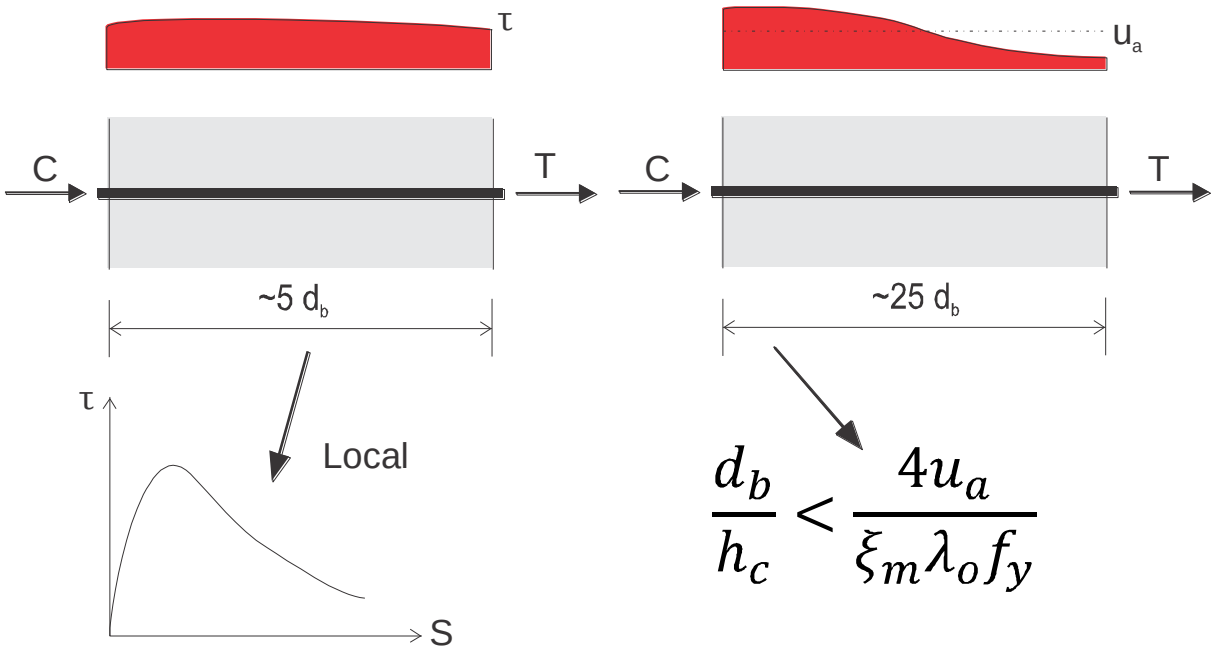

(a) Local bond stress (b) Design bond stress

Figure 3-1: *Clarification of local and design bond stress distributions*

Hence to avoid confusion in this thesis, *local* bond stress, τ, refers to the bond stress obtained using Equation 3-1 where the embedment length is generally on the order of $5d_b$. Conversely,

average bond stress, u_a, refers to the resultant bond stress obtained by applying Equation 3-1 to embedment lengths typical of actual design on the order of $15d_b$ or greater and is the form most commonly used in this thesis. Note that some variables within Equation 3-1 have been altered from the form in which they appear in the texts.

$$\tau, u_a = \frac{q}{p} = \frac{C+T}{\Delta L p} = \frac{\Delta f_s[\pi d_b^2/4]}{\Delta L[\pi d_b]} = \frac{d_b \Delta f_s}{4\Delta L} \qquad \text{Equation 3-1}$$

Where q is the change of bar force per unit length of bar, p is the nominal bar perimeter, ΔL is the length of bar over which bond stress is computed, and Δf_s is the change of steel stress over length ΔL. However, Δf_s and the length over which it acts, ΔL, are relatively difficult to determine accurately. Thus the local bond stress, τ, is very difficult to quantify. Moreover, it is dependent on many variables (Federation internationale du beton, 2000).

Before covering the main topic of concern, bond under cyclic loading, the relatively simpler mechanism of bond under monotonic loading must be understood. Bond under monotonic loading refers to the mechanism through which bond between reinforcing steel and concrete is developed when the loading is in a single direction. An important aspect of monotonic bond behaviour is that, when the bars are cast and loaded horizontally, the stress-slip hysteresis is effectively the same for both tension and compression loading of the bar (Eligehausen, Popov & Bertero, 1983).

3.1.2 Uncracked Concrete

The process of bond under monotonic loading can be characterised by four stages. In the first stage, during which the concrete remains uncracked and bond stress values are on the order of $0.2 - 0.8f_t$, where f_t is the tensile strength of the concrete, bond is provided mostly through chemical adhesion and friction (Federation internationale du beton, 2000; Choi & Lee, 2002; Harajli, Hamad & Karam, 2002). Highly localised stresses build up in the concrete close to the lug tips due to the microscopically rough bar surface providing some friction at this level. Note that 'lug' refers to the raised sections along deformed bars; these are sometimes referred to in literature as 'ribs' but this thesis will refer to them only as 'lugs'. During this stage there is no bar slip and, as a result, the bond stress-slip hysteresis is initially steep (ACI Committee 408, 1992) as illustrated in Figure 3-2(a). The deformation that occurs during this stage is instead due to shear deformation in the concrete as shown in Figure 3-3. Note that relative displacement of the bar is always measured with reference to undisturbed concrete.

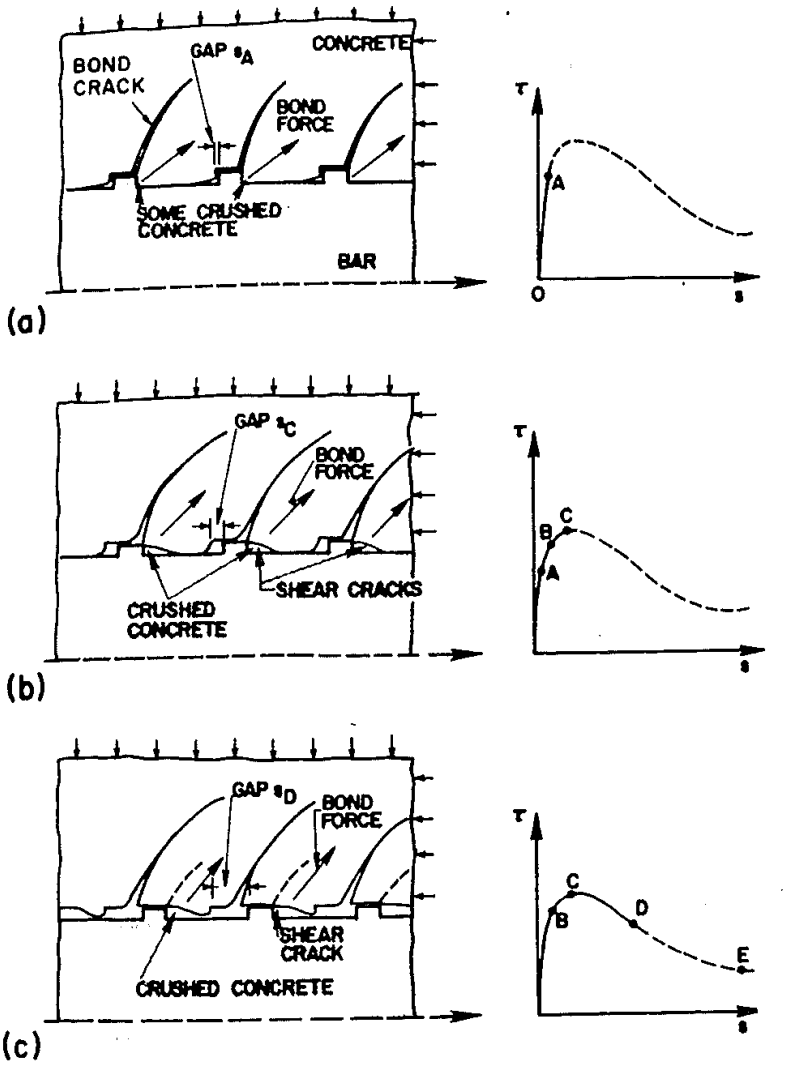

Figure 3-2: *Bond stress-slip relationships for monotonic loading (ACI Committee 408, 1992)*

3.1.3 Formation of Transverse Cracking

During the second stage, cracks begin to develop in the concrete as the bond stress moves into the range $0.8 – 1.0f_t$, or $0.4 – 0.5\sqrt{f_c'}$, using the relationship proposed by Paulay and Priestley (1992). The chemical adhesion breaks down causing the lugs to induce large bearing stresses, p^*, in the adjacent concrete which are set up at approximately 30˚ to the bar axis. Coupled with stress concentrations due to concrete shrinkage around the lug tips (ACI Committee 408, 1992), p^* results in the formation of transverse cracks from the lug tips allowing the bar to slip at the bar-concrete interface by a distance δ_t as illustrated in Figure 3-4(b). Due to this slip, frictional forces are mobilised along the bar surface, but these are small in comparison to bearing resistance (ACI Committee 408, 1992). As shown in Figure 3-2(b), the stress-slip hysteresis begins to soften due to these cracks allowing movement. Wedging action of the lugs, which refers to the lugs being forced into the concrete surrounding the undeformed sections of the bar, remains limited such that the concrete does not split (Federation internationale du beton, 2000).

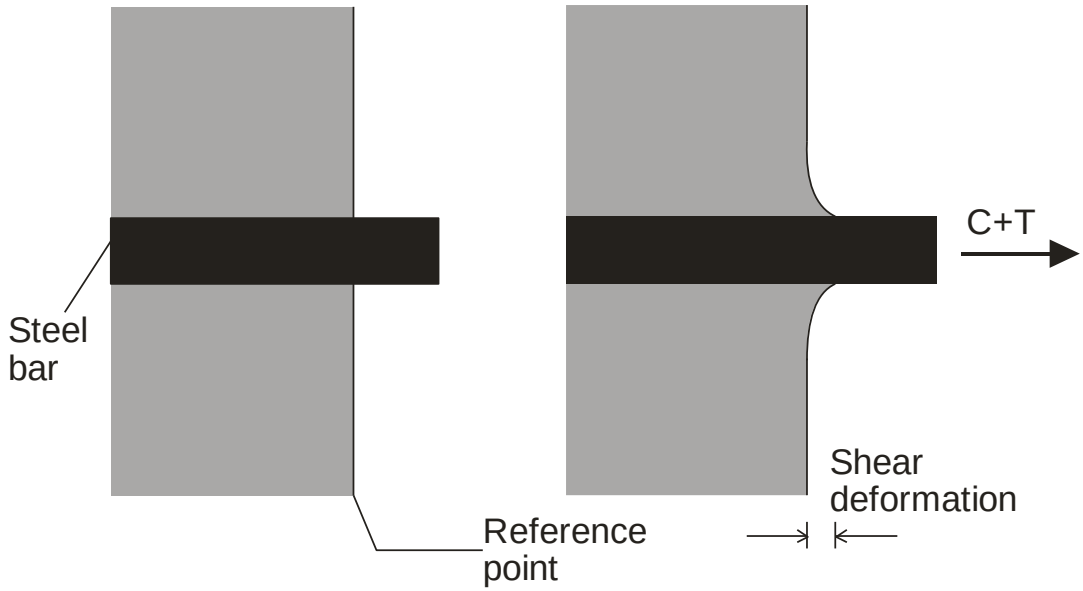

Figure 3-3: *Concrete shear deformation during stage 1*

3.1.4 Splitting Failure

When the bond stress reaches $1.0 – 3f_t$ (Federation internationale du beton, 2000), or between $0.5 – 1.5\sqrt{f_c}'$ using the aforementioned relationship, the third stage begins with the formation of longitudinal splitting cracks spreading radially in front of the lugs as shown in Figure 3-4(a) and Figure 3-5. Note that N is equivalent to the bar forces $C + T$ introduced previously. Spreading of these cracks is driven by wedging action (Choi & Lee, 2002) which is enhanced by the presence of crushed concrete stuck in front of the lugs as shown in Figure 3-6.

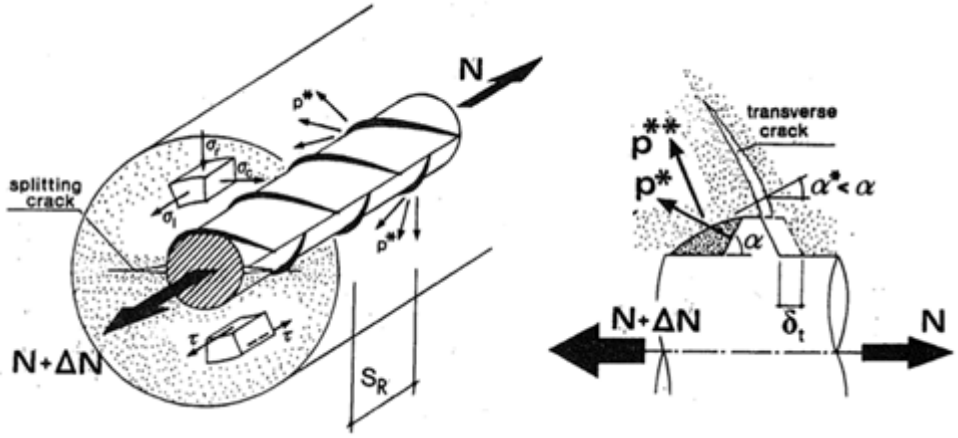

(a) Formation of longitudinal splitting cracks (b) Formation of transverse cracks

Figure 3-4: *Forces and cracking patterns associated with bond mechanisms (Federation internationale du beton, 2000)*

Illustrated in Figure 3-4(b), the outward component of the wedging pressure, p^{**}, is resisted by hoop stresses set up in the surrounding concrete which remains uncracked (Esfahani & Rangan, 1998). This component of stress is aligned at the steeper angle of 45˚ to the bar axis (ACI Committee 408, 1992; Ogura, Bolander & Ichinose, 2008) most likely due to complete

loss of the cohesion component which previously acted parallel to the bar longitudinal axis. These radial stresses in turn exert additional confinement forces on the bar such that bond strength and stiffness are provided by the interaction between interlocking reinforcement, concrete struts radiating from the bar, and the undamaged outer concrete hoop (Federation internationale du beton, 2000; Tastani & Pantazopoulou, 2010).

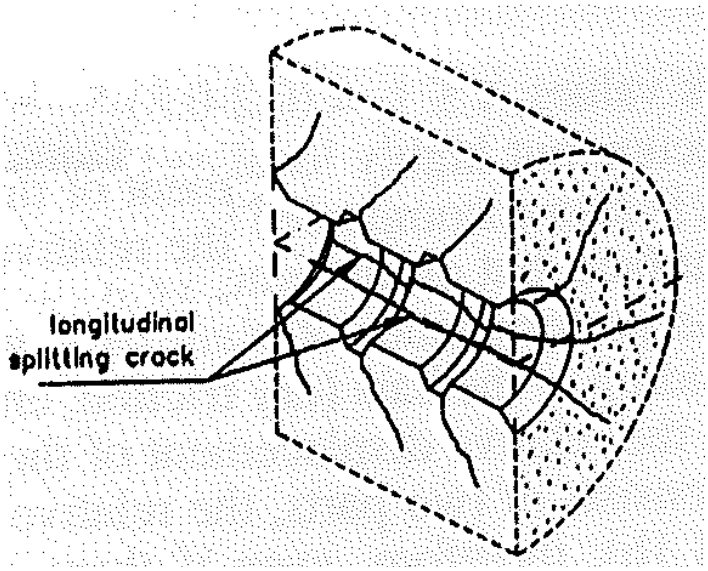

Figure 3-5: *Longitudinal splitting and transverse cracks (Federation internationale du beton, 2000)*

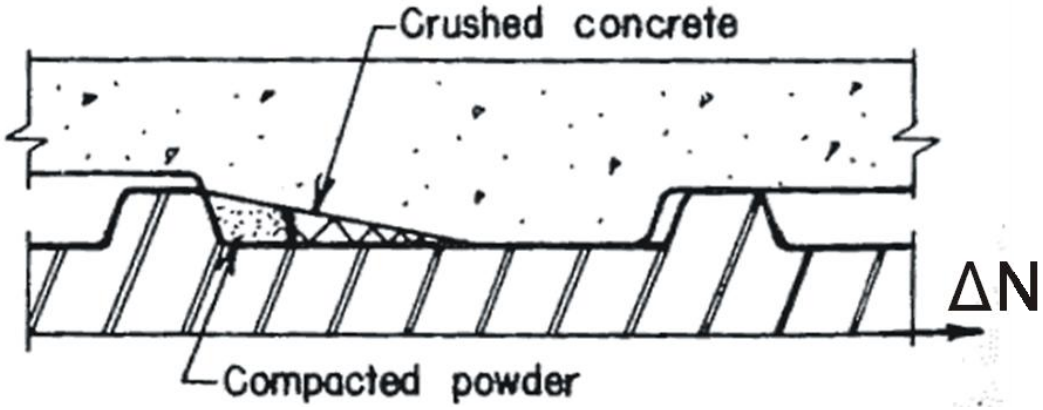

Figure 3-6: *Crushing of concrete in front of lugs. Adapted from ACI Committee 408 (1992)*

From this stage onwards, the mechanism of failure depends on the level of confinement provided to the bar under bond. In members with little or no transverse reinforcement, insufficient cover concrete, or tension perpendicular to the bond interface, the level of confinement is minimal and splitting failure will generally result (Plizzari, Deldossi & Massimo, 1998; Ichinose, Kanayama, Inoue & Bolander, 2004; Tastani & Pantazopoulou, 2010). This is a brittle failure mechanism and occurs when splitting cracks reach the outer surface of the member. The rate at which these cracks propagate to the surface is dependent on the exact level of confinement provided by transverse reinforcement (ACI Committee 408, 1992). This failure mechanism is generally rapid and associated with significant bar slip often

in excess of $0.05d_b$. Depending on the level of transverse reinforcement, bond stress values can reach $1/3 - 1/2\sqrt{f'_c}$ (Federation internationale du beton, 2000).

3.1.5 Bar Pullout Failure

In members such as beam-column joints which have a high level of transverse reinforcement, the failure mechanism is instead due to bar pullout (ACI Committee 408, 1992; Choi & Lee, 2002; Ogura et al, 2008). The heavy confinement present in such members ensures longitudinal splitting is contained within a cracked core around the bar and, as a result, the mechanism of bond transfer changes from bearing on the lugs to shear within the concrete (Federation internationale du beton, 2000) along a failure surface between bar lugs as shown in Figure 3-7. As the ultimate bond stress is approached locally, shear cracks along the failure surface begin to form until the concrete shear key is lost between the corresponding lugs. Subsequently, bond capacity is lost and significant slip occurs leading up to the ultimate ductile failure, as shown by the hysteresis in Figure 3-2(c) path D - E. Due to the loss of equilibrium previously achieved through bond, the local stress in the steel increases. It is consequently redistributed to stronger concrete further within the member and the process continues. This progressive failure due to strain penetration continues until no further resistance is available and bar slip results.

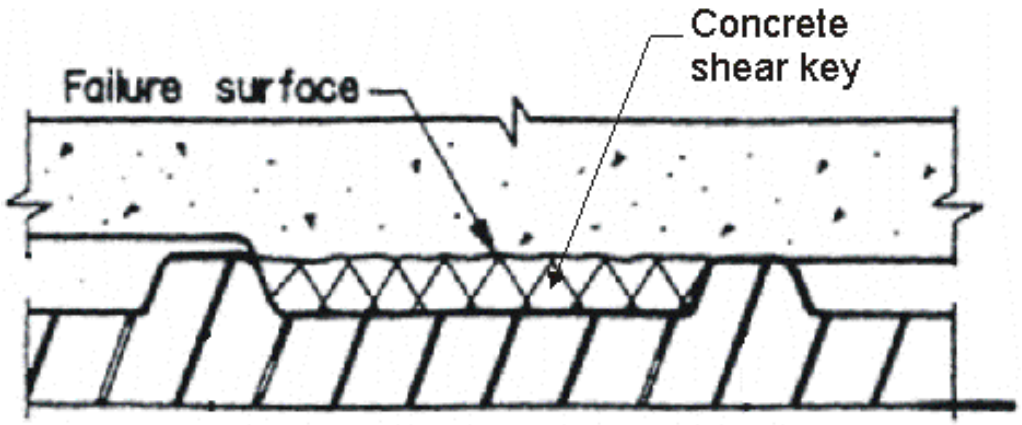

Figure 3-7: *Bar pullout failure mechanism. Adapted from ACI Committee 408 (1992)*

However, because of friction and interface shear between the bar lugs and surrounding concrete, some capacity will exist even after large bar slip has occurred (ACI Committee 408, 1992). This is evident by the long tail shown on the stress-slip hysteresis loops in Figure 3-2. Restrepo (1992) found that this frictional resistance is very low, on the order of 0.18 MPa. Eligehausen et al (1983), Malvar (1992), and Cheng, Restrepo, and Park (2000) observed that the bond capacity levels off at a slip value comparable to the clear distance between each lug. This is because, beyond this level of slip, all concrete shear keys have been lost and the remaining resistance is due to friction alone.

It should be noted that, if the bonded bar is subject to tension upon exiting the concrete – such as at the gap between the beam and column on a slotted beam – bar pullout failure can be accompanied by concrete cone formation. This was observed in experimental testing by Viwathanatepa et al (1979), Engstrom, Magnusson, and Huang (1998), and Au (2010), and is due to strain penetration associated with the higher bar stresses able to be achieved when bar pullout is the mechanism of failure. Strain penetration causes the bar to move relative to the surrounding concrete thus exerting a pressure from the lug tips (Eligehausen et al, 1983) which is enough to burst out the already weakened concrete in this area.

3.2 Cyclic Bond

Section 3.1 described the mechanisms of bond under monotonic loading; however, for seismic applications which involve a small number of large excursions into the inelastic range, cyclic bond with stress reversal is the mechanism of concern. With less than 100 load cycles and a bond stress range typically greater than 4.1 MPa, the bond mechanism during seismic loading can further be classified into the 'low cycle, high stress' category. Fortunately, the previously discussed bond mechanisms for monotonic loading are similar to those observed during low cycle loading (ACI Committee 408, 1992).

During the first loading cycle, the cyclic bond behaviour follows the monotonic backbone curve described in Section 3.1. However, during subsequent cycles, the behaviour is highly sensitive to the level of slip at which load reversal occurs (ACI Committee 408, 1992). There are three possible behaviour models which depend primarily on whether or not transverse cracks have formed; these three models are discussed below. Note that these models apply to well confined concrete, such as that which exists within beam-column joints.

3.2.1 Load Reversal before Formation of Transverse Cracks

In the first model, a load reversal is imposed after following the monotonic loading curve up to a slip level below which transverse cracks form. The corresponding unloading curve – curve AF in Figure 3-8(a) – is initially stiff because only a small portion of the slip is associated with inelastic concrete deformation. Once slip begins in the opposite direction – path FH – friction is the mechanism of resistance and the corresponding section of the hysteresis curve is relatively flat. After any microcracks have closed and bearing again becomes the mechanism of resistance, the corresponding loading curve HI differs little from the initial monotonic one.

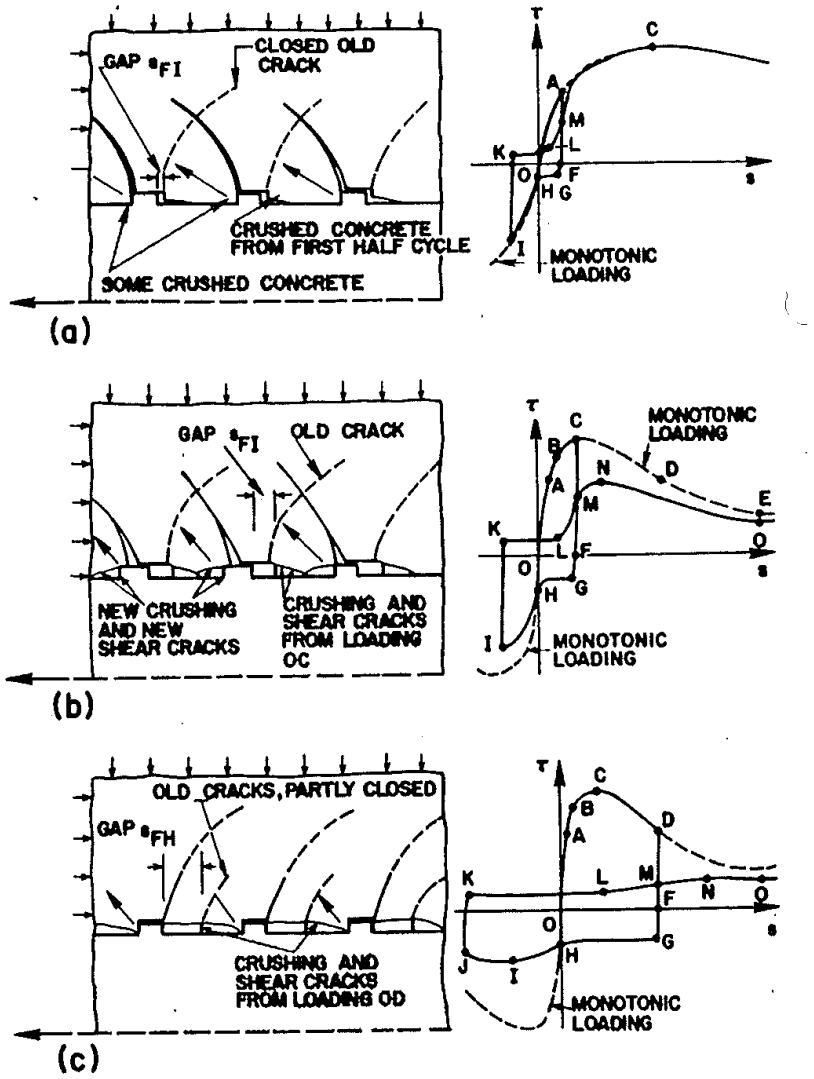

Figure 3-8: *Bond stress-slip relationships for cyclic loading (ACI Committee 408, 1992)*

Unloading from point I at the same slip value as that reached during the first half cycle, the path IKL is very similar to the initial unloading path AFH. However, due to previous cracking and crushing of concrete in front of the lugs as shown in Figure 3-6 and Figure 3-8(a), there is an amount of 'slack' that must be picked up before the concrete lugs reach their full bearing capacity which is mobilised at point M. Continued loading then follows the stress-slip curve until the monotonic curve is reached (ACI Committee 408, 1992). As illustrated in Figure 3-9, this process can be repeated for up to 10 cycles without any significant strength degradation or additional slip. In other words, the monotonic stress-slip curve can be achieved consistently when load reversals are imposed at small slip values corresponding to between 70 – 80% of the maximum monotonic bond stress (Eligehausen, Popov & Bertero, 1982).

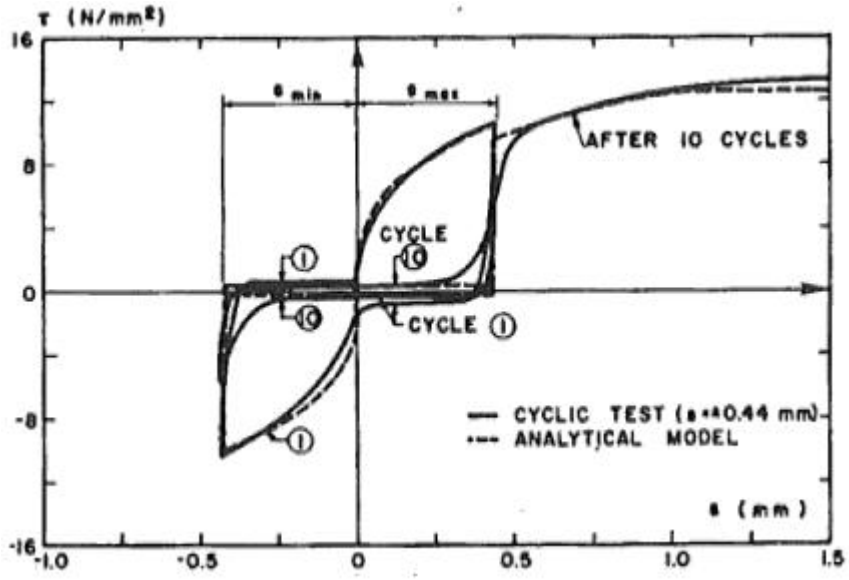

Figure 3-9: *Cyclic response for load reversals imposed at 70 – 80 % of maximum monotonic bond stress (Eligehausen et al, 1982)*

3.2.2 Load Reversal before Ultimate Bond Strength Reached

If a load reversal is imposed after formation of transverse cracks, a different model applies. Figure 3-8(b) shows a similar unloading path to that of the first model up to point F. Because there is more damage and crushing of the concrete in this case, more friction is mobilised and point G thus occurs at a higher stress level. After an increased amount of slip – curve GH – the lugs again bear on the concrete and the stiffness of the response increases. However, because the concrete shear key has been damaged by transverse cracking during the first half cycle, its resistance is lowered. Consequently, the peak strength reached at point I is significantly less than that exhibited during the first half cycle to point C.

Reversing the load again results in a further loss and delay of peak strength (point N) due to increased slack and further damage to the remaining concrete shear keys (ACI Committee 408, 1992). The effect of this process over 10 cycles is shown in Figure 3-10 in which both the decrease in peak strength and increase in slip at its onset are clearly visible.

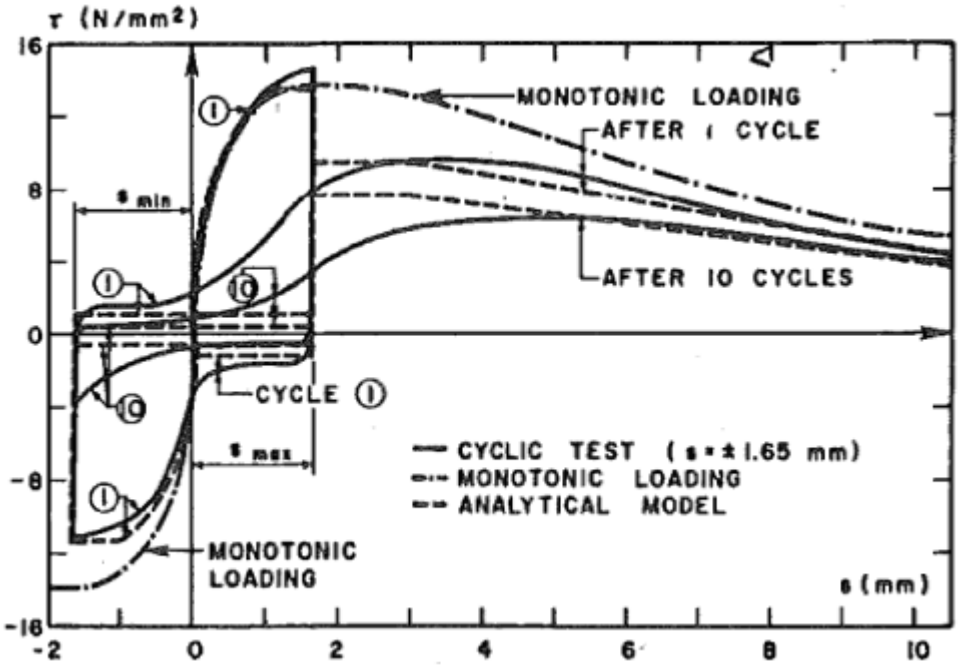

Figure 3-10: *Cyclic response for load reversals imposed above 80 % of maximum monotonic bond stress (Eligehausen et al, 1982)*

3.2.3 Load Reversal after Ultimate Bond Strength Reached

In the final model, a load reversal is imposed after the slip has passed the value at maximum strength. The significant damage to the concrete means that point G – which corresponds to the frictional resistance – occurs at a higher level of stress than in both previous cases. Due to the large slip imposed during the first half cycle, the recovery of lug bearing is much slower as shown by the elongated curve GH. Even once bearing is recovered, the capacity is significantly diminished because the concrete shear keys have been completely lost, and the curve HI to peak strength is severely degraded. If the system is loaded again in the original direction along path JKLMNO, the capacity is minimal and due to friction only (ACI Committee 408, 1992). Figure 3-11 illustrates the significant increase in the rate of bond strength loss; the stress-slip profile after a single cycle now comparable to that after 10 cycles in the previous scenario.

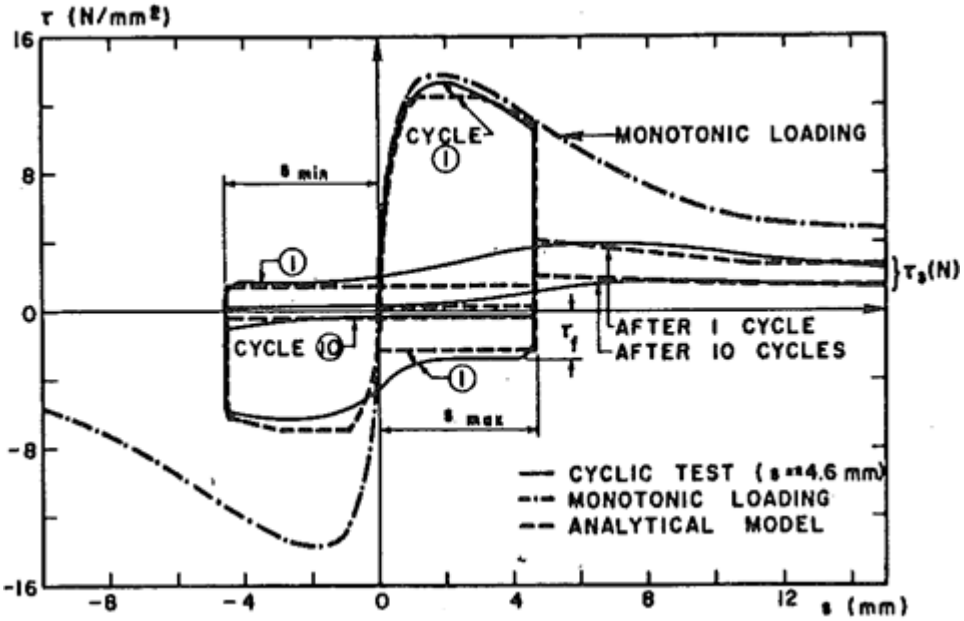

Figure 3-11: *Cyclic response for load reversals imposed above maximum monotonic bond stress (Eligehausen et al, 1982)*

3.3 Factors Affecting Bond Performance

As outlined in Section 3.1, bond is a function of many different variables including concrete and steel strength, bar geometry, level of confinement, and loading conditions. It is important to understand the influence of each of these variables on bond performance such that, where possible, they can be exploited in order to improve it. The following section discusses these variables in detail. Note that, unless otherwise stated, this section refers to the effect of each variable on local bond stress as defined in Section 3.1.1.

3.3.1 Concrete and Steel Material Properties

As a relatively easy variable to change, concrete compressive strength is inevitably one of the key parameters of interest. While some aspects of bond performance are linked to the shear and tensile capacity of concrete, these are inherently dependent on concrete compressive strength (ACI Committee 408, 1992; MacGregor & Wight, 2005; Mehta, Kumar & Paulo, 2005; Arioglu, Arioglu & Girgin, 2006). Based on over 100 experimental tests, Eligehausen et al (1983) found that bond resistance is approximately proportional to $\sqrt{f'_c}$. Similarly, Esfahani and Rangan (1998) showed that, for constant cover to bar diameter ratios, bond strength increases with the tensile strength of concrete. The ACI Committee 408 (1992) identifies one of the key drivers behind enhanced bond performance when stronger concrete is used as the increased bearing and shear resistance provided. The mechanism of failure is also dependent on concrete strength with pullout and splitting failure affected by compressive and

tensile strengths, respectively (Federation internationale du beton, 2000; Canbay & Frosch, 2005).

Steel grade is also easily changed and, as such, is another variable of interest in terms of bond performance. Since bond stress is directly related to the force in the bar, using a lower strength steel will clearly reduce the bond stress demand (ACI Committee 408, 1992). The strain level within reinforcement also becomes important when the bar is loaded in tension. While high steel strains within the elastic range can be activated in real structures where significant anchorage exists, the effect of such strains can be neglected when lug bearing is the primary method of force transfer because transverse deformation due to Poisson's effect is much less than lug height. Nonetheless, bond performance is found to deteriorate when steel strains reach the inelastic range as shown in Figure 3-12. This is because, in later stages of the bond process, friction plays a major role in force transfer. If the bar has moved into the inelastic range, and thus decreased in cross sectional area due to Poisson's effect, the outward components of p^* and p^{**} – as defined in Figure 3-4 – will decrease resulting in a reduced contribution from macro friction. It is also possible that yielding affects the lug geometry which in turn affects bond performance as discussed in the following section. Conversely, compression loading will enhance bond performance (Federation internationale du beton, 2000).

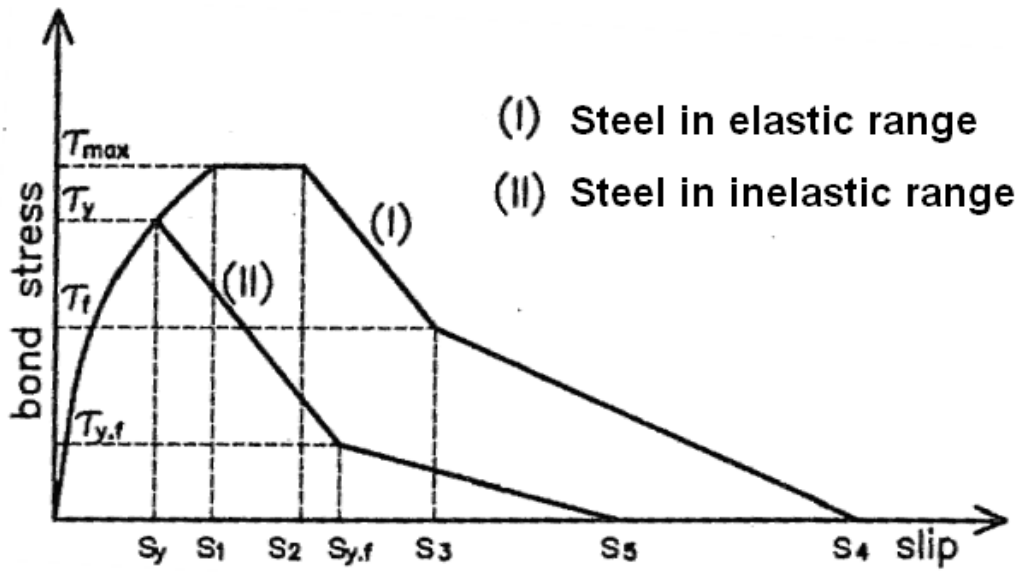

Figure 3-12: *Effect of steel inelasticity on monotonic bond stress-slip relationship (Federation internationale du beton, 2000)*

3.3.2 Bar Geometry

The geometry of the bars, both locally and with respect to the pour, is another key factor that can be controlled to some extent. Geometry of the bar itself includes bar diameter and lug face

angle, inclination, height, and spacing, as illustrated in Figure 3-13 and Figure 3-14, with each of these having various effects on bond performance. Together, several of these geometric features are used to calculate the relative indentation area, or RIA, which is a geometric index that can be used for quick and easy comparison between different bars. Given in Equation 3-2 (Esfahani & Rangan, 1996; Federation internationale du beton, 2000), RIA has an impact on bond performance as discussed in the following section. Note that some variables in Equation 3-2 have been altered from the form in which they appear in the texts.

$$RIA = \frac{A_L}{\pi d_b S_L} \qquad \text{Equation 3-2}$$

Where A_L is the projected area along the bar axis of both lugs at a given bar section and S_L is the spacing between lugs as shown in Figure 3-13. Note that d_b refers to the nominal bar diameter. Dancygier and Katz (2009) found that bond strength for pullout failure increases with RIA as shown in Figure 3-15. This is because increasing RIA enhances wedging action between the bar and concrete. Coupled with the relatively high level of confinement required to produce pullout failure, the surrounding concrete is able to sustain the increased radial stresses and, as a result, the bond strength is increased.

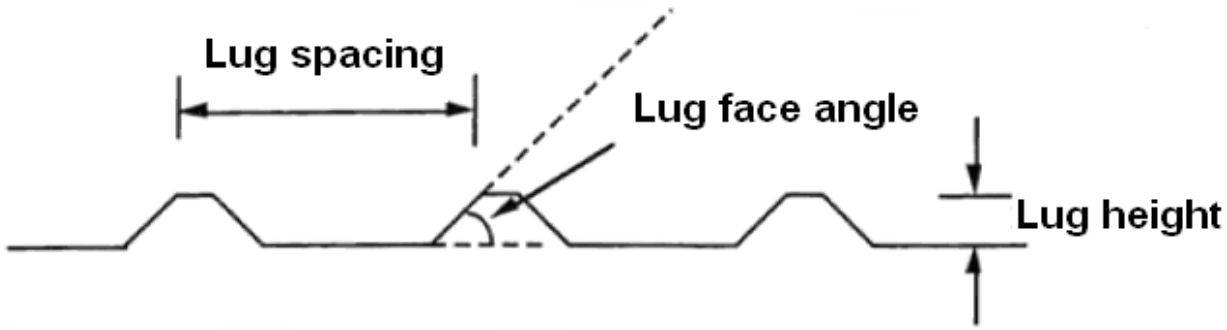

Figure 3-13: *Deformed bar surface features (Esfahani & Rangan, 1996)*

However, the same increases are not observed when failure is due to splitting cracking because of the typically lower levels of confinement present. Subsequently, the increase in wedging action drives expansion of splitting cracks instead of increasing radial bearing forces. This was confirmed in tests by Zuo and Darwin (2000) where increasing RIA failed to improve bond performance when transverse reinforcement, and thus sufficient confinement, were not present. Provision of confinement from other means was not a possibility in these tests as they were conducted on beams with only a small amount of cover. Analytical modelling by Choi and Lee (2002) and experimental testing by Hamad (1995) further verifies these results.

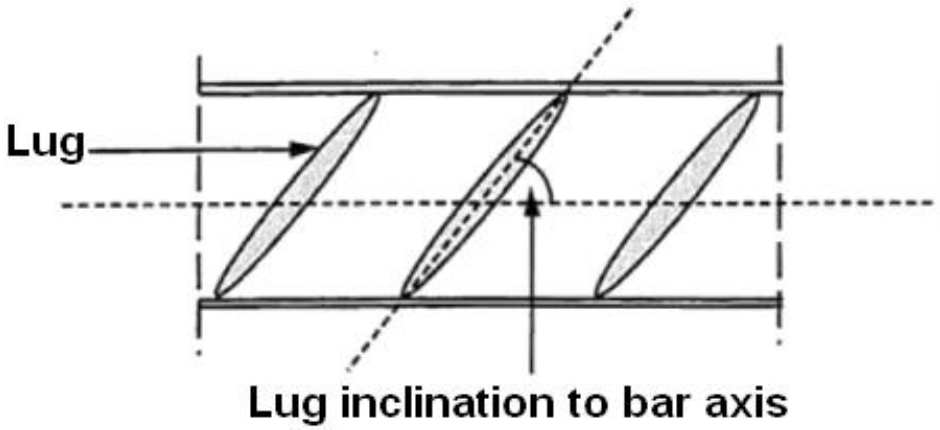

Figure 3-14: *Definition of lug inclination (Esfahani & Rangan, 1996)*

In terms of achieving practical RIA values with sufficient cover, Esfahani and Rangan (1996) recommend a larger lug area at a reduced spacing for increased bond strength and stiffness. Use of a smaller lug height and spacing will result in lower bond strength at failure; this is most likely due to the increased availability of lugs with which to remove concrete from the shear failure surface resulting in a more rapid loss of bond capacity. It is generally accepted that RIA values between 0.05 and 0.1 represent a good compromise in terms of ultimate bond strength, industrial requirements, and good service load performance including limited crack opening and cover splitting (Federation internationale du beton, 2000).

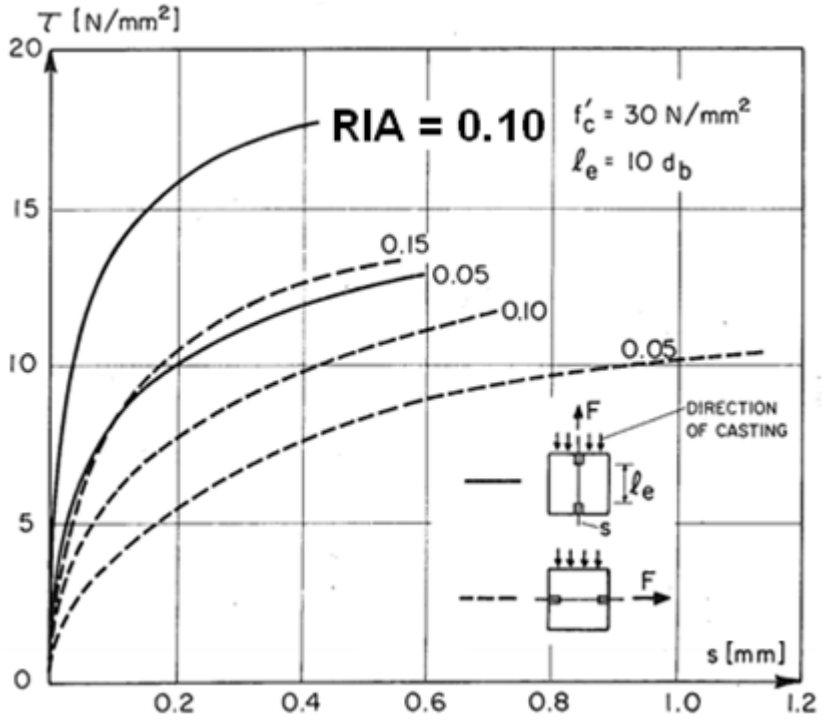

Figure 3-15: *Influence of relative indentation area and direction of casting on monotonic bond stress-slip relationship (Eligehausen et al, 1983)*

The bar geometric features can also have individual effects on bond performance. Bar diameter leads to a phenomenon known as ‘size effect’ which refers to the tendency for bars

of different diameter to exhibit different bond performance. Eligehausen et al (1983) found that bond strength decreases by between 5 and 10% with a decrease in bar diameter from 32 to 25 mm, or from 25 to 19 mm; Viwathanatepa et al (1979) agree with these findings and state similar reductions. However, Ichinose et al (2004) further studied size effect experimentally and found that it can be reduced by ensuring sufficient confinement of the bonding bar. The reason confinement is an effective solution is because size effect is attributed mainly to splitting cracks rather than local crushing of concrete in front of the lugs. Because adequate confinement is present within beam-column joints, size effect need not be considered in determining the appropriate column depth for prevention of bar slip failure.

Lug geometry is another important factor to be considered. Canbay and Frosch (2005) found that, if lugs are spaced far enough apart, pullout failure due to shearing of the concrete between lugs does not occur. Failure is instead due to propagation of splitting cracks once the concretes tensile strength has been exceeded due to radial stresses induced by wedging action. Tastani and Pantazopoulou (2010) recognised the importance of lug height where doubling this dimension consistently led to higher bond strengths in an experimental study on 50 test specimens. Both of these findings agree with the recommendations of Esfahani and Rangan (1996) discussed earlier.

Several researchers have noted the varying influence of lug face angle, α (as defined in Figure 3-4), on bond performance. Given other variables are held constant, increases to lug face angle above 30˚ result in negligible improvement to bond performance (Esfahani & Rangan, 1996; Federation internationale du beton, 2000). Choi and Lee (2002) reach a similar conclusion but suggest the critical angle is closer to 48˚. The reason bond performance does not increase further beyond this lug angle is because steeper lugs tend to become clogged with crushed concrete thus reducing the effective lug angle, α^*, available for bearing as shown in Figure 3-4 and Figure 3-6. The effective lug angle is always lower than the actual lug angle and is generally between 25 and 30˚ for realistic friction coefficients. As expected, bond strength increases with increasing effective lug angle (Choi & Lee, 2002). However, when the actual lug angle is below 30˚, bond performance is reduced (Esfahani & Rangan, 1996, 1998). Increasing lug inclination with respect to the bar axis also leads to a slight increase in bond strength (Esfahani & Rangan, 1996).

Hamad (1995) concludes that the ideal bar geometry consists of a lug face angle of 60˚, lug spacing of $0.5d_b$, and lug height of $0.1d_b$. During experimental tests on over 50 specimens, such an arrangement produced the stiffest stress-slip response, highest ultimate bond strength,

and least free end slip at failure for a pullout test. This customised bar achieved a 45% improvement in ultimate load compared with the nearest standard bar available. Unfortunately, fabrication of customised reinforcing steel is not a feasible means of improving bond performance.

While not applicable to real structures, the effect that strain gauges have on the geometry of bars should be taken into consideration for laboratory situations. In an attempt to reduce interference with the bond mechanism, Viwathanatepa et al (1979) machined grooves into the bars in which to attach strain gauges. These researchers found that the bond stress can vary by up to 10% between grooved and normal bars. This variation is due to the greater perimeter offered by a grooved bar which increases the shear resistance that can be built up against the surrounding concrete. Scott (1996) removed the issue entirely by using internal strain gauges; these were installed by cutting the bar in half along its axis, milling a small groove, attaching the strain gauges, and gluing the half-bars back together. However, because this research is not focussed on the bond mechanism itself, normal bars will be used and the small influence on performance accounted for by adjusting the column depth.

3.3.3 Reinforcement Layout

Research has also found that the position of bars within a pour significantly affects bond performance. Bars at the top of a pour will perform worse due to the lower strength concrete at this level and the presence of air voids trapped below the bars during mix consolidation (ACI Committee 408, 1992); this is known as the ‘top bar effect’. Evidence of this is illustrated in Figure 3-16 where a gap is clearly visible beneath the bar cast at the top of the specimen. The magnitude of this effect varies but experimental testing by Thrane, Pade, Idzerda, and Kaasgaard (2010) shows that it can be limited by casting under controlled conditions. Cheng et al (2000), in multiple tests on beam-column sub-assemblies, consistently observed greater bar slip in the top beam reinforcement compared to the bottom. Similar results were also found by Restrepo (1992).

The reduction in concrete strength is due to mix segregation driving water to the top of the pour such that the water to cement ratio – which is directly proportional to the compressive strength (Yasar, Erdogan & Kilic, 2004; Mehta et al, 2005) – is reduced. Conversely, it is found that bond performance for horizontal bars is best when they are placed close to the bottom of a pour and, for vertical bars, when they are loaded against the casting direction (Federation internationale du beton, 2000). The influence of casting direction on bond strength was also recognised by Eligehausen et al (1983) and is illustrated in Figure 3-15

where increases on the order of 30% are evident. While this effect cannot be realised for beam bars within in-situ joints, the benefits can possibly be extended to precast members. However, because the specimens in this research were cast horizontally, this effect can be neglected.

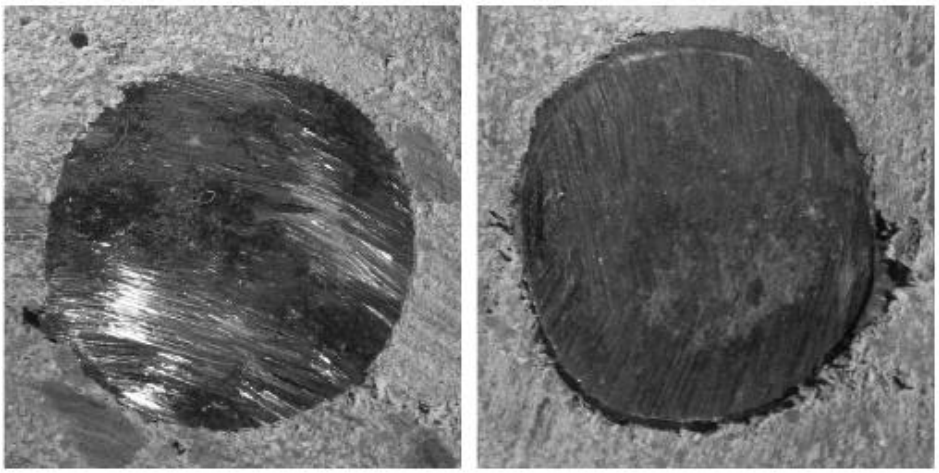

(a) Bottom bar (b) Top bar

Figure 3-16: *Evidence of effect casting position has on bond performance* (Soylev, 2011)

Clear spacing between bars within a layer and amount of cover are also both important factors. As illustrated in Figure 3-17, Eligehausen et al (1983) found that a 20% increase in bond strength can be gained by increasing the bar spacing from 1 to $4d_b$; further increases in spacing were ineffective at increasing strength. The strength increase is likely due to less overlapping of tension hoop regions when large bar spacings are used; this overlapping would otherwise result in more rapid crack propagation leading to premature splitting failure. As outlined previously, providing thicker cover increases the confinement and, therefore, resistance to splitting failure. However, as cover increases, the efficiency with which it increases bond performance is reduced (Canbay & Frosch, 2005). Tastani and Pantazopoulou (2010) found that an 85% increase in cover thickness resulted in only a 20% increase to bond strength, and that this is associated with an increase in bar slip due to the higher damage and cracking able to be sustained before failure. The ACI Committee 408 (1992) also recognises that the cover to bar spacing ratio is a critical factor in determining the crack pattern at failure. Additionally, Harajli et al (2002) note that it is the cover to bar diameter ratio, not the thickness of cover alone that increases bond strength. Fortunately, cover requirements are not an issue for horizontal beam reinforcement within beam-column joints. Nonetheless, it is suggested that clear spacing between bars within each layer of reinforcement is at least $2d_b$ to ensure minimal loss of bond stress in accordance with Figure 3-17.

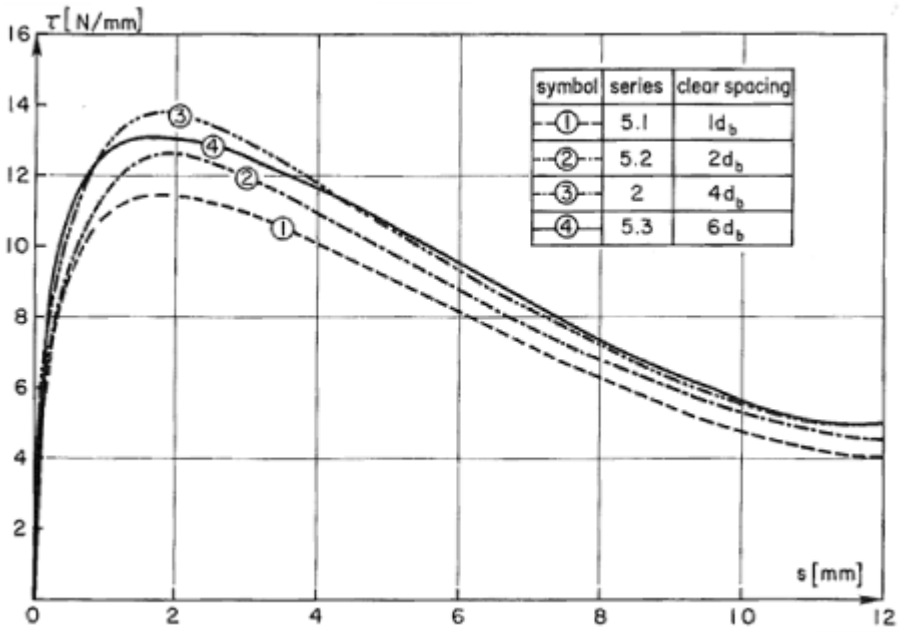

Figure 3-17: *Influence of clear bar spacing on bond stress-slip relationship (Eligehausen et al, 1983)*

3.3.4 Confinement

Throughout this section confinement has been referred to as a factor that can enhance the success of other bond performance improvement measures. As referenced in Section 3.1, many researchers have outlined its role in prevention of the brittle failure associated with splitting cracking and the promotion of ductile pullout failure. In addition to cover concrete, one of the easiest ways to provide confinement is through addition of transverse reinforcement. However, this is only effective when the transverse reinforcement is aligned perpendicular to the bar axis such that the potential splitting failure plane is confined (Eligehausen et al, 1983; Canbay & Frosch, 2005) and after cracks have opened sufficiently for the reinforcement to be activated; for this reason, it is classified as 'passive' confinement (Federation internationale du beton, 2000). Engstrom et al (1998) found that confinement provided by hoop stirrups to corner bars is more effective than that provided by straight stirrups simply hooked around a middle bar. This is likely due to the leg of the hoop stirrup having bearing resistance in addition to bond resistance such that less crack opening is required to activate the clamping response of the stirrup.

Nonetheless, the relationship between increasing levels of transverse reinforcement and bond strength through increased confinement is well recognised (Eligehausen et al, 1983; ACI Committee 408, 1992; Federation internationale du beton, 2000). The upper bound to this increase is pullout failure, after which further increases in transverse reinforcement provide no additional benefit (Eligehausen et al, 1983; ACI Committee 408, 1992; Gambarova & Rosati, 1997). This is clearly illustrated in Figure 3-18 where Ω is an index of confinement and is

discussed in more detail in Section 4.2.3. Another possible issue with excessive amounts of transverse reinforcement is that compressive stresses transferred from the bar into the surrounding concrete can become so large that bond strength is governed by concrete compressive failure (Ogura et al, 2008). Constructability must also be considered when detailing heavy transverse reinforcement.

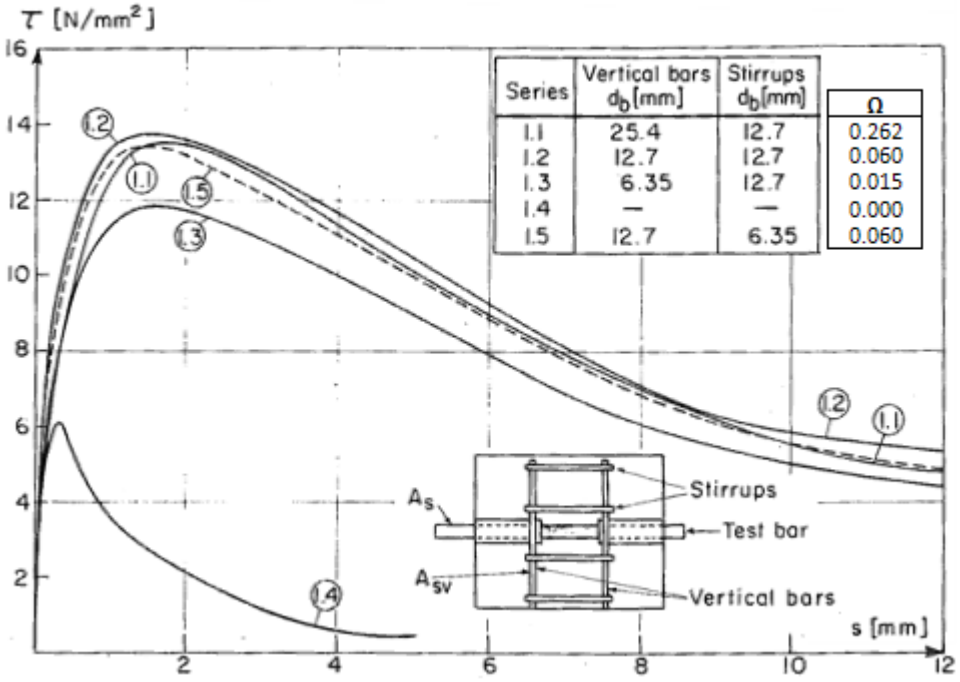

Figure 3-18: *Influence of transverse reinforcement on bond stress-slip relationship. Adapted from Eligehausen et al (1983)*

Another possible means of providing confinement is through axial load. This is possible in members such as beam-column joints and is accounted for by current NZS3101:2006 provisions as discussed in Section 4.1.2. As with confinement provided by transverse reinforcement, this pressure must be aligned perpendicular to the bond interface. However, unlike transverse reinforcement, cracking is not required to activate the beneficial effects of confinement and, as such, it is referred to as 'active' confinement (ACI Committee 408, 1992). For this reason, active confinement is more efficient than passive confinement as no activation in the form of crack opening is required to improve bond performance (Federation internationale du beton, 2000).

Eligehausen et al (1983), Malvar (1992), and Gambarova (1997), all found a strong correlation between increasing transverse pressure and bond performance as shown in Figure 3-19 and Figure 3-20. Eligehausen et al (1983) also found that, just as for confinement due to transverse reinforcement, there is an upper bound to the effectiveness of increasing transverse pressure. This is clearly illustrated in Figure 3-19 where maximum bond stress reaches an

asymptote of around 17 MPa given a transverse pressure of 10 MPa or more. The findings of Gambarova and Rosati (1997) support this observation; as shown in Figure 3-20, increases in transverse confining pressure above $0.25\sigma_c/f_c'$ are significantly less effective at increasing bond stress.

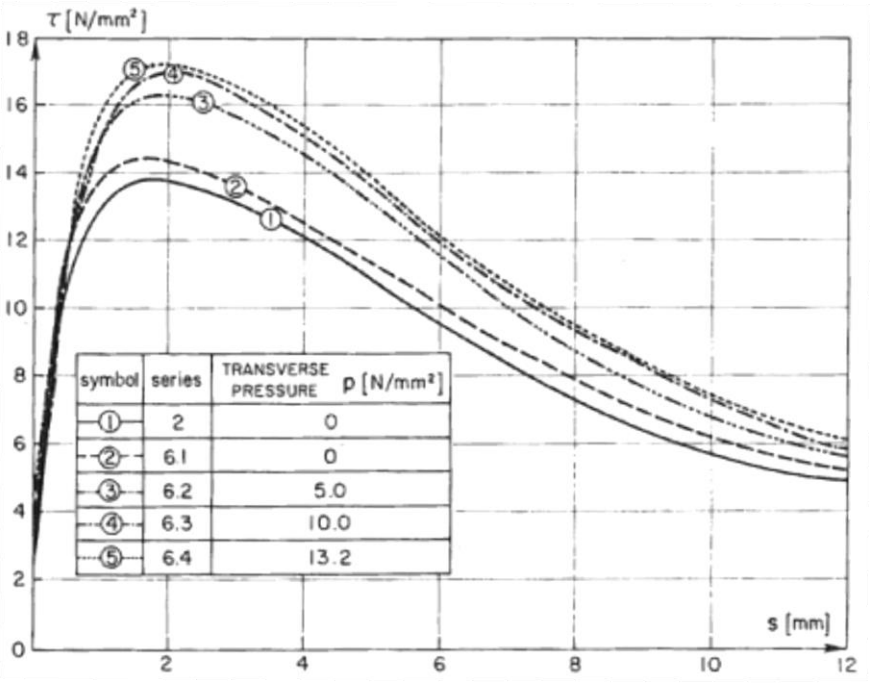

Figure 3-19: *Influence of transverse pressure on bond stress-slip relationship (Eligehausen et al, 1983)*

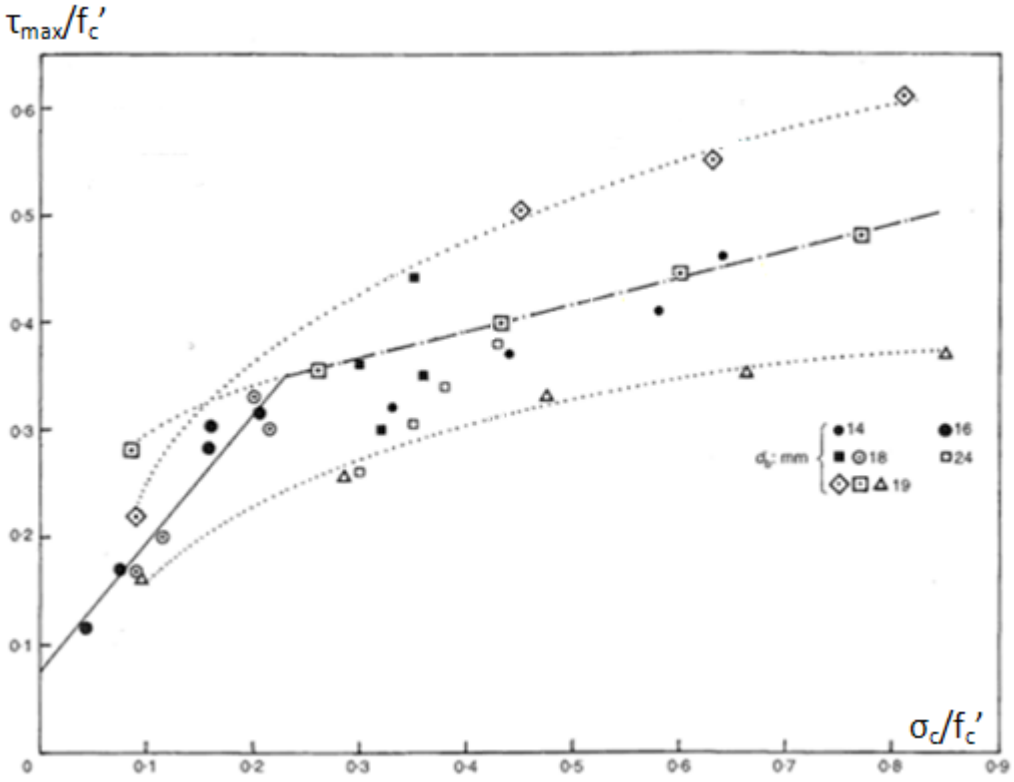

Figure 3-20: *Influence of transverse pressure on maximum bond stress. Adapted from Gambarova and Rosati (1997)*

When the bearing component of bond is compromised such as during cyclic loading with large imposed slips, friction becomes the critical factor in bond performance. Tastani and Pantazopoulou (2010) found that the coefficient of friction which governs the force transferred through this mechanism is dependent on normal pressure, surface roughness, lug profile, and slip magnitude. While the primary mechanism of frictional resistance is contact at the bar-concrete interface, it also occurs between crushed concrete in front of the lugs and surrounding intact concrete (Choi & Lee, 2002). Given typical conditions within a beam-column joint, the aforementioned authors suggest a coefficient of friction on the order of 0.9. Eligehausen et al (1983) found that frictional bond resistance is improved with confinement but unaffected by bar diameter, lug spacing, or relative indentation area.

3.3.5 Load Characteristics

Loading type and rate are also important factors to consider in bond performance and both are critical for seismic applications. As outlined in Section 3.2, seismic actions introduce stress reversals in the low cycle, high stress loading category with bond mechanisms similar to those observed during monotonic loading (ACI Committee 408, 1992). However, stress reversals are more demanding in terms of bond performance than both monotonic and pulsating cyclic loads (Federation internationale du beton, 2000). Eligehausen et al (1983) found that the overall shape of the bond stress-slip relationship does not change significantly with the loading rate. As shown in Figure 3-21, decrease of the loading rate by 5 orders of magnitude results in a decrease to bond strength of less than 25%. Given the relatively smaller range of loading rates experienced by structures during seismic excitation, the effect of loading rate on bond performance can safely be ignored.

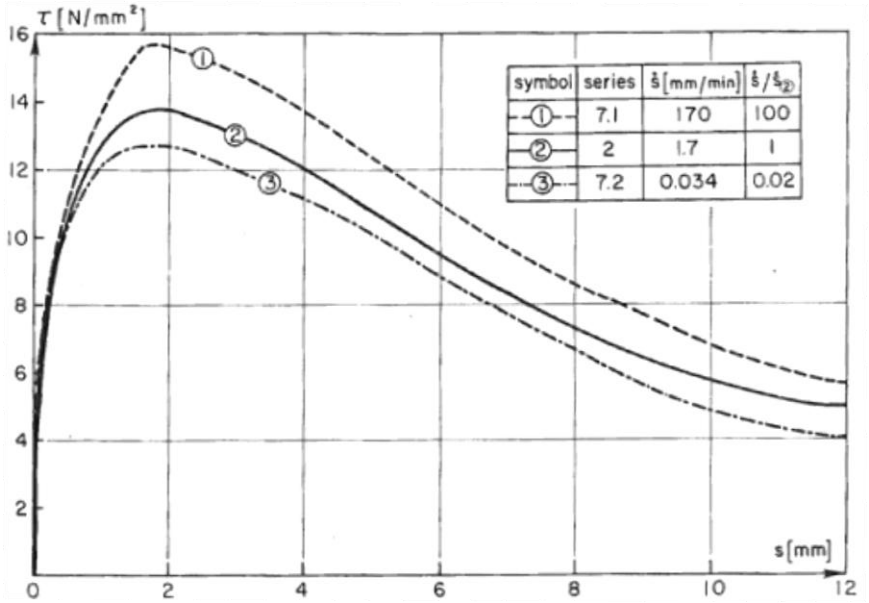

Figure 3-21: *Influence of loading rate on bond stress-slip hysteresis (Eligehausen et al, 1983)*

3.3.6 Embedment Length

Embedment length and loading conditions are also important factors in bond performance. Testing is common on shorter embedment lengths up to $5d_b$ (Federation internationale du beton, 2000) where the bond stress distribution can be approximated as uniform (Esfahani & Rangan, 1996) and Equation 3-1 applied with reasonable accuracy. Indeed, such tests are necessary to create and validate local bond stress-slip laws. Unfortunately, the resulting ultimate local bond stresses, τ, can be up to 4 – 5 times higher (10 – 20MPa) than the values observed in tests with longer, more realistic embedment lengths (ACI Committee 408, 1992) meaning they have limited applicability in real design situations. This is because, when shorter embedment lengths are used, the ultimate bond stress is mobilised along the entire bar and the resulting mean stress is higher as illustrated qualitatively in Figure 3-1(a). Alternatively, as shown in Figure 3-1(b), a bias in bond strength is observed towards the compression side of the specimen where significant active confinement is present. It is therefore commonplace in design to express the average bond stress as a portion of the observed maximum local bond stress (Paulay & Priestley, 1992) as determined under the controlled conditions obtained when using small embedment lengths.

Not surprisingly, the ACI Committee 408 (1992) recommends that bond testing be carried out on specimens with embedment lengths of at least $15d_b$. This is to ensure that the lower bound of embedment lengths within actual structures is replicated. However, in such realistic conditions, the bond stress distribution is non-uniform (Esfahani & Rangan, 1998; Tastani & Pantazopoulou, 2010) and Equation 3-1 therefore does not apply. Due to this non-uniformity, bond stress must be measured indirectly through the change in stress along the bonded bar.

In experimental pullout tests, Tastani and Pantazopoulou (2010) found that an increase in embedment length from 5 to $12d_b$ did not increase the average bond strength, u_a. This is because, in Equation 3-1, increases in ΔL are offset by development of higher elastic strains within the bar. However, with embedment lengths greater than $12d_b$, the average bond strength was found to decrease; beyond this limit, only a portion of the bar closest to the loaded end is initially activated. As loading increases, bond degradation reduces the effectiveness of this portion of the bar and the bond force is redistributed to portions of the bar still surrounded by intact concrete.

For specimens subject to monotonic compression and tension at either side, or ‘push-pull’ specimens, Ciampi, Eligehausen, Bertero, and Popov (1982) observed a negligible increase in maximum average bond stress for an increase in embedment length from 15 to $25d_b$. As

shown in Figure 3-22, embedment lengths above $25d_b$ followed the same stress-slip profile but were able to achieve higher maximum average bond stresses at the expense of increased slip. This increased bond strength is due to the relative portion of well confined, core concrete within the member increasing with embedment length. Similarly, the increased slip is due to the increased length of concrete over which stress redistribution, as discussed above, can occur before failure results. While the ACI Committee 408 (1992) agrees with these findings, it does state that, for cyclic loading, the number of cycles to failure increases with embedment length.

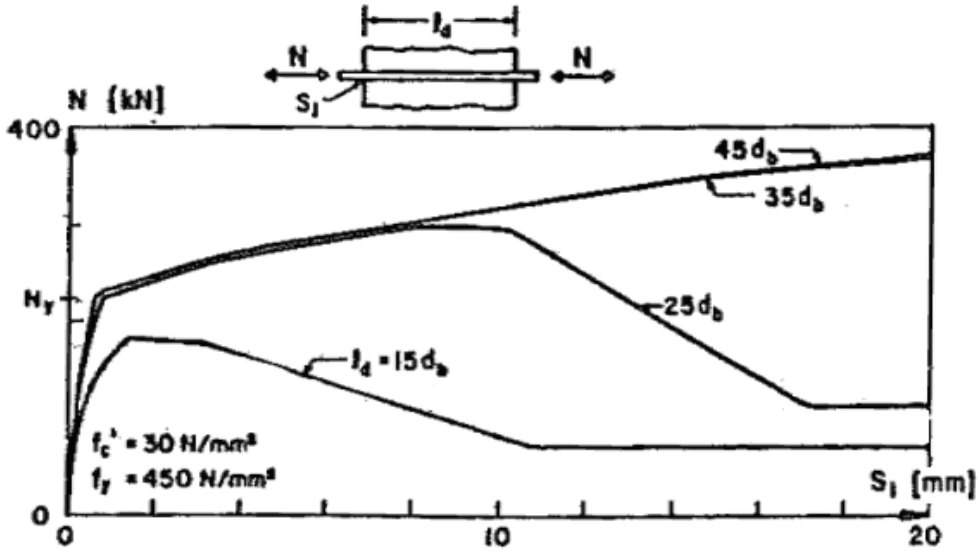

Figure 3-22: *Influence of embedment length on bond stress-slip hysteresis (Ciampi et al, 1982)*

3.4 Previous Dedicated Bond Tests

This section presents a detailed analysis of several extensive bond test programmes which are referenced throughout this thesis. The purpose of this is to provide some background to these tests and to relate experimental observations back to the theory discussed previously in this chapter. As the key focus of this research, this section only reports on bond tests which have been designed to simulate the conditions encountered within beam-column joints. The applicability of these tests to design values in beam-column joints is also discussed.

3.4.1 Viwathanatepa et al (1979)

Recognising a gap in existing knowledge, research by Viwathanatepa et al (1979) focussed on determining the bond behaviour within beam-column joints during seismic excitations. The test set up, illustrated in Figure 3-23, was designed to reproduce conditions within a beam-column joint as accurately as possible.

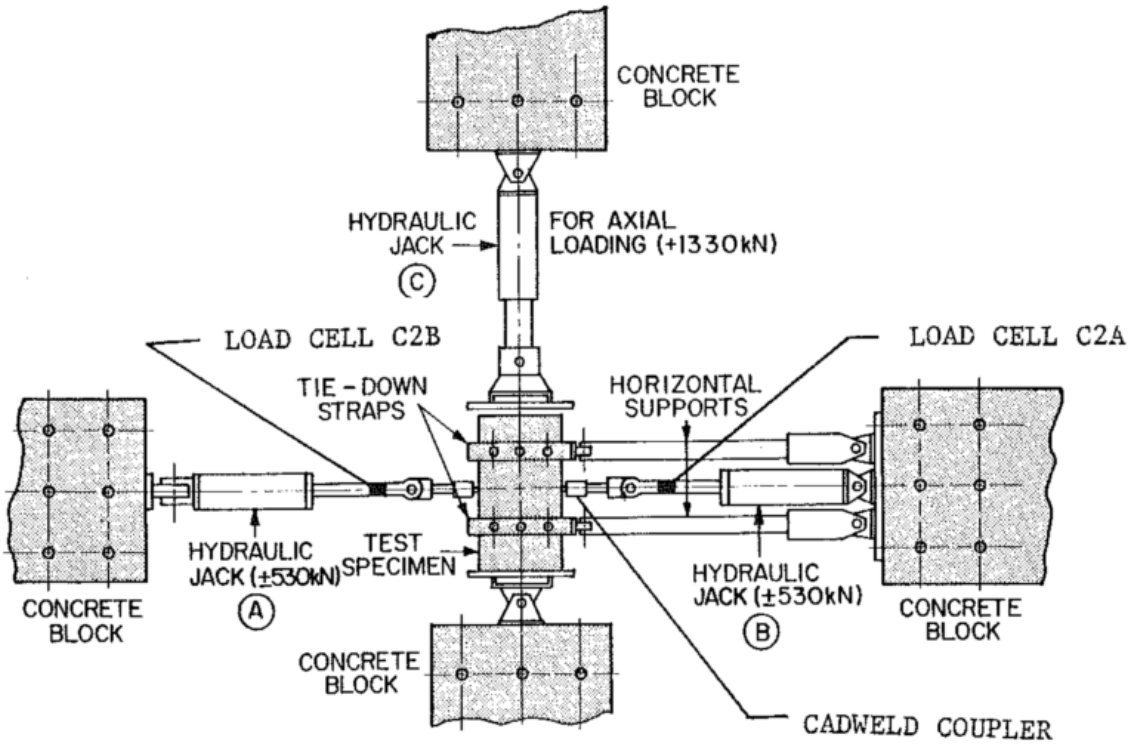

Figure 3-23: *Pullout test set up (Viwathanatepa et al, 1979)*

Horizontal straps were used to provide restraint in the plane of the bar such that tension and compression regions were set up perpendicular to the bond interface at alternate ends of the specimen; longitudinal reinforcement was required to carry the resultant flexural demands. Transverse reinforcement was provided for passive confinement using a similar layout to that within a typical joint. No supplementary vertical stirrups were used and intermediate column bars were only present in one of the three test set ups. Finally, axial load was applied to some specimens using a hydraulic jack in order to simulate active confinement. 17 well confined specimens with realistic beam-column embedment lengths between 15 and 27d_b were tested under simultaneous push-pull loading; available data on each of these is given in Appendix A. Around half of the tests used monotonic loading while the other half used cyclic loading. However, all failed through bar pullout as expected for well confined specimens. All specimens were cast in the weak direction; i.e. with the pour parallel to the bars.

Figure 3-24 and Figure 3-25 show typical cracking patterns for the monotonically loaded specimens. Note that the numbers correspond to steel stresses at crack formation as a proportion of the bars nominal yield strength of 420 MPa. Figure 3-24(a) shows the development of splitting cracks on the pull face beginning well within the elastic range of the bar. Combining values from all tests, the corresponding bond stress at the first splitting crack appearance was approximately $0.65\sqrt{f_c'}$ which is in agreement with the range proposed in Section 3.1.4. Note that these cracks assemble in a circular region around the bar and correspond to the cone pullout area discussed later in this section. Conversely, the cracking on

the push face is significantly reduced and likely linked to circumferential expansion due to Poisson's effect associated with high compression stress within the bar (Viwathanatepa et al, 1979). The difference in crack patterns on the two faces can be attributed to the active confinement due to axial compression present only on the push side of the specimen.

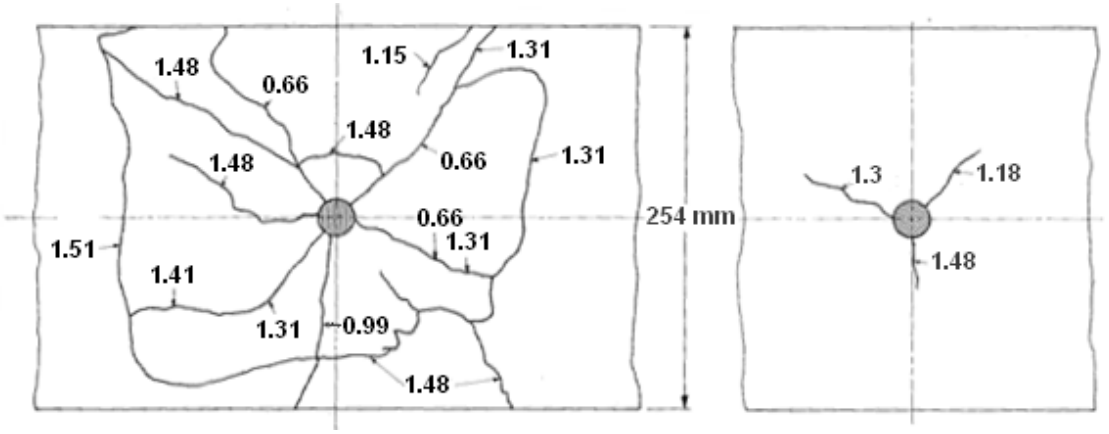

(a) Pull face (b) Push face

Figure 3-24: *Typical crack pattern on bar faces of monotonically loaded specimen. Adapted from Viwathanatepa et al (1979)*

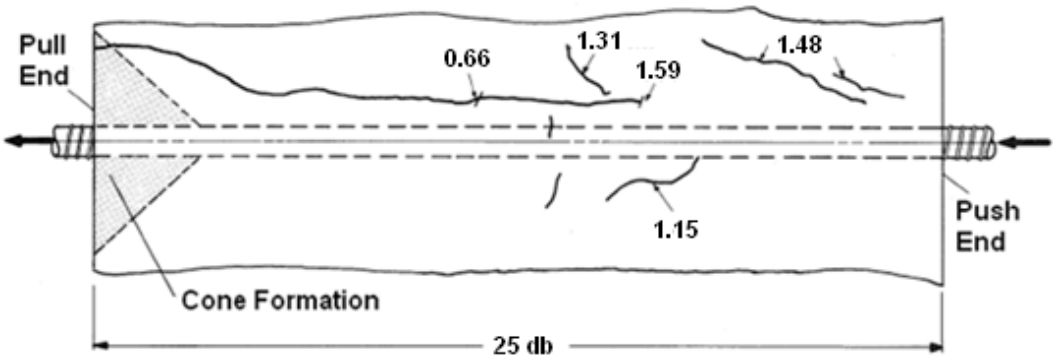

Figure 3-25: *Typical crack pattern on top side of monotonically loaded specimen. Adapted from Viwathanatepa et al (1979)*

Figure 3-25 shows one of the splitting cracks which has propagated to the top side of the specimen. While such cracking is not visible on the push side, it has penetrated well into the confined core of the specimen. However, inclined cracks are visible on the push side. The high confinement and angle these occur at indicate they are due to significant mobilisation of bearing pressure radiating from the bar lugs. This is consistent with the theory discussed in Section 3.1. The corresponding steel stresses, which have been allowed to reach into the inelastic range, reinforce the importance of confinement in achieving good bond performance as discussed in Section 3.3.4.

These high steel stresses also indicate that significant yielding, and thus strain penetration, has occurred within the specimens. As discussed in Section 3.1.5, strain penetration causes a build up of pressure extending radially from the bar lugs which induces further cracking within the

already weakened and unconfined cover concrete. When the stress becomes high enough, these cracks combine and break out a cone of concrete surrounding the bar on the pull end as shown in Figure 3-26.

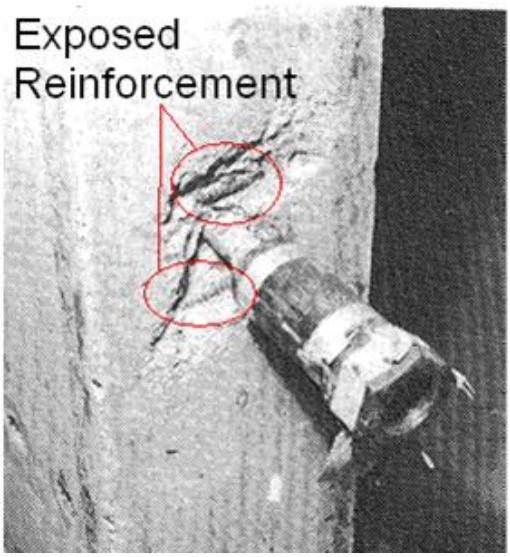

Figure 3-26: *Specimen after breaking out of concrete cone (Viwathanatepa et al, 1979)*

These cones typically separate completely from the specimen. As illustrated in Figure 3-27(a), the cone size at the depth of the reinforcement is limited by the space available between the reinforcement. Similarly, as shown in Figure 3-27(b), the cone forms at angle of approximately 45˚ which governs its depth and also size at the member face; this formation angle was also observed by Au (2010). For most situations, the depth is therefore limited to little more than the concrete cover. However, in tests on well confined concrete, Engstrom et al (1998) found that the cone depth was limited to approximately $1.7d_b$ regardless of cover.

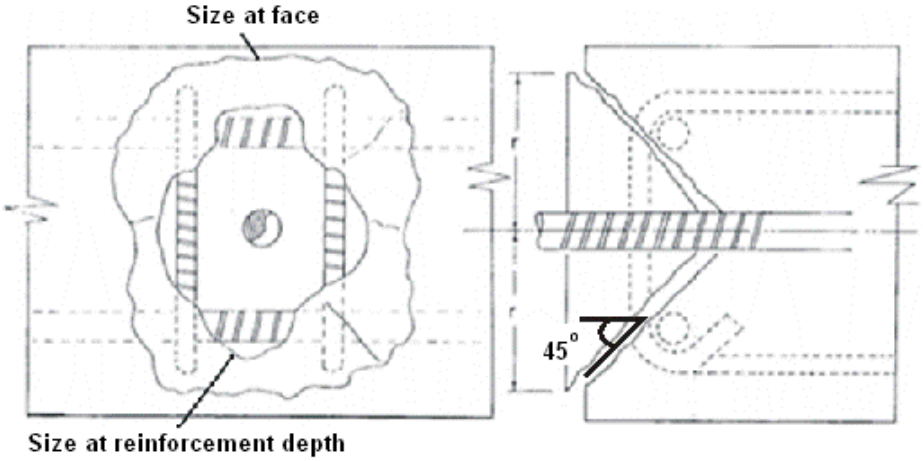

(a) Pull face (b) Section

Figure 3-27: *Geometry of typical cone pullout failure. Adapted from Viwathanatepa et al (1979)*

Given the reduced strength of concrete in this region and the relatively small reduction in embedment length, the cone pullout can be considered to have a negligible impact on the overall bond performance of the specimen. However, it is important to note that, in the multiple tests conducted by Viwathanatepa et al (1979), the cone consistently formed at a stress level between 74 – 92% of the bars nominal yield strength. Given the bottom reinforcement within slotted beams is expected to yield during even moderate seismic loading, cone formation in such scenarios is likely to be unavoidable. The best case scenario is to limit the extent of cone formation using suitable reinforcement as discussed above. Alternatively, modification to the column face in the form of confinement plates, would prevent cone formation altogether. However, the latter method would require specialist components not currently used in industry – an approach outside the goal of this research.

After relatively linear bond stress distributions prior to the bar reaching yield, Figure 3-28 shows the behaviour in the post yield range. The inset figure shows the relative steel strain at each loading point where a distribution was recorded. It is immediately clear that the bond stress is higher towards the push side of the specimen, relatively constant in the core, and minimal on the pull side, just as predicted from earlier external observations. The effect of strain penetration, as described in Section 3.1.5, is also evident with the uptake of peak bond stress moving further into the member with increasing steel stress. It follows from this that, due to the reduced bar length available with which to equilibrate an increasing force, the bond stress within the remaining intact core will increase; this is illustrated in Figure 3-28.

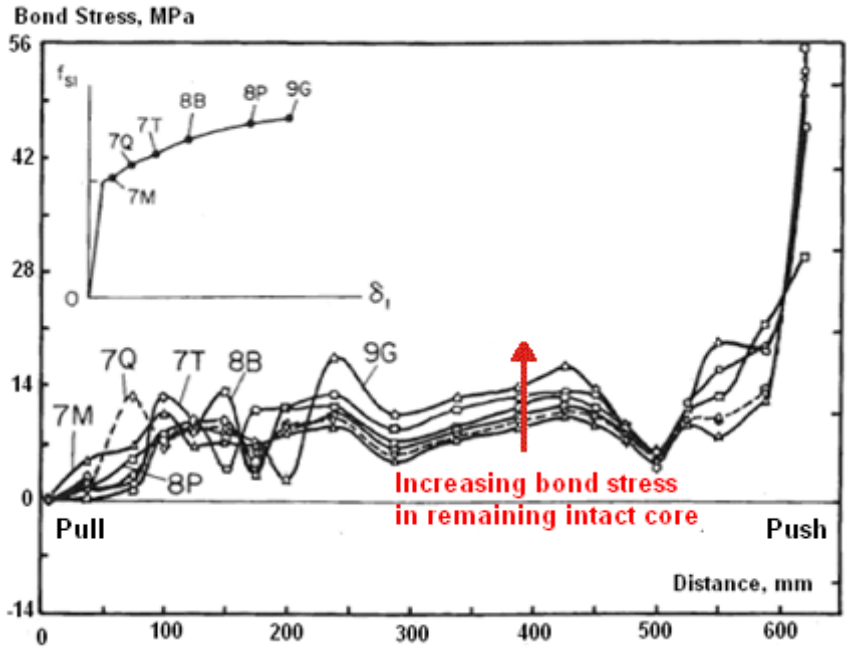

Figure 3-28: *Bond stress distributions in the post yield range for monotonic loading. Adapted from Viwathanatepa et al (1979)*

The resulting stress-slip profiles for each region of a typical specimen are shown in Figure 3-29. As expected, bond performance increases with the degree of confinement. The unconfined region at the pull end, Region 1, consistently exhibits the lowest peak local bond strength and fails in a brittle manner due to splitting and cone pullout. It is also subject to the negative effects of reduced bar diameter due to Poisson's effect (Viwathanatepa et al, 1979). Region 2, the confined core of the specimen, achieves higher peak local bond strength but is still subject to strain penetration and splitting towards the tension side of the specimen. More importantly, due to availability of sufficient embedment length, bond capacity is maintained for some time after strain penetration has begun. The push end, Region 3, reaches the greatest peak local bond strength and maintains bond performance for the largest range of slip values. This is because it is subject to significant confinement and not affected by strain penetration, as evidenced in Figure 3-25 by failure of the longitudinal cracking to extend sufficiently far. Combining the results of all applicable monotonic specimens, the resulting average maximum bond strength is found to be $2.9\sqrt{f_c'}$.

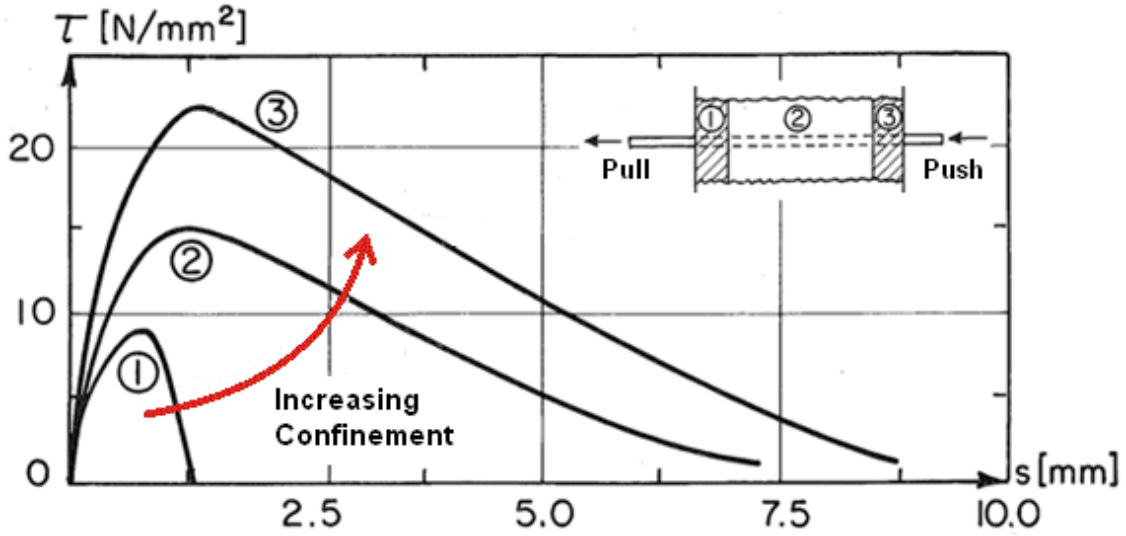

Figure 3-29: *Bond stress dependence on region. Adapted from Viwathanatepa et al (1979)*

Specimens subject to cyclic push-pull loading also exhibited similar cracking patterns on each face to those loaded monotonically. However, unlike in the monotonic specimens, longitudinal splitting cracks penetrated through the member from one face to the other. These cracks propagated from the alternating pull ends and combined near the middle of the specimen at a bar stress of around $0.9f_y$ as shown in Figure 3-30. Cones also formed at both ends of the specimen at around this time; consequently, only the core of the specimen was effective at providing bond resistance beyond this point.

As a result, the maximum average bond strength of $2\sqrt{f_c'}$ is found to be somewhat lower than that observed during the monolithic tests. This is approximately 20% greater than the average

bond stress of $0.67 \times 2.5\sqrt{f_c'} = 1.68\sqrt{f_c'}$ assumed by Paulay and Priestley (1992) and used for design as discussed in Section 4.1.1. However, considering transverse pressure on the order of 10 – 13 MPa in addition to an unknown axial load providing further confinement on the compression side of the specimens, the increase is accounted for. Thus the design value above is further justified. Note transverse pressure was applied via post tensioned straps attached to the specimen as illustrated in Figure 3-23.

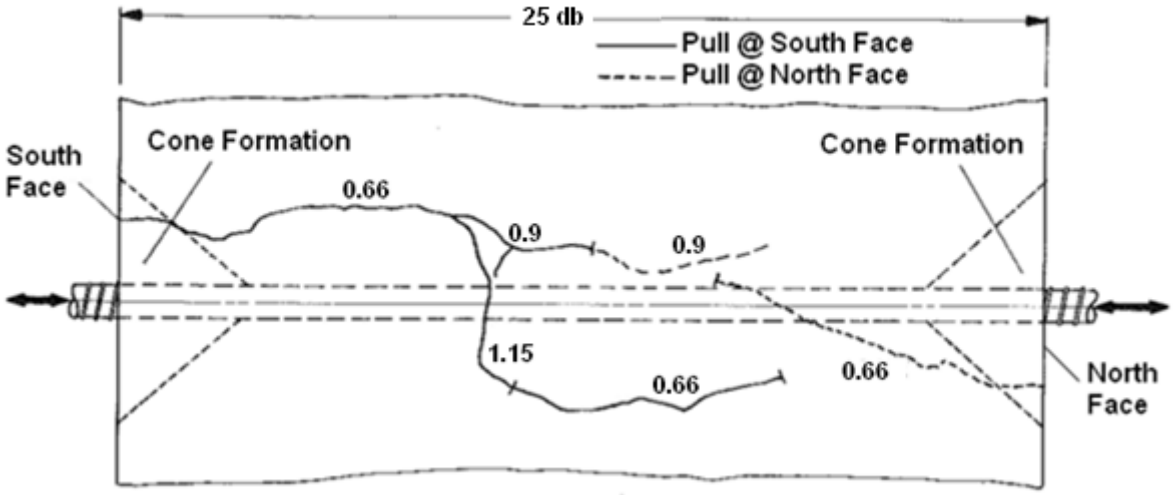

Figure 3-30: *Typical crack pattern on top side of cyclically loaded specimen. Adapted from Viwathanatepa et al (1979)*

3.4.2 Eligehausen et al (1983)

Eligehausen et al (1983) conducted an extensive experimental programme on some 125 pull-out specimens. A relatively short embedment length of $5d_b$ was used in order to develop the maximum bond strength over the entire length of the bar such that Equation 3-1 was valid. Tension or compression loading was applied to one end of the specimen only, by a movable head. As shown in Figure 3-31, each specimen bears on a steel plate in order to simulate the lateral confinement provided by the adjacent beams to the joint face. Concrete was cast parallel to the bond interface (weak direction) with the bars installed at mid-height in the specimen. As such, the resulting bond performance was not representative of either a top or bottom beam bar. A thin plastic sheet was installed along the splitting plane in order to predetermine the location of any splitting cracks that formed and to ensure the effect of confining reinforcement on restraining such cracks could be isolated. Around half the specimens were tested under monotonic loading and half under cyclic loading. The tests were conducted in series with a key variable – each one is discussed in Section 3.3 – being changed between series.

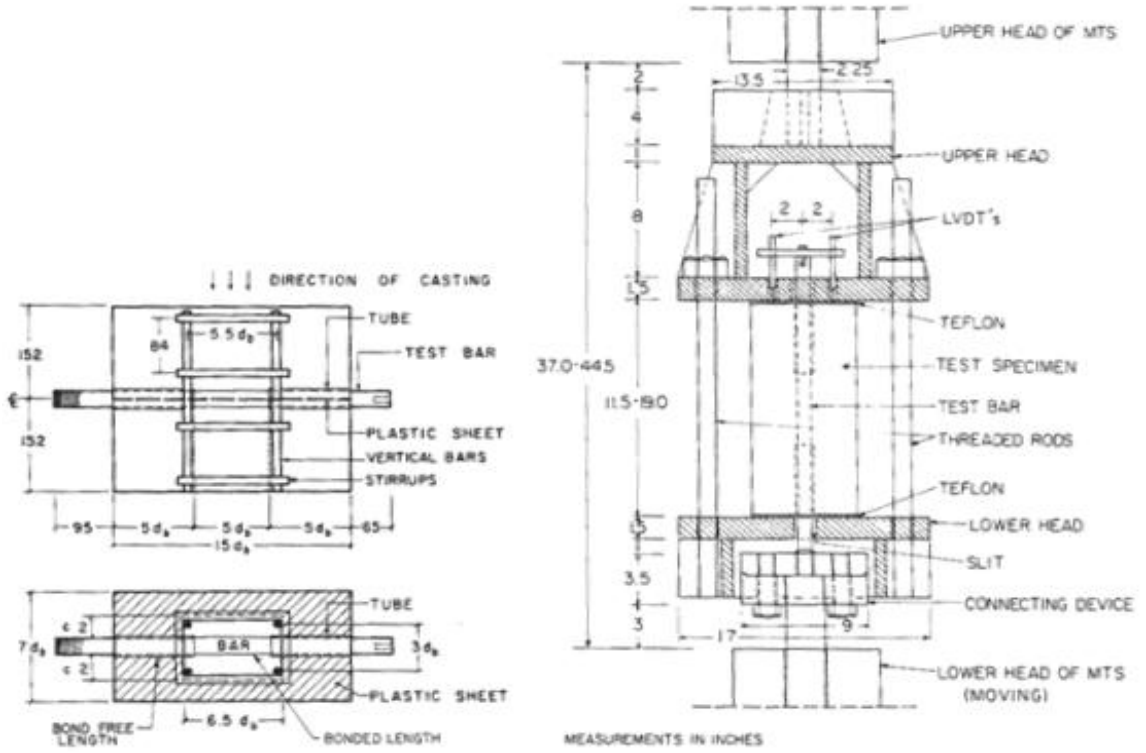

(a) Specimen details (b) Experimental set up

Figure 3-31: *Test set up showing end confinement provided by plates (Eligehausen et al, 1983)*

The majority of specimens tested had passive confinement provided by transverse reinforcement but no active confinement. In testing of such specimens, a splitting crack would develop prior to failure in the plane of the bar. The crack consistently formed at a bond stress between 0.7 – 1.6$\sqrt{f_c'}$ but was restricted to less than 0.1 mm width by the presence of confining reinforcement. This small crack width meant that lug bearing was not compromised and, as such, all specimens with transverse reinforcement failed through bar pullout. A good example of bar pullout failure is illustrated in Figure 3-32(a) where a smooth surface remains after all the concrete shear keys have been lost through the mechanism described in Section 3.1.5. Similar findings were observed by Restrepo (1992) after removing the cover concrete on a tested specimen. By comparison, Figure 3-32(b) shows a specimen with no transverse reinforcement which, predictably, failed by splitting. The concrete shear keys are intact and no shear cracking or crushing – both signs of significant lug bearing activation – are not present.

Eligehausen et al (1983) observed a maximum average bond stress of 2.5$\sqrt{f_c'}$ over approximately 60 tests on identical specimens as shown in Figure 3-33. These were tests conducted with a set of standard conditions typical of a beam-column joint; d_b = 25 mm, f_c' = 30 MPa, sufficient transverse reinforcement, 1.7 mm/minute load rate, clear spacing between bars of $4d_b$, and little or no transverse confining pressure. The only difference between tests

was the loading regime; both monotonic and cyclic loading were used with variable slip values at stress reversal. The embedment length of only $5d_b$ meant that the maximum bond strength was able to be achieved along the entire bar. Therefore, when the bond stress was back-calculated from the change in steel stress, the value would be the true maximum. For these reasons, adoption of $2.5\sqrt{f_c'}$ by Paulay and Priestley (1992) as the maximum bond stress within a beam-column joint seems reasonable; this is discussed further in Section 4.1.1.

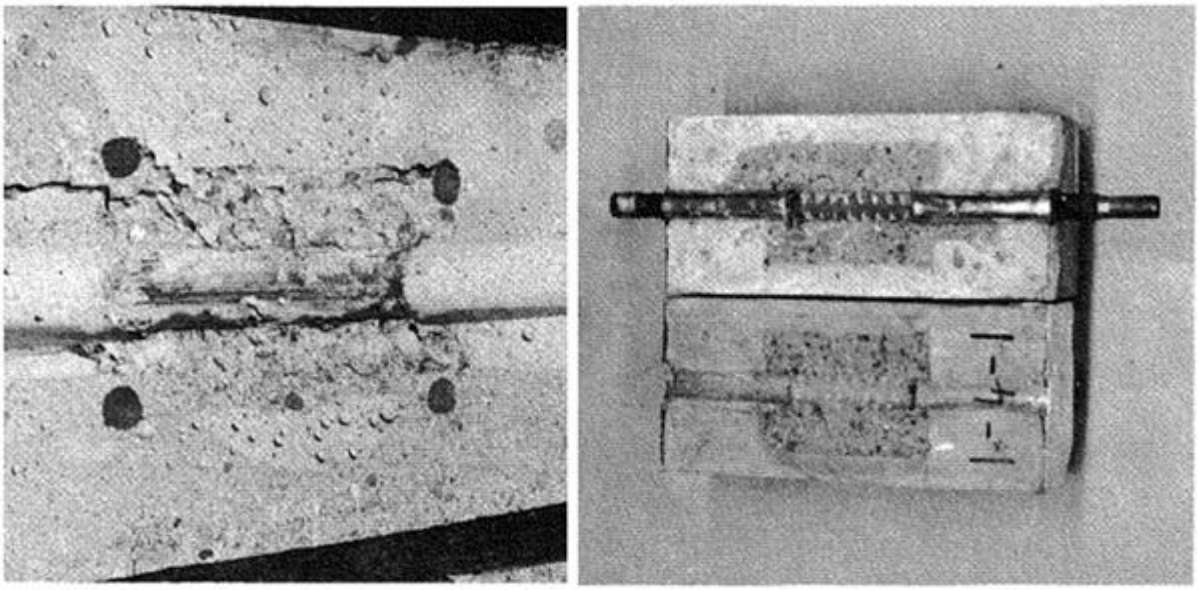

(a) Pullout failure specimen (b) Splitting failure specimen

Figure 3-32: *Sections through failed specimens (Eligehausen et al, 1983)*

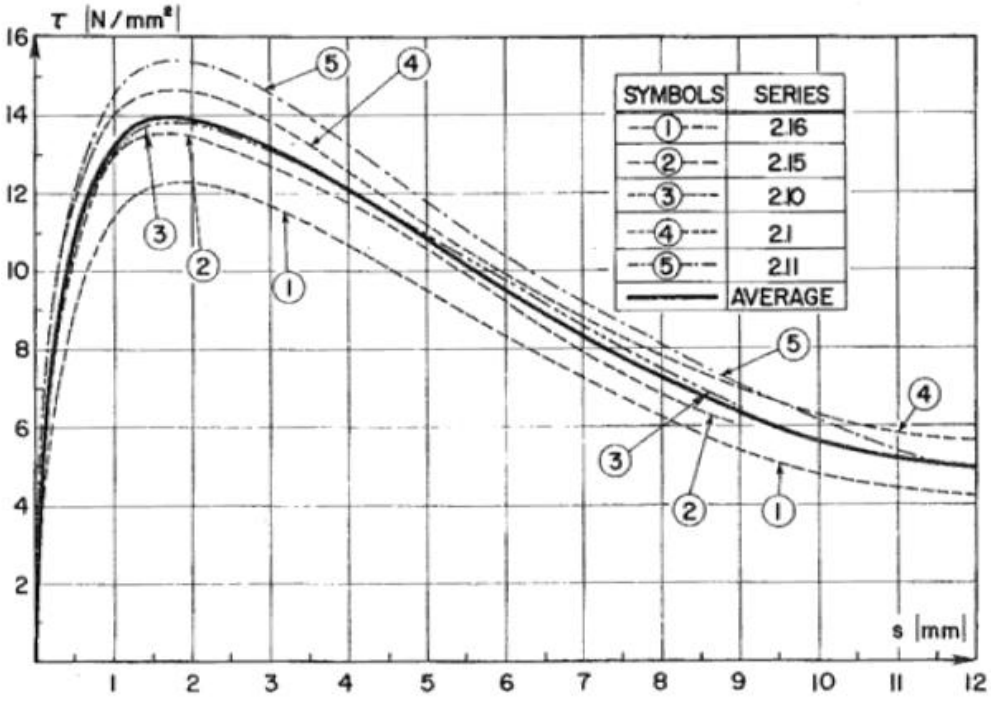

Figure 3-33: *Bond stress-slip relationships for multiple tests (Eligehausen et al, 1983)*

Chapter 4 - BEAM-COLUMN JOINT MECHANICS

4.1 Bond within Monolithic Interior Joints

4.1.1 Bond Demand

The bond demand within monolithic interior beam-column joints is based on equilibrium of forces entering and being resisted within the joint. However, due to the complexities and number of variables involved, experimental testing is required to calibrate and verify the relationships developed through such a theoretical approach. Consider a reinforcing bar passing through an interior joint as shown in Figure 4-1.

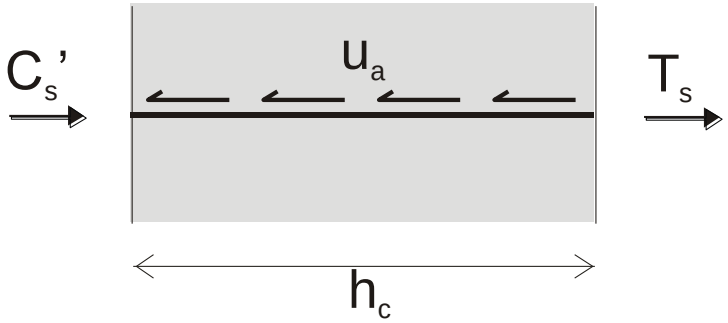

Figure 4-1: *Bond force within monolithic interior joint*

Conservatively assuming overstrength compression and tension on either side of the joint, Equation 4-1 from Paulay and Priestley (1992) is derived using equilibrium across the joint:

$$u_o = \frac{T_s + C_s'}{h_c}$$

$$= \frac{2\lambda_o f_y A_s}{h_c} \qquad \text{Equation 4-1}$$

Where u_o is the bond force per unit length of bar. In terms of average bond stress, u_a:

$$u_a = \frac{u_o}{\pi d_b}$$

$$= \frac{d_b \lambda_o f_y}{2h_c} \qquad \text{Equation 4-2}$$

Paulay and Priestley (1992) then assumed a maximum local bond stress, u_{max}, of $2.5\sqrt{f_c'}$ after this was observed by Eligehausen et al (1983) over a number of tests as described in Section 3.4.2. Engstrom et al (1998) found a similar relationship with the proportionality of

$0.45f_c'$ which gives a similar u_{max} for the usual range of f_c' values between 25 and 40 MPa. Database findings, from Section 4.1.7, suggest this value is achievable for well reinforced joints with an axial load ratio of 0.05 or more. However, as discussed in Section 3.4.1, the bond stress distribution is not uniform over the column depth and the maximum local bond stress must be altered accordingly.

Bond strength is greatest within the side of the joint subject to compression from the moment couple within the column in addition to any axial load on the column. In this region, the compression provides active confinement to the longitudinal reinforcement thus increasing the bond capacity as discussed in Section 3.3.4 and ensuring a ductile pullout failure mechanism occurs. Further confinement is provided to this region by beam compression which, combined with column compression and the concrete strut within the joint, increases the concrete compressive strength (Harries & Kharel, 2003). As discussed in Section 3.3.1, this is beneficial to bond strength. Bar expansion due to Poisson's effect also increases bond performance (Eligehausen et al, 1983) as lugs are forced into the surrounding concrete which, due to the active confinement discussed above, is able to prevent splitting cracking and take advantage of the resulting radial pressure.

On the tension side of the joint, the bond performance is significantly worse. The tensile force acting perpendicular to the bond interface causes a splitting crack to form along the beam bar (Eligehausen et al, 1983; Paulay & Priestley, 1992) promoting a weak, brittle splitting failure. This can be seen in the testing of Viwathanatepa et al (1979) as discussed in Section 3.4.1. Although vertical reinforcement is present, it is only effective at providing passive confinement in the area immediately surrounding the bar as discussed in Section 4.1.5. Furthermore, vertical reinforcement is typically limited to column bars only and these do not map onto all the beam bars, particularly middle bars within the joint core. Column bars on joint faces are also activated significantly in flexure, further reducing any benefit they provide to bond performance.

To account for these differences in bond performance, Paulay and Priestley (1992) adopted the bond stress distribution shown in Figure 4-2 in which the average bond stress, u_a, is expressed as a portion of u_{max}. The location of u_{max} is skewed towards the compression side of the joint core to reflect the beneficial effects of axial confinement. Bond stress also decreases rapidly outside this region, especially on the tension side of the joint where strain hardening and bond degradation occur more rapidly. Because these inelastic effects are accounted for, this bond profile is applicable for joints experiencing a moderate level of inelastic loading in the range of displacement ductility 4 to 6 (Paulay & Priestley, 1992). Beyond this, sufficient

bond cannot be guaranteed because the conditions under which the bond profile was assumed no longer exist. In other words, these recommendations are performance based.

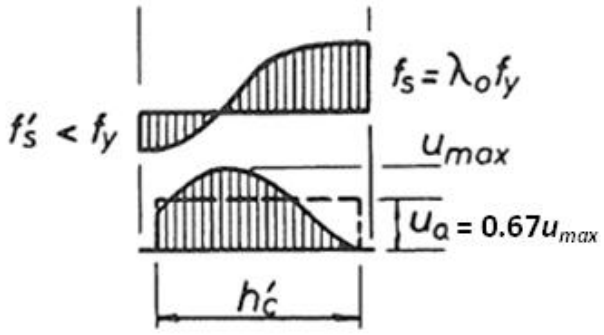

Figure 4-2: *Typical bond stress distribution allowing for inelasticity. Adapted from Paulay and Priestley (1992)*

In Figure 4-2, h_c' is the effective column depth providing bond resistance and is generally taken to be 80% of the total column depth, h_c (Standards Association of New Zealand, 2006). This reduction accounts for the cover and some core concrete on the tension side of the column which, as discussed in Section 3.4.1, are both relatively ineffective at providing bond resistance. Note that this is a different reduction to that considered for strain penetration and bond degradation; the excluded regions for the case of h_c' are assumed to be ineffective at providing bond regardless of the loading stage. The resulting average bond stress across the entire column depth is thus $0.8\times0.67\times2.5\sqrt{f'_c} = 1.34\sqrt{f'_c}$. Substituting this bond stress into Equation 4-2 gives the basic column depth requirement as given by Equation 4-3:

$$u_a = 1.34\sqrt{f_c'} = \frac{d_b \lambda_o f_y}{2h_c}$$

$$\therefore \quad \frac{d_b}{h_c} \leq 2.68\frac{\sqrt{f_c'}}{\lambda_o f_y} \qquad \text{Equation 4-3}$$

This equation is generally expressed with the associated bond modification factors as discussed in Section 4.1.2 to give Equation 4-4 from Paulay and Priestley (1992):

$$\frac{d_b}{h_c'} \leq 2.68\frac{\sqrt{f_c'}}{\lambda_o f_y} \times \frac{\xi_p}{1} \times \frac{\xi_t}{1} \times \frac{\xi_f}{1} \times \frac{2}{\xi_m}$$

$$\therefore \quad \frac{d_b}{h_c} \leq 5.4\frac{\xi_p \xi_t \xi_f}{\xi_m \lambda_o}\frac{\sqrt{f_c'}}{f_y} \qquad \text{Equation 4-4}$$

The relevant equation in the New Zealand Concrete Structures Design Standard (Standards Association of New Zealand, 2006) is almost identical to the Paulay and Priestley (1992)

equation presented above. The code equation, Equation 4-5, is given below firstly in the format with which it appears in the code and then in an equivalent format. As discussed in Section 4.1.2, the bond modification factors are the same between both sources; therefore the only difference is the factor at the front of the equation. Thus the code equation is 10% less conservative than the Paulay and Priestley (1992) equation.

Although no specific explanation to this relaxing of bond requirements is given, the code commentary does provide a possible reasoning. One of the assumptions in the derivation of the Paulay and Priestley (1992) equation is that bar stresses range from tensile yielding to compressive yielding on either side of the joint. However, when gravity loading considerations govern, there may be a large excess of strength compared with seismic demands. In such a case, the beam bar stresses may be of the same sign throughout the joint thus lessening the bond requirements (Standards Association of New Zealand, 2006).

Code format: $$\frac{d_b}{h_c} \leq 6\left(\frac{\alpha_t \alpha_p}{\alpha_s}\right)\alpha_f \frac{\sqrt{f_c'}}{\alpha_o f_y}$$

Equivalent format: $$\frac{d_b}{h_c} \leq 6\frac{\xi_t \xi_p \xi_f \sqrt{f_c'}}{\xi_m \lambda_o f_y}$$ Equation 4-5

4.1.2 Bond Modification Factors

As discussed in Section 3.3, there are a number of factors that affect the bond performance within reinforced concrete members. Several of these were considered by Paulay and Priestley (1992) as shown in Equation 4-4 where ξ_p, ξ_t, ξ_f, and ξ_m account for confinement due to column axial load, bar depth within the pour, plastic hinge locations, and the degree of reinforcement activation across the joint relative to the tension reinforcement overstrength force, T_s, respectively. There are two types of factors that enhance bond performance; those that directly influence bond stress such as concrete grade and those that prolong favourable bond conditions such as confinement due to axial load. Given bond requirements are performance based as outlined in Section 4.1.1, both types are considered. The factors presented here are generally consistent with those in the current New Zealand Concrete Structures Design Standard (Standards Association of New Zealand, 2006) although the form of these may vary.

The link between confinement and bond performance has been discussed at length throughout this thesis. As given in Equation 4-6, ξ_p is a modification factor to account for the beneficial effects of column axial load at improving bond performance. This improvement is due to the

greater column area required to equilibrate the increased vertical component of the concrete strut. Thus, a greater area of the column is subject to active confinement and the bond performance is improved. To be conservative, the minimum design axial compression force at ultimate, P_u, should be used (Paulay & Priestley, 1992).

$$1.0 < \xi_p = \frac{P_u}{2f_c' A_g} + 0.95 < 1.25 \qquad \text{Equation 4-6}$$

As discussed in Section 3.3.3, the position of bars within a pour can affect bond performance. The factor ξ_t allows for the location of bars with respect to how much fresh concrete is poured below the bars. According to Paulay and Priestley (1992), if more than 300 mm of fresh concrete is poured below a layer of bars, ξ_t is taken as 0.85, otherwise it is taken as unity; these recommendations were adopted in NZS3101:2006.

Bond strength can also be adversely affected in two-way frames when plastic hinges form on all four faces of the beam-column joint. However, for the scope of this project, only one-way frames are being dealt with and, as such, the corresponding factor, ξ_f, is again taken as unity.

The degree of reinforcement activation across the joint is also an important aspect to consider, and is accounted for using the factor ξ_m. This factor varies depending on the beam reinforcement profile and, as such, it is discussed separately for each case in Sections 4.1.3 and 4.1.4.

4.1.3 Symmetrically Reinforced Beams

A symmetrically reinforced beam is one in which the top and bottom reinforcement areas are equal. Consider the top beam reinforcement in Figure 4-3; due to the concrete compression on the left side of the joint, C'_c, the force in the reinforcement on the left side of the joint, C'_s, will be less than the overstrength force activated in the reinforcement on the right, T_s.

This inability to activate overstrength actions on both sides of the joint simultaneously means that the force required to be resisted through bond within the joint is reduced compared with the initial assumption in Section 4.1.1. From horizontal equilibrium in the top beam reinforcement, the maximum bond force is given by the following equation from Paulay and Priestley (1992):

$$(T_s + C_s')_{max} = \lambda_o f_y A_s' + \gamma f_y A_s'$$

The above quantity is typically expressed in terms of the overstrength tension force, T_s, in the reinforcement as given by Equation 4-7:

$$(T_s + C_s')_{max} = \left(1 + \frac{\gamma}{\lambda_o}\right) \lambda_o f_y A_s'$$

$$= \xi_m \lambda_o f_y A_s'$$

$$= \xi_m T_s \qquad \text{Equation 4-7}$$

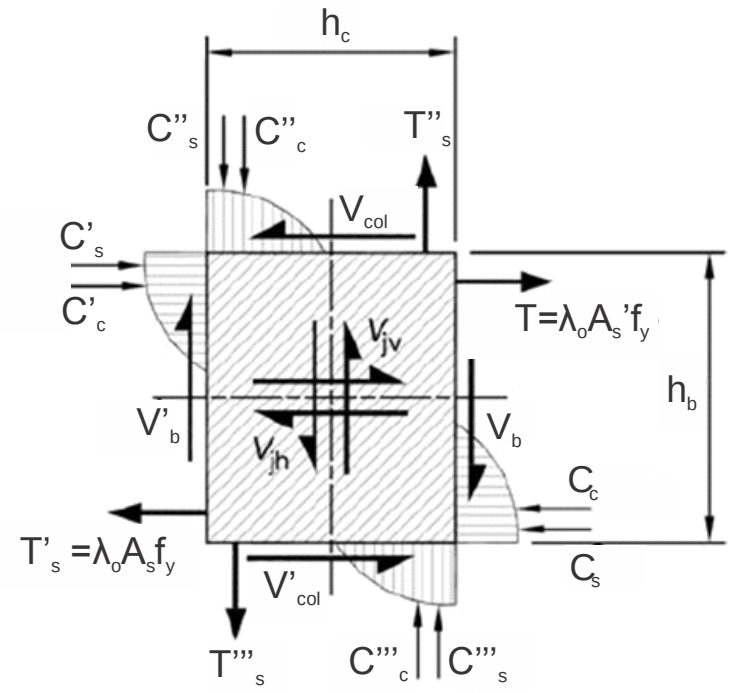

Figure 4-3: *External actions on an interior monolithic beam-column joint. Adapted from Au (2010)*

Due to strain penetration and associated bar slip that inevitably occurs once inelastic behaviour has begun, the compression reinforcement is not likely to exceed a stress of $0.7f_y$ (Paulay & Priestley, 1992). This was consistently observed in testing on symmetrically reinforced beams by Cheng et al (2000) where, as shown in Figure 4-4, compression reinforcement strains fail to exceed $0.5\varepsilon_y$. Database results in Figure 4-19 also show good agreement with this level of activation.

It should be noted that the $0.7f_y$ limit is only valid for the joint conditions from which the bond demand in Section 4.1.1 was derived; that is, strain hardening of the reinforcement with some bar slip. Several researchers have found that these conditions remain prevalent within monolithic joints up to a displacement ductility level of around 4 (Ruitong & Park, 1987; Cheng et al, 2000). The reason for this limiting stress is as follows; due to bar slip allowing some movement of the beam towards the column face, vertical cracks along the beam-column interface are able to close during compression cycles such that concrete is mobilised and the compression reinforcement is not required to yield in order to achieve equilibrium (Cheung, Paulay & Park, 1991). This behaviour is evident in Figure 4-5 where the beam elongation

follows a ‘saw tooth’ pattern as cracks open and close with alternating compression and tension inducing cycles.

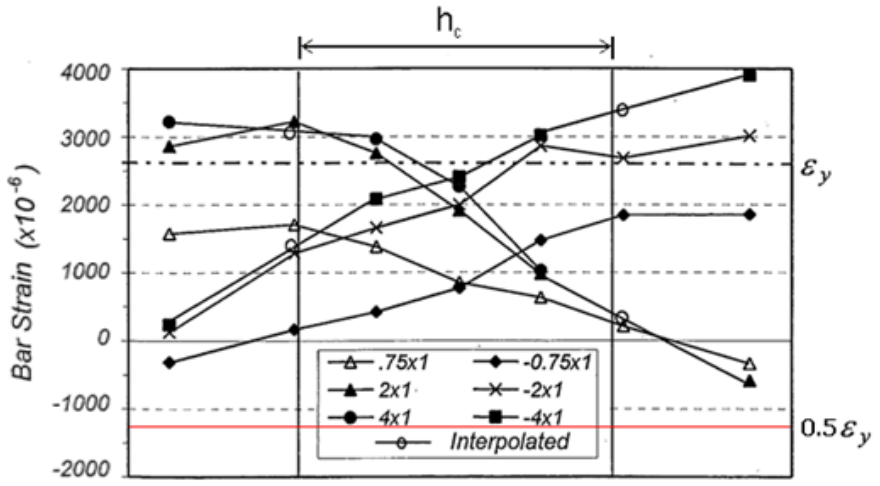

(a) Top reinforcement

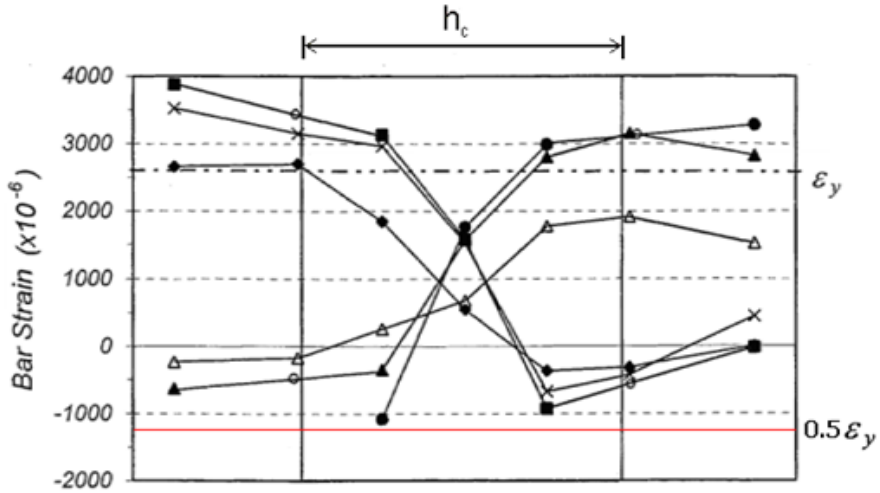

(b) Bottom reinforcement

Figure 4-4: *Symmetric beam reinforcement strain profiles. Adapted from Cheng et al (2000)*

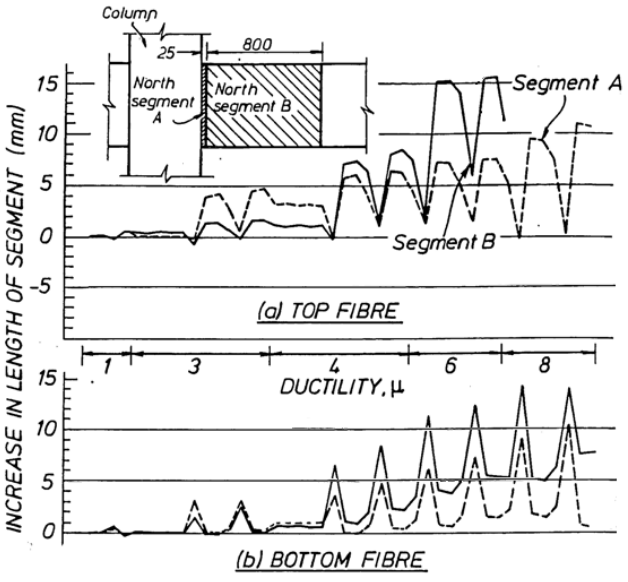

Figure 4-5: *Components of beam elongation (Cheung et al, 1991)*

For the case of a symmetrically reinforced beam, the factor ξ_m is thus defined by Paulay and Priestley (1992) for Grade 300 reinforcement in Equation 4-8:

$$\gamma = 0.7$$

$$\therefore \qquad \xi_m = 1 + \frac{\gamma}{\lambda_o} = 1 + \frac{0.7}{1.25} \approx 1.55 \qquad \text{Equation 4-8}$$

The factor ξ_m is not overly sensitive to the value of λ_o (Paulay & Priestley, 1992) and, subsequently, no allowance is made in the code for the grade of reinforcement. Experimental studies reported in the New Zealand Concrete Structures Design Standard suggest this simplification is adequate for Grade 500 bars (reinforcement with a 5th percentile characteristic yield strength of 500 MPa) provided interstorey drift does not exceed 1.8% (Standards Association of New Zealand, 2006).

4.1.4 Asymmetrically Reinforced Beams

In some design situations, it is desirable to use an asymmetric reinforcement profile within a beam in the region where it spans into the beam-column joint. However, this strength bias can significantly influence the relative reinforcement stresses on either side of the joint and, consequently, bond demand. For the larger area of reinforcement, bond demand is reduced, while the opposite is true for the smaller area. As for symmetrically reinforced beams, the theory presented here is only valid for the joint conditions assumed in Section 4.1.1.

Firstly, let the top beam compression reinforcement, A'_s, in Figure 4-3 be of greater area than the bottom tension reinforcement, A_s. Also let the ratio between the areas of compression and tension reinforcement be defined by Equation 4-9:

$$\beta = \frac{A_s}{A'_s} \leq 1 \qquad \text{Equation 4-9}$$

Considering the bond demand in the larger area of top reinforcement and taking equilibrium on the left column face in Figure 4-3, the maximum possible compression force, C'_s, that can occur within this reinforcement is equal to the overstrength tension, T'_s, in the bottom reinforcement. Thus the top compression reinforcement is only subject to a portion, γ, of its overstrength capacity, as defined in Equation 4-10:

$$C_s^{'} = T_s^{'} = A_s \lambda_o f_y$$

$$= \beta A_s^{'} \lambda_o f_y$$

$$= \gamma A_s^{'} f_y \qquad \text{Equation 4-10}$$

As illustrated in Figure 4-6, this portion is typically very low, on the order of 0.3 – 0.4f_y. However, during advanced inelastic displacments when the concrete contribution can no longer be relied upon and the bottom reinforcement is at overstrength in tension, this can increase to the theoretical limit given by Equation 4-11:

$$f_s^{'} = \beta \lambda_o f_y \qquad \text{Equation 4-11}$$

Which, for β = 0.5, is equal to 0.63f_y. Despite this theoretical limit, Paulay and Priestley (1992) use the 0.7f_y figure from Section 4.1.3; adoption of this value is supported by Figure 4-19 from the database. Combining the two governing cases gives the following limit on γ:

$$\beta \lambda_o \geq \gamma \leq 0.7$$

Given the usual range of reinforcement overstrength values, 1.25 < λ_o < 1.4, and β values above 0.5 for the most reinforcement layouts, γ is generally governed by the 0.7 limit.

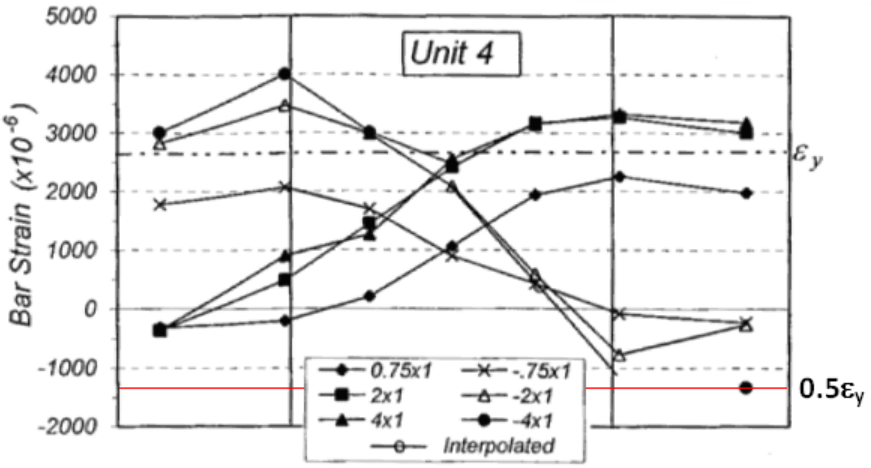

Figure 4-6: *Strain profiles for larger area of reinforcement within asymmetric beam. Adapted from Cheng et al (2000)*

Meanwhile, on the other side of the joint, high elastic to yield tensile stresses are activated in the larger top reinforcement by the compression reinforcement and concrete working together at the beam soffit. The strain profile in Figure 4-6 from testing by Cheng et al (2000) clearly illustrates the high tension and minimal compression demands experienced by the larger top reinforcement. This is also illustrated by database findings in Figure 4-19 where tensile stresses reach 115% of specified yield strength. However, to be conservative, Paulay and

Priestley (1992) allow for the top reinforcement reaching full overstrength in tension. Combining the above considerations for the larger areas of compression and tension reinforcement, the factor ξ_m is given by Equation 4-12:

$$\xi_m = 1 + \frac{\gamma}{\lambda_o} = 1 + \frac{0.7}{1.25} \approx 1.55 \qquad \text{Equation 4-12}$$

On comparison with Section 4.1.3, Equation 4-12 clearly offers no advantage for the reduced bond requirements obtained by using a larger reinforcement area. However, some relaxation of this limit should be possible for the top longitudinal reinforcement within slotted beams; this is discussed further in Section 4.2.5.

For the smaller bottom reinforcement, the bond demand is much more severe. Due to its smaller area, this reinforcement is subject to inelastic tension demands on one side of the joint as shown in Figure 4-6. On the other side of the joint, compression reinforcement reaches large elastic strains but, due to assistance from the concrete, does not yield. This is shown in Figure 4-7 and is supported by the database findings in Figure 4-19 although the average stresses recorded here are somewhat lower.

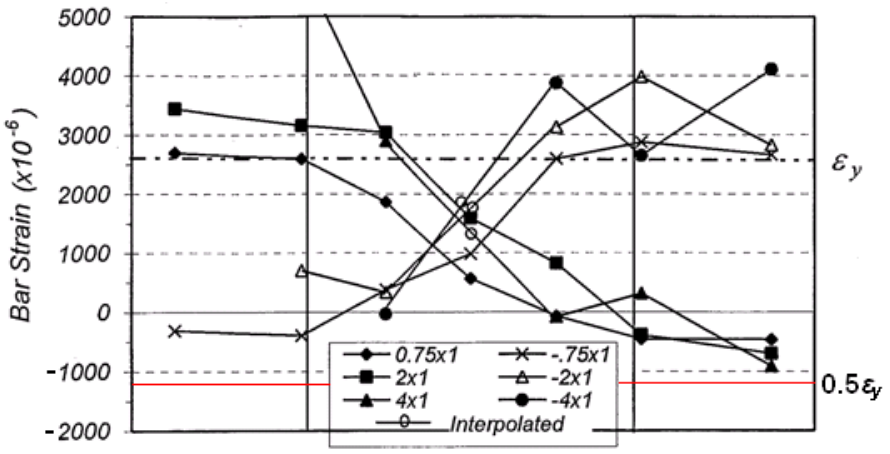

Figure 4-7: *Strain profiles for smaller area of reinforcement within asymmetric beam. Adapted from Cheng et al (2000)*

Paulay and Priestley (1992) propose the following limit on ξ_m for the smaller area of reinforcement within a beam. This assumes a maximum compression stress within the reinforcement of f_y which, according to the findings presented above appears rather conservative.

$$\xi_m = 2.55 - \beta \leq 1.8$$

4.1.5 Effect of Column Bars on Bond Performance

Bond performance within a beam-column joint is influenced by the presence of column bars. As discussed in Section 3.3.4, these can provide passive confinement to the bond interface which increases the maximum local bond stress that can be achieved. This becomes important when the beneficial effects of active confinement from axial load are unavailable. While such conditions obviously occur in joints with no axial compression from the column, they also occur during seismic loading when axial and lateral loads combine – due to the moment couple within a column, a large portion of the joint is subject to tension at any given time. Column bars enhance bond on the tension side of the joint by providing confinement, albeit the less effective passive confinement. Similarly, Brooke, Megget, and Ingham (2005) attribute the improved bond performance afforded by column bars to the resultant increased joint capacity and thus reduced damage. This section examines bond performance of beam bars in joints with both minimal and sufficient column bars and comments on the effectiveness of column bars compared with supplementary vertical stirrups discussed in Section 4.2.3.

Consider the beam-column joint in Figure 4-8(a) in which there are no interior column bars. In such a joint, bond deterioration begins on the tension side of the joint even during elastic loading (Cheng et al, 2000). This initial deterioration is due to formation of splitting cracks which are able to form on the tension side of the joint given the lack of confinement here. Such cracking was observed by Viwathanatepa et al (1979), as discussed in Section 3.4.1, and by Hakuto, Park, and Tanaka (1995) in testing of full-scale beam-column subassemblies with insufficient joint reinforcement. A typical example of this cracking is visible in Figure 4-9.

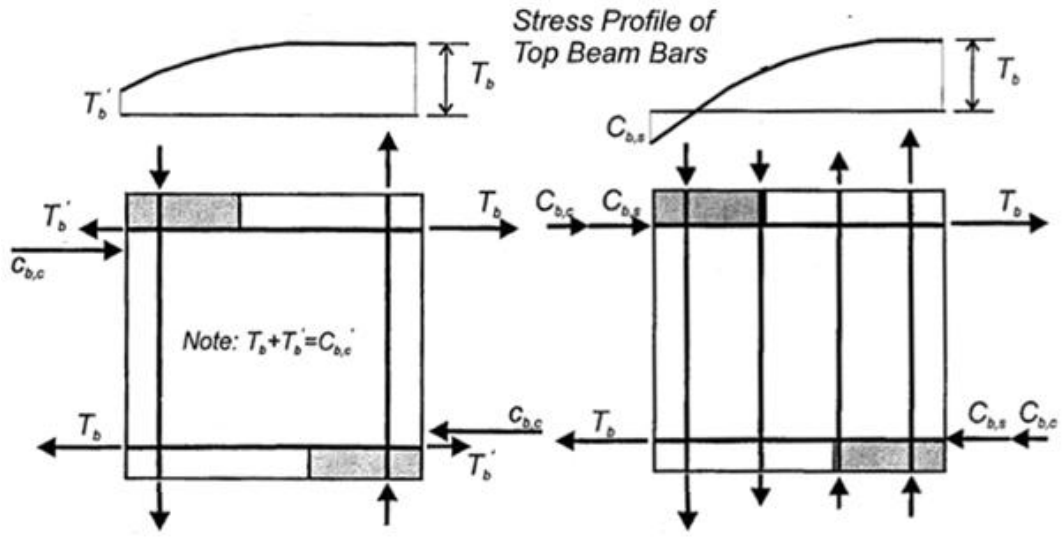

(a) No interior column bars (b) With interior column bars

Figure 4-8: *Beam reinforcement bond stress profile with varying column bar configurations (Cheng et al, 2000)*

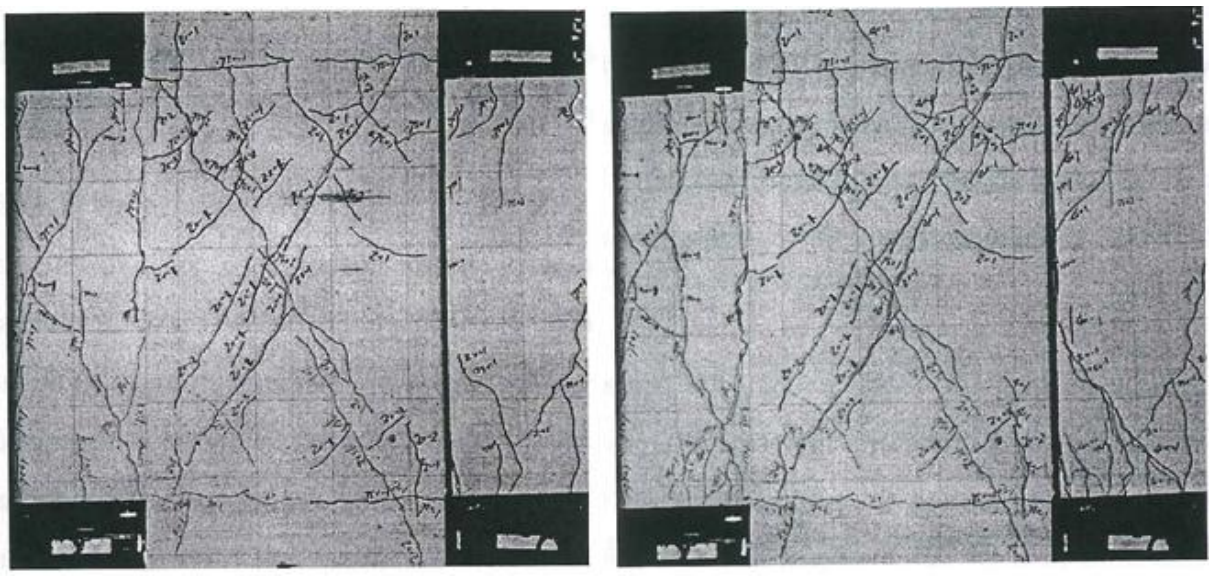

(a) Displacement ductility, $\mu_\Delta = 2$ (b) Displacement ductility, $\mu_\Delta = 4$

Figure 4-9: *Typical example of splitting cracks forming on the tension side of a beam column joint (Cheng et al, 2000)*

Due to this splitting cracking, the tension side of the joint is therefore ineffective at providing bond resistance. Evidence for this is provided in Figure 4-10 where bond stress remains negligible on the tension side of the joint until inside the first column bar.

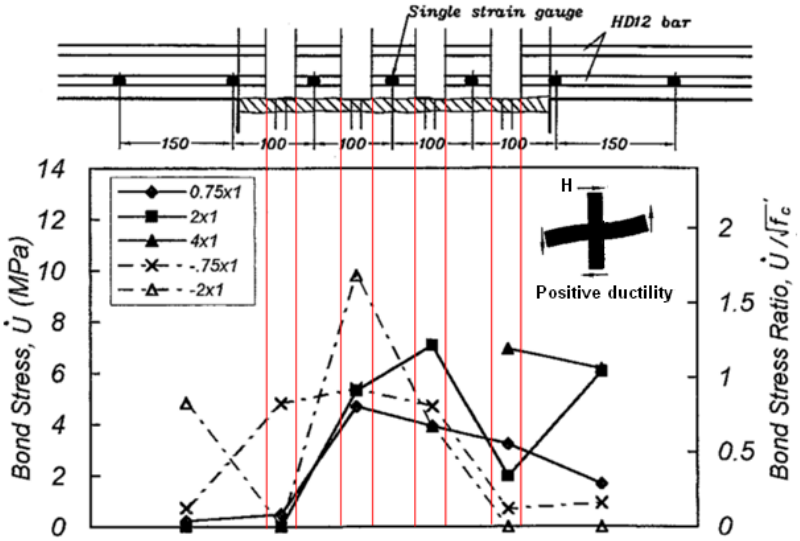

Figure 4-10: *Dependence of bottom beam bar bond stress profiles on column bar layout. Adapted from Cheng et al (2000)*

For this reason, the vast majority of the bond demand must be resisted by the region of the joint subject to confinement from axial compression; this is shaded grey in Figure 4-8(a). As discussed in Section 3.3.4, this confined region exhibits far superior bond strength. However, depending on the magnitude of the bond demand, this small region within the joint may be insufficient to achieve equilibrium; if this is the case, bar slip failure will result prematurely. Tensile stresses within the beam bar on both sides of the joint as shown in Figure 4-8(a) are indicative of such a failure as discussed in Section 4.1.6.

Consider now an interior beam-column joint which has several interior column bars as shown in Figure 4-8(b). These bars are able to provide a clamping force across the bond interface thus helping to restrict the formation of splitting cracks (Cheng et al, 2000); this clamping effect was also noted by Restrepo (1992). It is imperative that these bars remain elastic if the benefits to bond performance are to be realised. This is especially important as any bar inelasticity is likely to be on the tension side of the joint where the bars are required to provide passive confinement in the absence of active confinement from bending and any axial load that is present. Consequently, inelastic strains within the bars will allow splitting cracks to open somewhat before the confining effect is activated. If these cracks are allowed to open sufficiently far, pullout failure, as discussed in Section 3.1.5, cannot be guaranteed and bond performance will not be enhanced.

Further evidence supporting the clamping concept is shown in Figure 4-11 where local non-linearity in the stress profile of bar 4 is due to the bar being activated in tension as it attempts to prevent expansion of a splitting crack. Similar non-linearity can be observed in the column bar stress profiles of Beckingsale (1980) with several bars yielding upon bar slip failure. This delay in the formation of splitting cracks means that a greater portion of the joint remains effective at providing bond capacity for more cycles compared with the previous case (Cheng et al, 2000). Consequently, bar slip failure is delayed or, in the best case scenario, prevented. Indeed, database findings illustrated in Figure 4-21 show a positive relationship between increasing levels of vertical joint reinforcement and maximum bond stress.

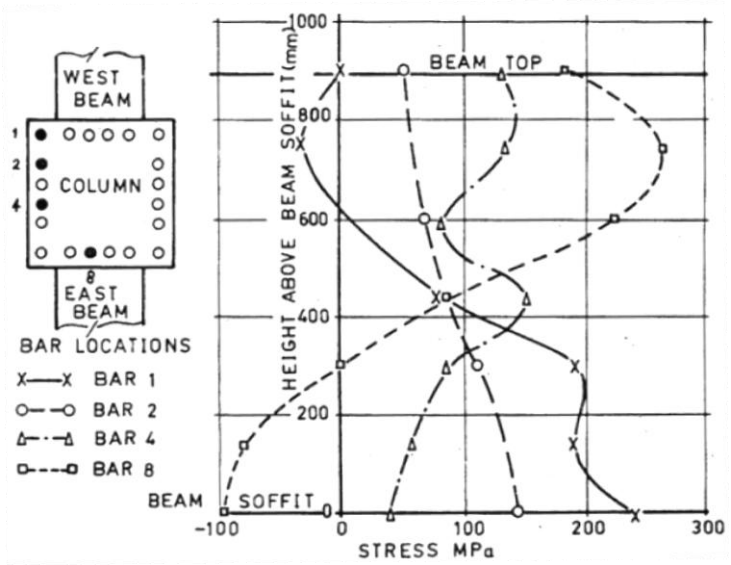

Figure 4-11: *Column bar stress profiles at ductility 6 (Blakeley, Megget & Priestley, 1975)*

Despite these positive findings, column bars are not ideally suited to enhancing bond within adjacent beam bars. Firstly, due to their relatively large size, only a small number of column

bars are required along the column face to provide sufficient vertical shear reinforcement within the joint. As a result, they are often spaced a relatively large distance apart which, as discussed in Section 4.2.3, is undesirable in terms of bond enhancement. Furthermore, because column bars are continuous through the joint, they are all activated in flexure to some extent. While the intermediate bars are activated less than those along the beam face, some elongation in these bars on the tension side of the joint is inevitable. For this reason, the clamping response that retards crack opening is compromised somewhat. In terms of practical implementation, the increasing using of 'drop in' column units incorporating Drossbach ducts for grouting of column bars means that bond improvements by these means is not always possible. The prospects for interior beam bars are worse; as illustrated in Figure 4-11, column bars are generally arranged around the perimeter of the column leaving a central core where beam bars pass through with no passive confinement. Subsequently, the use of dedicated bond enhancing vertical joint reinforcement should be investigated; this is discussed further in Section 4.2.3.

4.1.6 Bar Slip within Interior Joints

Bar slip within interior beam-column joints is not limited only to slotted beams; indeed, it has been observed in monolithic beam-column joints by researchers including Beckingsale (1980), Hakuto et al (1995), and Cheng et al (2000). Such failures can occur within joints whenever insufficient bond capacity exists; this is generally when the conditions assumed during design no longer exist within the joint such as during advanced inelastic displacements. This section discusses the changes in joint conditions caused by inelastic displacements and how these affect the assumptions in Section 4.1.1. The consequences of such failures are also discussed.

During advanced inelastic displacements, the forces within the beam reinforcement on either side of the joint can reach yield or even overstrength in some cases. Consider first the asymmetric beam in Figure 4-12(a) under seismic loading. On the right hand side the top longitudinal reinforcement yields in tension resulting in a crack progressing down the beam-column interface towards the neutral axis of the beam. With assistance from the concrete, the bottom longitudinal reinforcement is able to provide sufficient force to facilitate this yielding. However, because the concrete is acting in compression, any cracks in the beam remaining from the previous tension cycle are closed.

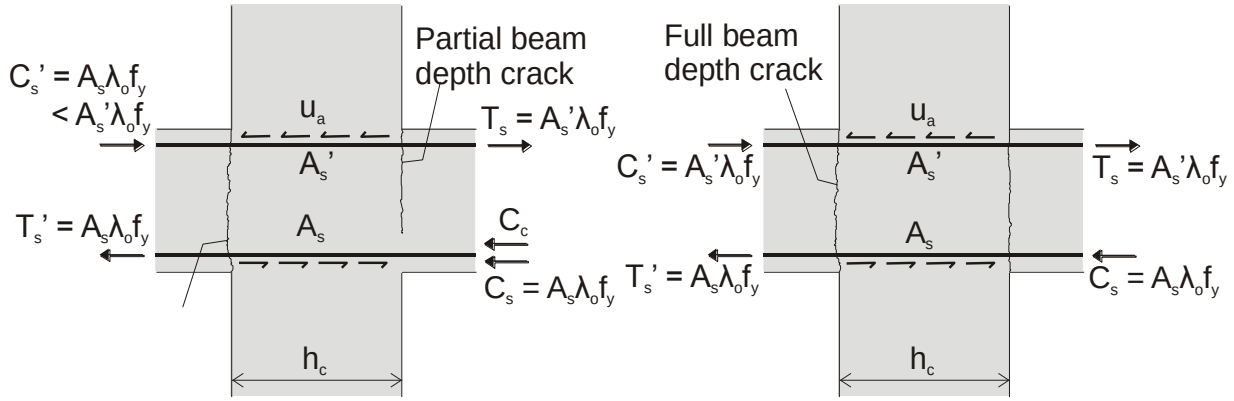

(a) $A_s/A'_s = 0.5$ (b) $A_s/A'_s = 1$

Figure 4-12: *Force magnitude and cracking behaviour after several inelastic cycles*

Meanwhile on the left side of the joint, the smaller bottom reinforcement reaches overstrength in tension and is easily equilibrated by the top steel without assistance from the concrete. Due to its greater area, the top reinforcement is not required to yield to achieve equilibrium (Ruitong & Park, 1987) and tensile plastic strains accumulate in the reinforcement. As a result, cracks formed during previous tension cycles are unable to close (Blakeley et al, 1975; Popov, 1980). Coupled with the newly formed cracks around the bottom steel, cracking is now observed down the full depth of the beam-column interface. As a result, the smaller area of bottom reinforcement is subject to simultaneous tension/compression yielding on either side of the joint while the larger top reinforcement is also subject to forces beyond those allowed for in design according to Section 4.1.1. If this increase in forces is unable to be resisted by spare bond capacity within the joint, bar slip failure will result.

For a symmetric beam as shown in Figure 4-12(b), tension yielding in the top reinforcement causes vertical cracks to open up along the beam-column interface. Meanwhile, due to assistance from the concrete, the bottom reinforcement is not required to yield. Thus cracks developed during previous tension cycles remain open which leads to the cracking pattern shown (Cheng et al, 2000). After many cycles, these permanently open cracks prevent the concrete from contributing and flexural capacity is consequently derived from the steel moment couple alone (Ruitong & Park, 1987). For this reason, tension/compression yielding occurs on either side of the joint and, as with the asymmetric beam described previously, bar slip generally results.

As discussed in Section 3.1.5, another bond degradation mechanism that develops in parallel with that discussed above is strain penetration. This progresses through the column from the tension side thus reducing the effective column depth available to resist the bond demand. Consequently, the bond stress required to achieve equilibrium across the joint is increased.

When the required stress increases above that able to be sustained by the concrete within the joint, bar slip failure will occur.

As discussed in Section 3.3, other factors such as the level of axial load and concrete strength can also affect bond strength. These influences must be considered by the designer.

Bar slip failure can have several consequences for the joint and frame system as a whole. Firstly, because equilibrium can no longer be achieved within the joint, beam bars will pull through the joint from the tension side and become anchored in the compression side of the beam (Leon, 1989; Restrepo, 1992). Evidence for this can be seen in Figure 4-13 taken from Hakuto et al (1995) and relating to a test specimen in which no joint reinforcement was provided. Consequently, equilibrium is compromised and flexural capacity is lost for the system. Furthermore, due to the build up of residual tensile strains in the compression reinforcement, the available curvature ductility in the beam will also be reduced, particularly in plastic hinge regions adjacent to the column face (Hakuto, Park & Tanaka, 1999).

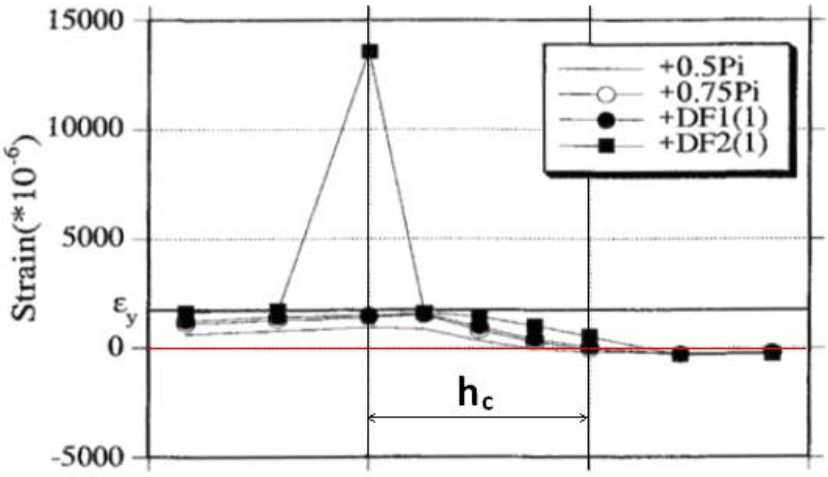

Figure 4-13: *Beam reinforcement in tension throughout joint due to poor bond conditions. Adapted from Hakuto et al (1995)*

At the same time, deformations attributed to bar slip can amount to as much as 50% of the total beam-column deformation (Paulay & Priestley, 1992). Naturally the combination of reduced capacity and increased deformation causes a stiffness degradation within the joint as evidenced in Figure 4-14. This can lead to increased levels of drift for the structure and, subsequently, more severe P-delta actions. Pinching of the hysteresis loop due to bar slip during load reversals is evident in Figure 4-14 and can also be seen in the work of Beckingsale (1980) and Ruitong and Park (1987). As a result, the ability of the system to dissipate seismic energy is compromised (ACI Committee 352, 2002). Bar extension within the joint due to strain penetration can also contribute to beam elongation (Paulay & Priestley,

1992). Differences in slip readings at opposite ends of a beam-column joint, as illustrated in Figure 4-15, support this finding as do similar figures in Hakuto et al (1995).

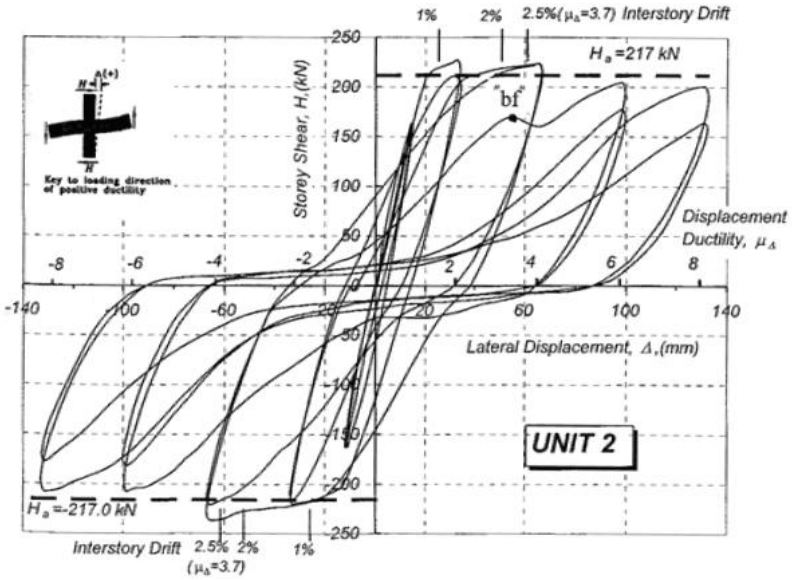

Figure 4-14: *Effect of bar slip failure on hysteretic response (Cheng et al, 2000)*

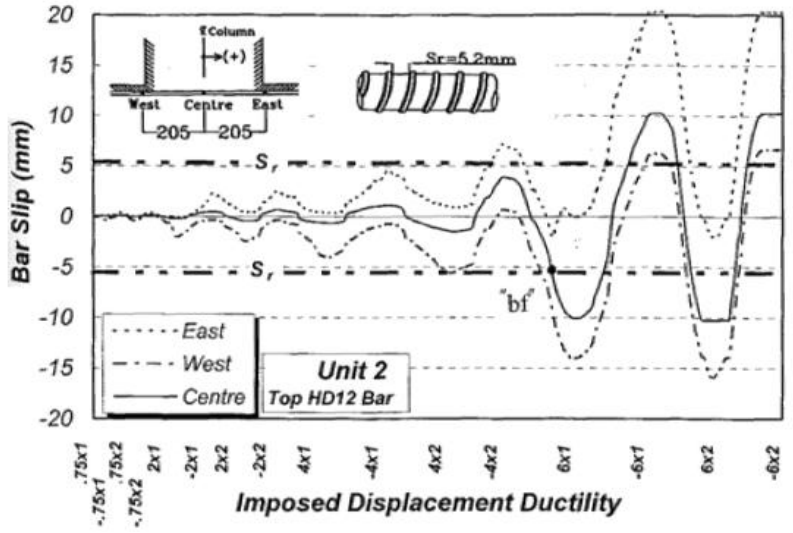

Figure 4-15: *Bar elongation due to strain penetration within joint region (Cheng et al, 2000)*

4.1.7 Findings from Database

Prior to the experimental phase of this research, a database was put together from a collection of past tests on interior beam-column joints. Details of test units in the database are given in Appendix A. The goal was to create a data set from which the effect of various parameters on bond performance within the joints could be determined. These could then be used to help make more informed decisions during the design phase for the test specimens. The main parameters investigated were axial pressure, joint shear reinforcement, and column depth. Bond performance was evaluated in terms of maximum bond stress, u_{max}, within the joint as opposed to maximum average bond stress, u_a, achieved over the entire column depth. This is

because average bond stress values can be misleading. For example, when a large column depth is used, bond demand will not be activated over the entire column and the resulting average bond stress will be decreased. Thus when commenting on tests with different column depths, those with smaller column depths would return relatively high average bond stresses compared with tests incorporating larger column depths. Maximum bond stress can then be related back to average bond stress using the relationships in Section 4.1.1. The findings of this study are presented in the following section and, where applicable, related to code requirements.

Figure 4-16 shows the maximum bond stresses, u_{max}, recorded in the database specimens plotted against axial pressure; average values for each region of similar axial pressure values are also shown in blue. The bond stress values were derived using the maximum beam bar stress gradient within the joint throughout the test. Note that the bond stress values have been normalised by the square-root of the measured concrete compression strength at testing. This is to enable comparison with the maximum bond stress value recommended by Eligehausen (1983) and adopted by Paulay and Priestley (1992) as discussed in Section 4.1.1.

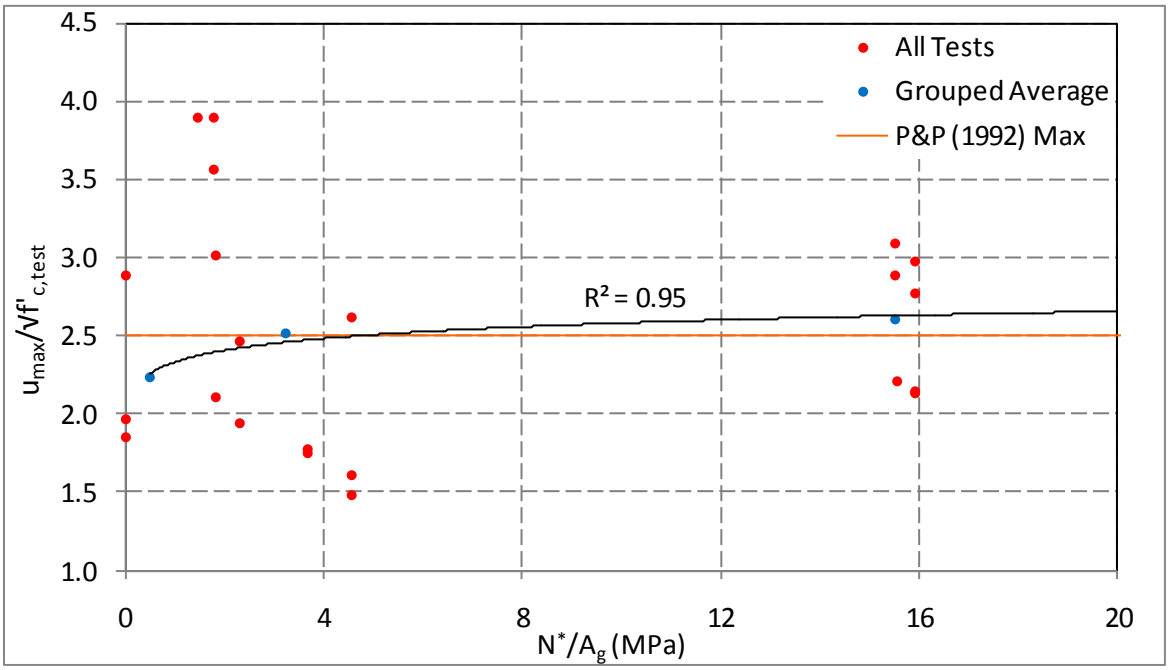

Figure 4-16: *Effect of axial pressure on maximum bond stress*

An overall positive trend is evident with maximum bond stress increasing with axial pressure. Outlying data points must be expected due to the effects of other variables such as beam reinforcement asymmetry and joint reinforcement quantity. The good correlation with a logarithmic function reinforces the material presented in Section 3.3.4 where bond stresses were found to be influenced less as transverse pressure increases. Comparison suggests that

the recommended value of $2.5\sqrt{f_c'}$ is somewhat unconservative for lower axial pressure with over half the data points falling below the line. However, the concrete compressive strength at testing is generally greater than that specified – approximately 20% greater for the database specimens, on average. Thus, when normalised by the square-root of the test strengths, the maximum bond stress values are around 10% lower than those that would arise at the design stage using the specified strength and the comparison improves.

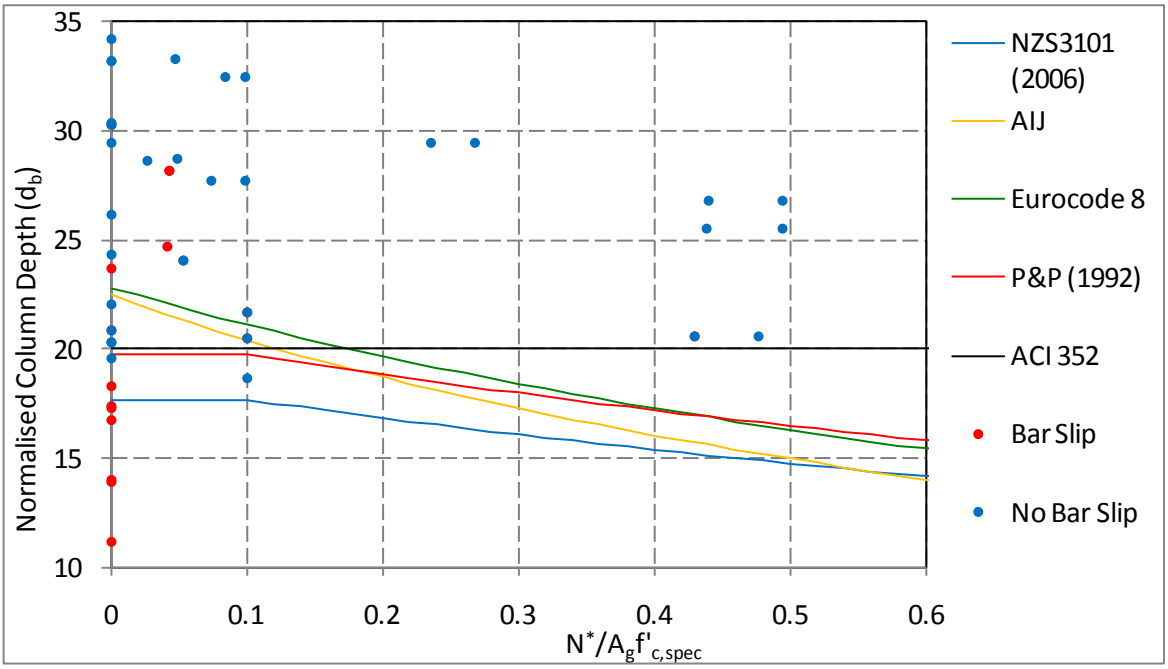

Figure 4-17: *Effect of axial pressure on design and actual bond performance*

It is clear that the NZS3101:2006 recommendations produce the smallest column depths, h_c, for a given beam bar diameter within the realistic range of $N^*/A_g f'_{c,spec}$ up to around 0.5. Unfortunately, only a handful of specimens were tested at such values of axial pressure and therefore no solid conclusions can be drawn. The NZS3101:2006 equation mirrors that of Paulay and Priestley (1992) one but is less conservative; this was discussed briefly in Section 4.1.1. Eurocode and AIJ requirements are approximately 20% more conservative than their New Zealand counterparts for low levels of axial pressure but return similar values at higher levels. The ACI recommendations are the simplest of those considered and do not account for the effects of axial pressure.

Compared with the test results, the recommendations appear to be overly conservative for higher values of axial pressure. This reinforces the discussion in Section 4.1.2 where it was noted that the effects of axial pressure are not fully accounted for in New Zealand recommendations. The NZS3101:2006 equation is unconservative for low values of axial load where numerous occurrences of bar slip are visible above the corresponding required column

depth. Thus the Paulay and Priestley (1992) recommendations will be used as a basis for development of the design equations; these appear suitable for non-zero values of $N^*/A_g f'_{c,spec}$, as will be used in the test specimens.

Beam reinforcement layout can also have an effect on bond performance. Figure 4-18 shows the required column depth according to various codes for different beam reinforcement layouts. Because the reinforcement bias was to the top of the beam in all database specimens, area ratios below one correspond to the top reinforcement while ratios above one correspond to bottom reinforcement. Column depth normalisation was carried out as discussed above except the factor accounting for asymmetric beam reinforcement profiles was replaced with the one corresponding to variation of axial pressure.

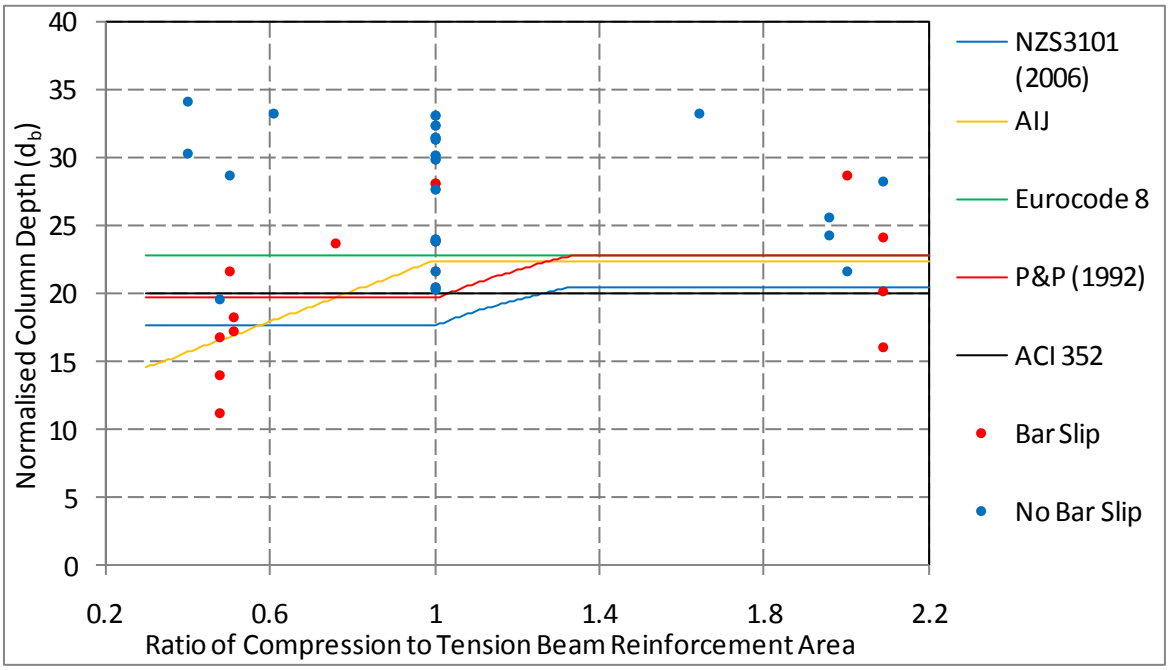

Figure 4-18: *Effect of beam reinforcement layout on design and actual bond performance*

Once again, the New Zealand based recommendations mirror one another and are the least conservative for lower reinforcement area ratios compared with other codes. The Eurocode and ACI recommendations do not allow for the effect of beam reinforcement asymmetry while the New Zealand and Japanese recommendations do but to different extents. The various code recommendations differ by 30% for the larger area of reinforcement, decreasing to approximately 15% for the smaller area. As the chosen basis for design, the Paulay and Priestley (1992) recommendations appear suitable with only two bar slip occurrences at $\beta = 2$, as is typical for a slotted beam. Bar slip occurrences in the top reinforcement are not as critical because bond requirements here generally do not govern for slotted beams.

Figure 4-19 illustrates the variation in maximum beam reinforcement stresses at the column face with changing reinforcement area ratio; the plotted stress values are averages of those from the specimens in the database. The horizontal orange line in the figure corresponds to the material overstrength factor, λ_m, for typical reinforcing steel – because specified yield strength is the 5th percentile strength for that grade of bar, the actual yield strength is likely to be somewhat higher. Taken to be 1.15 from Paulay and Priestley (1992), λ_m accounts for this variability. Combined with the overstrength factor to account for strain hardening, the characteristic overstrength factor, λ_o, is obtained – i.e. 1.25 for Grade 300 reinforcement and 1.4 for Grade 500.

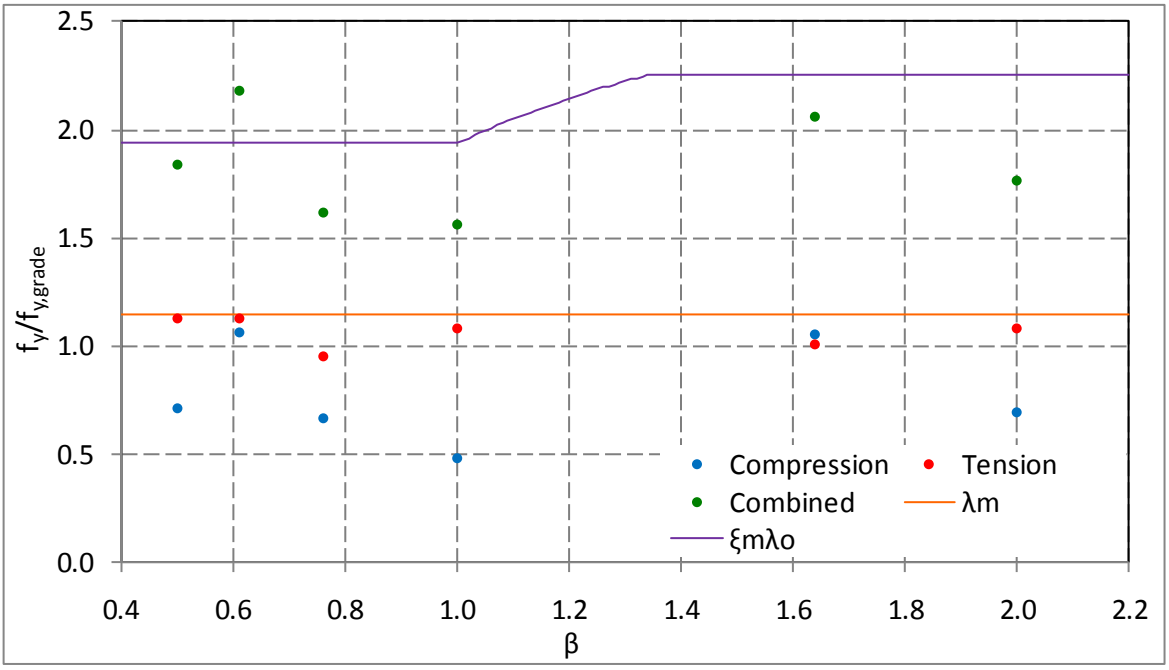

Figure 4-19: *Maximum reinforcement activation at column face as a function of reinforcement asymmetry*

As discussed in Sections 4.1.3 and 4.1.4, the maximum reinforcement demand is obtained on the tension side of the column and is generally taken to be overstrength. However, on inspection of Figure 4-19, it is clear that only the material overstrength is being achieved; i.e. strain hardening to reach full overstrength is not allowed to occur. This is because, upon yielding in tension, the bar elongates significantly before strain hardening begins – on the order of 2% for larger deformed bars according to the material properties presented in Section 5.2.5. During this period, which occurs over several inelastic cycles, strain penetration damages the concrete in the immediate area, rendering it ineffective at providing bond as discussed in Section 3.1.5. Thus local strain within the reinforcement cannot increase and, consequently, strain hardening cannot occur. The compression demands within the

reinforcement are consistently around the $0.7f_y$ figure suggested by Paulay and Priestley (1992) regardless of reinforcement area ratio.

When the average compression and tension demands are combined, the result is the total percentage of specified yield that must be resisted across the joint. In design, this is accounted for by the factor ξ_m as discussed in Sections 4.1.3 and 4.1.4. Combined with the characteristic overstrength factor, λ_o, the equivalent design value is obtained; this is also plotted in Figure 4-19. It can be seen that the degree of reinforcement activation in the tests is consistently below that allowed for in the design equations. While this indicates a suitable conservatism for monolithic joints, the design value is too conservative for a slotted joint as top reinforcement demand is driven primarily by stress in the bottom reinforcement due to a lack of concrete contribution at the beam soffit. This result does not apply to the bottom reinforcement where overstrength demands are activated on both sides of the joint simultaneously.

Although not accounted for in any of the selected code recommendations, joint reinforcement is another important factor to consider in investigation of bond performance. Figure 4-20 shows the relationship between the amount of horizontal joint reinforcement and maximum bond stress. It is clear that under-reinforced joints exhibit lower maximum bond stresses; this is likely due to premature breakdown of the truss mechanism, as discussed in Section 4.4.2, resulting in joint deterioration and corresponding degradation of bond conditions. Similarly, over-reinforced joints do not provide any appreciable increase in bond stress, as illustrated by the strong correlation with a logarithmic function.

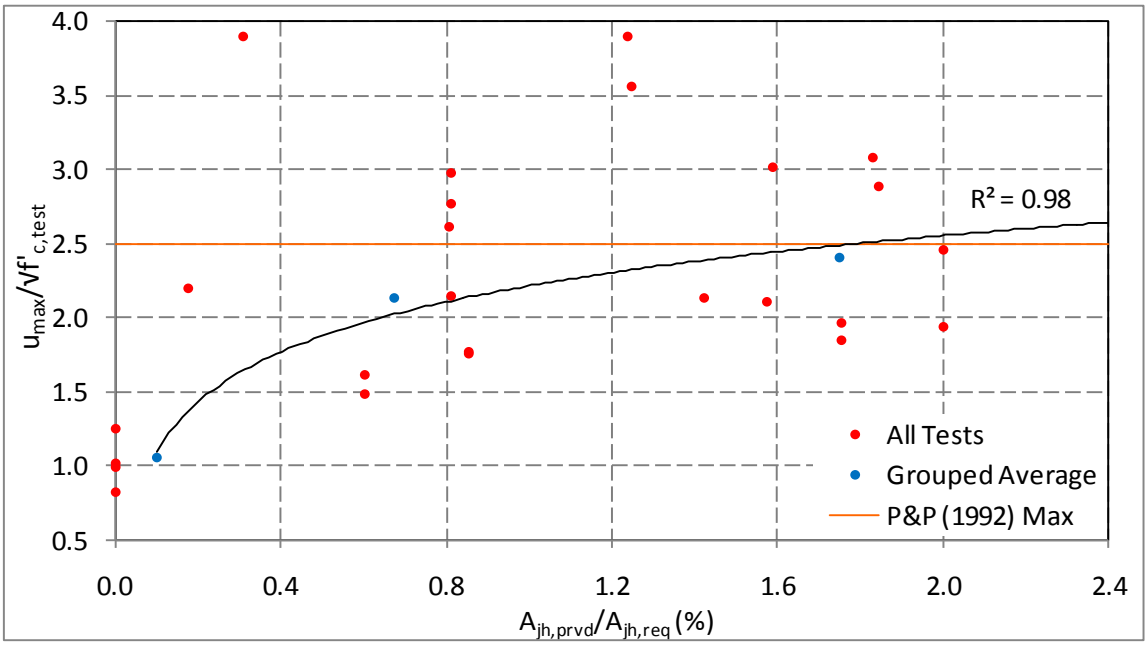

Figure 4-20: *Effect of horizontal joint reinforcement on maximum bond stress*

Note that $A_{jh,prvd}$ is the area of horizontal joint reinforcement provided in the test specimen and only includes stirrups or hoops that cross the entire joint. Furthermore, stirrup sets within $s/2$ – where s is the typical stirrup spacing within the joint – of the beam bars are excluded from the area count as discussed in Section 4.5.1. Similarly, $A_{jh,req}$ is the area of horizontal joint reinforcement required in accordance with NZS3101:2006 and is derived from the theoretical overstrength capacity of the beams.

A similar trend can be observed for the effect of vertical joint reinforcement on maximum bond stress, as illustrated in Figure 4-21. Under-reinforced joints exhibit a lower maximum bond stress due to a lack of passive confinement. This allows splitting cracks to form readily along the beam bars on the tension side of joint as discussed in Section 4.1.1 thus negatively affecting the bond performance of this region during subsequent reverse cycles. Joints with less shear reinforcement generally deteriorate more rapidly and this has been linked to decreased bond performance as discussed in Section 4.1.5. Similarly, over-reinforced joints do not provide any appreciable increase in bond stress. As discussed in Section 3.3.4, this is because bar pullout failure is an upper bound failure mechanism. Thus a well reinforced joint appears sufficient to ensure maximum bond stresses on the order of $2.5\sqrt{f_c'}$ can be achieved.

As per NZS3101:2006, $A_{jv,prvd}$ was taken as the total area of column bars excluding those on the beam faces; i.e. bars contributing predominantly to the column flexural capacity were ignored. Supplementary vertical stirrups were not present in any specimens. $A_{jv,req}$ was calculated using the same process as outlined above but with the corresponding vertical equilibrium equations.

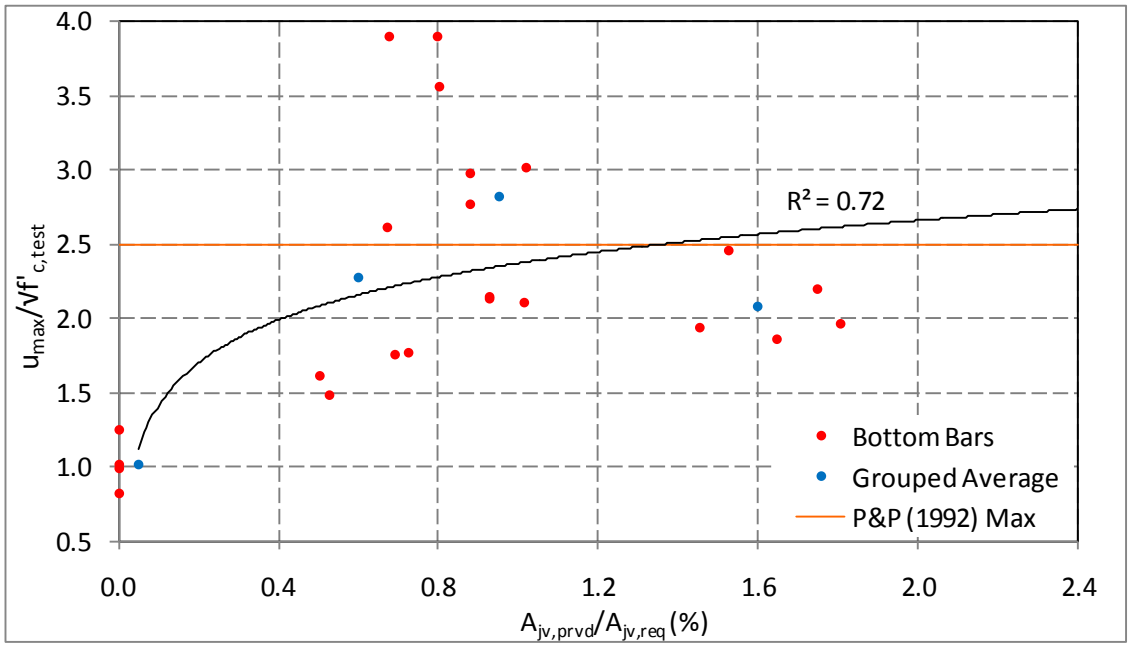

Figure 4-21: *Effect of vertical joint reinforcement on maximum bond stress*

4.2 Bond within Slotted Interior Joints

Bond conditions within slotted beam joints are much less favourable than those in monolithic joints. As outlined in Section 1.2, the larger column depths required to overcome increased bond demand of the bottom beam reinforcement within interior joints is one of the major issues standing between slotted beams and industry acceptance. The key to solving this problem lies in understanding the bond mechanics within slotted beam joints and developing solutions to the issues presented.

However, as evidenced in Section 2.2, previous testing in this area is limited to only a handful of reduced scale specimens. While these tests are a valuable source of information, the small amount of data available necessitates that the problem also be approached from first principles. Once these are understood, the findings presented previously in this thesis can be applied to the problem. The overall result is a much more informed design for the test specimens.

4.2.1 Overview of Bond Requirements

Bottom reinforcement in a slotted beam is subject to much greater bond requirements within the beam-column joint when compared to a monolithic system. Firstly consider the bottom reinforcement within the slotted joint illustrated in Figure 4-22. Due to the presence of the slot there is no concrete compression at the soffit of the right beam; the entire force from the beam moment couple must therefore be transferred into the joint through this reinforcement. Secondly, consider that the beam is asymmetrically reinforced with a strength bias at the top of approximately two-to-one. As discussed in Section 4.1.4, this ensures the smaller bottom reinforcement reaches overstrength during tension cycles. Furthermore, coupled with the lack of assistance from the concrete at the beam soffit, the compression reinforcement is also required to reach overstrength despite the small flexural contribution due to prying in the top hinge. The net result is simultaneous overstrength tension/compression on either side of the joint (Au, 2010; Leslie, 2010) – a scenario only encountered in monolithic joints during advanced inelastic loading.

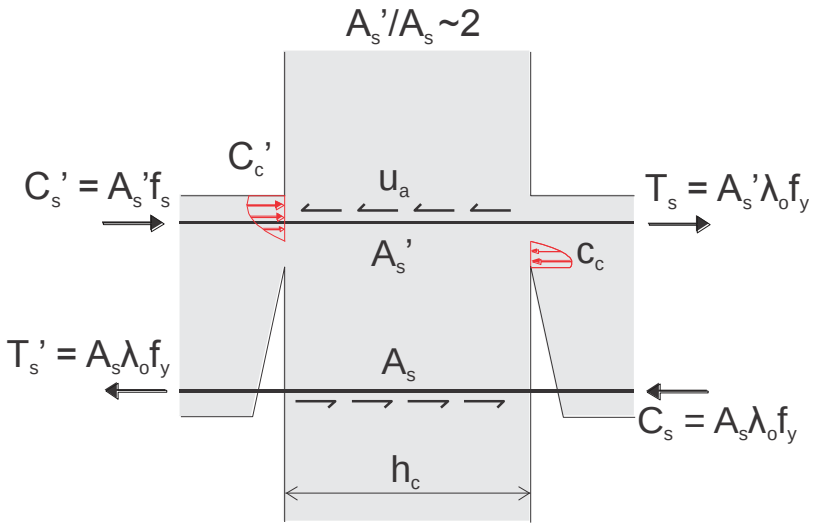

Figure 4-22: *Force magnitudes within a slotted beam joint*

The lack of confinement from adjacent beams produces another potential failure mechanism in which strain penetration within the joint can result in concrete cone pullout failure as discussed in Sections 3.1.5 and 3.4.1. This is illustrated in Figure 4-23(a) where the dashed lines represent the concrete cone pulled out by the bar and was observed in testing by Au (2010) as discussed in Section 2.2.3. Therefore, in order to ensure sufficient bond for the bottom beam reinforcement and prevent cone pullout failure, column depths for use with slotted beams are required to be larger than those used for equivalent monolithic systems; exactly how much larger is the question that needs to be answered before slotted beams can be used in practice.

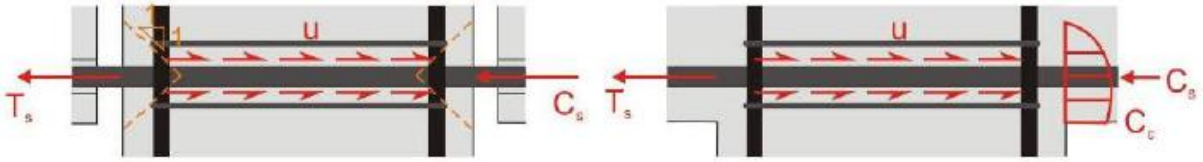

(a) Slotted (b) Monolithic

Figure 4-23: *Bond conditions within beam-column joint incorporating monolithic and slotted beams (Au, 2010)*

Bond requirements must also be met for the top beam reinforcement. Fortunately, these requirements are similar to those for the larger area of reinforcement within an asymmetric beam as discussed in Section 4.1.4. However, given the required strength bias and issues with congestion within the hinge, it is desirable to use fewer, larger bars. Combined with the reduced bond performance due to the top bar effect as discussed in Section 3.3.3, the bond requirements for this reinforcement must still be considered.

4.2.2 Forensic Analysis of Au (2010) Specimens

Having conducted two tests on interior beam-column joints incorporating slotted beam systems, one in which bar slip failure occurred, the data set created by Au (2010) is an

excellent source of information regarding the bond performance of such systems. Prior to the testing phase of this research, it was the only well documented source available. This section describes and comments on the process used by Au (2010) to determine the column depth for each of these two specimens.

As discussed in Section 2.2.3, the initial test by Au (2010), SB2, resulted in bar slip failure due to an insufficient column depth. In order to determine the required column depth for successful use of a slotted beam, Au (2010) used the Paulay and Priestley (1992) bond equation as discussed in Section 4.1.1. Assuming the standard value for the modification factors ξ_p, ξ_t, and ξ_f as given in Section 4.1.2 and working in terms of the effective column depth, h'_c, which was assumed to be $0.8h_c$, the resulting equation is given below:

$$\frac{d_b}{h'_c} \leq \frac{4u_a}{\xi_m \lambda_o f_y} \qquad \text{Equation 4-13}$$

Note that Au (2010) also applied a 5% safety reduction factor to his column depth equation. The reasoning behind this is not explicitly stated but it is likely to be similar to the strength reduction factors typically used in design. In the case of a slotted beam, where cone pullout failure can occur, the $h'_c = 0.8h_c$ assumption is only reasonable given such a failure does not reduce the effective column depth further. As discussed in Section 3.4.1, this can be ensured by providing a suitable reinforcement layout such that the cone pullout depth is limited. However, before the test of specimen SB2, Au (2010) was unaware of this failure mechanism and, consequently, did not account for its occurrence. Incidentally, the cone failure which occurred reduced the effective column depth to around $0.7h_c$ – less than that in the design assumptions. This oversight contributed to the bar slip failure observed in specimen SB2, but was allowed for in the design of specimen SB3 as discussed later in this section.

In his design process, Au (2010) assumed a material overstrength factor, λ_o, of 1.25, the standard value for Grade 300 reinforcement. This proved to be unconservative and, as further testing revealed, values of 1.3 and 1.4 were more appropriate for positive and negative moments, respectively. These increased overstrength factors are due to the larger top longitudinal reinforcement and lack of bottom concrete compression combining to activate high stresses in the bottom longitudinal reinforcement. Because overstrength occurs simultaneously on either side of the joint, a combined overstrength factor of 1.35 seems reasonable. However, analytical studies by Muir, Bull, Au, and Pampanin (2010) suggest the values could be as low as 1.22 and 1.25 thus highlighting the care required in selection of an appropriate value and the need for experimental confirmation.

Envisaging similar conditions within the joint core compared with a monolithic joint, Au (2010) adopted a maximum local bond stress of $2.5\sqrt{f_c'}$. This seems reasonable given that maximum local bond stress occurs within the joint core and the conditions found here are comparable between a monolithic and slotted joint. However, assuming the same bond stress distribution as proposed by Paulay and Priestley (1992) for a monolithic joint, as shown in Figure 4-2, was subsequently found to be unconservative. This resulted in an average bond stress of $1.68\sqrt{f_c'}$ which is approximately 12% greater than the maximum measured average bond stress before bar slip failure of $1.48\sqrt{f_c'}$ as shown in Figure 4-24.

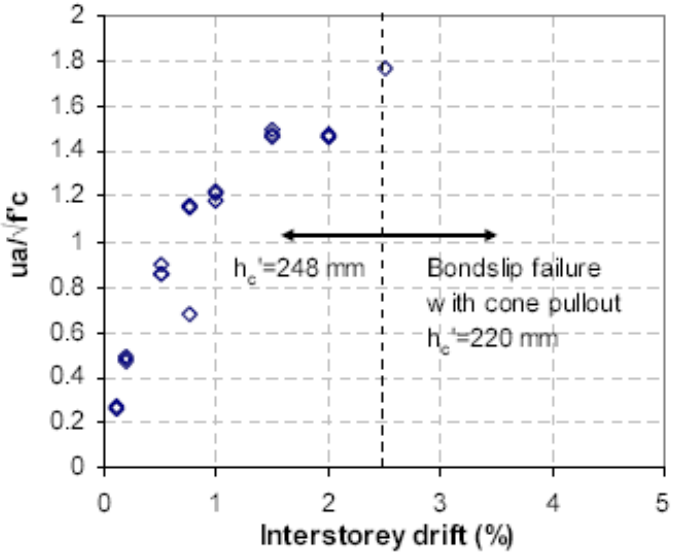

Figure 4-24: *Average bond stresses observed during testing of SB2 (Au, 2010)*

Figure 4-2 shows the reinforcement strain profile corresponding to the assumed bond stress distribution adopted by Paulay and Priestley (1992). This distribution assumes that reinforcement remains within the elastic range on the compression side of the joint while reaching overstrength on the tension side. However, as shown in Figure 4-25, strain in the bottom compression reinforcement consistently exceeds yield even within the specified $0.8h_c$ boundary and at drift levels as low as 1.5%. One of the primary reasons for this excessive strain penetration is due to the simultaneous tension/compression yielding on either side of the joint, and suggests a reduced h'_c should be adopted. Additionally, the lack of concrete compression from the adjacent beam significantly reduces the confinement of this region. As discussed in Section 3.3.4, confinement is closely related to bond performance and, without it, this region of the joint was inferior compared with the monolithic joint from which its performance was assumed. Neglecting these key differences was, in all likelihood, one of the primary reasons why specimen SB2 failed through bar slip.

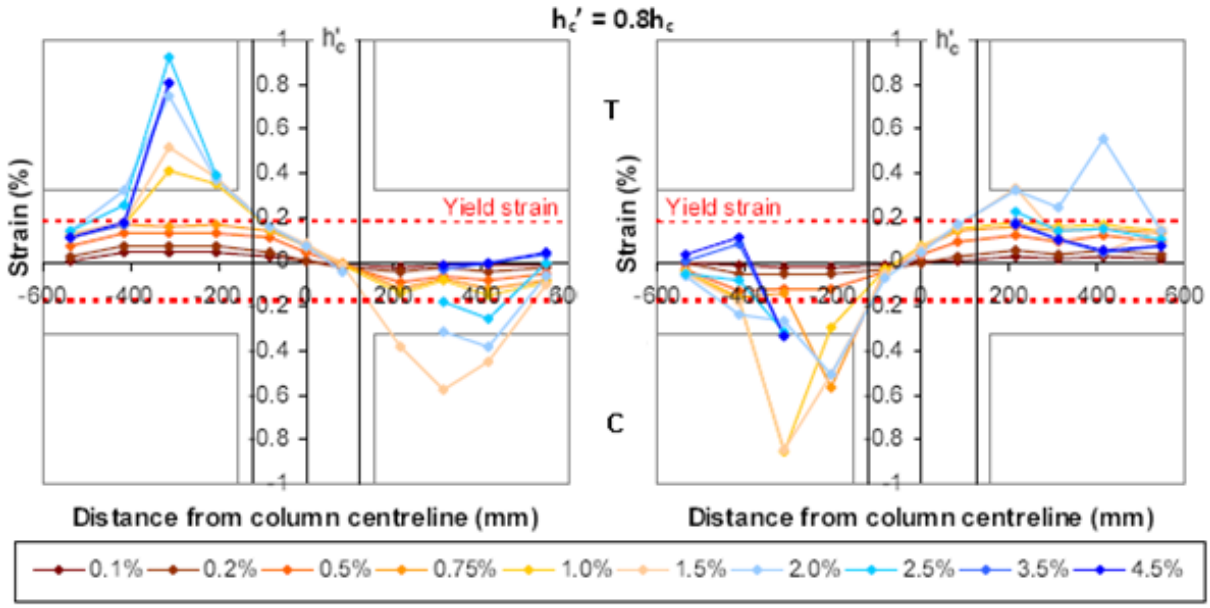

(a) Positive drifts (b) Negative drifts

Figure 4-25: *Bottom reinforcement strain profile with adopted effective column depth for specimen SB2. Adapted from Au (2010)*

The only factor to be modified by Au (2010) for bond calculations in the first test, SB2, was ξ_m; the factor accounting for the degree of reinforcement activation across the joint. This was revised from the monolithic value of 1.55 to 2 in order to reflect overstrength actions occurring on both sides of the joint simultaneously. Figure 4-25 shows inelastic strains occurring in the bottom reinforcement at the column face during drifts of 1 – 1.5%. This observation supports the decision to adopt an increased ξ_m value, and the theory leading to this decision. Combining all of the above into a rearrangement of Equation 4-13, the column depth adopted by Au (2010) for test SB2 is obtained in Equation 4-14:

$$h_c \geq \frac{\xi_m \lambda_o f_y}{4u_a}\frac{d_b}{0.8} = \frac{2 \times 1.25 \times 300 \times 12}{4 \times 1.675 \times \sqrt{30} \times 0.8} = 25.5d_b \approx 310\ mm \qquad \text{Equation 4-14}$$

This is approximately 33% less than the revised column depth obtained using the refinements discussed above and shown in Equation 4-15:

$$h_c > \frac{2 \times 1.3 \times 300 \times 12}{4 \times 1.48 \times \sqrt{30} \times 0.7} = 34.3d_b \approx 410\ \text{mm} \qquad \text{Equation 4-15}$$

In order to prevent bar slip failure from occurring again in the testing of SB3, Au (2010) increased the concrete strength from 30 to 40 MPa and used more conservative assumptions in Equation 4-13 to determine an appropriate column depth. Firstly, to account for the possibility of a cone pullout failure reducing the effective column depth beyond the standard $0.8h_c$ limit, Au (2010) imposed a further limit on h'_c as illustrated in Figure 4-26.

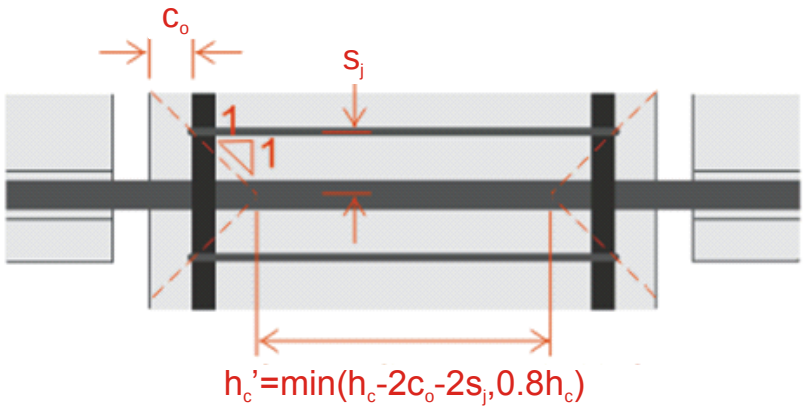

Figure 4-26: *Effective column depth for bond calculations. Adapted from Au (2010)*

Additional vertical stirrups were also installed in the cover concrete and horizontal joint stirrups were placed closer to the bottom beam bars in an attempt to reduce the extent of any cone pullout failure that occurred. Au (2010) assumed that these measures would be sufficient to prevent or minimise cone formation thus reducing strain penetration and increasing the effective column depth. However, this did not prove correct and, as illustrated in Figure 4-27, yield penetration reduced the effective column depth to around $0.75h_c$ by 2% drift. Because this joint did not experience bar slip due to conservative assumptions relating to other aspects of design, this value is suitable for a design basis.

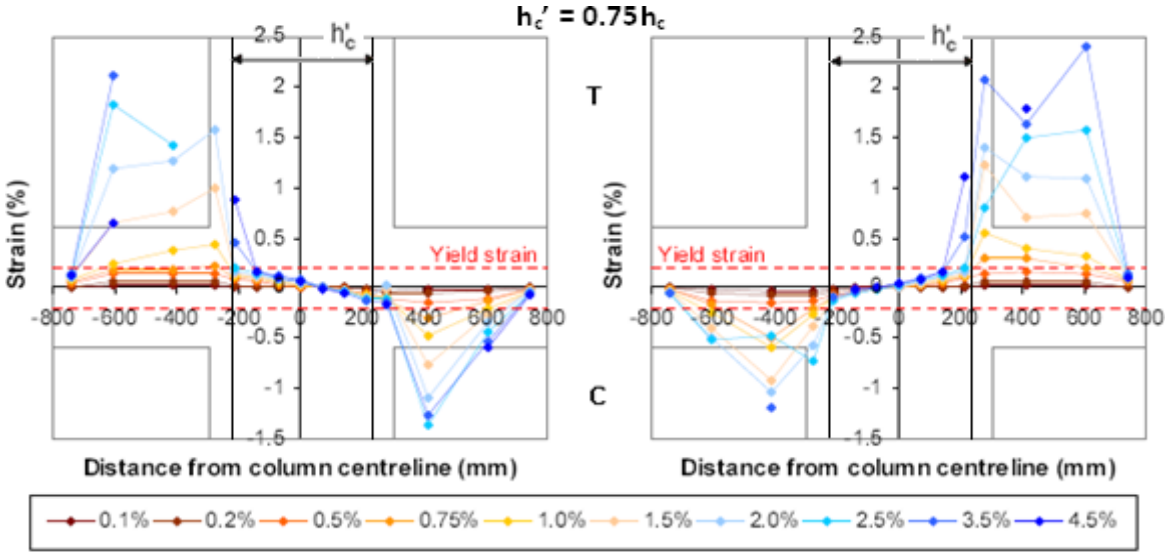

(a) Positive drifts (b) Negative drifts

Figure 4-27: *Bottom reinforcement strain profile with revised effective column depth for specimen SB3. Adapted from Au (2010)*

Given the reduced value of h'_c, the requirements for cone pullout failure discussed above are unlikely to govern. Referring to Figure 4-26 and assuming a sensible cover thickness, c_o, of 30 mm and reduced joint stirrup spacing, s_j, immediately adjacent to the beam bars of 20 mm, the $0.75h_c$ limit governs for column depths greater than 410 mm. Given the smallest practical beam bar size of 20 mm, such a column depth would not provide sufficient bond for a slotted

beam system. In other words, the $0.75h_c$ limit governs for the majority of slotted beam applications even when allowances are made for cone formation.

The overstrength factor was also increased to the very conservative value of 1.5 in an attempt to avoid another bar pullout failure. Similarly, the average bond stress was reduced from 1.68 to $1.2\sqrt{f_c'}$ to reflect the less favourable bond conditions within a slotted beam joint. This revised value corresponds to u_a/u_{max} = 0.48 which is approximately 28% more conservative than the value of u_a/u_{max} = 0.67 adopted by Paulay and Priestley (1992) for monolithic joints as discussed in Section 4.1.1. However, while effective at preventing bar slip failure, the column depth presented in Equation 4-16 was excessive to the extent that horizontal joint reinforcement was not activated until a drift of 3.5% as discussed in Section 4.5.1. Given architectural and economic restraints, such a column depth might be unacceptable in current industry practice.

$$h_c > \frac{\xi_m \lambda_o f_y}{4u_a}\frac{d_b}{0.8} = \frac{2 \times 1.5 \times 300 \times 16}{4 \times 1.2 \times \sqrt{40} \times 0.8} = 37d_b \approx 600 \text{ mm} \qquad \text{Equation 4-16}$$

As shown in Figure 4-28(a), the measured overstrength factor never exceeded 1.4 during the test of specimen SB3, and was in fact closer to 1.35 as shown in Figure 4-29. Given bar slip failure and significant joint deterioration did not occur in this test, the overstrength values achieved here should be an upper bound and are thus suitable for design. For this reason, the back-calculation to obtain the bond stresses in Figure 4-28(b) overestimated the maximum value at around $1.17\sqrt{f'_c}$. Adopting a more appropriate overstrength factor of 1.35, the maximum average bond stress is found to be around $1.1\sqrt{f_c'}$, or approximately $0.44u_a/u_{max}$. While similar to the assumed bond stress value, this is unrealistically low because the entire core of the column was not activated due to the excessively large column depth.

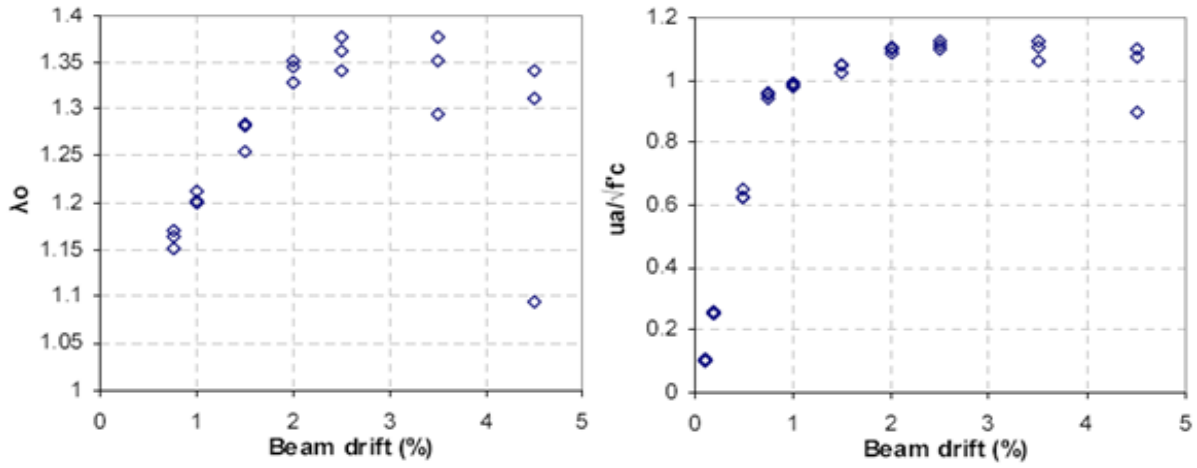

(a) Overstrength factor (b) Average bond stress

Figure 4-28: *Experimental bond and overstrength values for specimen SB3 (Au, 2010)*

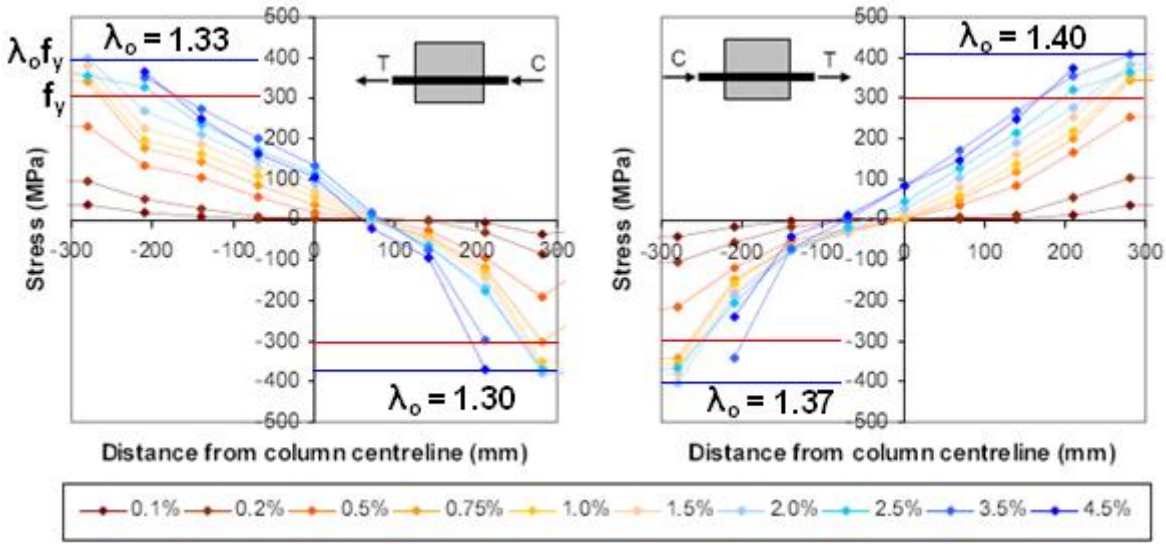

(a) Positive drifts (b) Negative drifts

Figure 4-29: *Bottom reinforcement stress profile for specimen SB3. Adapted from Au (2010)*

Au (2010) then proposed a revised column depth based on the factors discussed above. Firstly, a more probably average bond stress value of $1.4\sqrt{f'_c}$ (u_a/u_{max} = 0.56) was assumed. This is equal to the maximum average bond stress achieved during the testing of SB2 with a 5% safety reduction factor applied as discussed previously. The overstrength factor was conservatively taken as 1.4 as discussed previously and h'_c remained unchanged at $0.8h_c$. The resulting column depth, presented in Equation 4-17, was found to be approximately 25% less than that provided:

$$h_c > \frac{\xi_m \lambda_o f_y}{4u_a}\frac{d_b}{0.8} = \frac{2 \times 1.4 \times 300 \times 16}{4 \times 1.4 \times \sqrt{40}\text{x}0.8} = 29.6\text{d}_\text{b} \approx 475 \text{ mm} \qquad \text{Equation 4-17}$$

4.2.3 Supplementary Vertical Stirrups within Joint

Based on the findings of Sections 4.1.5 and 4.1.7, bond performance within a joint can be influenced by vertical joint reinforcement. While column reinforcement fulfils this role to some extent, it is not ideally suited to the task as discussed in Section 4.1.5 – as such, the use of supplementary vertical stirrups to enhance bond performance is proposed. If these measures prove to be successful, the column depth required to achieve sufficient anchorage in the beam bars will be reduced. This section discusses how such reinforcement should be detailed and attempts to quantify a suitable amount.

Past tests incorporating supplementary vertical stirrups within the joint are almost non-existent. This is because column bars alone generally fulfil vertical joint reinforcement criteria. While Au (2010) did provide several supplementary vertical stirrups in a test incorporating slotted beams, these were not strain gauged or reported on. Furthermore, there

was no control specimen with which to compare the effects of adding supplementary vertical stirrups. Relevant testing is thus limited to dedicated specimens that do not emulate the conditions within beam-column joints.

In order to realise the full bond enhancing potential of supplementary vertical stirrups, these must meet certain requirements. First and foremost, the stirrups must remain elastic as discussed in Section 4.1.5 such that the clamping response is as stiff as possible. As such, the vertical stirrups should not extend beyond the joint panel to ensure they are not activated in flexure along with the column bars. Secondly, the stirrups must have sufficient anchorage such that they can be activated to high elastic strains with minimal slip. This is to ensure a stiff response such that the degree of crack opening to achieve clamping action is minimised. Given the stirrups are to remain within the joint panel this necessitates the use of hoops or hooked stirrup ties to achieve sufficient anchorage.

Experimental testing by Plizzari et al (1998) indicates that individual stirrups hooked around each beam bar, as opposed to hoop stirrups, is the most effective approach in terms of maximising bond performance. Similar findings were observed by Engstrom et al (1998) and Ogura et al (2008). The comparison between longitudinal bars confined by each type of stirrup is illustrated in Figure 4-30 and Figure 4-31 where confinement index, Ω, is plotted against an index of maximum bond stress, u_{max}/f_c'. Confinement index, the measure used by Plizzari et al (1998) to define the degree of confinement provided by the stirrups, is given in Equation 4-18. Note that the variables have been changed from the form in which they appear in the text.

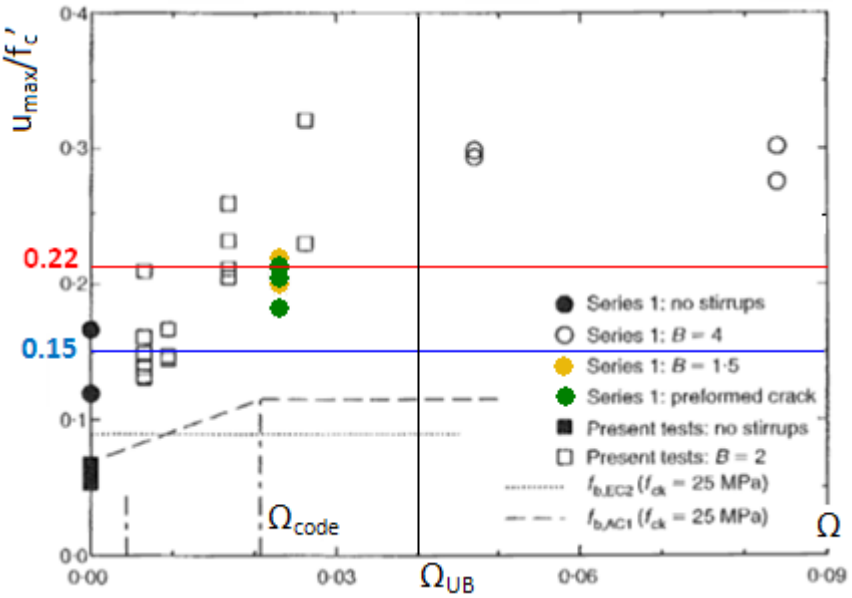

Figure 4-30: *Influence of confinement index on maximum bond stress within corner bars. Adapted from Plizzari et al (1998)*

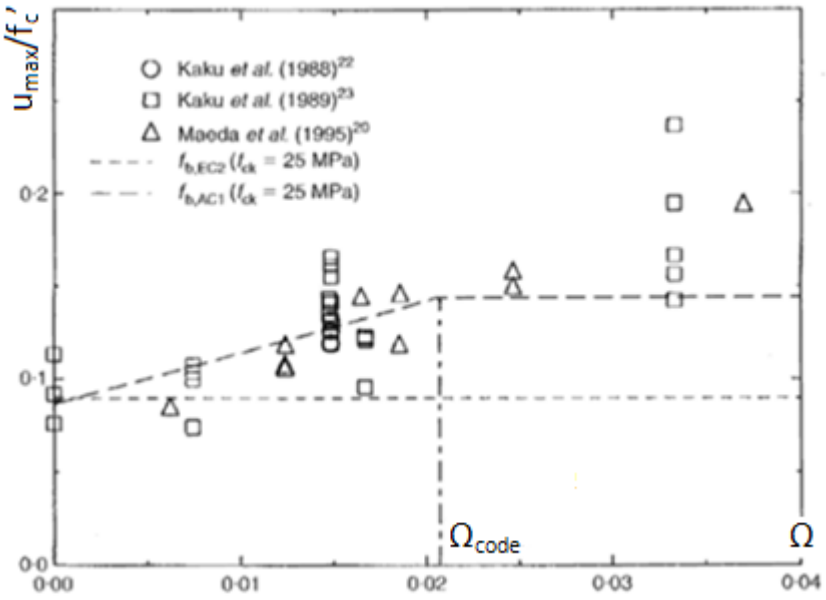

Figure 4-31: *Influence of confinement index on maximum bond stress within intermediate bars. Adapted from Plizzari et al (1998)*

$$\Omega = \frac{n_{st} A_{st}}{n_b A^*} = \frac{n_{st} \pi d_{st}^2}{4 n_b d_b s} \qquad \text{Equation 4-18}$$

Where A_{st} is the cross-sectional area of stirrup legs crossing the bond interface and A^* is the projected area of the bonded bar onto the bond plane. The number of stirrups at each location is represented by the term n_{st} while the spacing of each stirrup set along the bonded bar is given by s. Finally, n_b corresponds to the number of bonded bars reliant on the stirrups for confinement. This is illustrated in Figure 4-32.

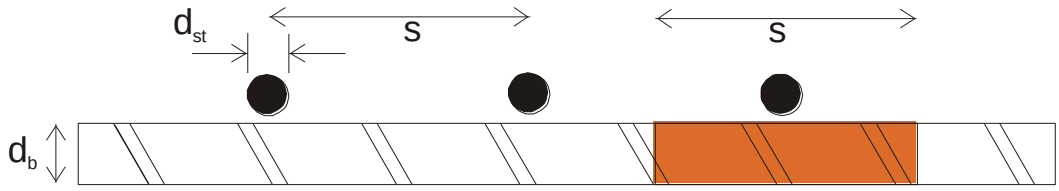

Figure 4-32: *Confinement index parameters*

While a positive relationship exists for both intermediate and corner bars confined by hoop stirrups, the latter clearly achieves up to 50% higher bond stresses. This can be explained by the effectiveness of confinement provided by each type of stirrup and the maximum bond stresses that can subsequently be achieved. As illustrated in Figure 4-33, maximum radial stress within concrete surrounding the bonded bar is compared between corner and inner bars. Based on the concrete stress profiles around each bar type, it is clear that corner bars are subject to more confinement with peaks visible in the vertical, horizontal, and diagonal planes reflecting the corner stirrup layout. Conversely, the stress profile around the inner bar only peaks in the horizontal direction reflecting the stirrups presence in the same plane.

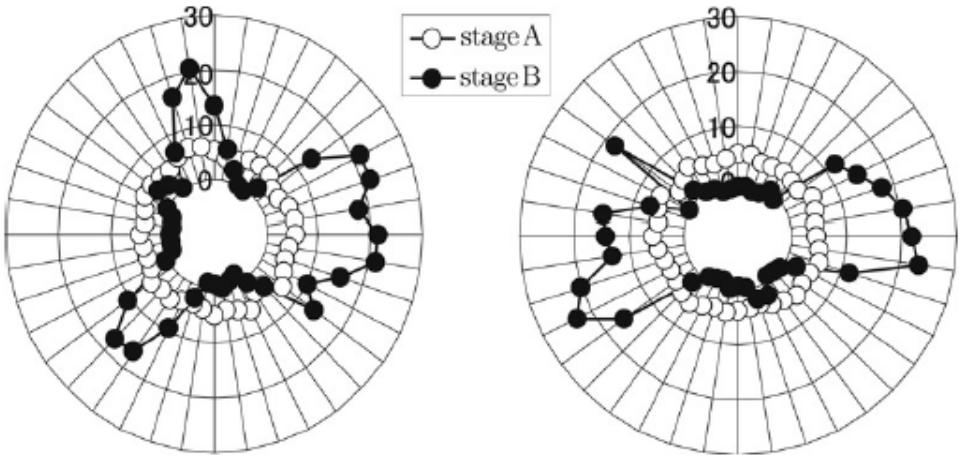

(a) Corner bar (b) Inner bar

Figure 4-33: *Influence of stirrup type on radial stress in concrete surrounding bonded bar (Ogura et al, 2008)*

These results must be used with care when applying to bond enhancement within beam-column joints. As shown in Figure 4-30, the ratio between the net area of concrete and primary bars, *B*, also has an influence on the degree of bond enhancement due to transverse reinforcement. This ratio, defined in Equation 4-19, is an indicator of congestion and how much concrete must be damaged in order for cracks to propagate between individual reinforcement bars such that a continuous splitting crack causing failure results. Note that the variables have been changed from the form in which they appear in the text.

$$B = \frac{(b - n_b d_b)s}{n_b d_b s} \qquad \text{Equation 4-19}$$

Where b is the section width and the other variables are as for Ω. Given a typical B value of around 3 for the beam bars within a joint, an upper bound bond stress index of approximately 0.28 appears reasonable as shown in Figure 4-30. However, considering column and horizontal joint reinforcement, the joint becomes more congested and B decreases. As such, an upper bound bond stress index closer to $u_{max}/f_c' = 0.22$, corresponding to B on the order of 1.5 – 2 is more appropriate. Assuming a conservative lower bound bond stress index of $u_{max}/f_c' = 0.15$, based on the results of specimens in which no stirrups were provided, properly detailed vertical stirrups generate bond enhancement on the order of 45%.

As shown in Figure 4-30, such enhancement can be achieved at a confinement index on the order of 0.04; this value is marked in Figure 4-30 by the Ω_{UB} line. Further increases to Ω beyond this level are ineffective; this is in agreement with theory discussed in Sections 3.3.4 and 4.1.7. Figure 3-18 supports this observation although the upper bound value for Ω is closer to 0.06. However, this increased value is likely due to the transverse reinforcement

being some distance away from the bonded bar such that the in-plane confinement it provides is less effective – in the tests by Plizzari et al (1998), the stirrups were placed immediately adjacent to the bonded bars as would be the case within a beam-column joint. Furthermore, Eligehausen et al (1983) used larger stirrups at a greater spacing – this is not conducive to good bond performance as noted by Plizzari et al (1998) who recommend the use of smaller bars with reduced spacing such that splitting cracks between stirrup sets is limited. For this reason, the upper bound confinement index will be taken as 0.04 for design purposes. In terms of detailing, this can be provided by hooked R10 stirrup legs at 100 mm centres within the joint for each D20 beam bar.

The 45% bond enhancement determined above is not directly applicable to beam-column joints. Because this value was sourced from monolithic pullout tests, it must be further reduced to account for the poorer bond performance expected under cyclic loading. Figure 4-34 shows the effect of loading type on normalised average bond stress for specimens with excessive passive confinement in the form of transverse stirrups; these results are from the testing of Viwathanatepa et al (1979) as discussed in Section 3.4.1. Because bond performance is unaffected at such high Ω values, as discussed previously, and all other variables are unchanged, these results allow a good comparison for the effects of loading type on bond performance. Thus it can be seen from Figure 4-34 that bond performance is reduced by approximately 30% when loading is cyclic as opposed to monolithic.

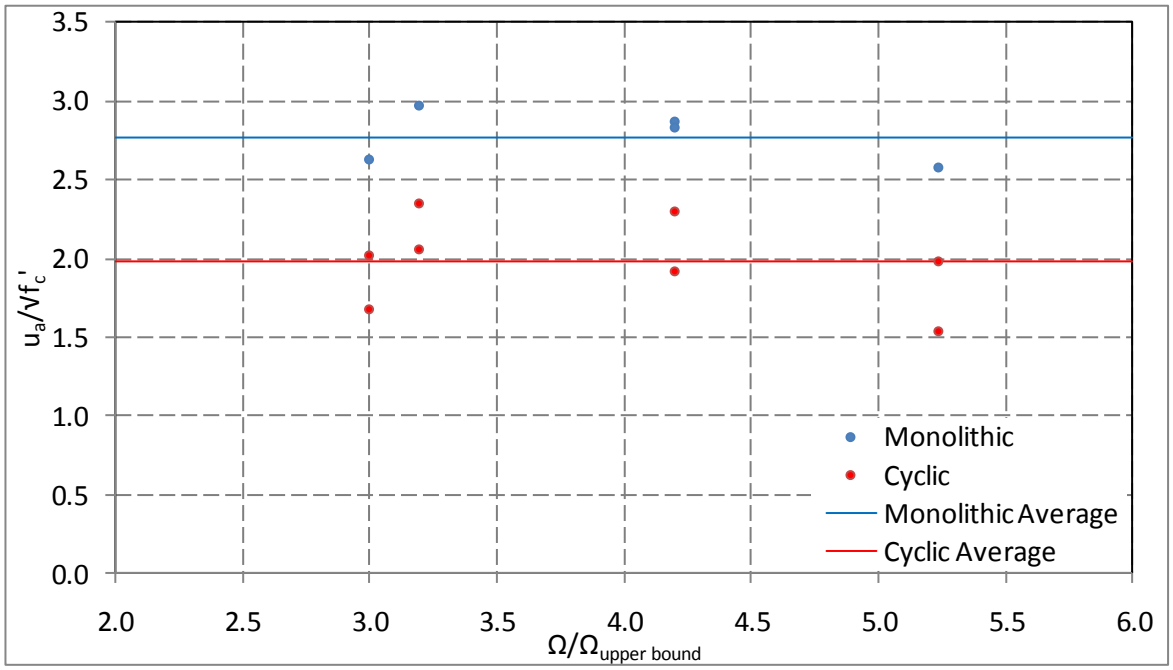

Figure 4-34: *Effect of loading type on bond performance in specimens with high passive confinement*

A further reduction is necessary due to the presence of column bars within beam-column joints. While the effect these have on bond performance is questionable as discussed in Section 4.1.5, their presence means that the baseline for bond enhancement is not zero as was assumed previously for determination of the bond enhancement. A further 25% reduction is thus applied. While this may be conservative, bar slip failure is an undesirable result and so it is better to introduce any new modification factors with caution. Allowing for these reductions and combining with previous findings, it is expected that bond performance within a beam-column joint can be enhanced by approximately 20% when properly detailed supplementary vertical reinforcement is provided.

4.2.4 Bond of Bottom Reinforcement

This section combines findings presented previously in order to develop recommendations for column depth such that bar slip failure is prevented in the bottom longitudinal reinforcement. These recommendations will then form the design basis for the test specimens. Similar to the Paulay and Priestley (1992) bond equation discussed in Section 4.1.1, the recommendations presented here are performance based; i.e. they are only relevant when the conditions under which they were derived exist within the beam-column joint. Finally, the column depth design equation is modified based on experimental results.

As discussed in Section 4.2.1, slotted beams experience simultaneous overstrength demands in the bottom beam reinforcement on either side of the joint. The average bond stress demand, u_a, is thus equal to that given in Equation 4-2 and is the starting point for determination of the required column depth. Prior to the testing phase of this research, the correct overstrength factor for bond demand within slotted joints was yet to be determined. Based on the findings of Section 4.2.2 the value of 1.35 appears appropriate and will thus be adopted for design.

The average bond stress within the joint core is a function of both the maximum bond stress, u_{max}, and the bond stress profile. As discussed in Section 4.1.1, maximum bond stress is achieved within the compression side of the joint core. Given confinement here is due to joint/column reinforcement, compression due to the moment couple within the column, and any axial load that may be present as opposed to beam compression, the bond conditions are likely to be very similar to those within a monolithic joint. For this reason, u_{max} is assumed to be equal to that within a monolithic joint. As discussed in Section 4.1.1, u_{max} is taken as $2.5\sqrt{f_c'}$ after results from dedicated bond experiments.

Due to the effects of strain penetration and lack of confinement from adjacent beams, the average bond stress, u_a, within a slotted joint is less than that within a typical monolithic joint.

As discussed in Section 4.1.1, the average bond stress within a monolithic joint according to Paulay and Priestley (1992) is assumed to be $0.67u_{max}$. However, the results of experimental testing by Au (2010) suggest a value of $0.56u_{max}$, or 80% of the monolithic value, is more appropriate for slotted joints. Furthermore, this is only assumed to act on a portion of the column depth, h'_c, due to ineffective cover concrete and the effects of strain penetration; for monolithic joints, h'_c is generally taken as $0.8h_c$. However, as discussed in Section 4.2.2, the effects of strain penetration are more severe in a slotted joint and the value $0.75h_c$ is more appropriate. Combining the above considerations into Equation 4-2 gives the following basic bond equation for bond of bottom reinforcement within a slotted joint. This represents a reduction in bond effectiveness of 20% compared with a monolithic system.

$$u_a = 0.56u_{max} = 0.75 \times 0.56 \times 2.5\sqrt{f_c'} = \frac{d_b \lambda_o f_y}{2h_c}$$

$$\therefore \quad \frac{d_b}{h_c} \leq 2.1 \frac{\sqrt{f_c'}}{\lambda_o f_y} \qquad \text{Equation 4-20}$$

Just as with bond within a monolithic joint, there are a number of modification factors that need to be considered for slotted joints. Perhaps most important of these is the factor accounting for confinement due to axial load, ξ_p. Given the conditions within the core of a slotted joint are similar to those within monolithic joints and assuming significant bar slip does not occur, this factor should vary little from that presented in Section 4.1.2.

The factors ξ_t and ξ_f accounting for bar position within the pour and joint type, respectively, are as per monolithic specimens. As such, ξ_f can be excluded because this research is only focussed on one-way frames. Furthermore, the factor ξ_m which accounts for the degree of reinforcement activation across the joint is not required. This is because overstrength is activated on both sides of the joint simultaneously and Equation 4-2, from which Equation 4-20 was derived, is based on this assumption.

As discussed in Sections 4.1.7 and 4.2.3, both horizontal and vertical joint reinforcement have an effect on bond performance. However, neither NZS3101:2006 or the Paulay and Priestley (1992) text on which the code bond equations are based make any allowance for these parameters. Thus any modification to bond performance relating to joint reinforcement should be made conservatively. Firstly, consider bond enhancement due to supplementary vertical stirrups. As discussed in Section 4.2.3, these provide passive confinement across the bond interface thus limiting the growth of splitting cracks on the tension side of the column and changing the failure mode from splitting to bar pullout.

Firstly, as discussed in Section 3.1.5, bar pullout is a more ductile failure mechanism which occurs at higher bond stresses. As a result, the reliable bond stress on the tension side of the joint increases; this is illustrated qualitatively in Figure 4-35. Note that the maximum bond stress on the compression side of the joint is unaffected as this region already benefits from active confinement due to the moment couple within the column and any axial load that is present. As discussed in Section 4.2.3, this mechanism is readily quantifiable with bond stress able to be increased by approximately 20% within the region of the beam-column joint subject to axial tension.

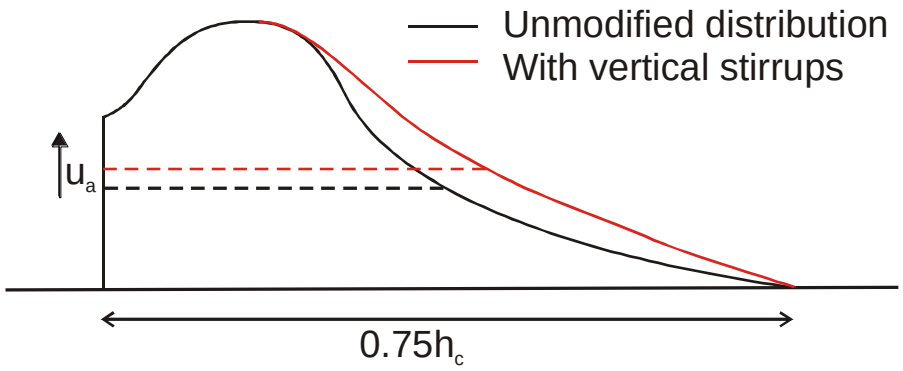

Figure 4-35: *Effect of supplementary vertical stirrups on bond stress distribution*

The presence of supplementary vertical joint stirrups also acts to slow the propagation of splitting cracks thereby reducing the rate of bond deterioration and delaying bar slip failure. As a direct result of this, strain penetration into the joint is reduced. Subsequently, the joint can sustain an increased number of inelastic cycles before bar slip failure occurs. While these mechanisms are difficult to quantify in terms of design, these do improve bond from a performance based perspective and, as such, should not be discounted.

In order to be used in practice, the quantifiable bond enhancement must be expressed in a term familiar to designers. This is achieved by coupling the 20% bond stress enhancement with the Paulay and Priestley (1992) equation for column neutral axis depth. The resulting vertical joint reinforcement modification factor, ξ_r, is given by Equation 4-21:

$$\xi_r = 1 + 0.2\left(1 - \frac{c}{h_c}\right)$$

$$= 1 + 0.2\left(1 - \left(0.25 + 0.85\frac{N^*}{A_g f_c'}\right)\right)$$

$$\xi_r = 1.15 - 0.17\frac{N^*}{A_g f_c'} \qquad \text{Equation 4-21}$$

With the limitation:

$$1.0 \leq \xi_r \leq 1.15$$

Although a link between maximum bond stress and amount of horizontal joint reinforcement was established in Section 4.1.7, a bond modification factor to account for this is not appropriate. As can be seen in Figure 4-20, increases in horizontal joint reinforcement above 80% of that specified in NZS3101:2006 do not result in any appreciable bond stress improvement above the standard $u_{max} = 2.5\sqrt{f_c'}$ value. Given any new structures are required to meet the requirements of NZS3101:2006, the amount of horizontal joint reinforcement provided would fall within the ineffective range specified above.

Combining the findings of this section, the required column depth for prevention of bar slip in the bottom reinforcement is given in Equation 4-22. This equation will be used as the basis for design of the experimental specimens along with the recommendations to account for strain gauge installation and top bar effect as discussed in Section 5.2.4. Note that λ_o is taken as 1.35 as discussed in Section 4.2.2.

$$\frac{d_b}{h_c} \leq 2.1 \frac{\xi_p \xi_r \xi_t \sqrt{f_c'}}{\lambda_o f_y} \qquad \text{Equation 4-22}$$

Using experimental results from Chapter 5, Equation 4-22 can be refined slightly. Average bond stress, u_a, was found to reach $0.59u_{max}$ in the test of specimen B. Given no discernable bar slip had occurred and that the bond stress did not appear to be approaching an asymptote, this value appears suitable for design. Effective column depth, h'_c can also be revised given the limited extent of cone formation and strain penetration observed. The monolithic value of $h'_c = 0.8h_c$ is therefore adopted. Combined with the experimentally determined ξ_b value of 2, the bond stress profile for the bottom longitudinal reinforcement within a slotted joint is proposed in Figure 4-36.

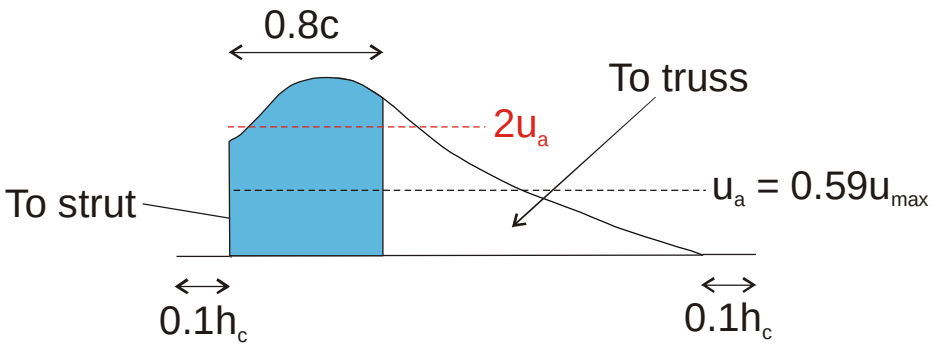

Figure 4-36: *Bond stress distribution for bottom longitudinal reinforcement*

These figures can then be incorporated into Equation 4-20 to produce Equation 4-23, the revised basic equation for required column depth when supplementary vertical joint stirrups are used:

$$u_a = 0.59u_{max} = 0.80 \times 0.59 \times 2.5\sqrt{f_c'} = \frac{d_b \lambda_o f_y}{2h_c}$$

$$\therefore \qquad \frac{d_b}{h_c} \leq 2.36 \frac{\sqrt{f_c'}}{\lambda_o f_y} \qquad \text{Equation 4-23}$$

Where λ_o is taken as 1.35. Note that while higher maximum bond stresses were observed as reported in Section 5.5.2, the Author is hesitant to increase this figure for design basis given the wealth of experimental testing indicating $2.5\sqrt{f_c'}$ to be the maximum attainable bond stress within well confined concrete as discussed in Section 3.4.2. The bond modification factors are then applied to the basic column depth equation as before to produce the detailed column depth equation given in Equation 4-24:

$$\frac{d_b}{h_c} \leq 2.36 \frac{\xi_p \xi_r \xi_t \sqrt{f_c'}}{\lambda_o f_y} \qquad \text{Equation 4-24}$$

Note that this equation is only applicable to joints in which supplementary vertical reinforcement is provided in accordance with Section 4.2.3. Where such stirrups are not provided, Equation 4-22 with ξ_r = 1.0 is tentatively recommended to determine the required column depth. However, further testing is necessary to confirm this.

Column depths determined using Equation 4-24 are approximately 10% less demanding than those produced using Equation 4-22. However, as discussed in Section 5.5.2, the column depth used for specimen B was effectively 14% less than that given by Equation 4-22 due to the reduced concrete strength. The fact that specimen B performed suitably from a performance based standpoint despite this shortcoming, suggests the level of bond enhancement afforded by supplementary vertical joint stirrups has been underestimated. This is not surprising given the conservatism employed in Section 4.2.3. Attributing this additional 4% bond enhancement to the vertical joint stirrups results in a revised ξ_r value as given by Equation 4-25:

$$\xi_r = 1 + 0.24\left(1 - \frac{c}{h_c}\right)$$

$$= 1 + 0.24\left(1 - \left(0.25 + 0.85\frac{N^*}{A_g f_c'}\right)\right)$$

$$\xi_r = 1.18 - 0.2\frac{N^*}{A_g f_c'} \qquad \text{Equation 4-25}$$

With the limitation:

$$1.0 \leq \xi_r \leq 1.18$$

In summary, the use of supplementary vertical joint stirrups improves bond performance through several mechanisms. The first of these – provision of passive confinement – is readily quantified and, as such, has been assigned a factor, ξ_r, for use by designers. The other two mechanisms – reduction of strain penetration and bar slip – are not readily quantified but are important nonetheless from a performance based standpoint. Further work is required to understand the latter two mechanisms such that the benefit these provide to bond performance can be realised in design.

4.2.5 Bond of Top Reinforcement

Although bond conditions for the top longitudinal reinforcement are less severe than those for the bottom longitudinal reinforcement within a slotted beam, bond requirements must still be adhered to. This is especially important given that the use of larger bars is more desirable in order to reduce hinge congestion while still achieving the required reinforcement strength bias. This section combines findings presented previously in order to develop recommendations for detailing of the top reinforcement such that strength bias, hinge damage, bond requirements and other parameters are respected. As in Section 4.2.4, experimental results are used to fine tune the governing equation for column depth.

As outlined above, slotted beams require a strength bias in order to limit elongation of the top beam bars through the hinge and thus damage in this area. Au (2010) found that $A'_s/A_s = 2$ is appropriate to meet these criteria; however, no recommendations were given regarding reinforcement grade. The findings of Section 2.2.3 show that Grade 300 reinforcement is sufficient to meet elongation and damage criteria. Furthermore, Grade 300 reinforcement is preferable from a bond standpoint. As such, it will be used for the experimental stage of this research.

Because top reinforcement within a slotted beam benefits from concrete compression in the adjacent beam, its bond conditions are largely similar to those of the larger reinforcement within an asymmetric monolithic beam. For this reason, the current NZS3101:2006 equation, as presented in Section 4.1.1, can be used as a basis for the bond requirements here. However, some alterations are required as outlined below. Firstly, because top longitudinal reinforcement activation is driven only by the bottom longitudinal reinforcement and a small amount of concrete prying in the hinge, the bond demand is decreased compared with a monolithic joint. Thus the factor accounting for the degree of reinforcement activation across the joint, ξ_m, should be reduced as proposed in Section 4.1.4.

Consider first the case for gap opening moments when the top reinforcement is in compression. As illustrated in Figure 4-22, concrete within the hinge is able to assist in achieving equilibrium and the bottom reinforcement is easily activated to overstrength; this is summarised by the following relationship:

$$C_c^{'} + C_s^{'} = T_s^{'}$$

$$\therefore \quad C_c^{'} + A_s^{'} f_s^{'} = A_s f_y \lambda_{ob}$$

Where f_s' is the elastic compressive stress within the top beam reinforcement and λ_{ob} corresponds to the bottom longitudinal reinforcement. If the concrete contribution within the hinge is ignored, the stress in the top compression reinforcement can be no greater than that given by Equation 4-26:

$$A_s^{'} f_s^{'} \leq A_s f_y \lambda_{ob}$$

$$\therefore \quad A_s^{'} f_s^{'} \leq \beta A_s^{'} f_y \lambda_{ob}$$

$$\therefore \quad f_s^{'} \leq \beta f_y \lambda_{ob}$$

$$\therefore \quad \frac{f_s^{'}}{f_y} \leq \beta \lambda_{ob} \qquad \text{Equation 4-26}$$

Given the standard values for β and λ_{ob} within a slotted joint, the degree of activation within the top reinforcement on the gap opening side of the joint is limited to the value given below:

$$\frac{f_s^{'}}{f_y} \leq 0.68$$

However, unlike in a monolithic joint, concrete compression within the hinge is always present due to the significantly reduced damage and elongation in this region as discussed in

Section 2.2.3. For this reason, the degree of activation within the top compression reinforcement can be reduced; determining an appropriate reduction is now the issue.

As evidenced in Figure 4-37, compression strains in the top reinforcement are negligible. Unfortunately, premature bar slip failure of the bottom bars was observed in this specimen and, as such, the maximum degree of top reinforcement activation observed during this test is less than what would be expected if bar slip failure had not occurred. Furthermore, due to multiple strain gauge failures, the corresponding results from specimen SB3 are unavailable.

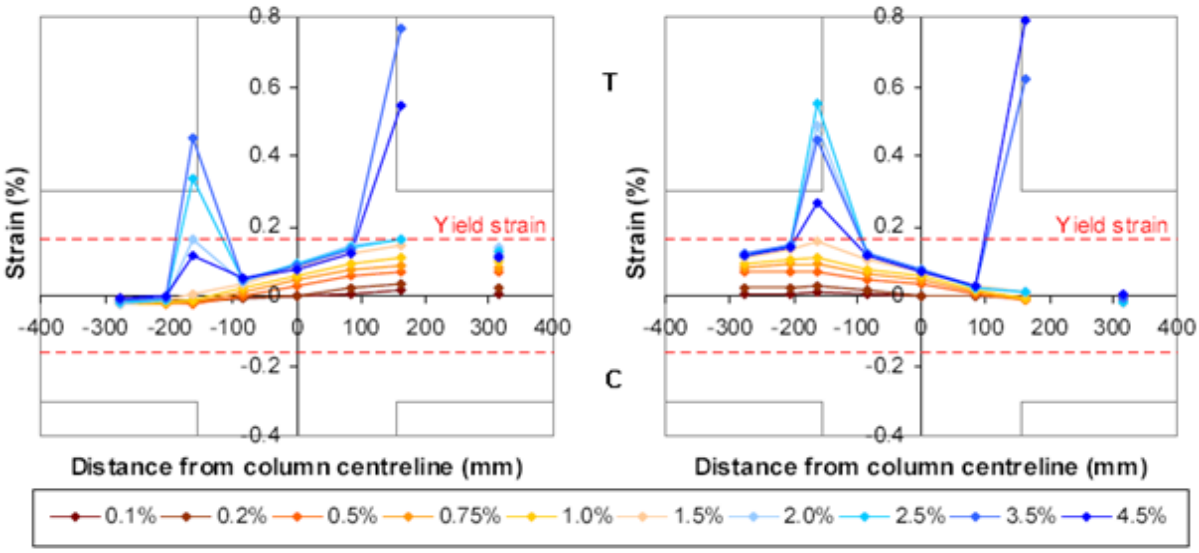

(a) Positive drifts (b) Negative drifts

Figure 4-37: *Top reinforcement strain profile for specimen SB2. Adapted from Au (2010)*

For these reasons engineering judgement must be used in proposing a suitable revised limit for the degree of activation within the top reinforcement. An appropriately conservative value is proposed for design basis in Equation 4-27:

$$\frac{f_s^{'}}{f_y} \leq 0.50 = \gamma^{+} \qquad \text{Equation 4-27}$$

Where γ is as defined in Section 4.1.4 and the '+' subscript indicates that the value is for gap opening moments.

Consider now the case for negative moments when the top reinforcement is in tension. As illustrated in Figure 4-22, the bottom reinforcement is assisted by concrete compression in the lower hinge region due to prying. Equilibrium is thus given by Equation 4-28:

$$C_c + C_s = T_s$$

$$\therefore \quad C_c + A_s f_y \lambda_{ob} = A_s^{'} f_y \lambda_{ot} \qquad \text{Equation 4-28}$$

Where λ_{ot} corresponds to the top longitudinal reinforcement. In this case, the concrete contribution from prying is working against the top reinforcement. This results in a similar situation to that within an asymmetric monolithic joint. However, in the case of a slotted joint, the top longitudinal reinforcement is expected to remain nominally elastic even in tension. This is due to the strength bias and reduced concrete contribution from the adjacent beam compared with an equivalent monolithic joint. The strain profiles in Figure 4-37 where the top reinforcement does not exceed $5\varepsilon_y$ support this claim.

As such, the NZS3101:2006 column depth requirements for joints where plastic action does not occur at the column faces appear to be a reasonable basis for design prior to further experimental work. Based on a reduced maximum bond stress of $1.5\sqrt{f_c'}$ (Standards Association of New Zealand, 2006), these requirements are reproduced below:

$$\frac{d_b}{h_c} = \frac{6\alpha_f \sqrt{f_c'}}{f_y\left(1 + \frac{f_s}{f_y}\right)} \qquad \text{Equation 4-29}$$

Where α_f = 1.0 for a one way joint. Recalling from Equation 4-27 that f_s'/f_y = 0.5 and accounting for only material overstrength, λ_m, in the tension reinforcement, Equation 4-29 becomes:

$$\frac{d_b}{h_c} = \frac{6}{f_y(1.15 + 0.5)} = \frac{3.6\sqrt{f_c'}}{f_y} \qquad \text{Equation 4-30}$$

Note that the material overstrength factor is not applied to the compression stress term because activation of this reinforcement is driven by the bottom reinforcement where full overstrength is already accounted for. Equation 4-30 is 10% more demanding than the NZS3101:2006 column depth requirements for nominally ductile joints.

Experimental findings from Chapter 5 indicate several changes should be made to Equation 4-30. Firstly, the maximum degree of reinforcement activation in compression was found to be $0.4f_y$ throughout the entire test sequence. Secondly, the current material overstrength factor, λ_m, appears to be too high for the larger bars generally used for top longitudinal reinforcement. Results from testing of D20, 25, and 32 bars as discussed in Section 5.2.5 indicate an average material overstrength factor of 1.02. Clearly this is not conservative enough as a design basis but the reduced value of 1.1 is suggested. Tensile reinforcement was found to remain nominally elastic and, as such, the factor corresponding to this does not need adjustment. Allowing for these observations in Equation 4-30 results in the current NZS3101:2006 equation for nominally ductile structures as given in Equation 4-31:

$$\frac{d_b}{h_c} = \frac{4\sqrt{f_c'}}{f_y}$$ Equation 4-31

4.3 Joint Shear Demand

4.3.1 Horizontal Joint Shear Demand within Monolithic Interior Joints

The shear transfer mechanism within monolithic beam-column joints is well documented in literature and, as such, is only discussed here briefly. As with bond demand, it is based on equilibrium of forces entering and being resisted within the joint. Figure 4-3 shows the external actions on an interior monolithic beam-column joint during seismic excitations; note that the contributions from floor diaphragm activation are ignored in this derivation. The corresponding horizontal joint shear demand, V_{jh}, is easily extracted from this figure using force equilibrium in the horizontal direction (Paulay & Priestley, 1992):

$$V_{jh} = C_s' + C_c' + T_s - V_{col} = T_s' + C_c + C_s - V_{col}$$

Where V_{col} is derived from overstrength beam actions computed at the column faces – the process of obtaining this value is readily available in NZS3101:2006 – while subscripts '*s*' and '*c*' donate a steel and concrete contribution, respectively. Note that it is assumed the beam and column shear forces, V_b and V_{col}, are primarily introduced into the joint at the corresponding flexural compression zones (Paulay & Priestley, 1992). Using equilibrium required for the moment couple within each beam, the above equation can be simplified as follows:

$$T_s' = C_c' + C_s'$$

$$\therefore \quad V_{jh} = T_s' + T_s - V_{col}$$

$$= \beta T_s + T_s - V_{col}$$

$$= T_s(\beta + 1) - V_{col}$$ Equation 4-32

Where $\beta = A_s/A'_s \leq 1$. If the overstrength factor, λ_o, and beam reinforcement areas are known V_{jh} takes its final form as Equation 4-33:

$$V_{jh} = (A_s' + A_s)\lambda_o f_y - V_{col}$$ Equation 4-33

4.3.2 Horizontal Joint Shear Demand within Slotted Beam Interior Joints

The horizontal joint shear demand for slotted beam systems is largely similar to that described above for monolithic joints (Au, 2010). However, due to the presence of a slot in each beam adjacent to the column face, there is no concrete compression contribution during gap-closing moments; this is clearly visible at the soffit of the right hand beam in Figure 4-38. Furthermore, due to the prying effect at the top of the right hand side beam, the tension force in the top reinforcement, T_s, is greater than the compression force in the bottom reinforcement, C_s. The horizontal joint shear demand is again determined using force equilibrium in the horizontal direction as given by Equation 4-34.

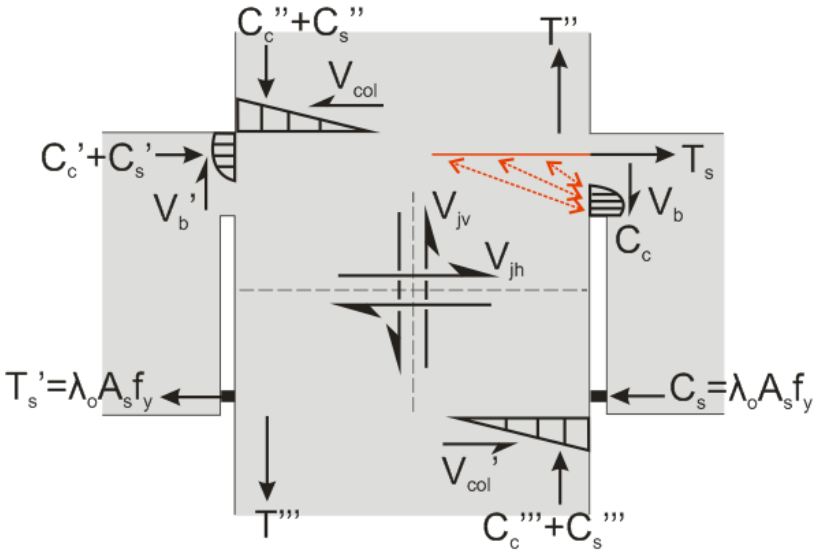

Figure 4-38: *External actions on an interior slotted beam joint (Au, 2010)*

$$V_{jh} = C_c^{'} + C_s^{'} + T_s - C_c - V_{col} = T_s^{'} + C_s - V_{col}^{'} \qquad \text{Equation 4-34}$$

Using equilibrium within each beam, Equation 4-34 can be simplified to the expression in Equation 4-35:

Right beam equilibrium: $T_s = C_c + C_s \rightarrow C_c = T_s - C_s$

$\therefore \quad V_{jh} = C_c^{'} + C_s^{'} + T_s - [T_s - C_s] - V_{col}$

Left beam equilibrium: $C_c^{'} + C_s^{'} = T_s^{'}$

$\therefore \quad V_{jh} = T_s^{'} + C_s - V_{col}$

$\therefore \quad V_{jh} = 2\lambda_o A_s f_y - V_{col}$ Equation 4-35

4.3.3 Vertical Joint Shear demand

While the process is similar for calculating the vertical joint shear, complexities arise due to the multiple layers typical of column reinforcement. For this reason, it is common practice to express the vertical joint shear as a fraction of the horizontal joint shear (Paulay & Priestley, 1992). The vertical shear demand, given in Equation 4-36, is therefore taken as that for the horizontal shear demand proportioned by the corresponding lever arms to the stress resultant in each direction:

$$V_{jv} = \frac{h_b}{h_c} V_{jh} \qquad \text{Equation 4-36}$$

When analysed in the vertical direction, the joint zone within a slotted beam system is effectively the same as for a monolithic system. For this reason, Equation 4-36 can also be used to determine the vertical joint shear within a slotted beam system (Au, 2010).

4.4 Monolithic Interior Joint Shear Mechanisms

Monolithic beam-column joints resist joint shear through a combination of two mechanisms, namely the concrete strut and reinforcement truss mechanisms (Blakeley et al, 1975; Beckingsale, 1980; Paulay & Priestley, 1992). This section gives a brief background to the mechanics of shear transfer within monolithic beam-column joints such that the concept can be extended to the more complex case of joints incorporating slotted beams in Section 4.5.

4.4.1 Concrete Strut Mechanism

Illustrated in Figure 4-39(a), the strut mechanism resists shear through a diagonal compression field within the concrete core of the joint and has a magnitude D_c. This strut is resisted at the joint boundaries primarily by concrete compression within the beams and column, although beam reinforcement contributes through bond to some extent.

Taking equilibrium across the top of the joint, the horizontal component of this strut, V_{ch}, is obtained using Equation 4-37:

$$V_{ch} = C_c' + \Delta T_c' - V_{col} = D_c \cos\alpha \qquad \text{Equation 4-37}$$

Where C'_c is the concrete compression within the beam and V_{col} is the shear force within the column. $\Delta T'_c$ refers to the small portion of the total force within the reinforcement, $T_s + C'_s$, that is resisted by bond over the region where the concrete strut lands and is therefore transferred into the concrete strut. As shown in Figure 4-39(b), this contribution is dependent on the bond stress profile and neutral axis depth, c. The bond stress profile on which this is

based was discussed in Section 4.1.1 while the neutral axis depth varies with axial load as given in Equation 4-38 according to Paulay and Priestley (1992):

$$\frac{c}{h_c} = \left(0.25 + 0.85\frac{P_u}{A_g f_c'}\right) \qquad \text{Equation 4-38}$$

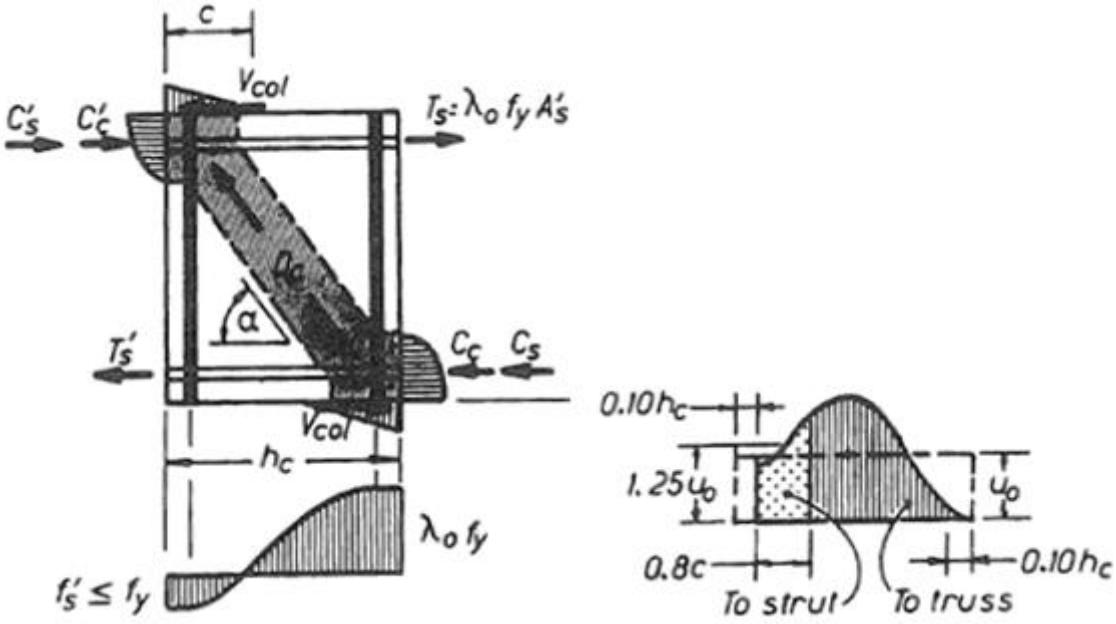

(a) Steel stresses (b) Bond forces

Figure 4-39: *Concrete strut mechanism (Paulay & Priestley, 1992)*

Where P_u is the minimum compression force on the column and A_g is the gross cross-sectional area of the column. Discounting the ineffective cover concrete and allowing for some strain penetration from inelastic loading, the strut is assumed to land over a distance $0.8c$. The average bond stress over this region is taken as $1.25u_o$ to reflect the more favourable conditions encountered within the compression region of the column as discussed in Section 4.1.1. Thus Paulay and Priestley (1992) assume the following value for $\Delta T'_c$:

$$\Delta T_c' = 0.8c \times 1.25u_o = u_o c$$

Because u_o represents the average bond stress across the entire column, the following is true:

$$\Delta T_c' = u_o c = (C_s' + T_s)\frac{c}{h_c}$$

The force in the compression reinforcement, C'_s, is then expressed in terms of the force in the top tension reinforcement, T_s, such that the final result is more uniform:

$$C_s' = \gamma f_y A_s'$$

and $$T_s = \lambda_o f_y A_s'$$

$$\therefore \quad C_s' = \frac{\gamma}{\lambda_o} T_s$$

Where γ is the proportion of yield stress activated in the compression reinforcement and is assumed to be 0.7 as per Section 4.1.4. Combining the above results and adopting the usual overstrength factor, λ_o, of 1.25, $\Delta T'_c$ takes its final form as expressed below:

$$\Delta T_c' = T_s \left(\frac{0.7}{1.25} + 1\right) \frac{c}{h_c}$$

$$= 1.55 T_s \frac{c}{h_c} \qquad \text{Equation 4-39}$$

It is also convenient to express the concrete contribution in terms of T_s before substituting into Equation 4-37. Taking equilibrium on the left side of the joint where the top and bottom reinforcement have areas A'_s and A_s, respectively, the following relationship is obtained:

$$C_c' = T_s' - C_s'$$

$$= \beta T_s - \frac{\gamma}{\lambda_o} T_s$$

$$= T_s(\beta - 0.55) \qquad \text{Equation 4-40}$$

Combining the results of Equation 4-39 and Equation 4-40 into Equation 4-37, the relationship for the horizontal component of the diagonal strut force, V_{ch}, is found:

$$V_{ch} = T_s(\beta - 0.55) + 1.55 T_s \frac{c}{h_c} - V_{col}$$

$$= T_s \left[1.55 \frac{c}{h_c} + \beta - 0.55\right] - V_{col} \qquad \text{Equation 4-41}$$

This equation is not simplified further because, as discussed in Section 4.4.2, it is common practice to express the shear demand in terms of required joint reinforcement area. This approach is used by the current Concrete Structures Design Standard as it inherently takes the concrete contribution into account. The vertical component of the concrete strut force, V_{cv}, is also expressed as a fraction of the horizontal component as given in Equation 4-42:

$$V_{cv} = V_{ch} \tan \alpha \approx \frac{h_b}{h_c} V_{ch} \qquad \text{Equation 4-42}$$

4.4.2 Truss Mechanism

The remainder of the force transferred from the reinforcement via bond is resisted through a truss mechanism set up within the joint shear reinforcement. As shown in Figure 4-40, this results in shear flow introduced along each of the four joint boundaries formed by the beam and column reinforcement (Paulay & Priestley, 1992). The shear is then transferred diagonally down the joint by concrete micro-struts with horizontal joint reinforcement providing ties across the joint as shown in Figure 4-40. Because these ties are in tension regardless of the loading direction, it is imperative they are detailed to remain elastic. Vertical joint stirrups are seldom used due to the associated constructability and congestion issues; fortunately interior column bars generally provide sufficient vertical reinforcement. The resultant force of magnitude D_s is aligned at an angle α assumed to be equal to that in the strut mechanism.

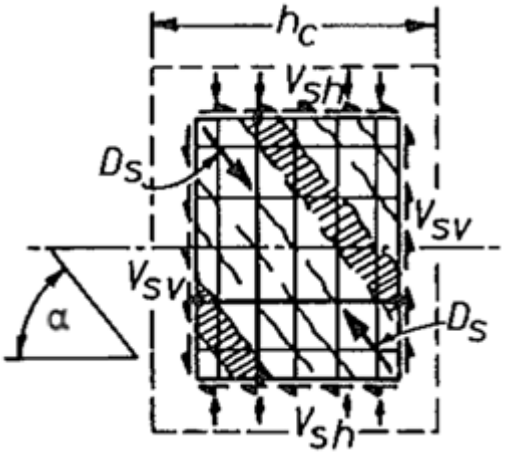

Figure 4-40: *Truss mechanism within monolithic beam-column joint (Paulay & Priestley, 1992)*

Again considering horizontal equilibrium within the top half of the joint in Figure 4-39(a), the resulting horizontal force resisted by the truss mechanism, V_{sh}, is given by Equation 4-43:

$$V_{sh} = V_{jh} - V_{ch} = D_s \cos\alpha \qquad \text{Equation 4-43}$$

Substituting Equation 4-32 and Equation 4-41 into Equation 4-43, it is possible to solve directly for V_{sh} as shown below:

$$V_{sh} = [T_s(\beta + 1) - V_{col}] - \left[T_s\left(1.55\frac{c}{h_c} + \beta - 0.55\right) - V_{col}\right]$$

$$= 1.55\left(1 - \frac{c}{h_c}\right)T_s$$

The ratio c/h_c is then taken as per Equation 4-38 to give the following:

$$V_{sh} = \left(1.15 - 1.3\frac{P_u}{f_c^{'} A_g}\right)\lambda_o f_y A_s^{'}$$

Where λ_o is generally taken to be 1.25. Substituting this into the above equation results in the design value for V_{sh} from Paulay and Priestley (1992) given in Equation 4-44:

$$V_{sh} = \left(1.4 - 1.6\frac{P_u}{f_c^{'} A_g}\right) f_y A_s^{'} \qquad \text{Equation 4-44}$$

Thus the required horizontal joint reinforcement can be found as follows:

$$A_{jh} = \frac{V_{sh}}{f_{yh}}$$

$$= \left(1.4 - 1.6\frac{P_u}{f_c^{'} A_g}\right)\frac{f_y A_s^{'}}{f_{yh}}$$

$$= \alpha_i \frac{f_y A_s^{'}}{f_{yh}} \qquad \text{Equation 4-45}$$

Equation 4-45 is slightly different to the current Concrete Structures Design Standard where a reduction factor is applied thus making the code provisions less conservative. A'_s is also replaced with A^*_s corresponding to the larger of the top and bottom reinforcement areas, to make the expression more general as shown in Equation 4-46 below:

$$A_{jh} = \left(\frac{6V_{ojh}}{f_c^{'} b_j h_c}\right)\left(\frac{\alpha_i f_y A_s^*}{f_{yh}}\right) \qquad \text{Equation 4-46}$$

Where V_{ojh} is the joint shear demand resulting from overstrength actions within the adjacent beams, b_j is the effective width of the column, and h_c is the column depth. The introduced factor is subject to the limitation below:

$$\frac{6V_{ojh}}{f_c^{'} b_j h_c} \geq 0.85 \qquad \text{Equation 4-47}$$

The reasoning behind this limitation has not been published but it effectively means that the joint shear reinforcement must take at least 85% of the shear demand. This limitation is most likely imposed to prevent designers from under-reinforcing large columns. Given the consequent lack of confinement, the strut mechanism within such columns could potentially break down during advanced inelastic loading resulting in joint failure. However, the lack of explanation is an unfortunate oversight given its tendency to govern the inequality for most

column dimensions and typical concrete strengths. The area of vertical joint reinforcement required, A_{jv}, is specified as a portion of A_{jh} as given in Equation 4-48:

$$A_{jv} = \alpha_v A_{jh} \frac{f_{yh}}{f_{yv}} \frac{h_b}{h_c} \qquad \text{Equation 4-48}$$

Where f_{yv} is the column reinforcement grade and h_b is the beam height. The factor α_v, given by Equation 4-49, is to account for the fact that column bars should remain elastic under design conditions. Increases in axial load will further reduce the tension forces these bars experience thus decreasing the change in stress, and therefore shear, experienced vertically across the joint.

$$\alpha_v = \frac{0.7}{1 + \frac{N_o^*}{A_g f_c'}} \qquad \text{Equation 4-49}$$

Where N^*_o is the minimum design axial compression force on the column.

4.5 Slotted Beam Interior Joint Shear Mechanisms

The shear transfer mechanism within interior joints when slotted beams are used is yet to be agreed upon. Although the joint shear force demand is similar to that of a monolithic joint as discussed in Section 4.4, the transfer of these external forces into the joint is very different as can be seen when comparing Figure 4-3 and Figure 4-38. This section aims to highlight the differences in force transfer between slotted beam and monolithic joints and to investigate the potential mechanisms through which these forces are transferred. The theoretical approach to proportioning shear to each resistance mechanism as described in Section 4.4 is also extended to slotted beams.

4.5.1 Mechanism Proposed by Au (2010)

The lack of concrete compression provided by adjacent beams has consequences beyond creating a more severe bond environment. Au (2010) proposed that, due to this lack of beam concrete compression at the bottom of a slotted beam-column joint, the strut mechanism as defined in Section 4.4.1 is different to that within a monolithic joint. As shown in Figure 4-41, a portion, V'_{ch}, of the diagonal concrete shear strut that, in a monolithic joint, would be resisted by compression from the adjacent beam is instead resisted by additional horizontal stirrups (shown in red) placed in the bottom half of the joint. Thus the additional stirrups are required to provide a resistance force ΔV_{sh} as given by Equation 4-50:

$$\Delta V_{sh} = V_{ch}^{'} - V_{ch} = V_{sh} - V_{sh}^{'}$$ Equation 4-50

It should be noted that Au (2010) did not use these additional stirrups in any test specimens but suggested they should be provided based on the evidence discussed below.

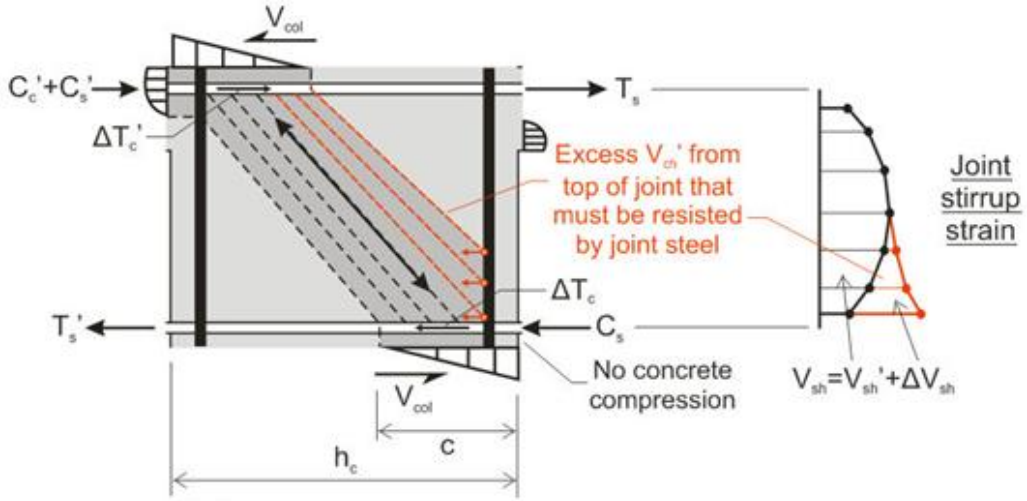

Figure 4-41: *Interior slotted beam joint mechanism proposed by Au (2010)*

One of the cornerstones of this assumption is that horizontal joint stirrups towards the bottom of the joint were activated more than those in the top in the test of specimen SB2 by Au (2010). While clearly visible in Figure 4-42(a), this bias in stirrup activation can be attributed to the bar slip that occurred in this test. Once the bars began to slip through the joint, their stiffness was reduced and the macro-truss mechanism incorporating the column and beam bars broke down. Thus with no possibility of force transfer to the beam concrete, the horizontal joint stirrups became the preferred means of resisting the horizontal component of the strut and the strains increased in this region. If bar slip had not occurred, it is likely that this strain bias would not have been observed. This was the case in the testing of specimen SB3 by Au (2010) where, as depicted in Figure 4-42(b), activation of the horizontal joint reinforcement was negligible and uniform. In this test, bar slip did not occur and the bottom longitudinal beam bars were able to remain effective as part of the truss mechanism.

Despite this bias, the degree of stirrup activation is limited – at the maximum shear demand which occurred at 2.5% drift as shown in Figure 4-42(a), these stirrups in the bottom half of the joint had only reached approximately half their measured yield strain of 0.0021. This cannot be attributed to a conservative design as the joint is well reinforced according to NZS3101:2006 with $A_{jh,prvd}/A_{jh,req}$ = 1.19 (see Appendix A). Note that strain data beyond 2.5% drift is not applicable as the joint strength degraded significantly due to bar slip. Indeed, the stirrup strain levels decreased markedly in response to this. As such, the results of this test should not be used for design basis.

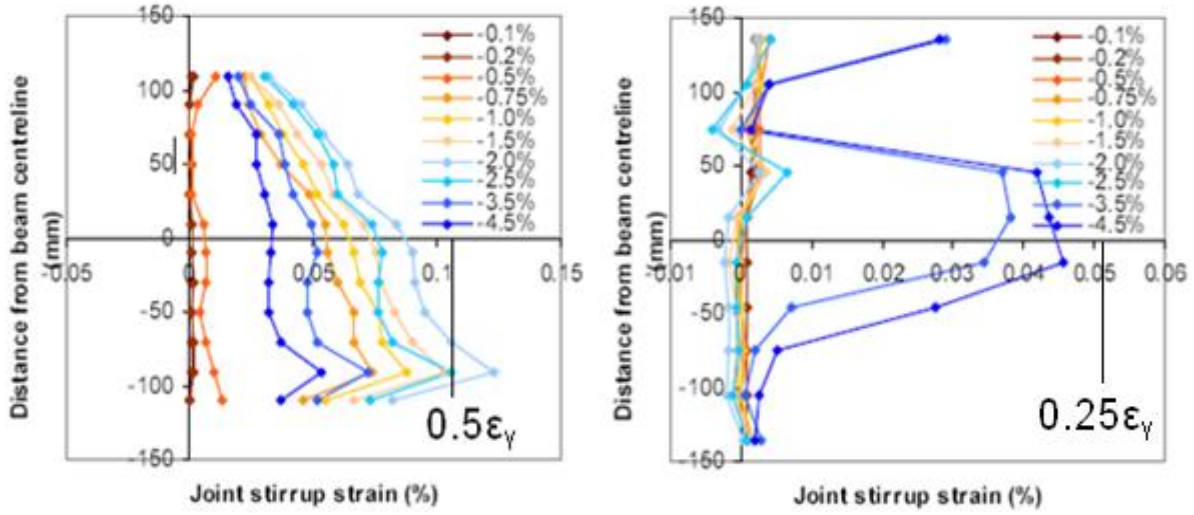

(a) Specimen SB2 (b) Specimen SB3

Figure 4-42: *Horizontal joint stirrup strain within interior beam-column joint specimens. Adapted from Au (2010)*

The question then arises that, if the joint had not failed due to bar slip and the shear demand continued to increase, would the additional stirrups have been activated sufficiently to justify the inclusion of these stirrups? To answer this question, one must first address the issue of bar slip. In order for bar slip to be prevented, the only readily available measures are to increase the column depth or concrete grade. Recognising this, Au (2010) conducted test SB3 with a much larger column depth and increased the concrete compressive strength from 30 to 40 MPa. Predictably, bar slip failure did not occur and a relatively stable hysteretic response was observed up to 4.5% drift as seen in Figure 4-43.

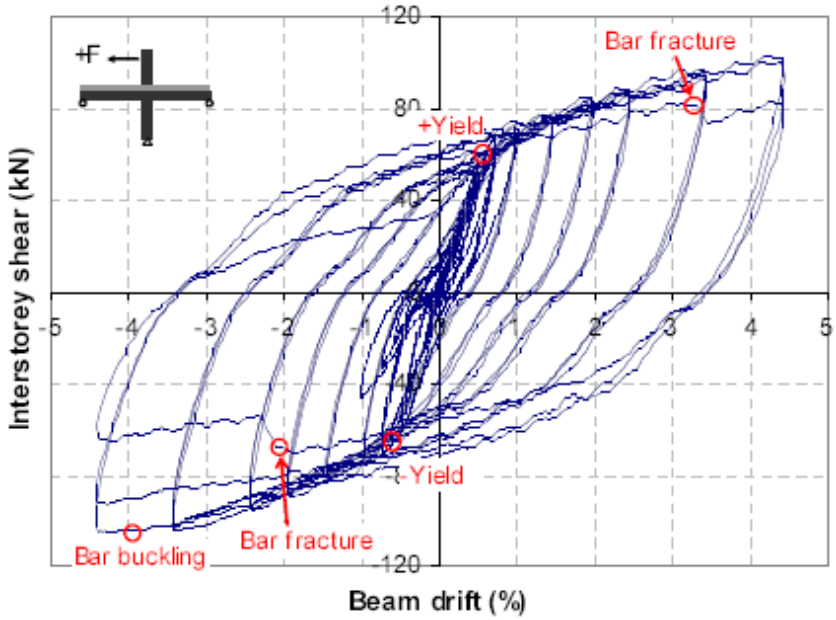

Figure 4-43: *Force versus displacement response for lateral loading of second interior slotted beam specimen SB3 (Au, 2010)*

In test SB3, the ratio $A_{jh,prvd}/A_{jh,req}$ was calculated to be 1.08, again indicating that the joint was well reinforced. The horizontal joint stirrups were not activated until 3.5% drift and even then were only found to reach around ¼ yield strain as shown in Figure 4-42(b). This finding is supported by experimental observations in which joint shear cracks did not appear until 3.5% drift. The asymmetric strain profile observed in the previous test is also not evident thus supporting the hypothesis that this was caused by slippage of the beam bars and not from resisting the concrete strut as Au (2010) proposed. With reference to the question posed above, in solving the issue of bar slip, the level of horizontal joint stirrup activation was significantly reduced. One would have to include that no, inclusion of the additional horizontal joint stirrups was not justified in this case.

The low level of stirrup activation suggests that the concrete strut mechanism is resisting the majority of the shear demand and that the truss mechanism is not being fully utilised. Ineffectiveness of the truss mechanism for joints with large column depths has also been recognised by Leon (1989). According to the theory proposed by Au (2010), reliance on the strut mechanism would cause additional demand in the stirrups within the bottom half of the joint. However, the low strains in Figure 4-42(b) do not support this. Given bond failure did not occur, it is more likely that horizontal equilibrium for the strut mechanism was provided by the beam bars, as discussed in Section 4.5.2.

However, the column depth successfully employed by Au (2010) for prevention of bar slip failure in test SB3 was overly conservative. Therefore, a reduction in column depth, while still preventing bar slip failure, would result in an increased level of horizontal joint stirrup activation. The parametric analysis in Section 4.5.4 attempts to quantify this activation such that design of the test specimens can be further refined and the question posed above can be answered. Prior to the experimental phase of this research, the degree of activation and, hence the justification for additional horizontal joint stirrups remains unknown. However, following the experimental programme as discussed in Chapter 5, the mechanism proposed by Au (2010) was found to be incorrect. The more probable mechanism is discussed in Section 4.5.2.

4.5.2 Revised Joint Shear Mechanism

It has recently been suggested by independent researchers (Fenwick, 2010) that the joint shear mechanism within a slotted beam-column joint is different to that assumed by Au (2010). In the proposed alternate mechanism, the concrete strut realigns itself such that it is landed entirely on the bottom beam reinforcement. The resulting horizontal joint reinforcement activation is then symmetrical as in a monolithic joint and additional stirrups are no longer

required within the bottom half of the joint as is currently assumed. Realignment of the strut is due to the beam bar being stiffer than the horizontal stirrups thus it attracts the excess strut force preferentially as shown by the red triangle in Figure 4-44. However, in order for this realignment to occur, it is imperative that bar slip failure does not occur. Such an event would result in nowhere for the strut to land, an inability to achieve equilibrium within the joint, and other consequences as discussed in Section 4.1.6. As such, the discussion in this section assumes that bar slip failure does not occur.

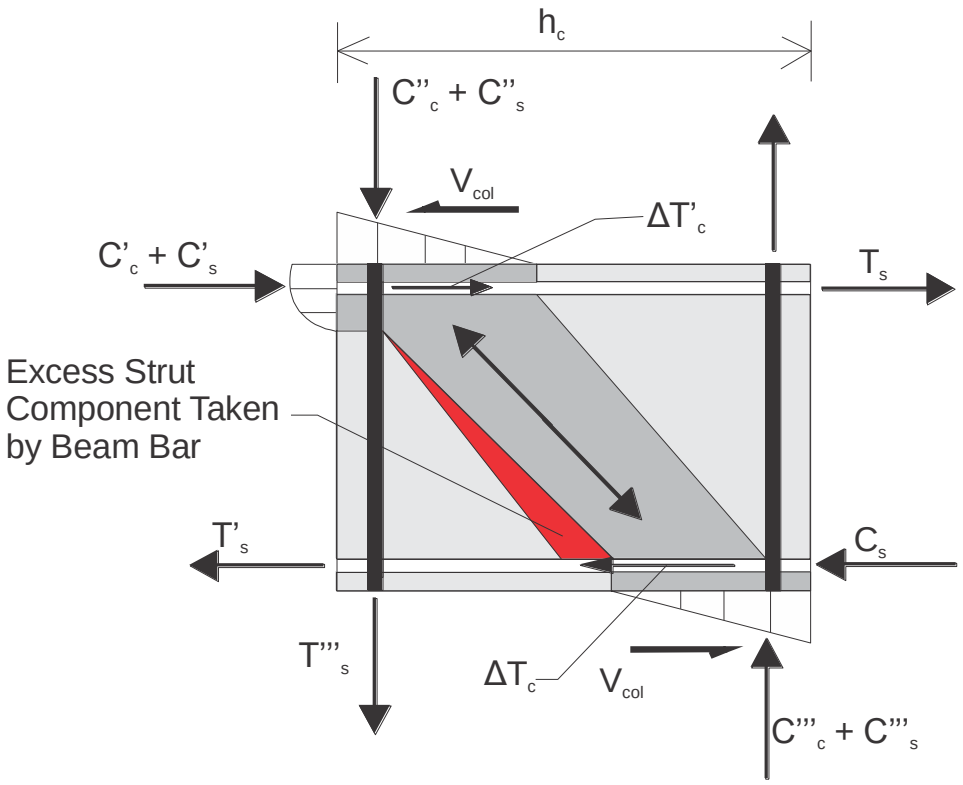

Figure 4-44: *Proposed alternative slotted beam joint mechanism*

The reasoning behind this alternate mechanism is supported by findings from previous testing on monolithic specimens. Figure 4-45(a) and (b) show typical horizontal joint reinforcement strain profiles for elastic and advanced inelastic loading stages, respectively. The specimen from which these profiles were derived has a relatively large column depth, as would be expected for a slotted beam specimen, but its beams are symmetrically reinforced. Due to the large column depth the strut resists a significant portion of the joint shear demand and, as a result, the ratio $A_{jh,prvd}/A_{jh,req}$ is around 2 corresponding to an over-reinforced joint. Consequently, stirrup strains are expected to be relatively low throughout the joint.

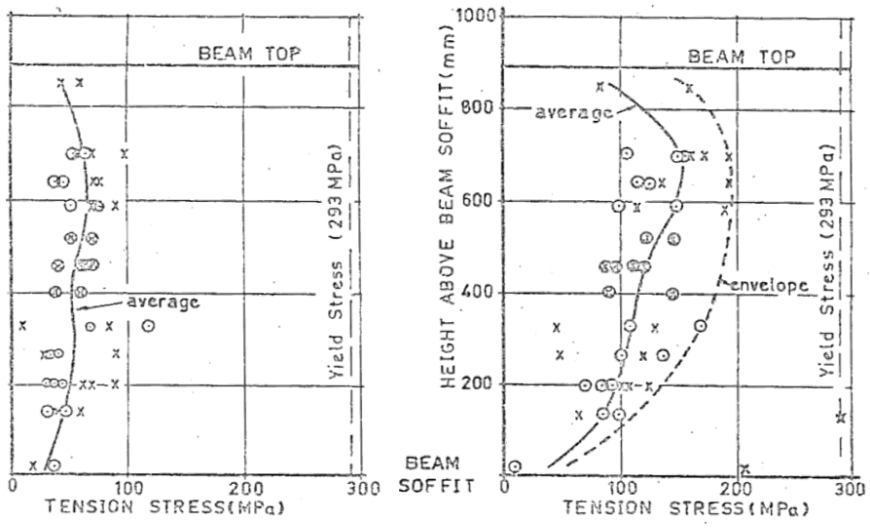

(a) Yield (b) Ductility 6

Figure 4-45: *Horizontal joint stirrup strain profile for specimen with large column depth (Blakeley et al, 1975)*

Comparison of the two profiles shows an increase in strain levels between recordings at yield and displacement ductility 6. This is due to disintegration of the joint concrete core with increasing inelastic action, and results in a significant reduction in the amount of shear taken by the concrete strut mechanism (Birss, 1978; Beckingsale, 1980). Consequently, the excess shear demand is transferred into the truss mechanism and the demand on joint stirrups increases. Closer inspection of these strain profiles reveals differential increases in the strain levels recorded over different stirrup sets. Strain levels in the stirrups situated in the middle of the joint increase by approximately 200% between yield and displacement ductility 6 while those nearest the beam bars increase by significantly less. Such non-linear increases in horizontal joint stirrup strain levels were also observed by Milburn and Park (1982). Indeed, this is a basis for the NZS3101:2006 requirement that, when located sufficiently close to the beam bars, stirrup sets do not contribute to the provided area of horizontal joint reinforcement. For this reason, these stirrups are often referred to as ‘dummy’ stirrups and are included for confinement and antibuckling requirements only. These dummy stirrup sets generally remain at or below yield as observed in the testing of Beckingsale (1980) and Restrepo (1992).

More importantly, the relatively small increase in strain levels for the dummy stirrups suggests that another mechanism is acting to achieve horizontal equilibrium within the vicinity of these stirrups. Concrete compression from the adjacent beams and preferential force uptake by the stiffer beam bars are the most likely means. However, given the significant concrete damage and full beam depth cracks associated with such an advanced inelastic level of loading as discussed in Section 4.1.6, the concrete is likely to be ineffective.

Therefore the probable mechanism of resistance is uptake by the beam bars – similar to the mechanism being proposed for joints with slotted beams spanning into them. However, in a slotted beam, it is not possible for the beam to provide concrete compression to the column to assist with horizontal shear equilibrium. For this reason, the excess horizontal shear demand from the strut would have to be equilibrated by the beam bars.

Thus if the beam bars are able to equilibrate the entire horizontal component of the strut within a slotted joint, the additional horizontal joint stirrups proposed by Au (2010) would be unnecessary and could therefore be excluded from design recommendations. This would help to reduce joint congestion and cost, while improving constructability. It is therefore imperative that the correct joint shear mechanism be established; this will be achieved through analysis of experimental results.

4.5.3 Components of Joint Shear Demand

In Section 4.4 the first principles theoretical analysis used by Paulay and Priestley (1992) to distribute shear to each of the resistance mechanisms was explained. Although slightly more complicated, this process can also be undertaken for joints incorporating slotted beams. Furthermore, due to differences in behaviour between the top and bottom reinforcement, the analysis should be carried out for each layer separately. Note that these equations are left in general form to enable ease of use in a subsequent parametric study presented in Section 4.5.4.

Consider first the top half of the joint shown in Figure 4-46. Because concrete within the adjacent beams is able to contribute to equilibrium within the joint, the analysis at this level is very similar to that of a monolithic joint as discussed in Section 4.4. However, as discussed in Section 4.2.5, the top reinforcement within a slotted joint is expected to remain nominally elastic; i.e. there is no strain hardening and overstrength is due only to material variation. For this reason, the bond stress distribution is assumed to be linear as proposed by Paulay and Priestley (1992).

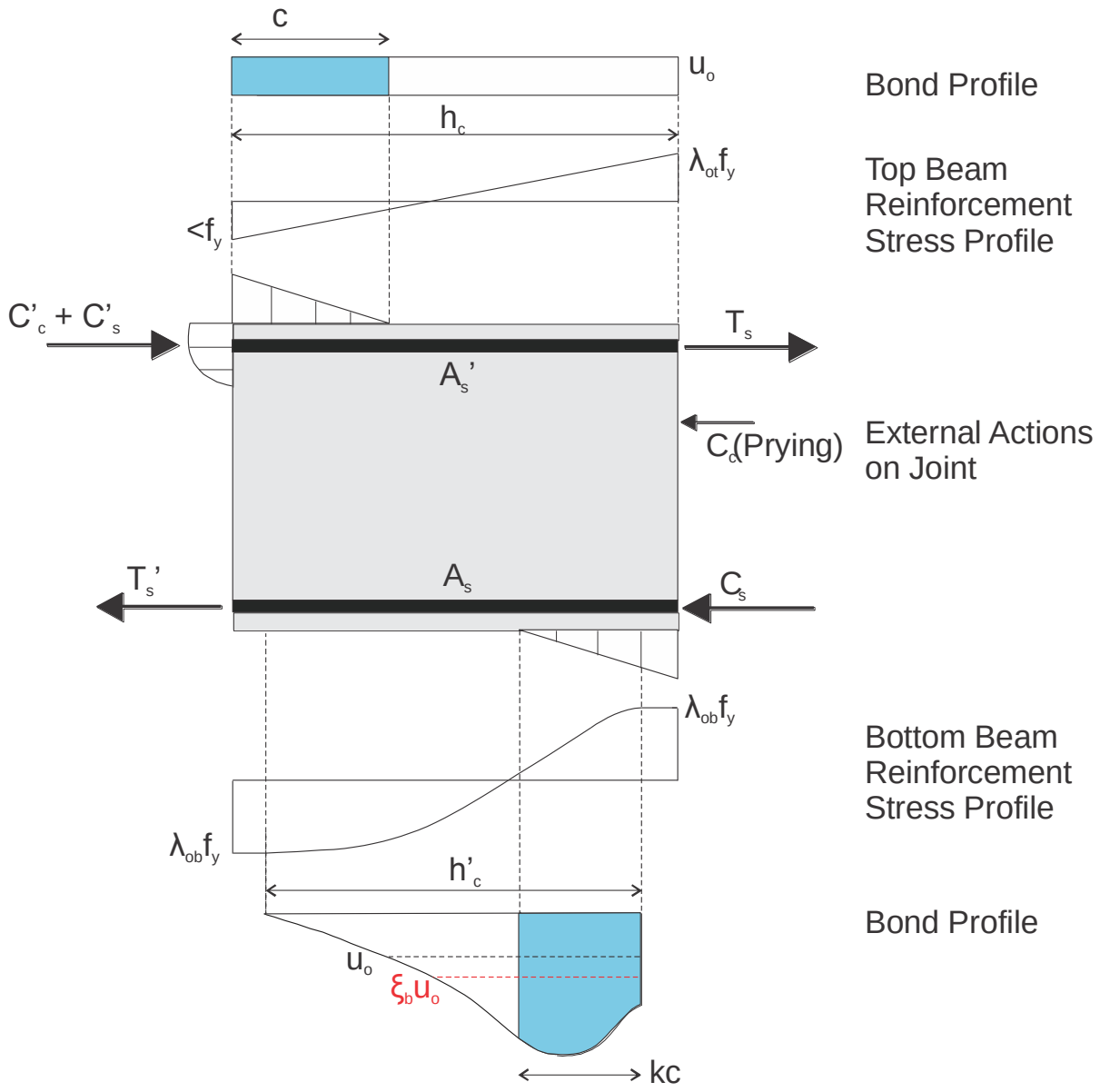

Figure 4-46: *Qualitative reinforcement and bond stress profiles for slotted joints*

Given the top region of slotted and monolithic joints is very similar, Equation 4-37 can be used to estimate the horizontal component of the concrete strut, V_{ch}. Indicated by the blue shaded region on the bond profile in Figure 4-46, $\Delta T'_c$ is then calculated using Equation 4-51. Recall from Section 4.4.1 that $\Delta T'_c$ refers to the small portal of the total force within the top longitudinal beam reinforcement, $T_s + C'_s$, that is resisted by bond over the region where the concrete strut lands and is therefore transferred into the concrete strut as opposed to the truss mechanism.

$$\Delta T_c' = c \times u_o = u_o c$$

$$= (C_s' + T_s)\frac{c}{h_c} \qquad \text{Equation 4-51}$$

Note that the length and height of the bond profile contributing to the strut mechanism have both changed due to the elastic reinforcement but the net contribution is the same as for a monolithic joint. It is then convenient to express C'_s in terms of T_s:

$$C'_s = \gamma A'_s f_y$$

and

$$T_s = \lambda_{ot} f_y A'_s$$

$$\therefore \quad C'_s = \frac{\gamma}{\lambda_{ot}} T_s \qquad \text{Equation 4-52}$$

Overstrength in the top longitudinal reinforcement is limited to material variation only as discussed in Section 4.2.5 with a corresponding value of 1.15 taken from Paulay and Priestley (1992). Combining the above results, $\Delta T'_c$ takes the following form:

$$\Delta T'_c = T_s \left(\frac{\gamma}{\lambda_{ot}} + 1 \right) \frac{c}{h_c} \qquad \text{Equation 4-53}$$

Now taking equilibrium on the left side of the joint in Figure 4-46 and using the result of Equation 4-52, C'_c can be simplified to:

$$C'_c = T'_s - C'_s$$

$$= T'_s - \frac{\gamma}{\lambda_{ot}} T_s$$

Recall that $\beta = A'_s/A_s$ and assume the bottom reinforcement is subject to overstrength λ_{ob} thus C'_c is further refined:

$$\therefore \quad C'_c = \beta T_s \frac{\lambda_{ob}}{\lambda_{ot}} - \frac{\gamma}{\lambda_{ot}} T_s$$

$$= T_s \left(\beta \frac{\lambda_{ob}}{\lambda_{ot}} - \frac{\gamma}{\lambda_{ot}} \right) \qquad \text{Equation 4-54}$$

Using equilibrium across the joint and incorporating the relationship in Equation 4-37, V_{sh} can be expressed as follows:

$$V_{sh} = V_{jh} - V_{ch}$$

$$= [T_s + T'_s - V_{col}] - [C'_c + \Delta T'_c - V_{col}] \qquad \text{Equation 4-55}$$

Combining the results of Equation 4-53 through Equation 4-55, it is now possible to solve for V_{sh} in terms of the force in the top tension reinforcement, T_s:

$$V_{sh} = T_s\left[1 + \frac{\gamma}{\lambda_{ot}} - \frac{c}{h_c}\left(\frac{\gamma}{\lambda_{ot}} + 1\right)\right] \qquad \text{Equation 4-56}$$

Consider now the bottom half of the joint in Figure 4-46. Because there is no concrete contribution from the adjacent beams, the reinforcement is subject to overstrength compression and tension demands simultaneously on either side of the joint. Thus the force in the concrete strut, V_{ch}, is due entirely to force transferred out of the beam bars within the region of the column subject to compression, ΔT_c:

$$V_{ch} = \Delta T_c - V_{col} \qquad \text{Equation 4-57}$$

As discussed in Section 4.2.4, the bond stress profile for the bottom reinforcement within a slotted joint is non-linear. Similar to the profile for the monolithic joint, it is more effective within the compression region of the column as illustrated in Figure 4-46. However, given a lack of previous experimental testing, the exact distribution is unknown. Thus the relative average bond stress within this region is expressed as a portion, ξ_b, of the average bond stress over the column depth, u_o. The factor ξ_b can thus be thought of as the degree of uniformity of the bond stress distribution where higher values correspond to a less uniform bond stress profile.

The width of the column neutral axis depth assumed effective in transferring bond to the strut mechanism, *kc*, is also not accurately quantified. However, it is expected to be less than that within an equivalent monolithic joint due to increased levels of strain penetration as discussed in Section 4.2.2. Combining these factors and expressing in terms of the reinforcement stresses, ΔT_c is found using Equation 4-58:

$$\Delta T_c = kc\xi_b u_o$$

$$= \xi_b(C_s + T_s')\frac{kc}{h_c}$$

$$= 2\xi_b T_s'\frac{kc}{h_c} \qquad \text{Equation 4-58}$$

It follows from Equation 4-57 that:

$$V_{ch} = 2\xi_b T_s'\frac{kc}{h_c} - V_{col} \qquad \text{Equation 4-59}$$

Using equilibrium across the joint and introducing the result of Equation 4-59, it is possible to solve for V_{sh}:

$$V_{sh} = V_{jh} - V_{ch}$$

$$= [T_s + T_s^{'} - V_{col}] - \left[2\xi_b T_s^{'} \frac{kc}{h_c} - V_{col}\right]$$

…..

$$V_{sh} = T_s^{'}\left[1 + \beta\frac{\lambda_{ot}}{\lambda_{ob}} - \frac{2\xi_b kc}{h_c}\right] \qquad \text{Equation 4-60}$$

Equation 4-60 is better expressed in terms of the force in the top tension reinforcement, T_s, to allow easy comparison with Equation 4-56:

$$V_{sh} = T_s\left[\frac{\beta\lambda_{ob}}{\lambda_{ot}} + 1 - \frac{2\beta\xi_b kc\lambda_{ob}}{h_c\lambda_{ot}}\right] \qquad \text{Equation 4-61}$$

4.5.4 Parametric Study on Joint Shear Demand

After establishing the governing equations for joint shear within a slotted joint in Section 4.5.3, the results can now be used to determine the sensitivity of V_{sh} to various parameters. This will enable a more accurate basis for detailing of the horizontal joint reinforcement within the test specimens compared with the suggestions of Au (2010) which, as discussed in Section 4.5.1, are not reliable. Furthermore, it will determine whether or not the current code provisions for horizontal joint shear reinforcement are applicable to slotted joints.

The first step is to make upper and lower bound estimates for each of the variables discussed in Section 4.5.3 along with estimates for the predicted values. Firstly consider the variable β, as discussed in Section 4.1.4, a known quantity at the discretion of the designer. The value recommended by Au (2010) is 0.5 but, due to the limited number of available bar diameters and the desire to keep reinforcement layouts symmetric, this figure cannot always be achieved. As such, lower and upper bound values of 0.4 and 0.6, respectively, are adopted.

Now consider the top and bottom reinforcement overstrength factors, λ_{ot} and λ_{ob}. As discussed in Sections 4.2.4 and 4.2.5, the predicted values for these factors are 1.15 and 1.35, respectively. The lower bound for λ_{ot} is taken as 1.0, corresponding to the case where the bar reaches yield as expected but the material overstrength factor is equal to 1.0; i.e. the bar yields at the characteristic yield strength. The upper bound is conservatively taken as 1.25, corresponding to the usual overstrength factor for Grade 300 reinforcement. Because the bottom reinforcement is detailed to yield in both compression and tension, the lower bound

for λ_{ob} is taken as 1.25. The upper bound value is taken as 1.45 from the results of experimental testing by Au (2010).

The value ξ_b is difficult to determine with accuracy because it cannot be directly measured. As discussed in Section 4.5.3, ξ_b is a function of the bond stress distribution – the more uniform the distribution, the lower the value of ξ_b. Because the bond stress distribution within a slotted joint is unlikely to be more uniform than that within a monolithic joint, the value of 1.25 from Section 4.4.1 provides a suitable lower bound. The upper bound is assumed to be 1.7 after this was back-calculated by Au (2010) from the test of SB2. Because strain penetration within a slotted joint is more severe than in a monolithic joint, the degree of bond profile uniformity is expected to decrease. However, the use of supplementary vertical joint stirrups, as discussed in Section 4.2.3, acts to improve bond performance on the tension side of the joint thus increasing bond uniformity. Combining the conflicting influences of these two factors, the predicted value for ξ_b is taken as 1.4.

Recall the variable k which represents the portion of the neutral axis depth effective in transferring stress from the reinforcement into the concrete strut mechanism through bond. As discussed in Section 4.4.1, k is taken as 0.8 for a monolithic joint with the remaining portion of c assumed ineffective due to cover concrete and the effects of strain penetration. Because the effects of strain penetration are more severe within a slotted joint, this value represents the upper bound for k. The lower bound is taken from the test of SB3 by Au (2010) where strain penetration, L_{sp}, reached $0.02 f_y d_b$. Corresponding values from SB2 are not applicable as bar slip failure occurred in this test. Given f_y = 316 MPa and d_b = 16 mm from material testing, L_{sp} is found to be 101 mm. It is assumed that 70% of this strain penetration occurred within the column. This is less than the recommendation given in Section 5.5.1 but is justified by the absence of supplementary vertical joint stirrups within specimen SB3. Adopting the revised neutral axis relationship for larger column depths as given in Equation 4-67, using the reported cover depth of 32 mm, and given h_c = 600 mm, k can be estimated from Equation 4-62:

$$kc = \left(\frac{c - 0.7L_{sp} - cover}{c}\right)c = \left(\frac{200 - 71 - 32}{200}\right) \approx 0.5c \qquad \text{Equation 4-62}$$

$$\therefore \quad k = 0.5$$

Note that the axial load ratio, $N^*/A_g f_c'$, was equal to 0.02 in specimen SB3.

The variable γ indicates the portion of yield stress activated within the compression reinforcement and is expected to be 0.5 as per Section 4.2.5. Monolithic theory from Section 4.1.4 provides a suitable upper bound of 0.7, while the lower bound is taken as 0.4 to reflect the case where concrete within the top hinge is contributing significantly to force equilibrium. An additional variable that must be considered is the ratio h_c/h_b. Assuming that D25s will be used for the bottom beam bars in practice and that the column depth is governed by Equation 4-22, the resulting range is 650 – 750 mm. Adopting a practical range of beam depths between 550 – 750 mm, h_c/h_b is found to range from 0.8 to 1.33.

Now that the upper and lower bound values for each variable have been determined, they can be used to find the theoretical range of horizontal joint shear demand to enable comparison with NZS3101:2006 provisions. Using the relationship for T_s in Equation 4-52, Equation 4-56 takes the form below:

$$V_{sh} = \lambda_{ot} f_y A_s' \left[1 + \frac{\gamma}{\lambda_{ot}} - \frac{c}{h_c}\left(\frac{\gamma}{\lambda_{ot}} + 1\right)\right]$$

This can then be rearranged to give:

$$\frac{V_{sh}}{f_y A_s'} = \lambda_{ot} \left[1 + \frac{\gamma}{\lambda_{ot}} - \frac{c}{h_c}\left(\frac{\gamma}{\lambda_{ot}} + 1\right)\right] \qquad \text{Equation 4-63}$$

Similarly, the NZS3101:2006 equation for the required amount of horizontal joint shear reinforcement within a monolithic joint can be expressed using the following relationship:

$$\frac{V_{sh}}{f_y A_s^*} = \frac{6 V_{oj\,h}^*}{f_c' b_j h_c} \alpha_i \qquad \text{Equation 4-64}$$

Where A^*_s corresponds to the larger of the top and bottom beam reinforcement area and α_i is calculated using Equation 4-65:

$$\alpha_i = 1.4 - \frac{1.6 N^*}{f_c' A_g} \qquad \text{Equation 4-65}$$

Equation 4-63 was then used to evaluate the sensitivity of joint shear demand to variations in each individual parameter. The results of this parametric analysis are presented in Table 4-1 in addition to comparisons with NZS3101:2006 provisions according to Equation 4-64.

Table 4-1: *Influence of joint parameters on accuracy of code equation applied to interior joints incorporating slotted beams*

	Lower Bound				Upper Bound			
Variable	**Value**	**$V_{sh,slot}/A'_sf_y$**	**$V_{sh,code}/A'_sf_y$**	**Difference as $\%V_{sh,code}/A'_sf_y$**	**Value**	**$V_{sh,slot}/A'_sf_y$**	**$V_{sh,code}/A'_sf_y$**	**Difference as $\%V_{sh,code}/A'_sf_y$**
β	0.4	1.15	1.11	4%	0.6	1.15	1.11	4%
λ_{ot}	1	1.05	1.11	5%	1.25	1.22	1.11	10%
λ_{ob}	1.25	1.15	1.10	4%	1.45	1.16	1.11	4%
ξ_b	1.25	1.15	1.11	4%	1.7	1.15	1.11	4%
k	0.5	1.15	1.11	4%	0.8	1.15	1.11	4%
γ	0.4	1.08	1.11	2%	0.7	1.29	1.11	17%
h_c/h_b	0.8	1.08	1.04	4%	1.4	1.15	1.11	4%
N^*/A_gf_c'	0.0	1.24	1.19	4%	0.2	0.96	1.02	6%
Standard values: f_y = 300 MPa, f_c' = 40 MPa, h_c = 690 mm, h_c/h_b = 1.20, N^*/A_gf_c' = 0.06								

Where $V_{sh,slot}/A'_sf_y$ and $V_{sh,code}/A'_sf_y$ are the joint shear demands according to Equation 4-63 and Equation 4-64, respectively.

From Table 4-1 it is clear that variations in most of the joint parameters do not cause the NZS3101:2006 joint shear demand equation to become inaccurate for use with slotted joints. For the variables β, h_c/h_b, and N^*/A_gf_c', this is because the code either directly accounts for these factors or inherently accounts for them in the derivation of Equation 4-64. The variables λ_{ob}, ξ_b, and k also have little effect but for a different reason. These relate to the smaller area of beam reinforcement and, as such, do not contribute to V_{sh} in either the slotted joint or NZS3101:2006 equation derivations. However, these parameters do influence the amount of shear that can be transferred from the bottom beam reinforcement into the strut mechanism and thus significantly affect the quantity ΔV_{sh} as discussed below.

Therefore λ_{ot} and γ are the only variables of interest in determining whether or not current code provisions for joint shear demand are adequate. These variables have a heavy influence because these feature prominently in the slotted joint shear equation but are assigned set values in the NZS3101:2006 derivation. In the code derivation, λ_{ot} is taken as 1.25 corresponding to the standard overstrength factor for Grade 300 reinforcement, while γ is assumed to be 0.7 in accordance with Section 4.1.4.

Finally, if the predicated values for every parameter are used simultaneously, the difference between the NZS3101:2006 and slotted equations is found to be 4% $V_{sh,code}/A'_sf_y$. Given this value is consistently observed throughout Table 4-1, the discrepancy between the code and slotted equations is most likely explained by rounding error in the derivation of Equation

4-65. This becomes evident when comparing the Paulay and Priestley (1992) derivation to the equation adopted by NZS3101:2006. As a result, the code equations appear to be suitable for design at this stage and will be reviewed based on experimental results when more appropriate values for each parameter are available.

As discussed in Section 4.5.3, there is also a difference in the shear force taken up by the truss mechanism at the top and bottom of the joint; this discrepancy is due to the lack of concrete compression in the adjacent beam soffit. Au (2010) found that this quantity, ΔV_{sh}, was on the order of 20 – 35% of $V_{sh,code}$ for an equivalent monolithic joint. Combining Equation 4-56 and Equation 4-61, ΔV_{sh} can also be found theoretically as given in Equation 4-66:

$$\Delta V_{sh} = V_{sh,bottom} - V_{sh,top}$$

$$= T_s\left[\frac{\beta\lambda_{ob}}{\lambda_{ot}} + 1 - \frac{2\beta\xi_b kc\lambda_{ob}}{h_c\lambda_{ot}}\right] - T_s\left[1 + \frac{\gamma}{\lambda_{ot}} - \frac{c}{h_c}\left(\frac{\gamma}{\lambda_{ot}} + 1\right)\right]$$

$$= T_s\left[\frac{\beta\lambda_{ob}}{\lambda_{ot}}\left(1 - \frac{2\xi_b kc}{h_c}\right) - \frac{\gamma}{\lambda_{ot}} + \frac{c}{h_c}\left(1 + \frac{\gamma}{\lambda_{ot}}\right)\right] \qquad \text{Equation 4-66}$$

The results in Table 4-2 are obtained by evaluating the effects of varying each parameter individually and expressing in terms of $\Delta V_{sh}/V_{sh,code}$, as was done for the previous study. It should be noted that the NZS3101:2006 limit of $6V_{ojh}/f_c'b_jh_c$ governed in all of the cases suggesting that the applicability of this may need to be investigated further for slotted joints.

Table 4-2: *Influence of joint parameters on* ΔV_{sh}

	Lower Bound		Upper Bound		Range
Variable	**Value**	**$\Delta V_{sh}/V_{sh,code}$**	**Value**	**$\Delta V_{sh}/V_{sh,code}$**	**$\Delta V_{sh}/V_{sh,code}$**
β	0.4	20%	0.6	30%	10%
λ_{ot}	1	20%	1.25	27%	7%
λ_{ob}	1.25	23%	1.45	26%	3%
ξ_b	1.25	29%	1.7	17%	12%
k	0.5	35%	0.8	20%	15%
γ	0.4	31%	0.7	12%	19%
h_c/h_b	0.8	28%	1.33	25%	3%
N^*/A_gf_c'	0.00	22%	0.20	31%	9%
Standard values: f_y = 300 MPa, f_c' = 40 MPa, h_c = 690 mm, h_c/h_b = 1.20, N^*/A_gf_c' = 0.06					

From the results shown in Table 4-2, it is clear that the range of $\Delta V_{sh}/V_{sh,code}$ is relatively insensitive to the parameters λ_{ot}, λ_{ob}, and h_c/h_b. Both of the overstrength factors have little effect because they do not influence the effectiveness of the strut mechanism at the top or bottom of the joint. Subsequently, they do not change the relative contribution of shear to

each mechanism. However, they do influence the magnitude of shear within the joint as evidenced in Table 4-1. In the work of Au (2010), the parameter h_c/h_b is found to have a significant influence on the range of $\Delta V_{sh}/V_{sh,code}$, becoming especially noticeable at h_c/h_b ratios above 1.4. Given the overly large column sizes Au (2010) was assuming for successful application of slotted joints, such high ratios were justified. However, in light of the findings of Section 4.2.4, smaller column depths are expected and the range of practical h_c/h_b ratios therefore decreases such that 1.4 represents the expected upper bound.

The variables β and $N^*/A_g f_c'$ both have a reasonable influence on the range of $\Delta V_{sh}/V_{sh,code}$. When all other variables remain unchanged, increasing β results in more force in the bottom reinforcement and thus increased shear demand across the bottom of the joint. Meanwhile, shear across the top of the joint remains relatively unaffected and, therefore, $\Delta V_{sh}/V_{sh,code}$ changes. As shown in Table 4-2, increasing $N^*/A_g f_c'$ causes $\Delta V_{sh}/V_{sh,code}$ to increase in what seems a counter-intuitive trend. As with a monolithic joint, one would expect increasing axial stress to increase c/h_c such that more force is transferred from the reinforcement into the strut mechanism via bond and V_{sh} to decrease as a result. This is in fact the case but, because bond transfer is more effective in the top reinforcement than in the bottom, the disparity between the two grows with increasing axial stress. The key parameters relating to effectiveness of bond transfer are k and ξ_b. Figure 4-47 shows that while increasing bond effectiveness reduces $\Delta V_{sh}/V_{sh,code}$, increases in axial stress exacerbate the discrepancy. A similar trend can be observed for k.

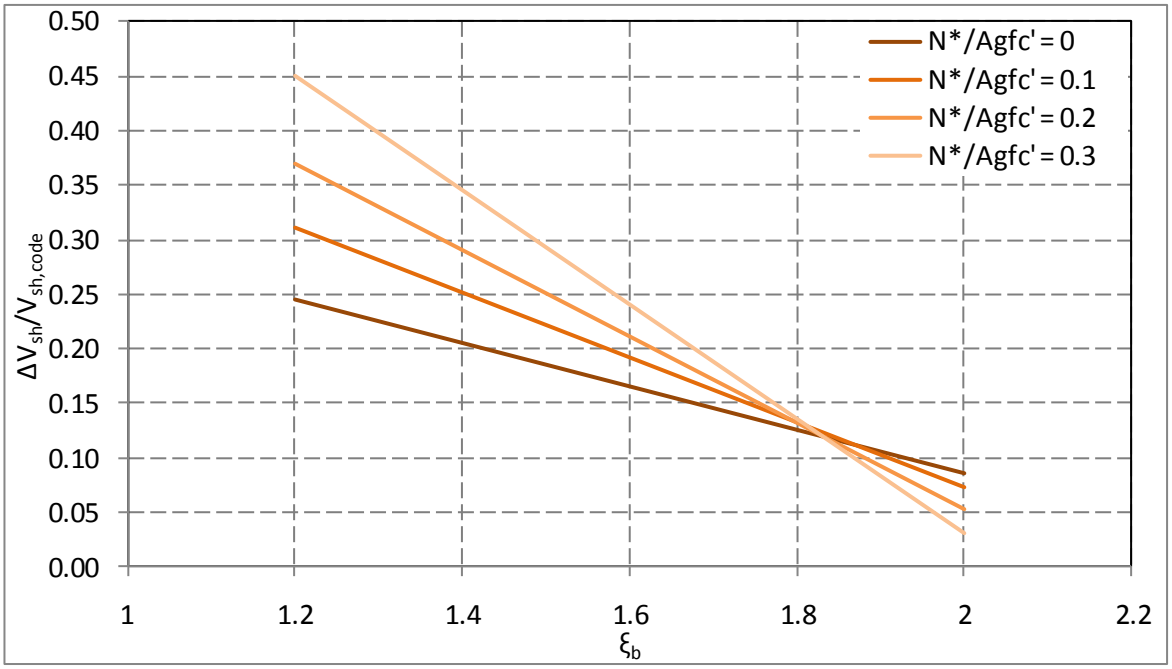

Figure 4-47: *Influence of bond non-linearity and axial load on* ΔV_{sh}

Table 4-2 indicates that the factors having the most influence on $\Delta V_{sh}/V_{sh,code}$ are γ, k, and ξ_b. As outlined above, k and ξ_b are both measures of bond efficiency and thus have the same effect. Figure 4-48 shows that increasing bond efficiency reduces $\Delta V_{sh}/V_{sh,code}$ as more force is able to be transferred from the bottom reinforcement into the strut mechanism. Increasing γ also reduces $\Delta V_{sh}/V_{sh,code}$ as more force is introduced to the joint by the top reinforcement. This additional force exceeds that able to be resisted by the strut mechanism and so the demand on the truss mechanism across the top of the joint increases. As such, it becomes closer in magnitude to the truss mechanism demands across the bottom of the joint and the difference between the two, $\Delta V_{sh}/V_{sh,code}$, decreases.

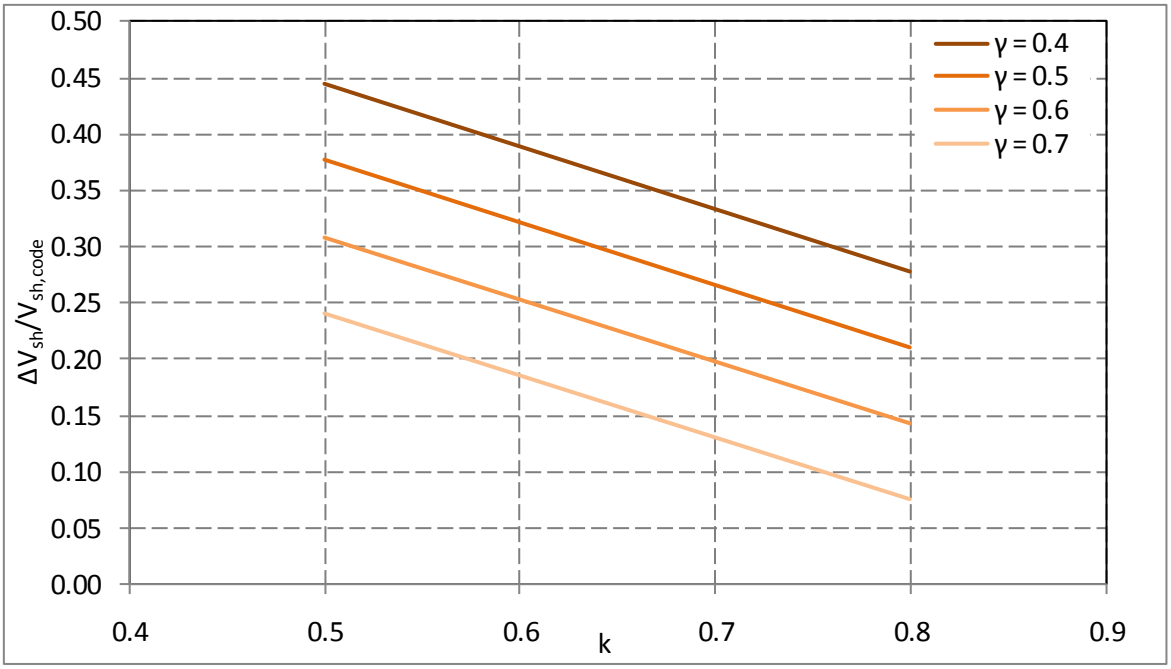

Figure 4-48: *Influence of key parameters on* ΔV_{sh}

Finally, if the result is computed when all variables are taken as predicted, $\Delta V_{sh}/V_{sh,code}$ is found to be 25%. The peak upper and lower bound values are 31 and 35%, respectively. Thus these results are in agreement with those of Au (2010), despite his results being based on a test in which premature bar slip failure occurred. Given this agreement, $\Delta V_{sh}/V_{sh,code}$ = 30% appears to be a reasonable value to use for design of the test specimens. In terms of joint detailing, this corresponds to 30% additional horizontal joint shear reinforcement, ΔA_{jh}, which should be placed within the bottom half of the joint. Unlike for monolithic joints where they are excluded due to their proximity to the beam bars, stirrups sets immediately adjacent to the bottom beam reinforcement can be considered to contribute to ΔA_{jh} (Au, 2010). This is because ΔA_{jh} is required to resist a component of the strut, not force transferred by bond from the immediately adjacent beam bars as would be the case in a monolithic joint. Thus fewer additional stirrup sets are actually required than it immediately appears. The specimens used

in the experimental phase of this research will have 35 and 20% ΔA_{jh}, in line with the range of values determined in the above parametric study. Note these additional horizontal joint stirrups are provided for redundancy should the revised joint shear mechanism in Section 4.5.2 prove incorrect. If the revised mechanism is correct, this would be reflected by a symmetric strain profile activated to a lower level.

4.5.5 Horizontal Joint Shear Reinforcement Provision

Using the results of Chapter 5 in conjunction with the generalised joint shear equations developed in Sections 4.5.3 and 4.5.4, the required amount of horizontal shear reinforcement within a slotted joint can be determined. Table 4-3 gives the various joint parameters as determined from experimental testing of the two specimens:

Table 4-3: *Experimentally determined joint parameters*

Variable	Value
λ_{ot}	1.1
λ_{ob}	1.35
ξ_b	2
k	0.8
γ	0.4
β	0.5
c/h_c	0.57

Note that the value c/h_c is the average observed during tests as calculated from moment-curvature analysis of the elastic column rather than Paulay and Priestley (1992) equation used for the parametric study. Using the values in Table 4-3, the relative joint shear demand based on activation of the top longitudinal reinforcement can then be calculated theoretically from Equation 4-56 to give $V_{sh} = 0.59T_s$, where T_s is the overstrength force in the top longitudinal reinforcement. This process can be repeated based on the bottom longitudinal reinforcement and results in $V_{sh} = 0.49T_s$ using Equation 4-61. These figures represent the horizontal joint shear demand that must be resisted by the truss mechanism.

The theoretical value of ΔV_{sh} can then be calculated by subtracting the top equilibrium V_{sh} value from the bottom to give $\Delta V_{sh} = -0.10T_s$. Note that the value of V_{sh} is almost identical when expressed in terms of $V_{sh,code}$ in this case, and can therefore be directly compared with the values in the parametric study of Section 4.5.4. The most important comparison to note is that the experimentally derived value is negative. This is in contradiction with the findings of both Au (2010) and the parametric study in Section 4.5.4 and implies that more force is being introduced to the truss mechanism at the bottom of the joint than at the top. Assuming this

value is correct it would mean that the joint shear mechanism proposed by Au (2010) does not govern the joint behaviour. From a design perspective, it means that equilibrium across the top of the joint governs the required area of horizontal joint reinforcement as opposed to equilibrium across the bottom as originally assumed.

A possible explanation for this unexpected result can be found by examining the parameters in Table 4-3. Low λ_{ot} and γ values show that the top longitudinal beam reinforcement is contributing a relatively small amount of force across the joint. Coupled with observations from Section 5.4.2 of limited damage to the hinge region, this suggests dominance of the strut mechanism at the top of the joint. It is also likely that the supplementary vertical joint reinforcement is influencing the joint behaviour – an important factor which is not accounted for in the theoretical approach.

V_{sh} can also be calculated directly from experimental data by summing forces within the horizontal joint reinforcement. This approach is based on the assumption that all horizontal joint reinforcement activation is due to horizontal joint shear demand; i.e. any activation of the horizontal joint stirrups due to confinement of the joint core and buckling restraint in the column bars is ignored. When expressed in terms of T_s, the equivalent experimental values of V_{sh} are found to be 0.26 and 0.31T_s at ULS drift for specimens A and B, respectively. These values are up to 50% lower than those calculated using the experimentally validated theoretical approach above. This suggests that another mechanism – one unaccounted for by the theoretical approach – is contributing to equilibrium across the joint. The most likely explanation is that the supplementary vertical joint reinforcement is acting to make the strut mechanism more efficient such that it is able to take a greater portion of the horizontal joint shear demand. However, conservatism in adopting the design values in Table 4-3 is also a contributing factor. Nonetheless, given the significant difference observed between theoretical and experimental values, it is imperative that the effects of supplementary vertical joint reinforcement on the joint shear mechanisms be further investigated.

Note that experimental values for ΔV_{sh} could not be calculated with sufficient accuracy to warrant discussion here. This was due to the difficulty associated with calculating V_{sh} across the bottom of the joint where post-yield strain gauge data was found to be unreliable. Back calculation of the bottom longitudinal steel forces using equilibrium at the beam face was also not possible due to the inability to quantify the concrete hinge prying mechanism.

While the V_{sh} values determined from experimental data suggest less horizontal joint reinforcement is required within joints incorporating slotted beams, there are a number of

other factors that must first be considered before any such design recommendation is made. Firstly, the current Concrete Structures Design Standard recommendations limit the strut mechanism contributions in larger columns by imposing the condition $V_{sh}/V_{jh} \geq 0.85$ as discussed in Section 4.4.2. Thus, according to NZS3101:2006, even the more conservative estimate of $V_{sh} = 0.59T_s$ is easily governed by this limit. However, this limit is somewhat arbitrary and disadvantaging to joints incorporating large column depths where the strut mechanism is highly effective. Leon (1989) suggests that, in joints where the column depth exceeds $24d_b$, column confinement provisions are sufficient for detailing the horizontal joint reinforcement. Based on Equation 4-24, the column depth for use with slotted beams is unlikely to be less than this value for typical concrete strengths on the order of 40 MPa. Furthermore, Cheng et al (2000) found NZS3101:2006 provisions to be overly conservative in terms of the amount of joint shear assigned to the truss mechanism even for typical monolithic column depths on the order of $20d_b$ when normalised to $f_c' = 30$ MPa and $f_y = 300$ MPa. Throughout a range of tests, these researchers found $A_{jh,prvd}/A_{jh,code}$ values on the order of 0.8 to be sufficient to achieve a nominally elastic joint response. Experimental observations of limited joint shear activation in Section 5.6.4 are in agreement with the above recommendations, as are the results of Au's (2010) test SB3 which also incorporated a relatively large column depth.

Secondly, concrete stress within the joint should be limited to ensure crushing does not occur. This is currently facilitated in NZS3101:2006 by limiting the overstrength joint shear demand, V_{ojh}, and should also be enforced for slotted joints. However, given the relatively large column depths required for successful implementation of slotted beams, this is not expected to govern in most cases.

Any reduction in V_{sh} requirements must also account for variation in parameters at the designer's discretion. These include axial load ratio, $N^*/A_g f_c'$, beam reinforcement asymmetry, β, and beam/column geometry, h_c/h_b. The latter two parameters are inherently accounted for within the derivation of V_{sh} given in Equation 4-63 while axial load ratio is accommodated within this equation through embedment of a relationship for the neutral axis depth. While Paulay and Priestley (1992) have developed such a relationship as defined in Equation 4-38, this was found to underestimate the neutral axis depth for large columns, such as those required for successful implementation of slotted beams. This is evident in Figure 4-49 which compares the column neutral axis depth ratio, c/h_c, for various column depths, h_c, as calculated through moment curvature analysis and using the Paulay and Priestley (1992)

equation. It was found that the Paulay and Priestley (1992) equation underestimated c/h_c by 20 – 30% compared with the moment-curvature analysis.

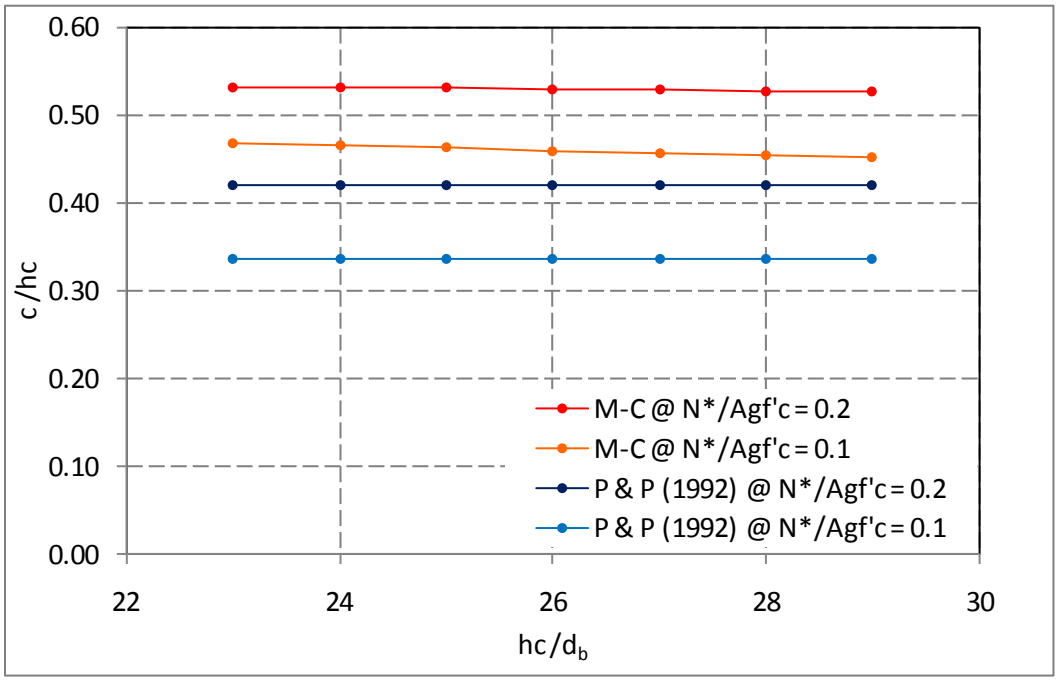

Figure 4-49: *Paulay and Priestley (1992) and moment-curvature estimates for column neutral axis depth ratio*

As such, a revised *c/h* ratio as determined from moment-curvature analysis will be adopted for determination of V_{sh}. Illustrated graphically in Figure 4-50, this relationship was developed based on a parametric analysis of large column depths operating within the elastic range. A moment ratio of $M_{y,col}/M_{o,b}$ of 1.5 and column depths ranging from 23 to 29d_b, consistent with those required for slotted beams, were adopted in the analysis. Note that $M_{y,col}$ and $M_{o,b}$ correspond to the column yield and beam overstrength at the column face moments, respectively.

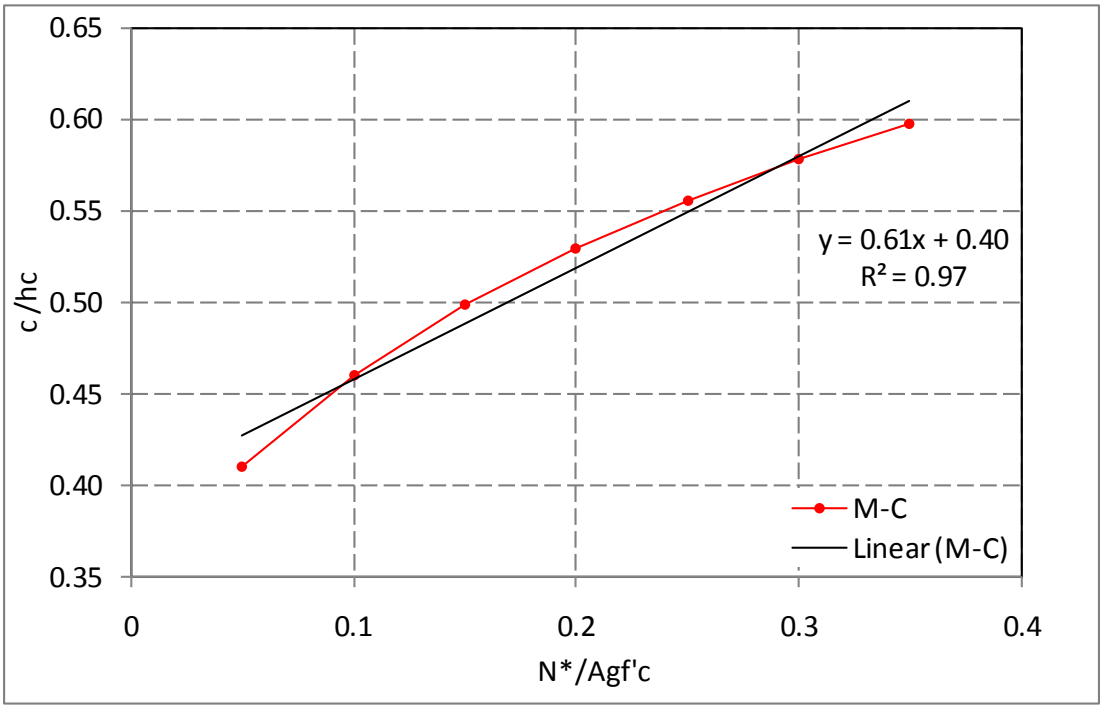

Figure 4-50: Moment curvature estimate for column neutral axis depth

Equation 4-67 gives the resulting column neutral axis depths as a function of axial load ratio. Note that the base value of c/h_c has been reduced by 20% – lower c/h_c ratios result in higher V_{sh} requirements – to account for variables outside the scope of the parametric analysis undertaken:

$$\frac{c}{h_c} = 0.61\frac{N^*}{A_g f_c'} + 0.32 \qquad \text{Equation 4-67}$$

Combining Equation 4-63 and Equation 4-67, the following relationship for V_{sh} is obtained based on equilibrium across the top of the joint after this was found to give the most conservative estimate as discussed above:

$$\frac{V_{sh}}{f_y A_s'} = \lambda_{ot}\left[1 + \frac{\gamma}{\lambda_{ot}} - \left(0.61\frac{N^*}{A_g f_c'} + 0.32\right)\left(\frac{\gamma}{\lambda_{ot}} + 1\right)\right]$$

The values in Table 4-3 are then substituted in and the expression simplified to give Equation 4-68:

$$V_{sh} = A_s' f_y \left(1.02 - 0.92\frac{N^*}{A_g f_c'}\right) \qquad \text{Equation 4-68}$$

Finally, a 10% reduction is made to account for interaction of the supplementary vertical joint stirrups with confinement and shear capacity of the joint as discussed in Section 5.6.5. Note

that this reduction is not applied to the axial stress term as the change in neutral axis is assumed to be independent of the presence of supplementary vertical joint stirrups. The resulting design recommendations for determining the required horizontal joint reinforcement area within a slotted joint is given in Equation 4-69:

$$A_{jh} = 0.92A_s' \frac{f_y}{f_{yh}}\left(1 - \frac{N^*}{A_g f_c'}\right) \qquad \text{Equation 4-69}$$

This is approximately 20% less conservative than current NZS3101:2006 requirements for one-way joints subject to nominal values of axial stress ($N^*/A_g f_c' = 0.1$). Note that the above equation is only applicable when supplementary vertical joint reinforcement is provided. In cases where such reinforcement is not present, current NZS3101:2006 provisions should be more than sufficient. However, these are likely to be overly conservative given a required column depth on the order of $28d_b$ according to Equation 4-22.

It is generally accepted that increased axial load reduces the joint shear reinforcement requirements. This is reflected in both the NZS3101:2006 requirements and Equation 4-69 above. However, there is a practical upper limit to the beneficial effects provided by increased axial load, when crushing of the joint begins to occur. Research by Cheng et al (2000) indicates this change in behaviour occurs around $N^*/A_g f_c' = 0.3$. As such, $N^*/A_g f_c'$ should not be taken as greater than 0.3 in Equation 4-69.

Given the revised mechanism has been established to govern joint shear behaviour as discussed in Section 5.6.4, the bottom stirrups should also now be considered ‘dummy’ stirrups as described in Section 4.5.2. Unlike in the Au (2010) joint shear mechanism, these are no longer required to equilibrate a portion of the joint strut. Instead, these stirrups function in the same way as horizontal stirrups within a monolithic joint, resisting shear through the truss mechanism. When this is the case, stirrup sets immediately adjacent to the beam bars are not considered effective in resisting joint shear given their close proximity to the beam bars.

Chapter 5 - EXPERIMENTAL PROGRAMME

5.1 Overview

For the experimental phase of this research, two 80% scale slotted beam-column joint subassemblies were tested under quasi-cyclic loading. The design of these specimens was based on the results of testing by Au (2010), findings from Chapter 4, and NZS3101:2006 provisions. Testing was carried out in accordance with American Concrete Institute guidelines (ACI Committee 374, 2005).

The purpose of this testing was to:

- Determine whether or not the initial column depth provisions developed in Section 4.2 are adequate to prevent bar slip failure in the bottom longitudinal beam reinforcement.
- Assess the effectiveness of using supplementary vertical stirrups within the joint to enhance bond performance.
- Determine whether or not additional horizontal joint shear reinforcement is required when bar slip is not the method of failure.
- Determine which mechanism governs the behaviour within the beam-column joint:
    - Mechanism proposed by Au (2010) as per Section 4.5.1 or,
    - Revised mechanism as per Section 4.5.2
- Assess the suitability of using Grade 300 reinforcement in the top of the beam in terms of observed damage and level of activation.
- Investigate failure mechanisms when bar slip failure does not occur.
- Refine initial design recommendations based on test findings.

5.2 Test Specimens

5.2.1 Prototype Building

The test specimens were taken from the prototype 7-storey office building shown in Figure 5-1. This structure consists of moment resisting frames in both directions with Hollowcore flooring units spanning in the transverse direction. It was designed for Wellington seismicity

founded on Class C soil with an importance level of 2 and 50 year return period earthquake according to NZS1170.5:2004 (Standards Association of New Zealand, 2004). Seismic loading was derived from non-linear time history analyses using a batch of scaled earthquake records. These analyses were carried out using Ruaumoko 2D (Carr, 2005) on the transverse frame incorporating Au (2010) type multi-spring models. Moment redistribution was then carried out according to NZS3101:2006 on the resulting average moment and scaled appropriately for design of the subassemblies.

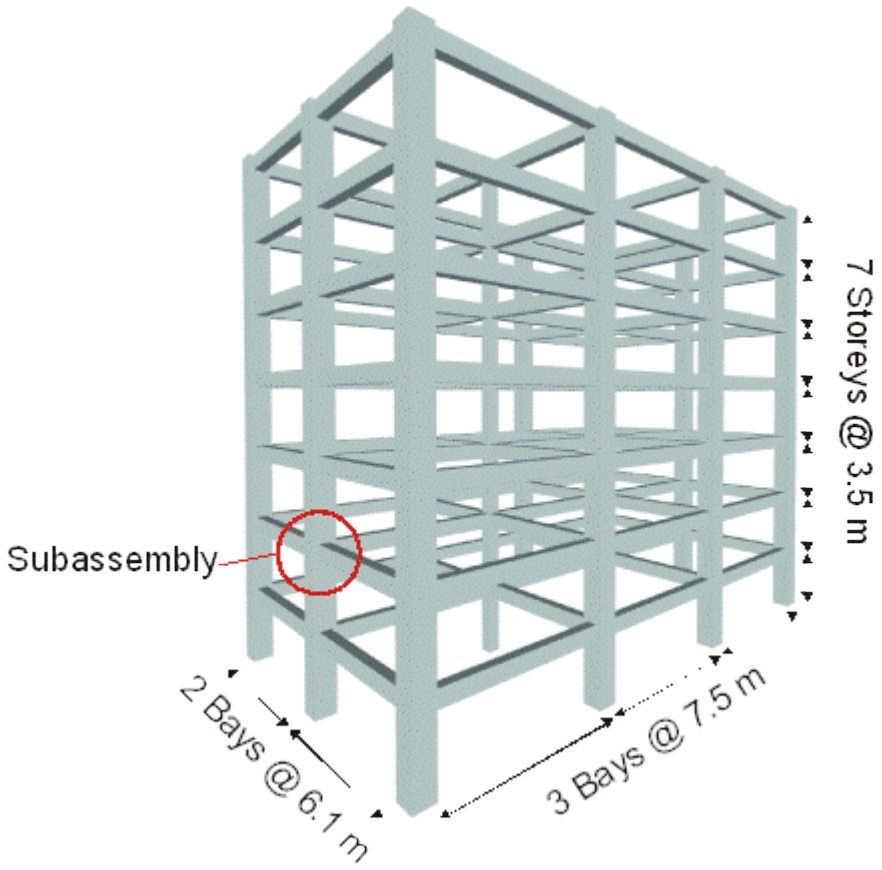

Figure 5-1: *Prototype building from which test specimens were taken. Adapted from Muir, Bull & Pampanin (2010)*

5.2.2 Specimen Design

Detailed design of specimens A and B was undertaken according to NZS3101:2006 requirements with some changes. These included beam stirrup density within the unbonded region, hanger design, unbonding of the bottom beam reinforcement, and top to bottom reinforcement bias, which were detailed according to Au (2010) recommendations. Horizontal and vertical joint reinforcement were determined in accordance with findings from Chapter 4 of this thesis. As a critical aspect of this research, the calculation used to determine the column depth for testing has been reproduced in Equation 5-1; again, this was based directly on findings from Chapter 4.

$$\frac{h_c}{d_b} \geq \frac{\lambda_o f_y d_b}{2.1 \xi_p \xi_r \xi_t \sqrt{f_c'}} = \frac{1.35 \times 300}{2.1 \times 1.14 \times \sqrt{40}} = 26.7 d_b \approx 535\ mm \qquad \text{Equation 5-1}$$

Where ξ_p and ξ_t were taken as unity and d_b is equal to 20 mm. The geometry and reinforcement layout for specimens A and B is illustrated in Figure 5-2. Note that an additional 50 mm has been added to the above figure to account for the effects of strain gauge installation; this is discussed further in Section 5.2.4.

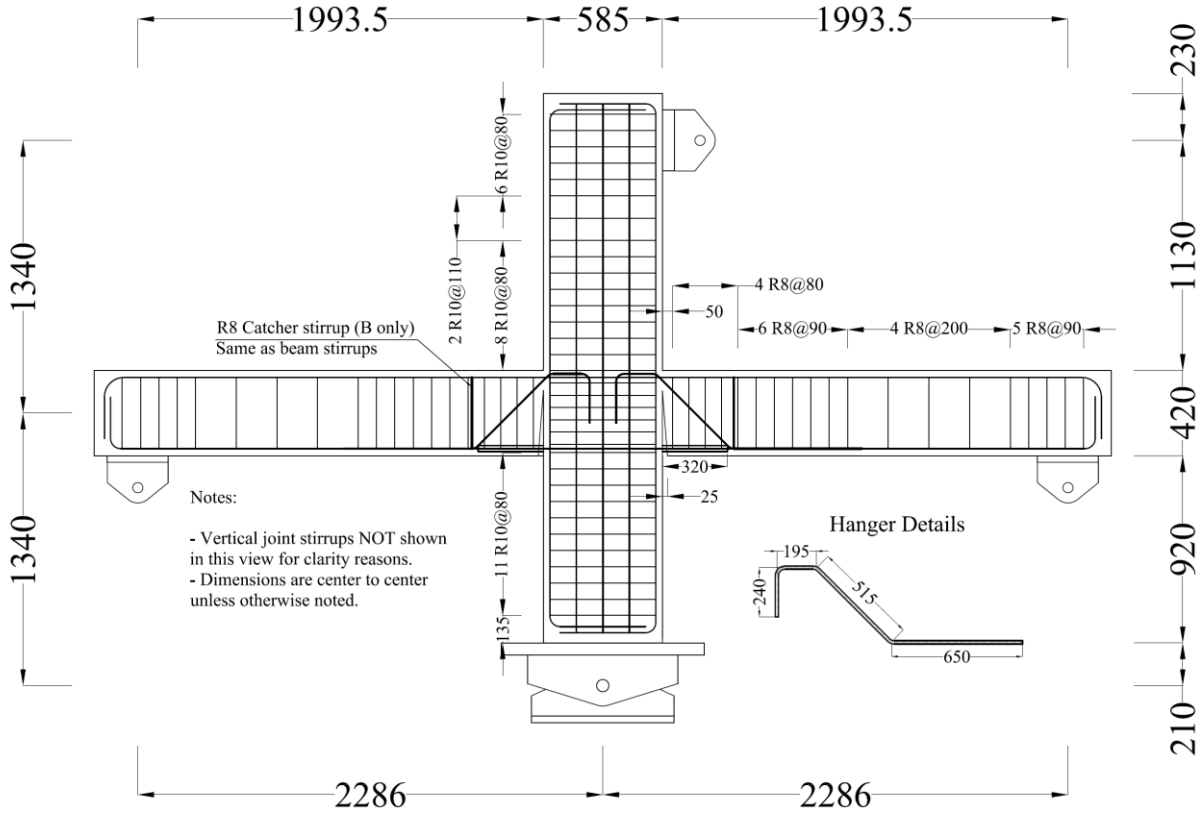

Figure 5-2: *Specimen geometry and general reinforcement layout*

As shown in Figure 5-3, the horizontal joint reinforcement provisions were slightly different between specimens. Specimen A was detailed to have 135% $A_{jh,code}$ while specimen B had 120% $A_{jh,code}$ in accordance with Section 4.5.4. Supplementary vertical joint stirrups were provided through a combination of R10 and R12 bars at a confinement index, Ω, of 0.04 as discussed in Section 4.2.3. Different bar sizes were used as illustrated in Figure 5-4 to assess the effect of spacing on bond performance. Fewer bars at larger spacing is preferential from a constructability point of view, but is less beneficial for bond improvement as discussed in Section 4.2.3.

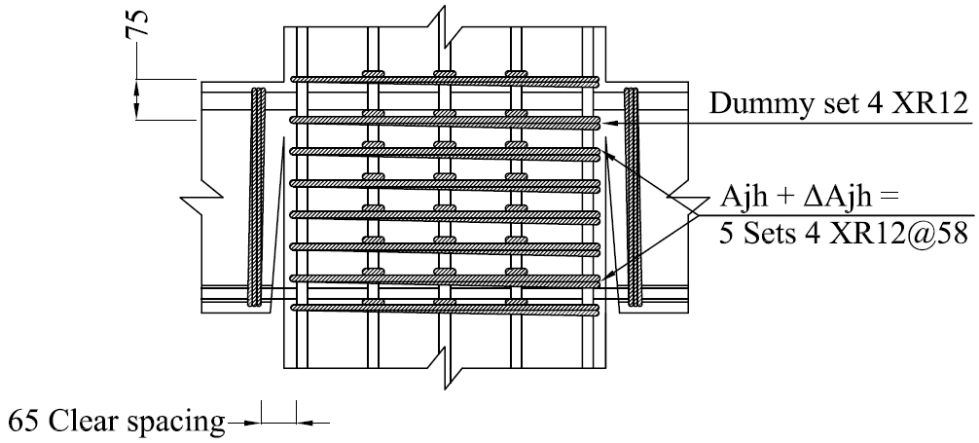

(a) Specimen A

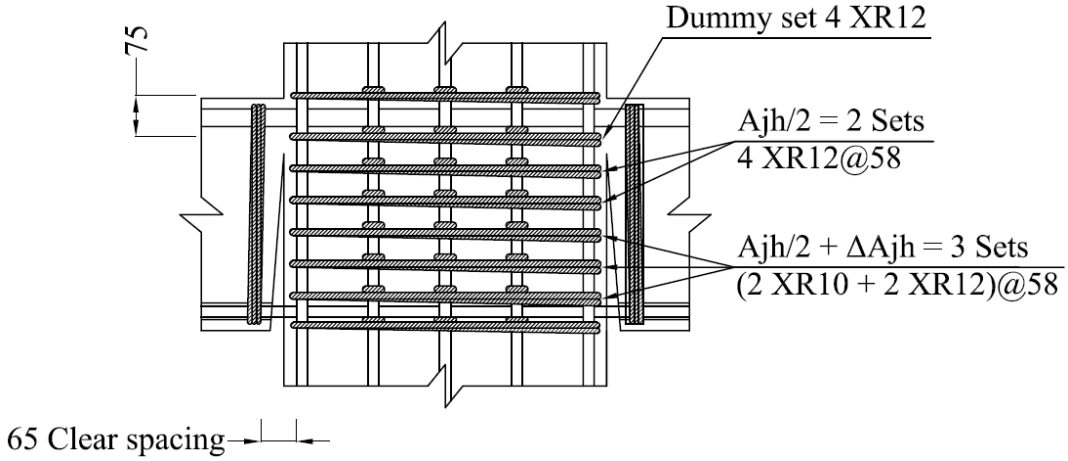

(b) Specimen B

Figure 5-3: *Horizontal joint sections*

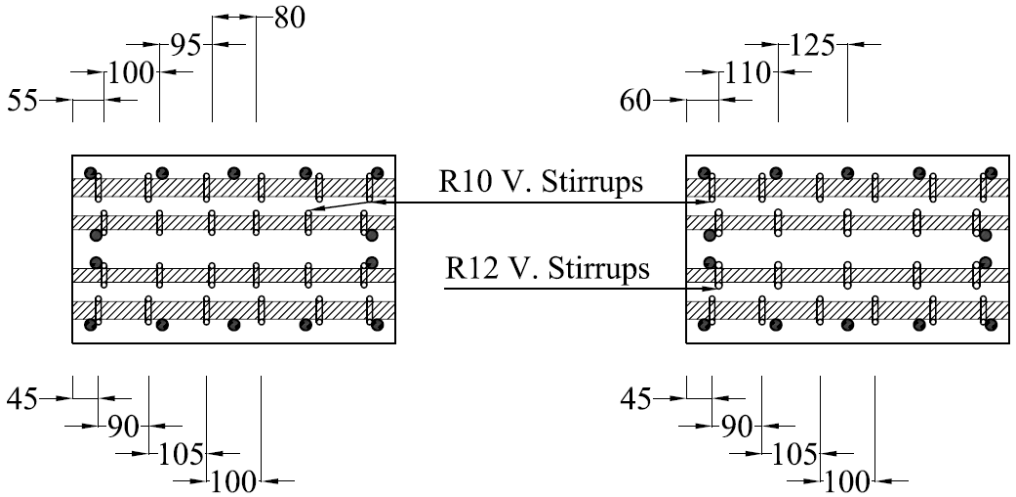

(a) Specimen A (b) Specimen B

Figure 5-4: *Vertical joint sections*

The beam and column sections used in both specimens are illustrated in Figure 5-5 and Figure 5-6. Shear hangers were provided by dual HD16 bars and dedicated catcher stirrups were installed at the hanger bend in specimen B. Bottom reinforcement unbonding tubes were mild steel with 25 mm inside diameter and 3.2 mm wall thickness. As discussed in Section 2.2.3,

these were terminated short of the hanger bend to ensure tension demands were not passed into the concrete at this point. Top to bottom beam reinforcement ratio, A'_s/A_s, was detailed to be 2.06 in accordance with Au (2010) recommendations. A column depth of 585 mm was provided in accordance with Equation 4-22 – it should be noted that this included an additional 50 mm to allow for disruption of bond due to strain gauge installation as discussed in Section 5.2.4. The column yield to beam overstrength strength ratio, $M_{y,col}/M_{o,b}$, was 1.8. Interior column bars on the beam faces were offset such that interior stirrup hoops could be installed in the same plane as exterior ones. This increased the clear spacing of stirrup sets, helping to decrease joint congestion and make construction easier.

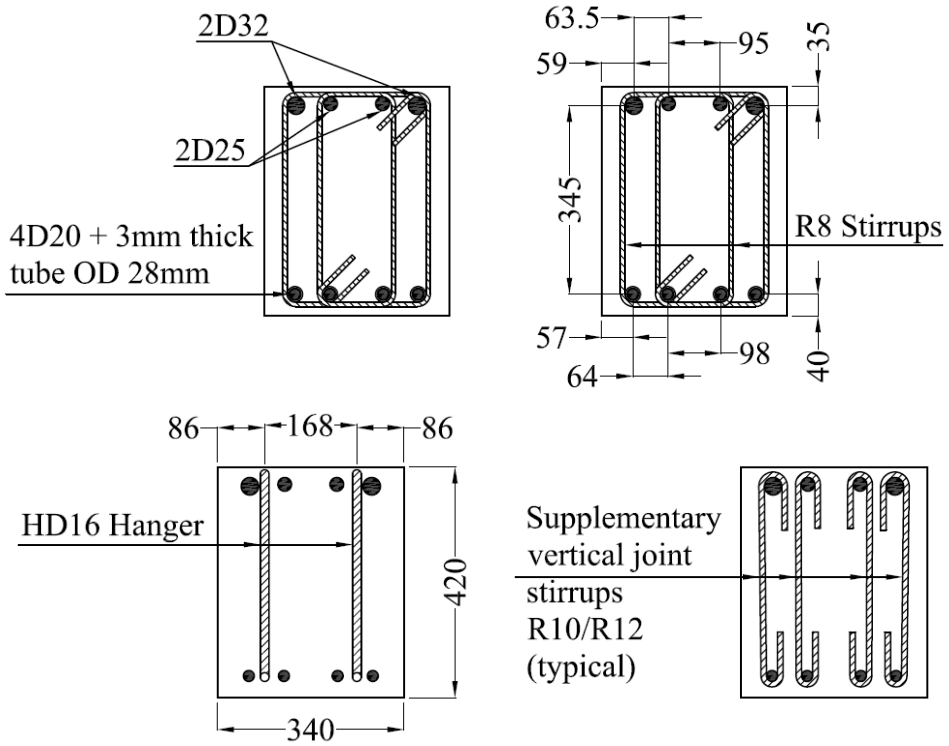

Figure 5-5: *Beam sections specimens A and B*

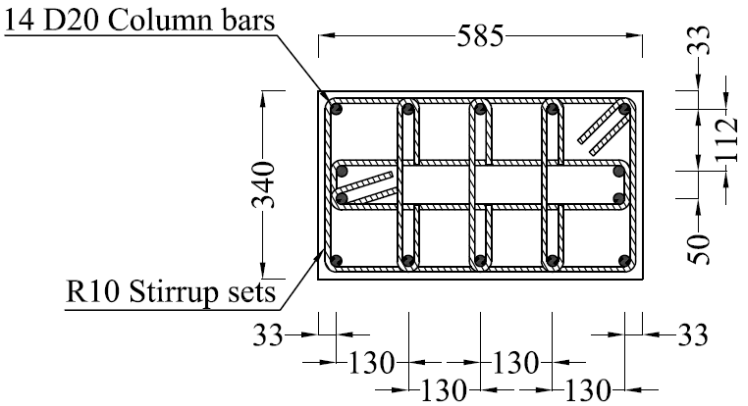

Figure 5-6: *Column section specimens A and B*

5.2.3 Specimen Construction

The specimens were constructed at the University of Canterbury by the Author with assistance from a fellow postgraduate student and laboratory technicians. Reinforcing steel was supplied cut and bent ready for caging which was carried out in stages. Firstly, the vertical joint stirrups and unbonding tubes were threaded over the beam bars with the horizontal joint stirrups placed between the two layers of longitudinal reinforcement. Strain gauges on the bottom longitudinal reinforcement were installed at this stage as access to this region would be lost once the unbonding tubes were in place.

The beam bars were then tied to the beam stirrups as illustrated in Figure 5-7(a). Unlike in the construction of Au's (2010) specimens, grout was not used in the unbonding tubes as this can lead to increased stiffness during compression inducing rotations. Instead, the tubes were left empty and the ends plugged with silicone to prevent concrete entering the unbonded length. After completion of the beam cage, it was then rotated so the column bars could be threaded through the joint as shown in Figure 5-7(b). Restricted access to the vertical joint stirrups necessitated these be tied and strain gauged first. The column bars were then fixed in place and tied to the horizontal joint stirrups. To reduce the extent of cone formation in joint, it was important that the bottom joint and first column stirrup sets be located immediately adjacent to the bottom beam bars. Finally the column stirrups were tied and external strain gauges installed on the horizontal joint reinforcement, beam stirrups, and column bars resulting in the finished cage as illustrated in Figure 5-7(c).

(a) Beam cage (b) Beam-column joint assembly

Figure 5-7: *Specimen Construction Photos*

(c) Caged beam-column joint

(d) Specimen formwork

Figure 5-7: *Specimen Construction Photos (Continued)*

The formwork for casting was constructed of plywood and No. 1 framing timber as shown in Figure 5-7(d). In order to form the slotted sections, a special form mould was required. Illustrated in Figure 5-7(e), the form was cut from high-density polystyrene and backed with sheet metal to give added stiffness and a smooth finish to the concrete surface. The form was cut in two and fitted over the bottom beam reinforcement before being fixed to the formwork. A plywood stiffener was then attached to the free end of the form extending above the formwork. Strain gauge wires were grouped and passed out of the specimen and reinforcing steel chairs were installed to ready the specimen for pouring as shown in Figure 5-7(f).

(e) Slot form and shear hangers

(f) Finished cage in formwork

Figure 5-7: *Specimen Construction Photos (Continued)*

Concrete was supplied by Allied Concrete and placed in the formwork using a crane mounted hopper as illustrated in Figure 5-7(g). The concrete was vibrated to ensure full compaction and good coverage of the bars. It was then trowel-finished as shown in Figure 5-7(h). The specimens were then covered in wet hessian sacks to assist with curing and prevent surface cracking. Once the concrete had reached target strength, the specimens were then lifted into the testing rig as illustrated in Figure 5-7(i). Linear potentiometers were then installed as shown in Figure 5-7(j). The mounting rods for these were embedded well into the specimen to ensure the potentiometers would remain in place even in the event of severe spalling of the cover concrete.

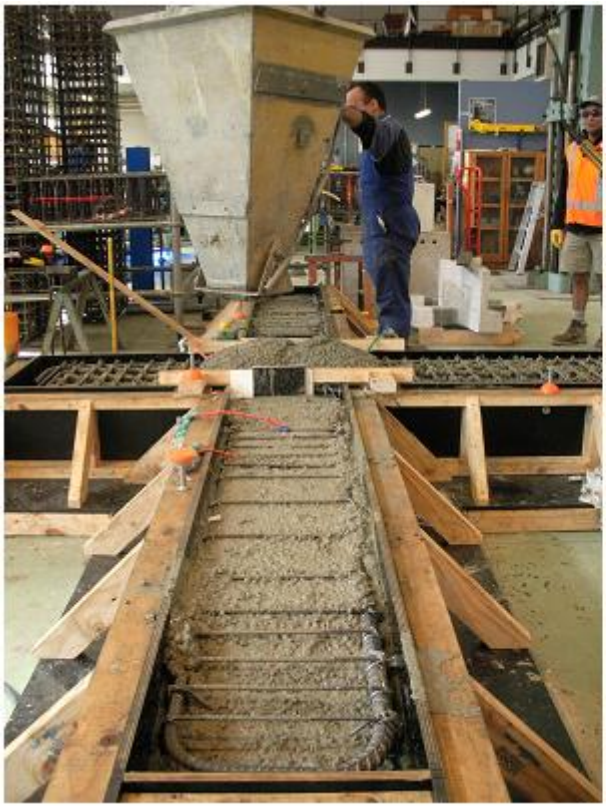

(g) Concrete pouring

(h) Cast specimen

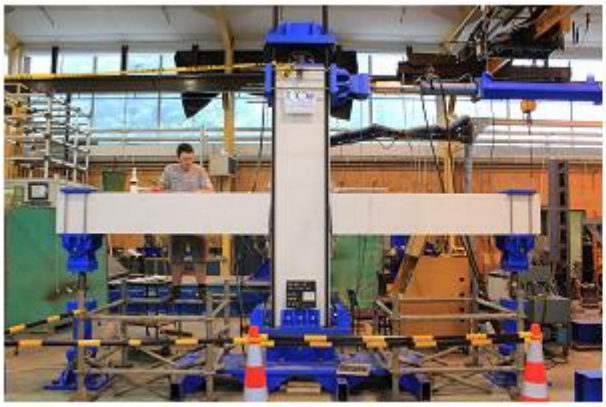

(i) Specimen in testing rig

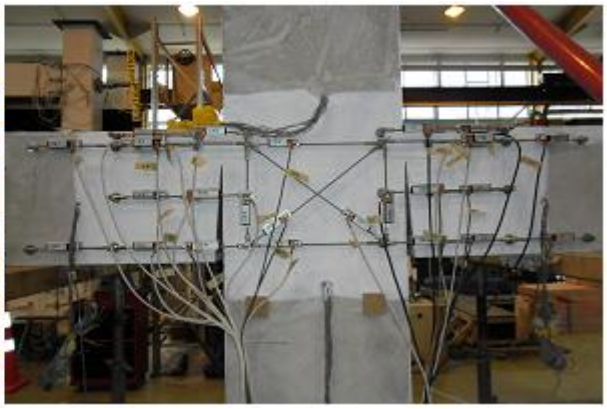

(j) Linear potentiometer installation

Figure 5-7: *Specimen Construction Photos (Continued)*

5.2.4 Strain Gauge Installation and Effect on Bond Performance

The strain gauge installation technique used for this project differed slightly from previous techniques employed on similar projects at the University of Canterbury. Initial bar preparation was unchanged; a linisher (small powered sanding tool) was used to smooth the bar surface and establish a suitable area for attachment of the strain gauge. The area was then cleaned using acetone and the strain gauge attached using a cyanoacrylate adhesive as shown in Figure 5-8(a). A waterproofing layer was then applied by painting the strain gauge with liquid paraffin oil as illustrated in Figure 5-8(b). This cooled and set rapidly saving time and resulting in a superior coating compared to previous waterproofing techniques. Rubber mastic tape was then placed over the paraffin layer to minimise any shear transfer between the concrete and strain gauge that could otherwise interfere with readings; this is shown in Figure 5-8(c). Finally, the bar was wrapped in electrical tape in the vicinity of the strain gauge as illustrated in Figure 5-8(d). This was necessary to ensure the mastic tape and waterproofing remained in place during handling of the cage and concrete pouring. Of 181 strain gauges installed using this technique, only 2 failed prior to testing.

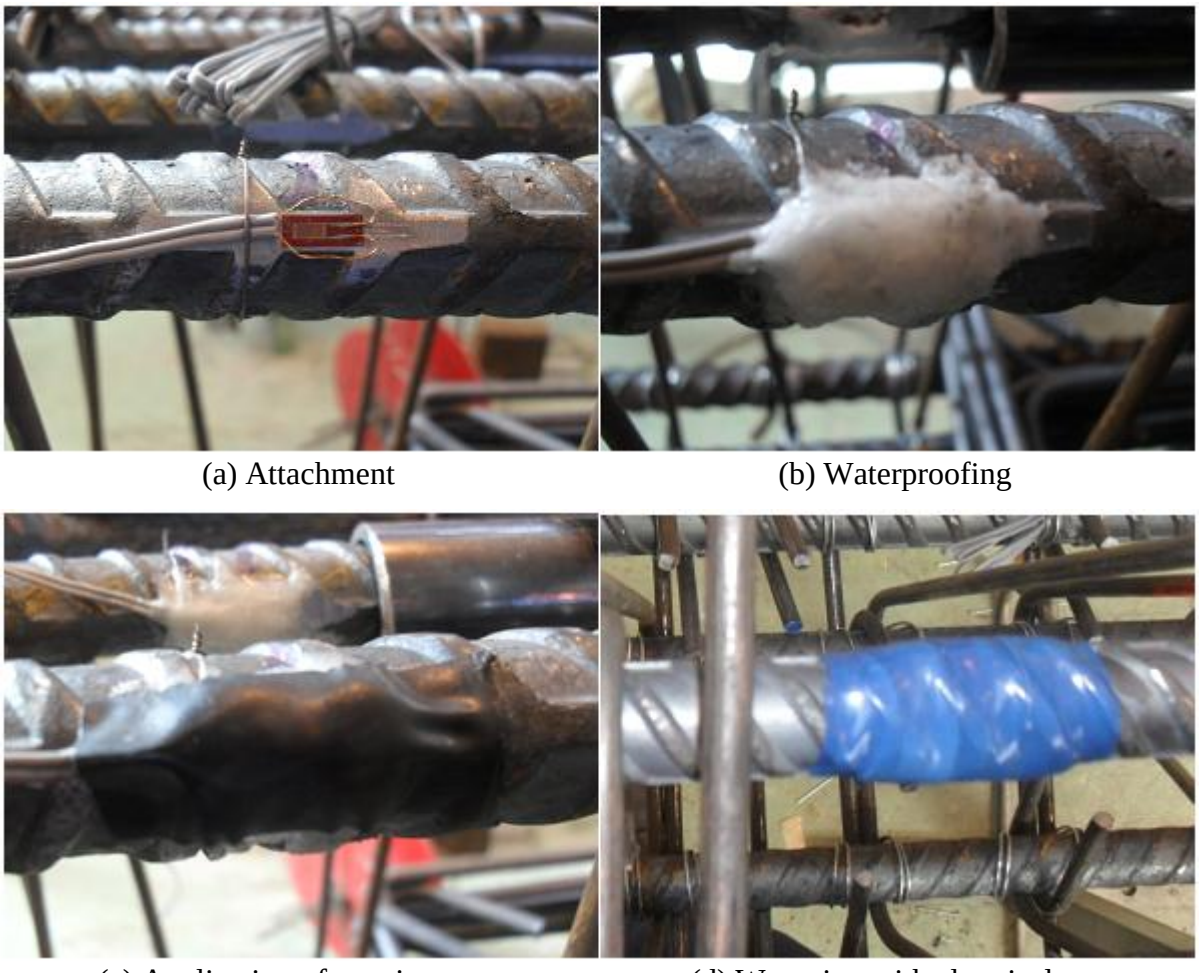

(a) Attachment (b) Waterproofing

(c) Application of mastic tape (d) Wrapping with electrical tape

Figure 5-8: *Strain gauge installation procedure*

In addition to being difficult to install, strain gauges are also detrimental to local bond performance of the bar. This is due to disruption of the bonded surface as a result of the strain gauge (Scott, 1996). While this is not important for the majority of the specimen, it is critical for the bottom longitudinal reinforcement within the joint. Using the installation technique described above, each strain gauge and its associated protection covers the entire circumference of the bar over a length of approximately 25 mm. As shown in Figure 5-8(d), this will inevitably encompass several of the lugs on the reinforcement bar from which the majority of bond is achieved via bearing as discussed in Section 3.1.3. For this reason, the ability of this region to achieve the same maximum bond stress as an unmodified region on the bar is compromised. Unfortunately, due to the lack of dedicated literature on this topic, the degree of reduction is unknown and an estimate must therefore be made with sufficient conservatism. Thus with three strain gauges installed across the joint and an assumed 70% reduction of bond capacity, the effective column depth is reduced by approximately 50 mm. Given D20 bars were used in the experimental tests, this equates to a loss of $2.5d_b$ which is on the order of $0.1h_c$.

While the reduction in effective column depth due to the presence of strain gauges is undesirable, it can easily be accounted for in design. However, because not all of the beam bars are strain gauged, some bars will experience relatively more favourable bond conditions than others. This can be somewhat accounted for in the method of casting. As discussed in Section 3.3.3, bars towards the top of a pour have inferior bond performance due to air pockets and bleed water segregating towards the top of the mix and getting trapped under the bars. This is reflected in the factor ξ_t which, as discussed in Section 4.1.2, gives a 15% reduction in bond stress if more than 300 mm of fresh concrete exists below the reinforcement layer under consideration.

This figure is likely too conservative for several reasons. Firstly, because the pour will be carried out under direct supervision of the author, strict quality control and proper vibration during casting can be ensured thus lessening the extent of mix segregation. Secondly, because of the horizontal casting position, any bleed lenses trapped underneath the bars will not be on the side subject to confinement from axial pressure and supplementary vertical stirrups. Therefore the bond performance on the more important bar faces is not compromised. For these reasons, the reduction factor is reduced to 10%. Finally, it seems logical that the reduction in concrete quality is not a step function, as assumed in NZS3101:2006, but is actually closer to exponential decay (Soylev & Francois, 2006). Thus the factor ξ_t would be more suitably expressed with a simple linear function as illustrated in Figure 5-9.

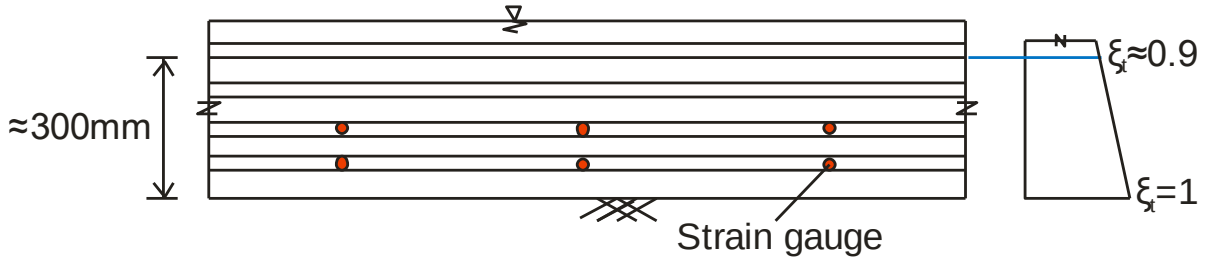

Figure 5-9: *Influence of strain gauge layout and mix segregation on each bar*

Because the specimens are cast horizontally, the effect of mix segregation will change over each layer of bars with bars closer to the top of the pour being affected more than those towards the bottom. Thus if strain gauges are installed on the lower bars, the overall impact on bond performance will be more uniform throughout each layer. This approach was used for the experimental stage of this research with approximately $2.5d_b$ added to final column depths to account for these factors.

5.2.5 Material Testing

The concrete ordered for both specimens had a specified 28 day strength of 30 MPa, maximum aggregate size of 13 mm, and target slump of 120 mm. From each mix, 18 concrete cylinders were taken for subsequent strength testing. These were wrapped in plastic film and cured under the same conditions as the specimens. To track the strength development of each specimen, groups of 3 cylinders were tested after 7, 14, 28, and 56 days. Final cylinders were tested on the day of specimen testing. Batching records indicated the concrete was supposed to plateau around the 40 MPa design strength after 56 days. This approach was used as opposed to ordering a 40 MPa concrete such that the testing window would be longer. Using this technique, specimen A reached 39 MPa on the day of testing while, unfortunately, specimen B reached only 29.5 MPa. This is shown in Figure 5-10 along with the strength values as given by the Allied Concrete laboratory who conducted their curing under ideal conditions. The lower strength of the specimen B mix was most likely due to additional water being used by the batchers in order to achieve the required slump. Regrettably, it had not been communicated to the batchers that strength was the more important aspect and that sufficient slump could be achieved upon delivery using super-plasticiser.

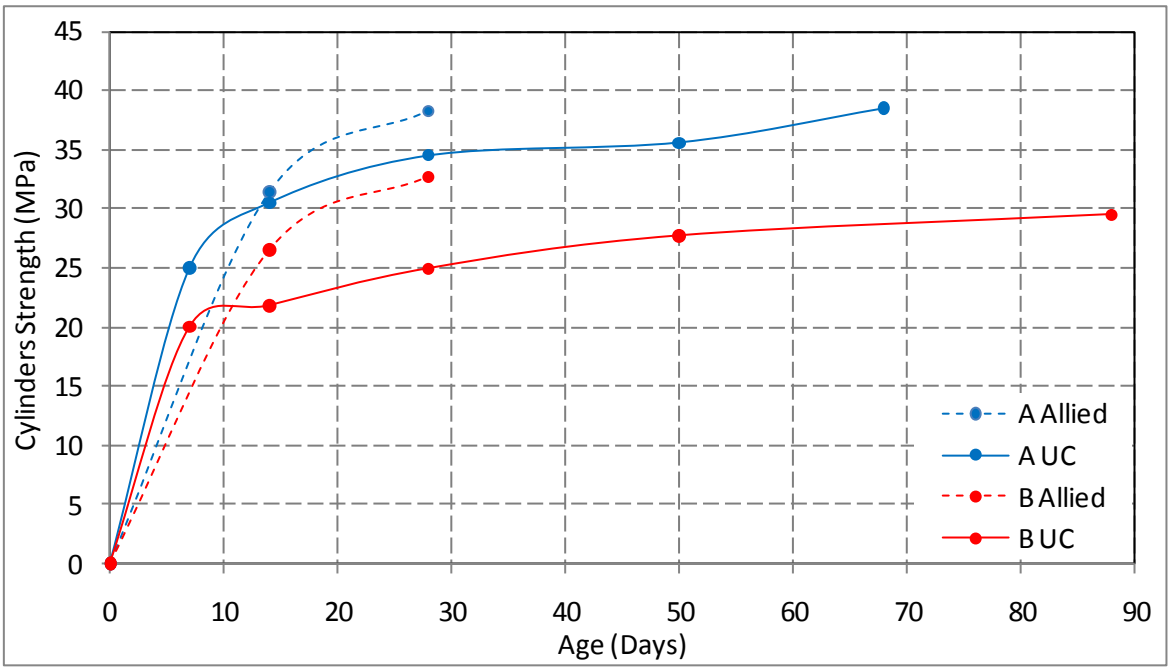

Figure 5-10: *Concrete strength progression for specimen A and B*

Steel testing was carried out using the Avery testing machine in the laboratory. Five samples were tested for each type of reinforcing steel used in the specimens. The average results are presented in Table 5-1 and Table 5-2 below with typical stress-strain profiles for each bar type shown in Figure 5-11. Note that the yield stress was defined as the initial point where the slope of the elastic curve decreased, thus the low yield strengths for some of the bars.

Table 5-1: *Mechanical properties for round reinforcing steel*

Sample	**R8**	**R10**	**HR10**	**R12**	**HR12**
Yield Stress (MPa)	382	258	372	336	369
Yield Strain	0.0019	0.0013	0.0020	0.0016	0.0020
Elastic Modulus (MPa)	201755	192741	185346	211897	181908
Strain @ Onset of Work Hardening	0.013	n/a	0.013	0.030	0.016
Ultimate Stress (MPa)	477	431	677	468	675
Ultimate Strain	0.105	0.174	0.107	0.203	0.116
Actual Overstrength Factor	1.25	1.67	1.82	1.39	1.83
Grade Overstrength Factor	1.59	1.44	1.35	1.56	1.35
Normalised Yield Strain	0.0015	0.0016	0.0027	0.0014	0.0017

Table 5-2: *Mechanical properties for deformed reinforcing steel*

Sample	HD16	D20	D25	D32
Yield Stress (MPa)	538	305	305	306
Yield Strain	0.0028	0.0016	0.0016	0.0016
Elastic Modulus (MPa)	191609	195757	190667	195683
Strain @ Onset of Work Hardening	0.021	0.022	0.018	0.018
Ultimate Stress (MPa)	664	448	465	466
Ultimate Strain	0.114	0.200	0.193	0.189
Actual Overstrength Factor	1.23	1.47	1.52	1.52
Grade Overstrength Factor	1.33	1.49	1.55	1.55
Normalised Yield Strain	0.0026	0.0015	0.0016	0.0015

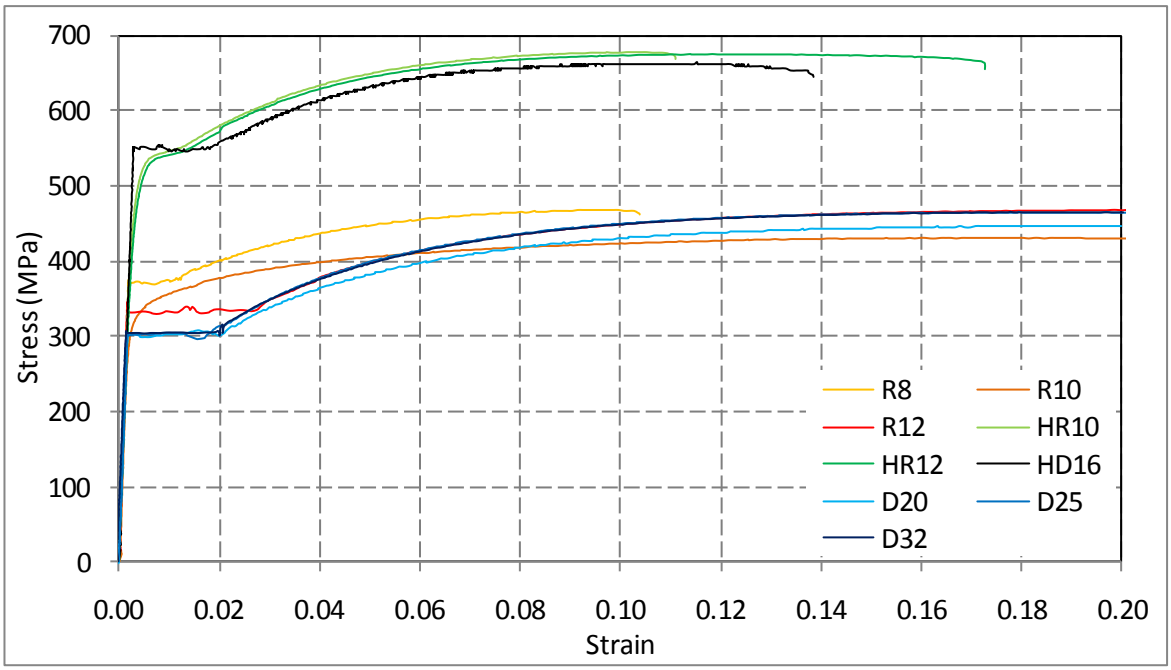

Figure 5-11: *Typical reinforcing steel stress-strain curves*

5.3 Experimental Set Up

5.3.1 Specimen Testing Rig

The rig used for testing of both specimens was designed in conjunction with a fellow postgraduate student and constructed by laboratory technicians. The rig is illustrated in Figure 5-12. In light of the recent Christchurch earthquake, double hinges were used on all connections to provide some out of plane capacity in the event of an aftershock. As further security, an "Acroprop" was used to brace the specimens while they were upright being prepared for testing.

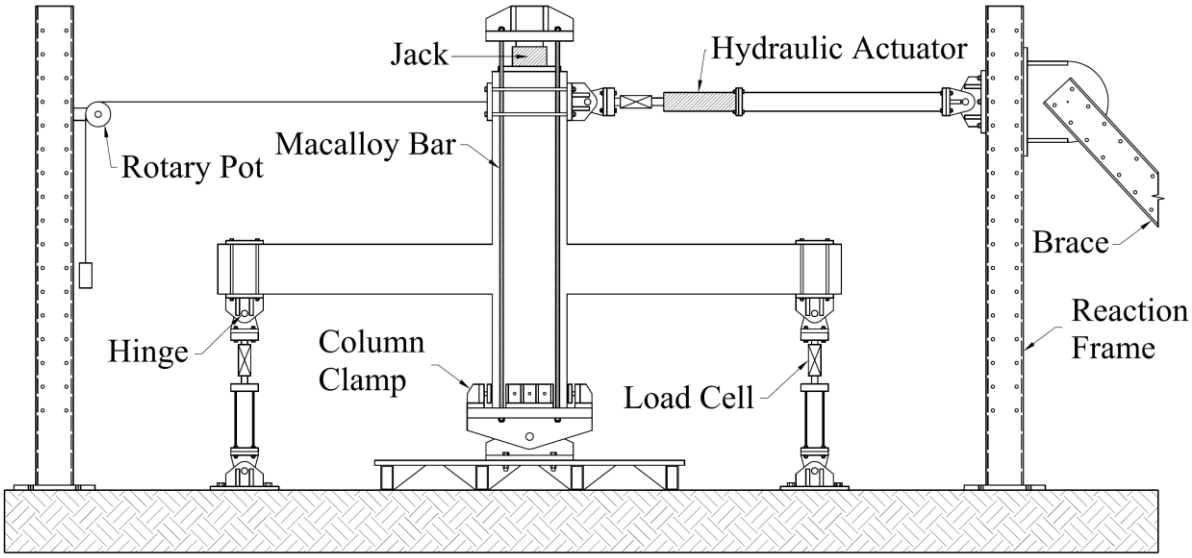

Figure 5-12: *Specimen testing rig*

The cyclic lateral drift sequence was applied at the top of the column using a hydraulic ram. This was logged against column displacement as measured by a rotary potentiometer attached to the other side of the column. Load cells attached to the ram and beam ends were used to measure specimen reactions. A string line was run along the front of the specimen between the frames in order to track any out of plane movement of the specimen during testing.

An axial load of 640 kN was applied to the specimen throughout testing using a jack attached between the top of the column and a reaction plate. This force resulted in a design axial load ratio of $N^*/A_g f'_c = 0.08$ – consistent with that used by Au (2010) and low enough such that the effect of the supplementary vertical joint stirrups on bond could be ascertained.

5.3.2 Loading Protocol

A cyclic quasi-static loading protocol was adopted in accordance with ACI guidelines (ACI Committee 374, 2005). Illustrated in Figure 5-13, this loading regime calls for 3 cycles at a given drift level followed by a single cycle at 1/3 of the previous drift magnitude. This is intended to simulate an actual earthquake where acceleration pulses vary in magnitude throughout the shaking. It also helps to close cracks formed during previous cycles. The drift level for subsequent cycles must be between 1.25 and 1.5 times the magnitude of the previous cycle. The loading sign convention adopted in this thesis is shown in Figure 5-14.

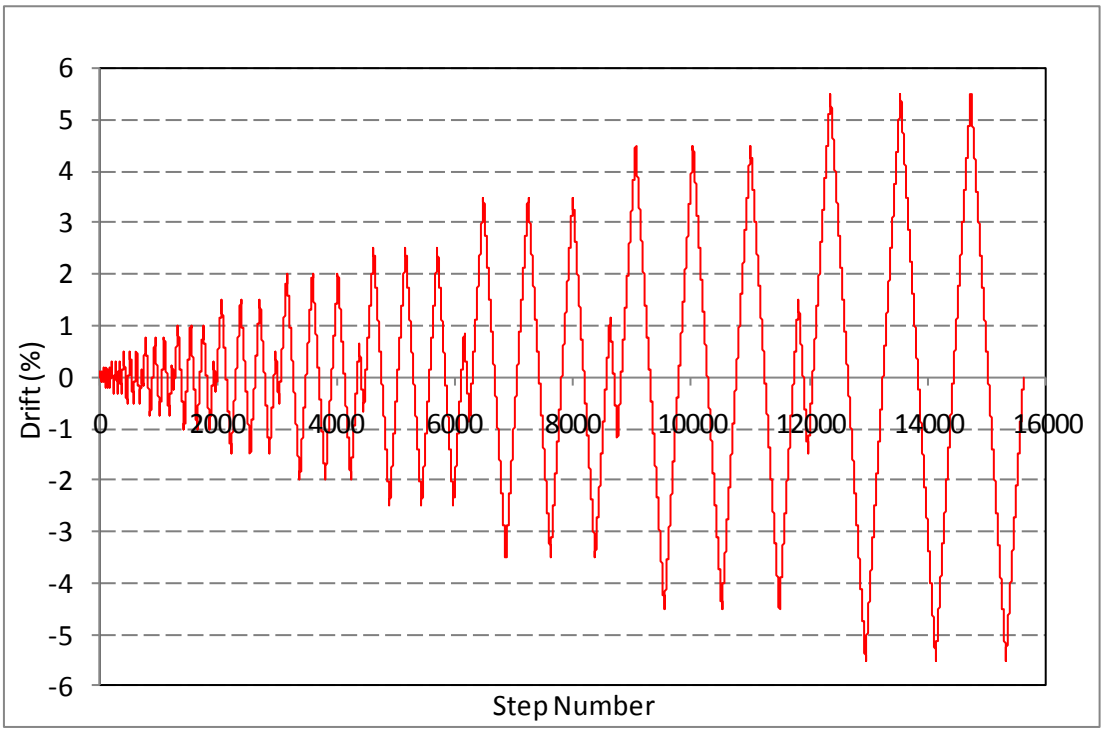

Figure 5-13: *Specimen loading protocol*

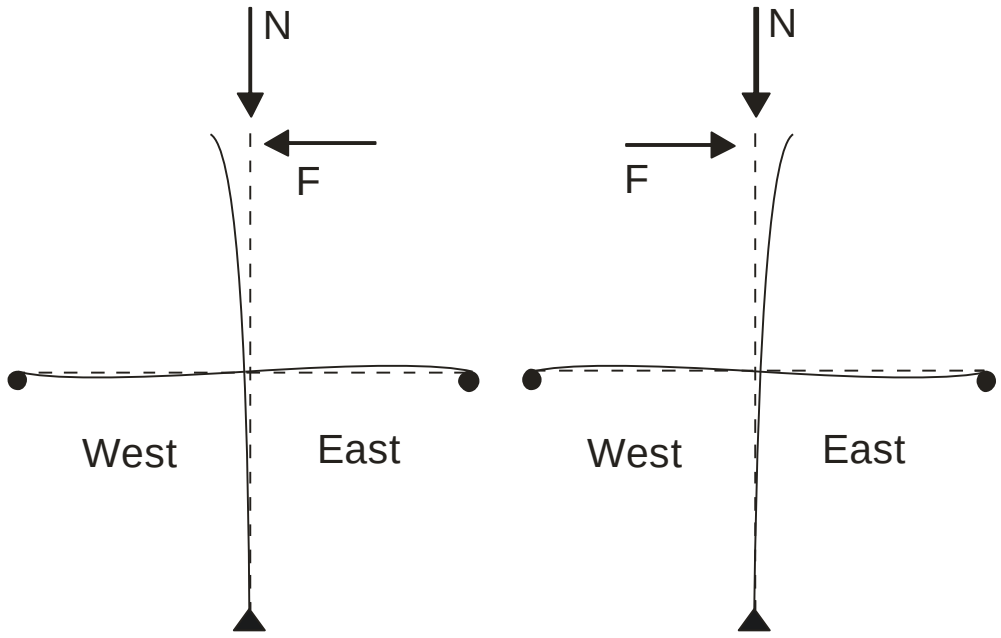

(a) Positive sign convention (b) Negative sign convention

Figure 5-14: *Loading sign convention*

5.3.3 Instrumentation

Four types of instrumentation were used in the test set up. Linear potentiometers were used to collect data relating to beam elongation, neutral axial depth estimation, and joint shear deformation. Spring potentiometers were used to measure vertical sliding across the beam hinges. The potentiometer layout is illustrated in Figure 5-15.

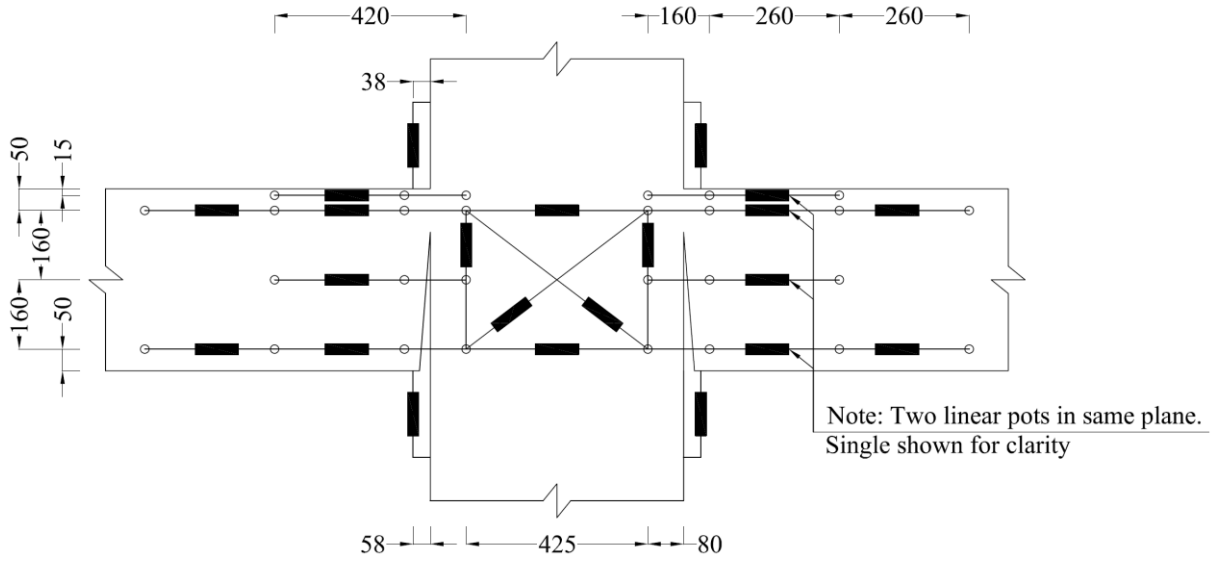

Figure 5-15: *Linear and spring potentiometer layout*

Strain gauges were installed on various reinforcing bars to measure the local strains. The gauge type used was 5 mm FLA-3-11 manufactured by Tokyo Sokki Kenkyujo Co. These were installed according to the methodology described in Section 5.2.4. The strain gauge layout was designed to ensure redundancy in the event of gauge failure with either multiple bars of the same type being gauged, multiple gauges being installed on the same type of bar, or single gauges being installed on symmetrical components on both sides of the joint. The strain gauge layout on each reinforcement type is shown in Figure 5-16.

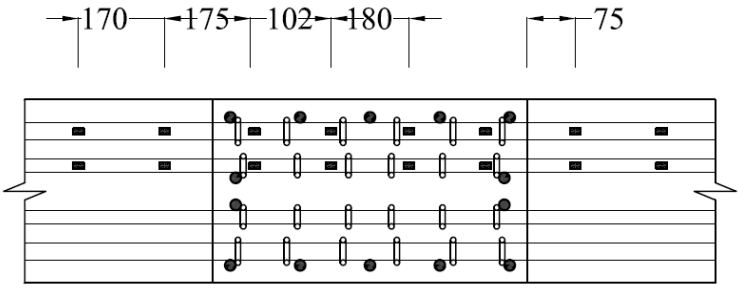

(a) Top beam bars

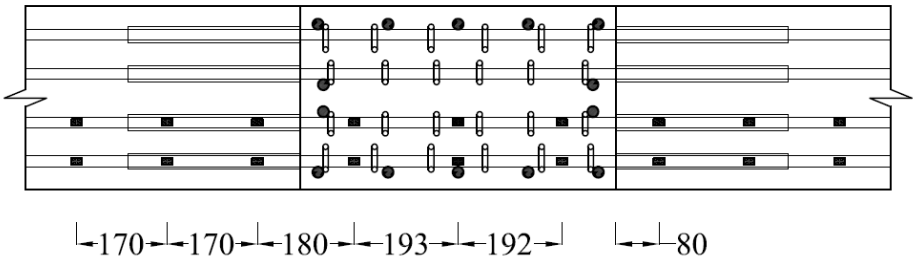

(b) Bottom beam bars

Figure 5-16: *Strain gauge layout for each reinforcement type*

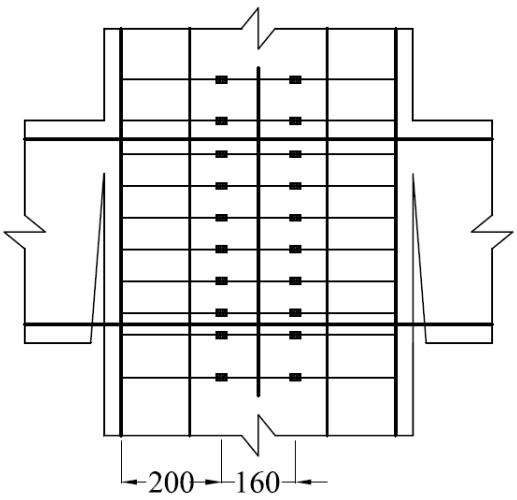

(c) Horizontal joint stirrups

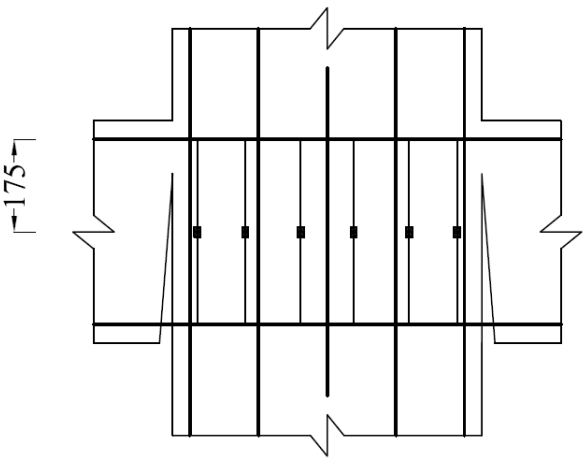

(d) Vertical joint stirrups

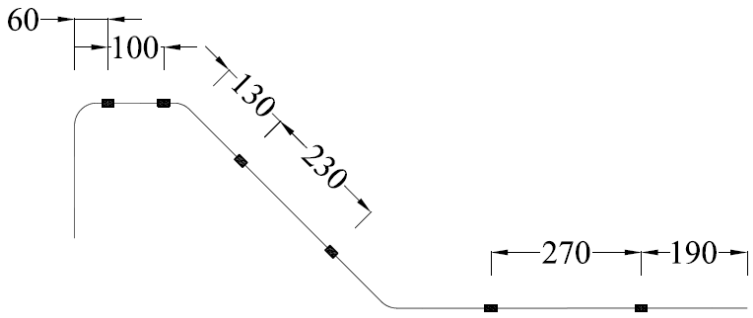

(e) Shear hangers

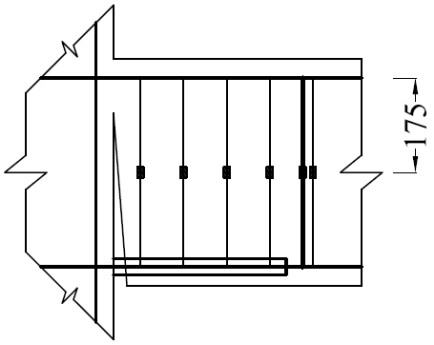

(f) Beam stirrups

Figure 5-16: *Strain gauge layout for each reinforcement type (Continued)*

The final type of instrumentation used was a rotary potentiometer. This was fixed to the east frame with a string under tension running to the specimen column and attached opposite the ram. Specimen deflection was measured by the rotary potentiometer which was in turn used to control the ram displacement for loading. Typical data processing techniques used are described in detail by Restrepo (1992) and Au (2010) and are therefore not repeated here.

5.4 General Experimental Results

This section of the experimental results relates to overall specimen performance. Comparisons with both the work of Au (2010) and monolithic systems are drawn where applicable.

5.4.1 Hysteretic Response and System Overstrength

The hysteretic response of specimens A and B is reproduced in Figure 5-17 and Figure 5-18 along with the individual beam contributions in Figure 5-19 and Figure 5-20, respectively. A summary of yield drifts and ram forces is given in Table 5-3 along with comparisons to the predicted values from monolithic theory.

Table 5-3: *Specimen yield forces and drifts*

	Gap opening A	Gap closing A	Gap opening B	Gap closing B
Ram force @ yield (kN)	114.0	108.0	109.0	106.0
Yield drift (%)	0.72	0.59	0.70	0.62
Predicted ram force @ yield (kN)	113.6	113.6	113.4	113.4
Predicted yield drift (%)	0.57	0.57	0.57	0.57

The difference between gap opening and closing yield drifts is consistent with the findings of Au (2010). Given the critical buckling load for the bottom reinforcement is on the order of $1.4F_{y,bar}$ when the bar is conservatively assumed to have pinned end connections, the discrepancy is unlikely to be due to this mechanism. Another possible explanation results from the presence of the unbonding length. Due to the prying effect within the top hinge during gap closing rotations, the force taken by the bottom longitudinal reinforcement is slightly greater during gap opening rotations. From this it follows that the bottom reinforcement would yield first in tension. Given the presence of the unbonding tube, the bar would theoretically be subject to uniform stress over its entire unbonded length. This could induce yielding at several locations along the unbonded length simultaneously, thus increasing the bar elongation and resulting yield drift of the specimen.

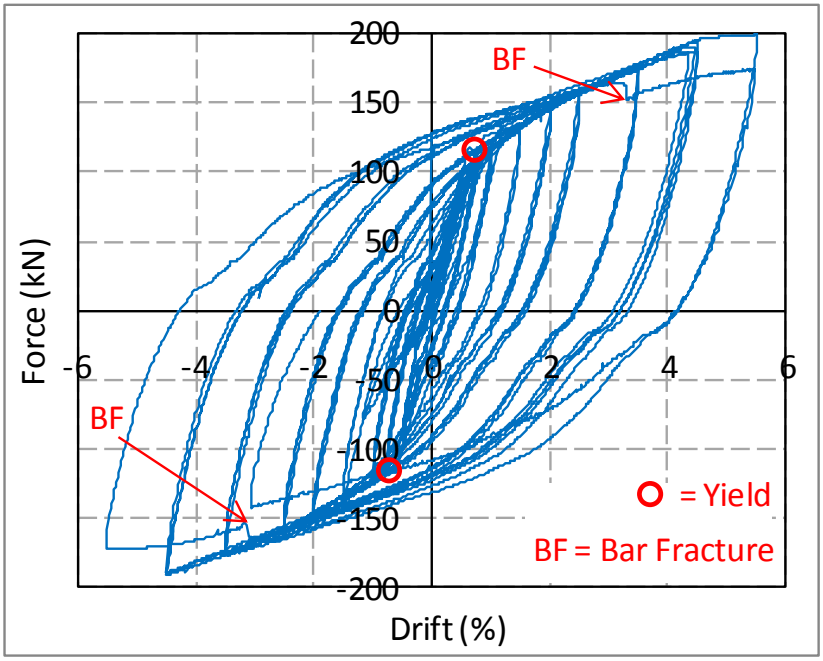

Figure 5-17: *Ram force vs. drift for specimen A*

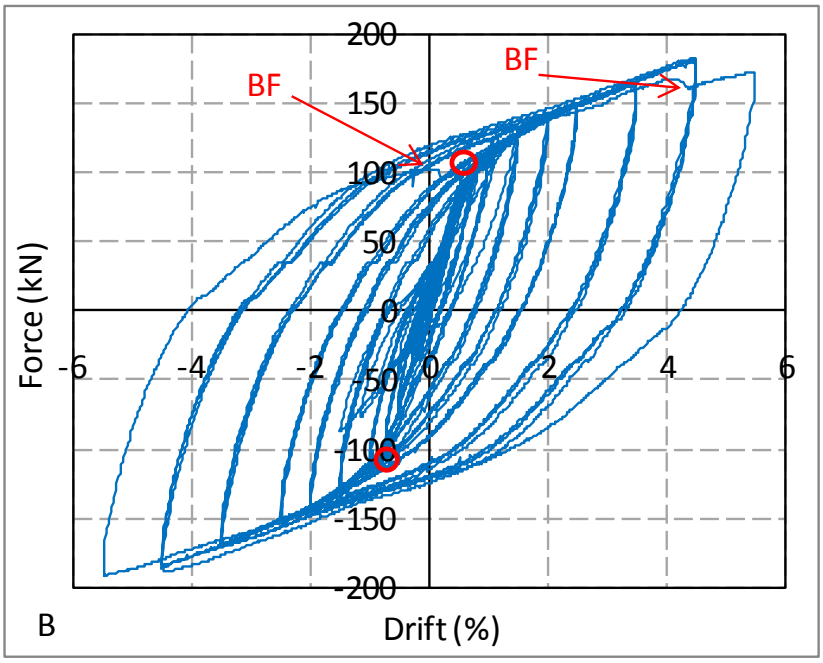

Figure 5-18: *Ram force vs. drift for specimen B*

Both specimens exhibited a 'fat' hysteretic response through 4.5% drift with no strength degradation. A small amount of pinching in the hysteresis loops is visible near regions of zero force. It should be noted that this corresponds to the bottom beam reinforcement on either side of the joint slackening as it comes out of tension during load reversal as opposed to bar slip through the joint. The first sign of strength degradation on both specimens was when a single bottom beam bar fractured in tension during load cycles at 5.5% drift. Both tests were stopped after fracture of a second bar due to concerns over system capacity in the event of another fracture. Highlighted in each figure, the bar fractures are associated with a sharp drop in

system load capacity. However, these events do not compromise the shape – and thus energy dissipation capacity – of the hysteresis loops in either specimen.

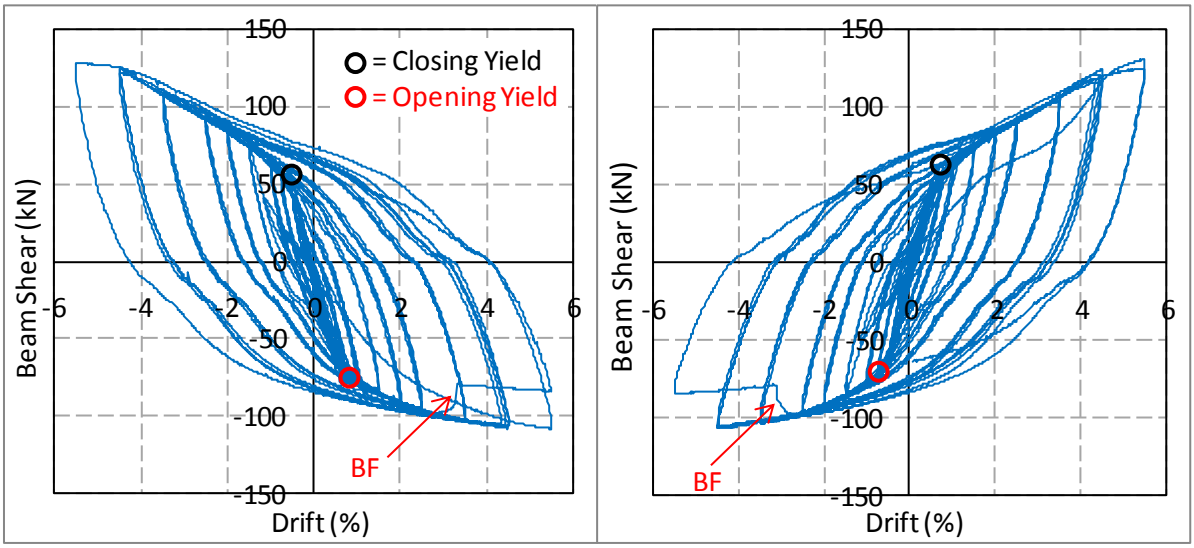

(a) West (b) East

Figure 5-19: *Beam contribution to overall response of specimen A*

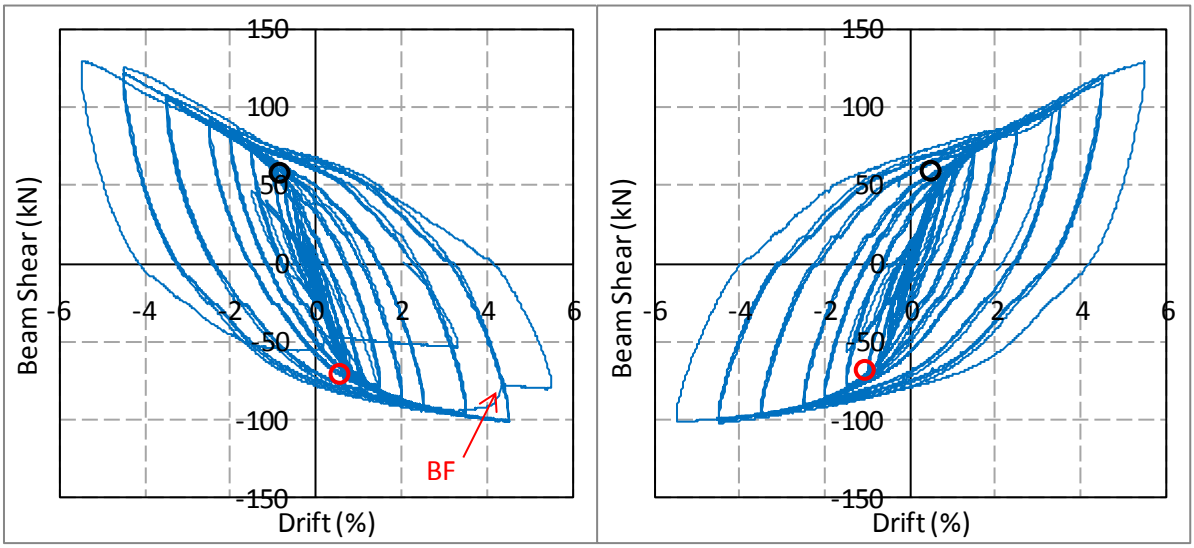

(a) West (b) East

Figure 5-20: *Beam contribution to overall response of specimen B*

System overstrength factors at 2.5%, corresponding to ULS drift limits, were found to be 1.42 and 1.43 for specimens A and B, respectively. These values show reasonable agreement with the figure of 1.35 adopted for design as discussed in Section 4.2.4. Following significant post-yield stiffening, overstrength factors at 4.5% drift were determined to be 1.73 and 1.72 for specimens A and B, respectively. These overstrength figures are consistent with those reported by Au (2010) for specimen SB3 where bar slip failure did not occur. Au (2010) had attributed this high overstrength factor to the presence of a floor slab. However, similar values observed in this testing indicate the overstrength response is independent of the floor slab.

This seems logical given the low degree of beam elongation and top beam reinforcement activation as discussed in Sections 5.4.3 and 5.5.3. In order to explain the high overstrength at 4.5% drift, one must consider the difference in beam response during gap opening and closing.

It is clear from examination of Figure 5-19 and Figure 5-20 that the overstrength for gap closing consistently exceeds that for gap opening during higher drift levels. This behaviour is summarised in Table 5-4 using average results from the beam load cells. The gap opening overstrength factor remains below the 1.5 upper bound value from reinforcement tensile testing through 4.5% drift for both specimens. That the bars were almost at their ultimate strength appears reasonable given fracture occurred during subsequent cycles at 5.5%.

Table 5-4: *Beam overstrength factors*

	Gap opening A	Gap closing A	Gap opening B	Gap closing B
Ave. beam shear @ yield (kN)	74.9	57.1	69.3	55.7
Ave. beam shear @ 2.5% (kN)	95.8	92.9	90.8	90.7
Ave. beam shear @ 4.5% (kN)	107.2	124.3	102.1	122.9
4.5% overstrength ratio	1.43	2.18	1.47	2.21
4.5% closing/4.5% opening shear	-	1.16	-	1.20

It is believed the large gap closing overstrength values are due to buckling restraint provided by the unbonding tube walls. After initial buckling, the bars become braced against the tube walls as illustrated in Figure 5-21. Given the small clearance between the bar and unbonding tube, this buckling would occur at a relatively high mode thus reducing the length of the unrestrained bar. With buckling well restrained, Poisson's effect results in an increased bar area under compression. While the stress reached in compression and tension is similar, the greater area means the bar is able to take an increased compressive load. Based on extensive experimental testing, Restrepo (1992) found that the increase in capacity is on the order of 25% under ideal conditions. This increase is similar to that given in Table 5-4 for gap closing forces compared with gap opening forces at 4.5% drift and offers a plausible explanation for the high gap closing overstrength values observed.

Minimal damage observed in the unbonded region as a result of high stirrup density and thick unbonding tubes would also have contributed to the success of the previously described mechanism. As the mechanism requires a certain degree of buckling to activate it, this would explain why the gap opening and closing beam shears are comparable at 2.5% drift as shown in Table 5-4. Because bar buckling had only just initiated, it was unlikely to have progressed

to the extent that it was in contact with the unbonding tube walls and thus able to set up the aforementioned mechanism.

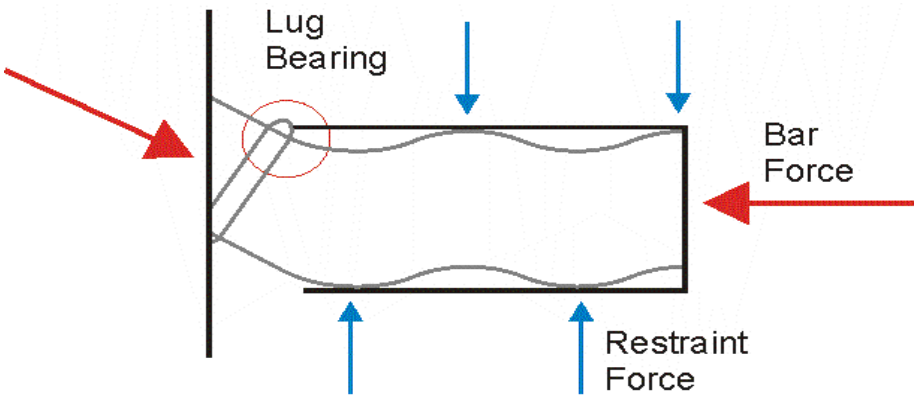

Figure 5-21: *Bar interaction with unbonding tube during gap closing rotations*

Bearing of the reinforcement bar lugs on the end of the unbonding tube is also a possible contributor to the high overstrength observed. As the bar becomes inclined entering the unbonding tube under downwards beam shear, the bar moves towards the top of the tube as illustrated in Figure 5-21. The lug is then able to bear on the wall of the unbonding tube thus increasing the capacity of the system.

5.4.2 Observed Damage and Crack Development Log

This section gives a detailed written and photographic account of the cracking and damage observed in each specimen. Both specimens exhibited very little damage compared with what would be expected from a typical monolithic specimen. Table 5-5 gives the maximum crack widths for each load cycle as measured while holding the specimen at the peak drift. Note that term ‘HL’ in Table 5-5 refers to cracks that are hairline in width. Figure 5-22 and Figure 5-23 show the crack development for specimens A and B throughout testing. These pictures were all taken at the 3rd negative cycle at each drift level in order to allow accurate comparison between specimens.

Table 5-5: *Measured crack widths for specimens A and B*

Maximum Crack Width (mm)														
Drift (%)	Joint Shear Crack		Bottom Beam		Top of Hinge Primary		Top of Hinge Secondary		Top of Beam		Above Slot		Column	
	A	B	A	B	A	B	A	B	A	B	A	B	A	B
0.1														
0.2			HL	HL	HL	HL			HL	HL	HL	HL		
0.3			HL	HL	HL	HL			HL	HL	HL	HL		
0.5			HL	0.04	HL	0.08			HL	HL	HL	HL		
0.75	HL	HL	0.06	0.08	0.15	0.2	HL	HL	HL	HL	HL	HL		
1.0	HL	0.03	0.06	0.08	0.4	0.5	HL	HL	HL	HL	0.1	0.15		
1.5	HL	0.04	0.1	0.15	0.5	0.75	0.1	0.1	0.04	0.04	0.45	0.55		
2.0	0.04	0.15	0.15	0.15	1.2	1.2	0.3	0.3	0.06	0.08	0.8	0.9		
2.5	0.1	0.2	0.15	0.2	1.5	1.4	0.5	0.55	0.06	0.08	1.2	1.3		HL
3.5	0.2	0.35	0.25	0.2	2.5	2.5	0.65	0.5	0.08	0.1	2.2	2.3	HL	HL
4.5	0.25	0.4	0.25	0.25	3.5	4	0.8	0.7	0.1	0.1	2.9	3.5	HL	HL

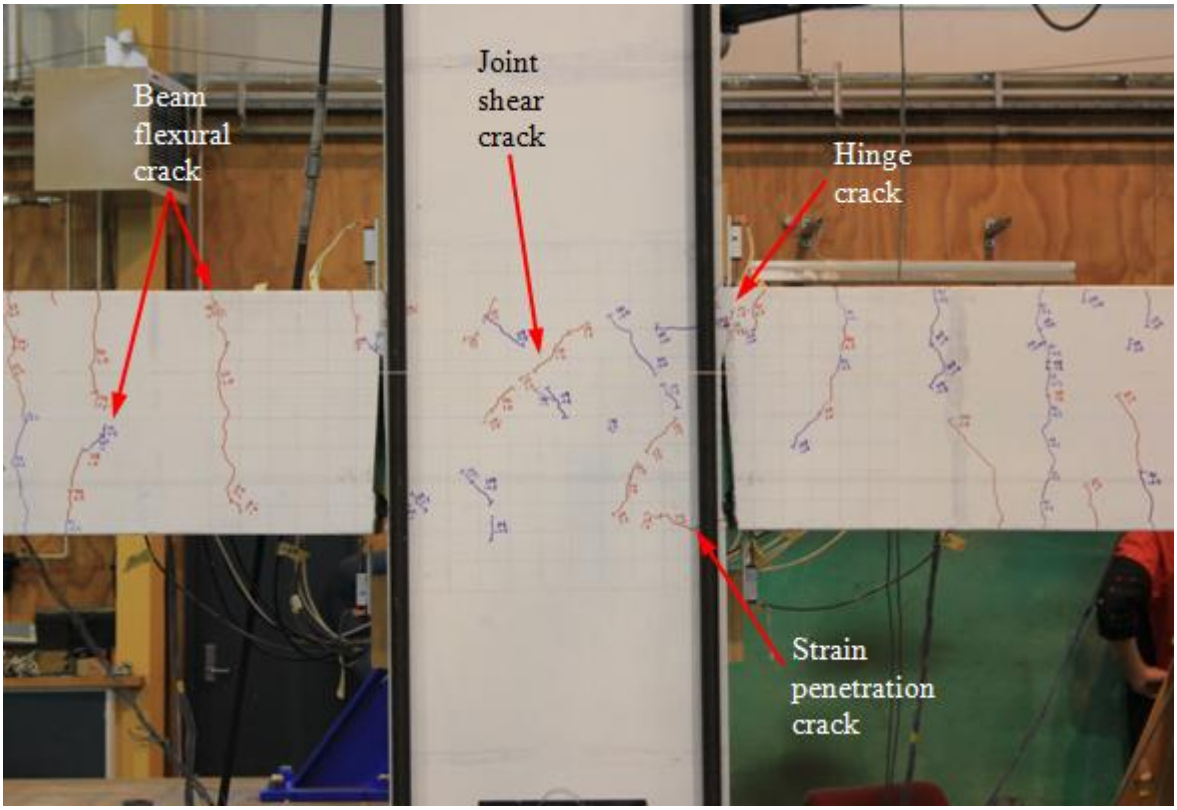

(a) -1.0% drift

Figure 5-22: *Crack development in specimen A*

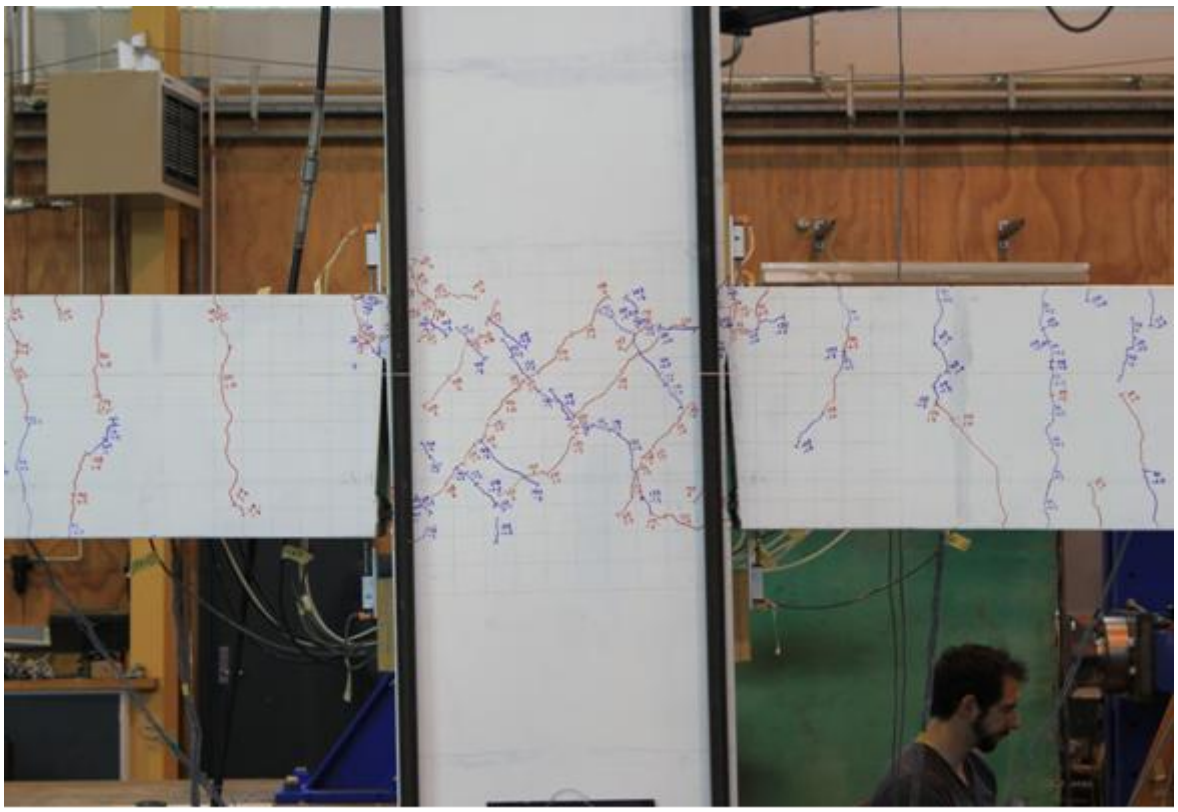

(b) -2.0% drift

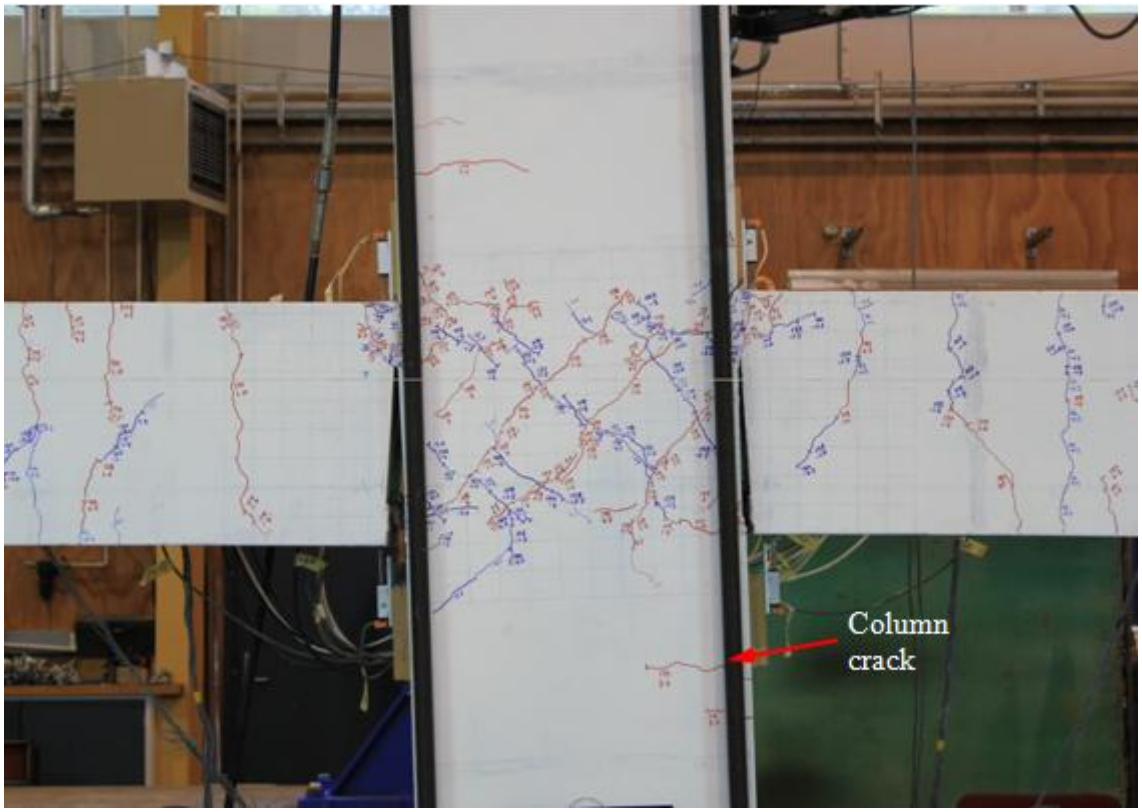

(c) -3.5% drift

Figure 5-22: *Crack development in specimen A (Continued)*

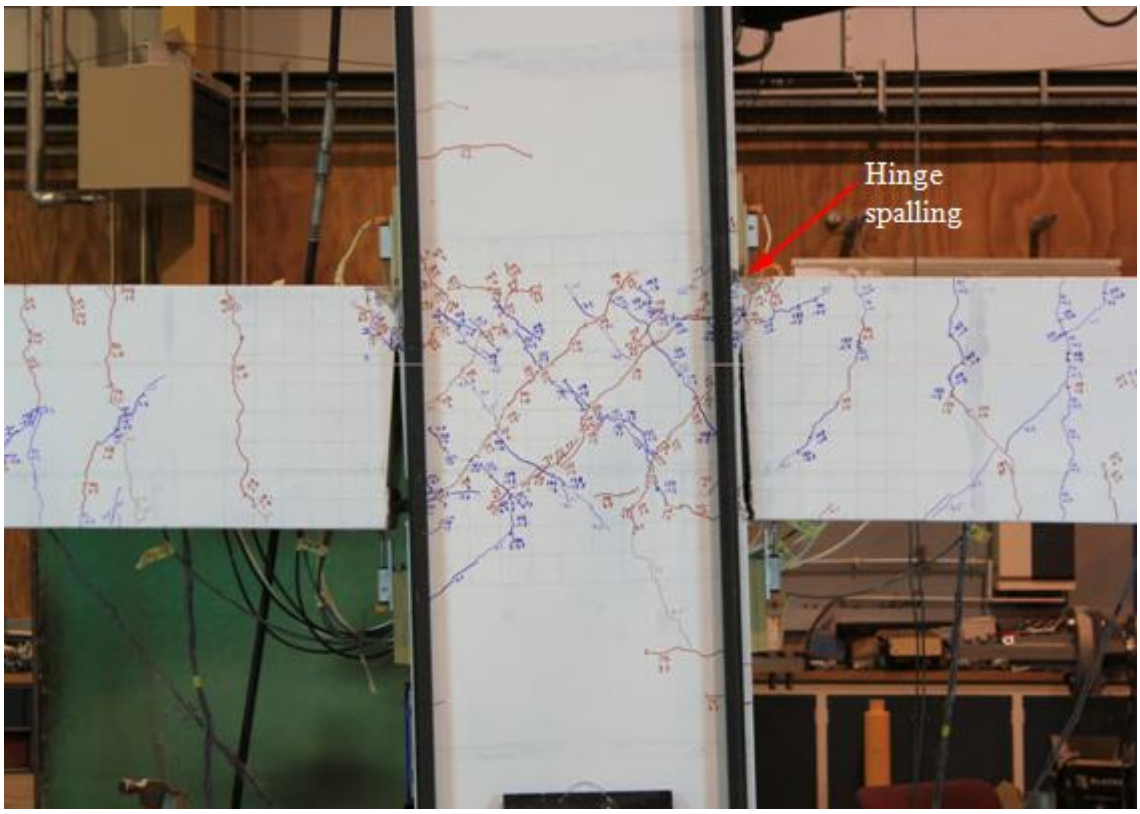

(d) -4.5% drift

Figure 5-22: *Crack development in specimen A (Continued)*

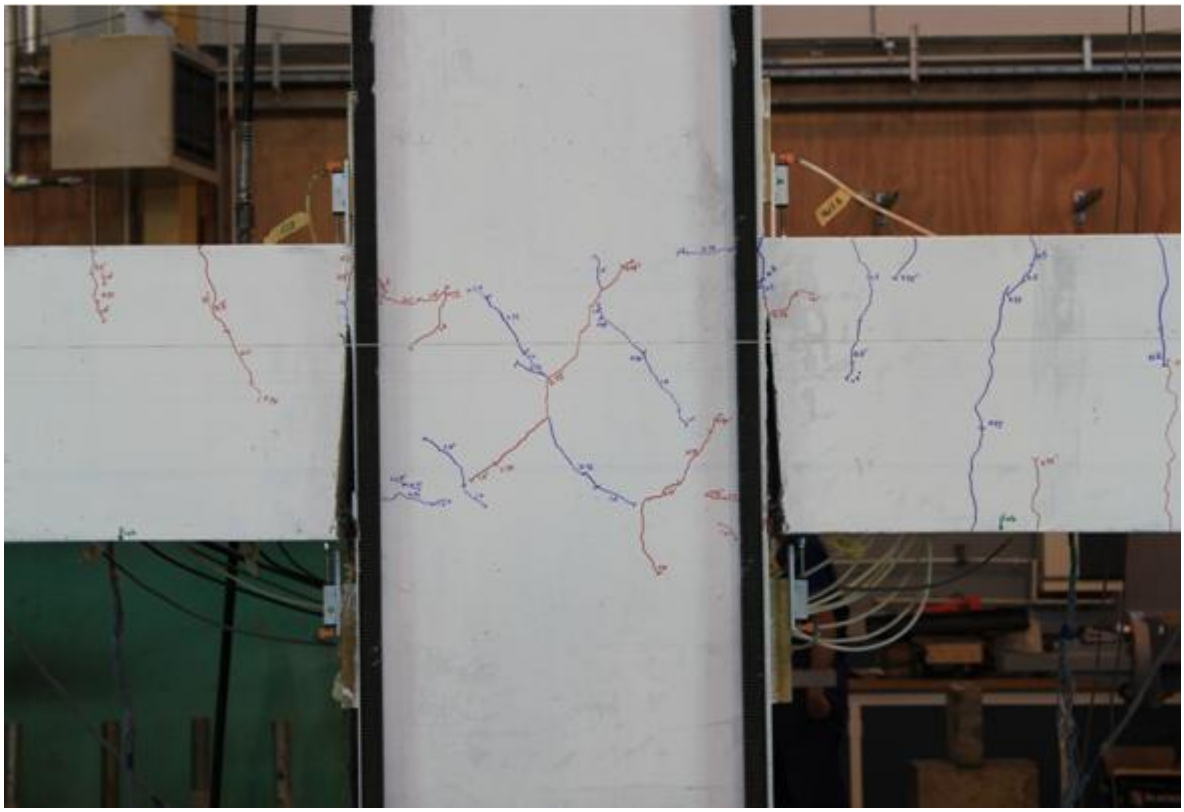

(a) -1.0% drift

Figure 5-23: *Crack development in specimen B*

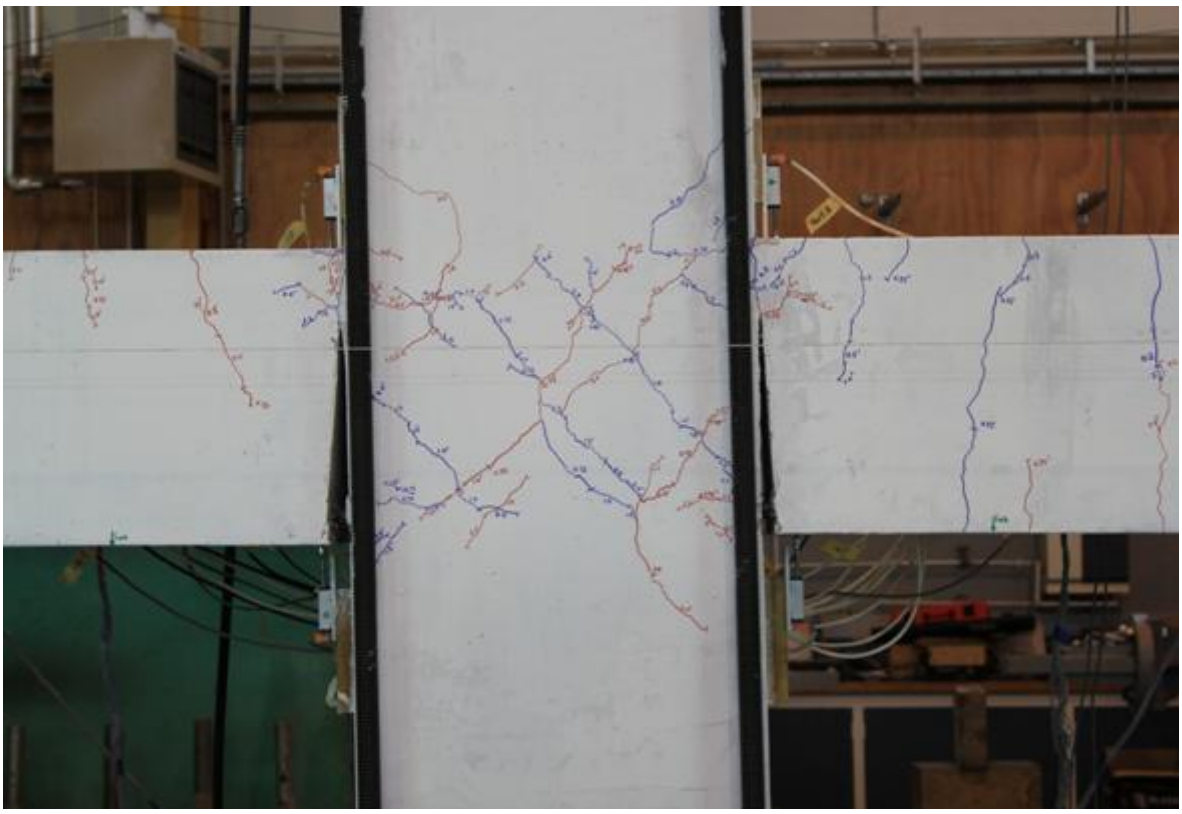

(b) -2.0% drift

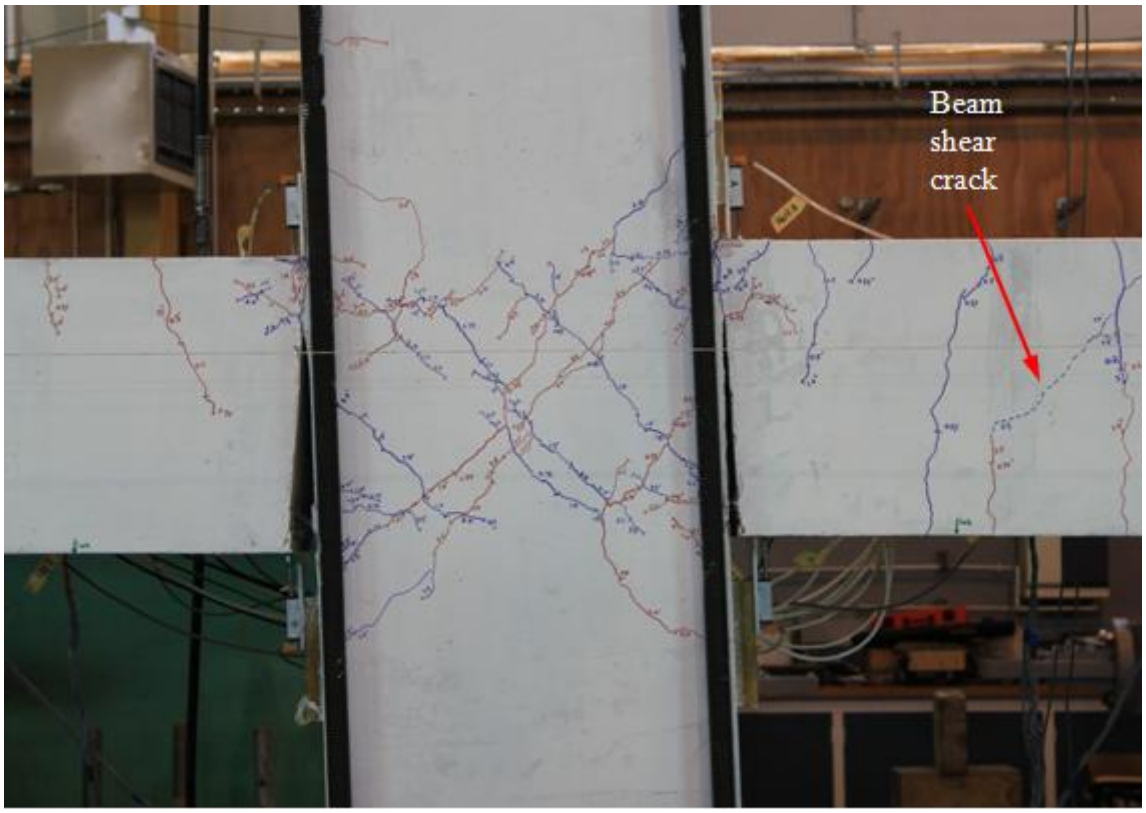

(c) -3.5% drift

Figure 5-23: *Crack development in specimen B (Continued)*

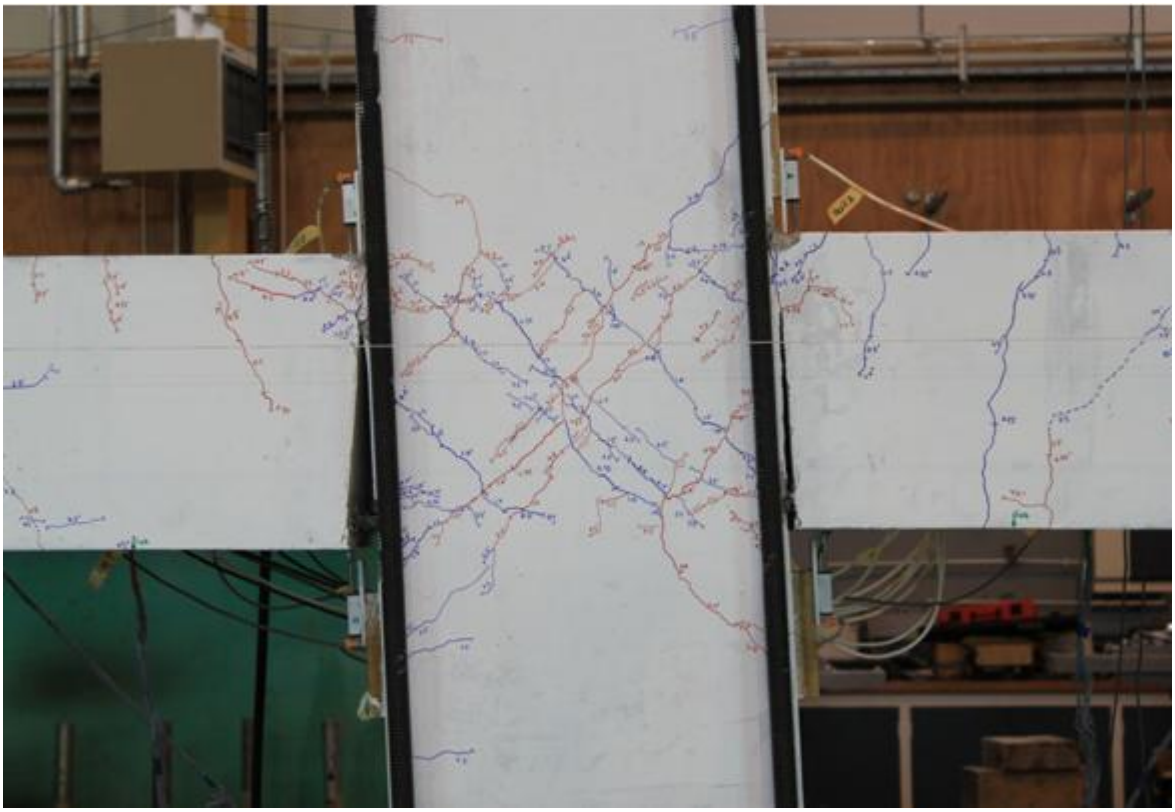

(d) -4.5% drift

Figure 5-23: *Crack development in specimen B (Continued)*

Crack Development up to Specimen Yield:

Initial cracking in both specimens occurred at 0.2% drift and consisted of an individual hairline crack moving up the hinge above each slot in addition to several hairline flexural cracks in the beams. During gap closing rotations, a hairline crack was also visible along the beam/column interface above the hinge. Apart from extension and formation of beam flexural cracks, no other types of cracking occurred in specimen A until 0.75% drift. Specimen B, however, began to develop strain penetration cracking in the joint during cycles at 0.5% drift. Extension of the hinge cracks was also observed. Strain penetration cracking first appeared on specimen A at the bottom east of the joint during the 3rd cycle at 0.75% drift. A common theme of strain penetration cracks on both specimens at this stage was their tendency to close completely during unloading cycles.

First hairline joint shear cracks were observed on both specimens during loading at 0.75% drift, although they appeared earlier on specimen B than on specimen A. The beam flexural cracks continued to extend and form on both specimens with the majority remaining hairline in width. Bottom strain penetration cracking at 0.75% drift reached a maximum of 100 mm into the joint on specimen A but was still observed to close during reverse cycles.

Crack Development and Observed Damage up to 2.5% Drift (ULS):

Figure 5-22(a) and Figure 5-23(a) show the crack development at 1.0% for specimens A and B, respectively. Several individual hinge cracks were now visible on specimen A, while a single crack was visible down the entire length of the hinge/column interface on specimen B. Cracking above the hinge on specimen B is shown in Figure 5-24(a) with a smaller secondary crack visible approximately 50 mm from the column face. Given the majority of flexural cracks on the top of each beam were still hairline in width it would appear the bulk of beam elongation was concentrated within the hinge over these two cracks. Strain penetration cracking was also observed to increase on both joints, but this was more prevalent in specimen B. This coincided with the appearance of a crack running along the inside of the west slot where the bars exited the joint.

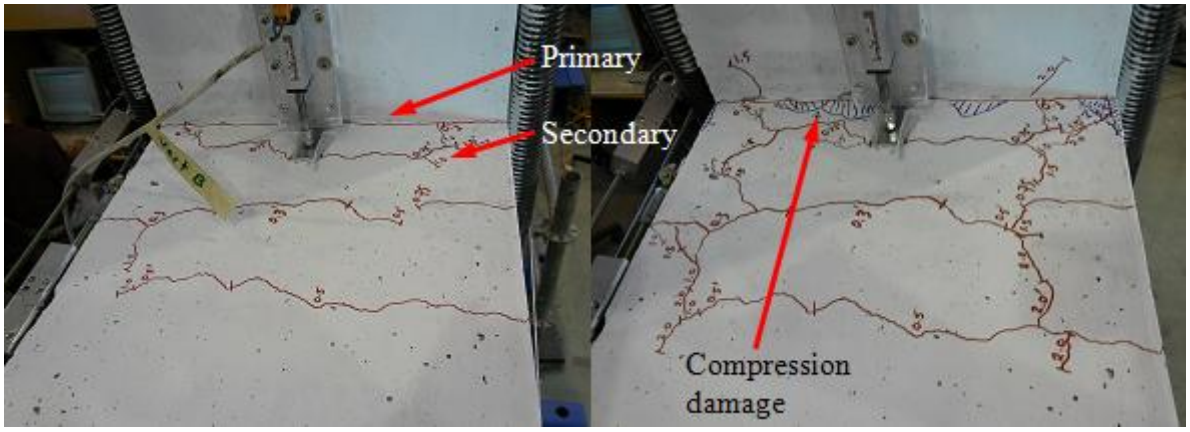

(a) 1.0% drift (b) 2.0% drift

Figure 5-24: *Progression of beam damage above the hinge on Specimen B*

The most noticeable progression in crack development at 2.0% drift was on the joints of both specimens. This increase in cracking is clearly evident in Figure 5-22(b) and Figure 5-23(b). Further strain penetration cracking was visible on both joints but these were still observed to close during unloading cycles indicating an effective clamping response from the elastic column bars. Note that the supplementary vertical joint stirrups are not expected to contribute to this clamping mechanism. This is because these stirrups are anchored around the longitudinal beam bars and, as such, cannot provide confinement to the adjacent concrete splitting plane. However, these stirrups are effective at clamping the longitudinal beam bars into the core as discussed in Section 4.2.3.

Formation of these splitting cracks coincided with initiation of cone pullout formation around the bottom bars exiting the joint as illustrated in Figure 5-25(a). By completion of the 2.0% drift cycles, this radial cracking had typically linked between individual bars and reached the column face as shown in Figure 5-25(b), although the damage was worse on specimen B.

After consistent widening during gap opening cycles at 1.5 and 2.0%, hinge cracks above the slot were now beginning to connect with nearby cracks on the joint face as can be seen in Figure 5-22(b) and Figure 5-23(b). Primary and secondary cracks above the beam hinges were also continuing to widen, but these closed completely upon unloading. Compression damage above the hinges began to appear on specimen B during gap opening rotations around 2.0% drift as shown in Figure 5-24(b). Cracking outside the hinge region on the beam tops remained predominantly hairline through 2.0 % drift.

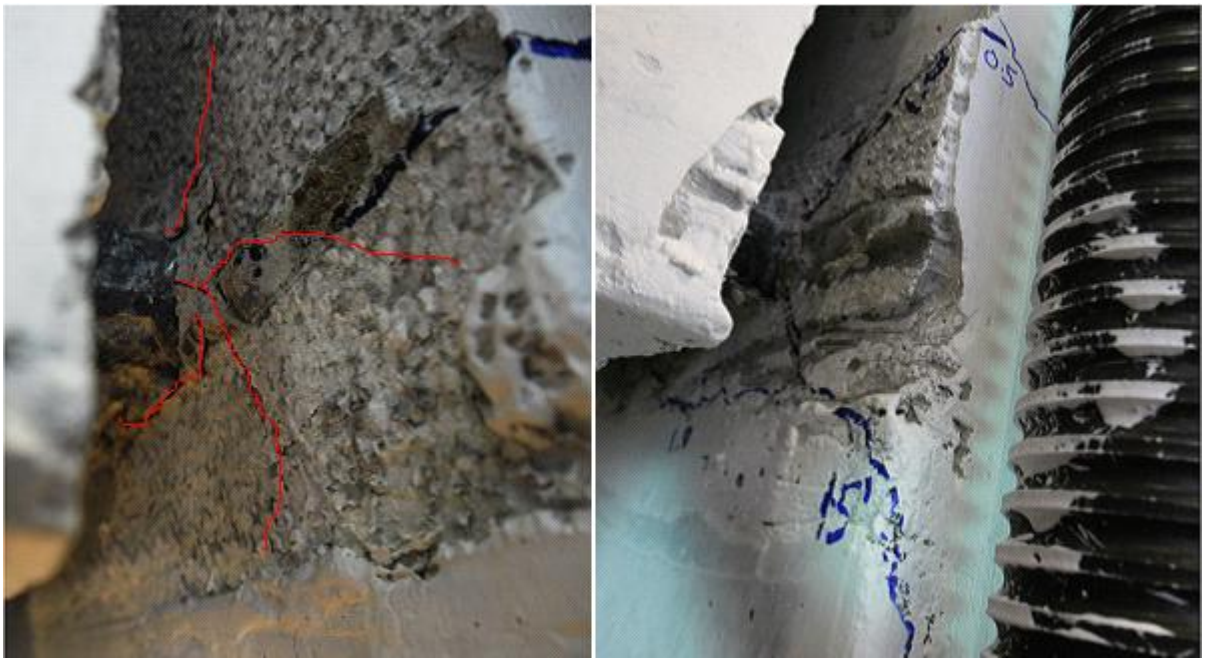

(a) Radial cracking (b) Radial cracking reaching column face

Figure 5-25: *Typical initiation of cone pullout of bottom bars exiting joint*

Damage at 2.5% drift, corresponding to the Ultimate Limit State, was more severe in specimen B. Figure 5-26(a) and (b) show typical hinge cracking in specimens A and B at this stage. Compression damage was now visible in the top hinge of specimen A and had advanced in specimen B. Crack widths on the rest of the beam tops remained predominantly hairline with flexural cracks on the bottom halves of the beam consistently wider. Strain penetration cracks on the joint extended and widened to 0.04 mm at most, with some now remaining open during unloading cycles. As shown in Figure 5-27(a), radial cracking around the bottom bars was continuing to develop in specimen A. Concrete flakes could be seen falling out of the slot during loading to 2.5%. Damage was worse in specimen B where the cone surface was beginning to pull away from the joint face. This is illustrated in Figure 5-27(b).

Several new types of damage became apparent during loading at 2.5% drift. Downwards inclination of the beam bars was evident across the slot on both specimens during

compression cycles indicating bar buckling and/or vertical dropping over the hinge. What appeared to be a shear crack formed in the bottom half of the east beam in specimen B, approximately 200 mm from the end of the unbonded length. Also, cracking across the beam soffit at the end of the unbonding tube appeared on specimen B.

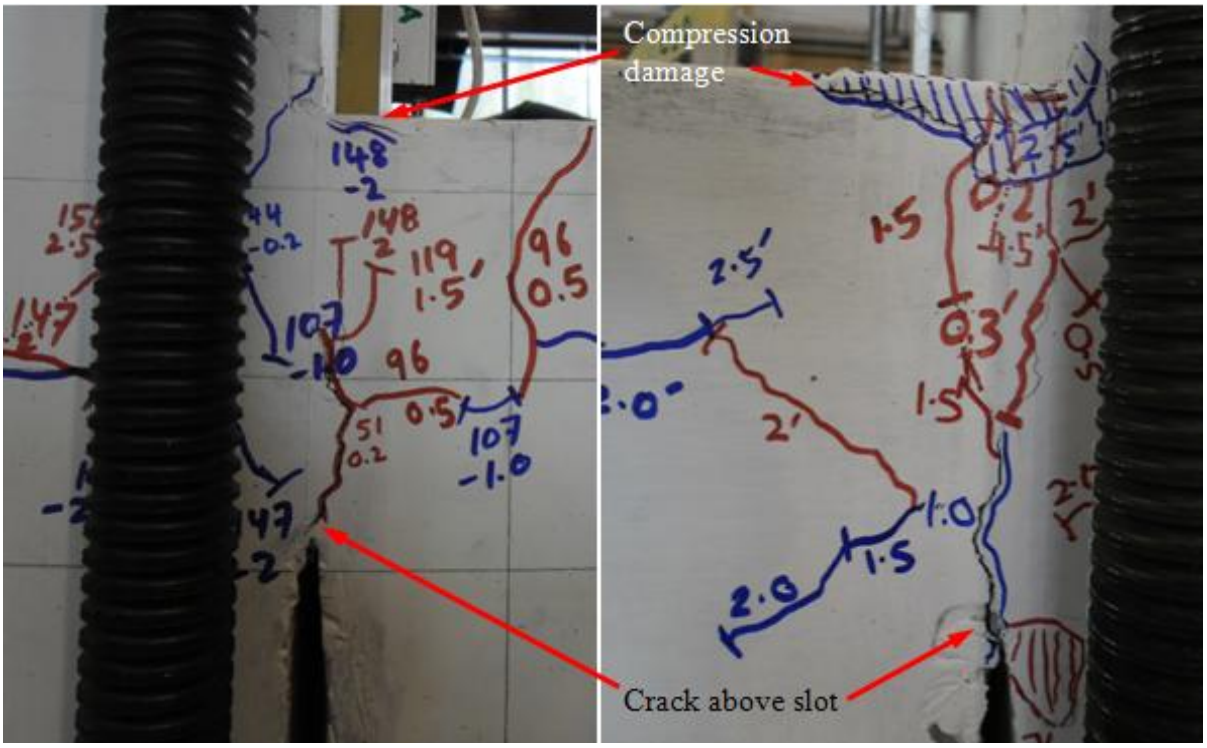

(a) Specimen A (b) Specimen B

Figure 5-26: *Typical hinge region cracking at 2.5% drift (ULS)*

(a) Specimen A (b) Specimen B

Figure 5-27: *Damage due to bar pullout at bottom joint region at 2.5% drift (ULS)*

Post-ULS Crack Development and Observed Damage:

Damage at 3.5% drift was still relatively minor. Highly inclined joint cracks were visible on the rear of both specimens as illustrated in Figure 5-28(a). The inclined nature of these cracks indicates the bottom longitudinal beam bars were still able to provide an effective landing zone for the concrete strut and suggests the revised mechanism discussed in Section 4.5.2 is governing joint shear behaviour. This high bond effectiveness is supported by the lack of strain penetration in each joint as shown in Figure 5-22(c) and Figure 5-23(c) with the maximum width of such cracks reaching only 0.08 mm. Several diagonal cracks also spread to the column just outside the joint region in both specimens, while the first hairline flexural cracks appeared on the column of specimen A. Some compression damage above the hinges was now visible in specimen A, while specimen B had significant compression damage at both the tops and side of the hinges. The comparison between specimens at this stage is illustrated in Figure 5-29. Cracks within the remainder of the beam tops generally remained hairline in width. Slot cracks continued to widen on both specimens with a secondary crack on the order of 0.65 mm visible on specimen A. In specimen B, these cracks remained open through the entire depth of the hinge during unloading through zero ram force indicating some permanent beam elongation.

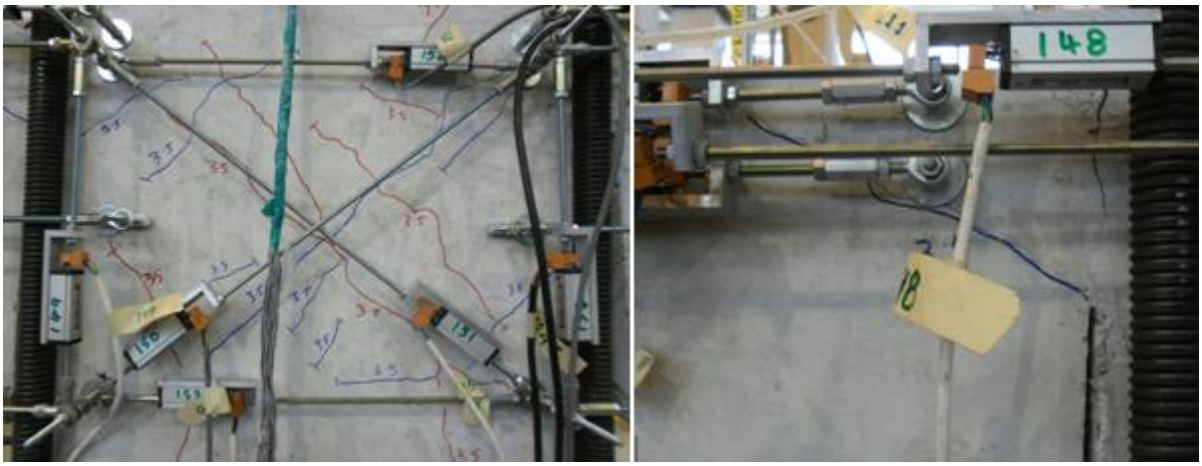

(a) Steeply inclined joint cracks (b) Diagonal hinge crack

Figure 5-28: *Typical joint and hinge cracking at 3.5% drift*

Further downwards inclination of beam bars entering the unbonded length was explained by diagonal hinge cracks indicating dropping of the beam over the hinge. One such typical crack is illustrated in Figure 5-28(b). Some vertical differential was also visible across cracks on top of the beam hinges. During the loading cycles at 3.5% drift, concrete began to loosen and spall off the joint faces around the beam bars. The stirrups were visible in places where all the concrete cover had been lost. Again, this damage was worse in specimen B. Cracks were observed for the first time on the beam soffit of specimen A in the vicinity of the unbonded

length. These initiated within the beam at the end of the unbonded length and ran axially along the beam. It is likely that these cracks were the surface presentation of radial cracks forming around the yielding bottom beam bars. Further cracking occurred across the soffit of specimen B just past the end of the unbonded length. The previously mentioned shear crack in specimen B widened to 0.2 mm while a second one formed on the west beam approximately half way up. No such cracks had yet formed in specimen A – probably due to the higher concrete strength within this specimen.

(a) Specimen A (b) Specimen B

Figure 5-29: *Beam damage above the hinge at 3.5% drift*

Damage to the hinge regions increased significantly in both specimens during the loading cycles at 4.5% drift. Increased crack widths along with spalling in this region can be seen in Figure 5-30. Further damage was also evident on the joint face in the vicinity of the bottom beam bars. Horizontal joint stirrups were now exposed across the joint face of both specimens due to cone pullout having occurred across the whole bottom bar group. This resulted in a greater length over which the beam bars were able to buckle during gap closing cycles. In conjunction with further dropping of the beam across the hinge, severe bar buckling occurred as illustrated in Figure 5-31(a). Despite the increased level of damage resulting from activation of the bottom beam reinforcement, diagonal joint cracks were still steeply inclined indicating the strut mechanism was still well intact. However, the amount of cracking on the joint had increased substantially to the point where it was difficult to differentiate between shear and strain penetration cracks. This can be seen in Figure 5-22(d) and Figure 5-23(d).

While the beam shear crack in specimen A reached 0.15 mm during loading to 4.5% drift, the development of similar cracking in specimen B was more significant. As shown in Figure 5-31(b), what appeared to be an ‘S’ crack had formed on the back of the beam. As discussed in Section 2.2.1, such cracking forms in slotted beams when inadequate continuity

reinforcement is provided across the end of the unbonded region. While this reinforcement was provided by the bottom horizontal portion of the shear hangers, it is possible these were not fully developed or had undergone some strain penetration. Either of these events would necessitate some bar slip and thus cracking before the restraining response was fully mobilised. Additional reinforcement in the form of deformed bars running parallel above the unbonding tubes with a hook for development at the column end can be installed to mitigate this cracking (Muir, 2011).

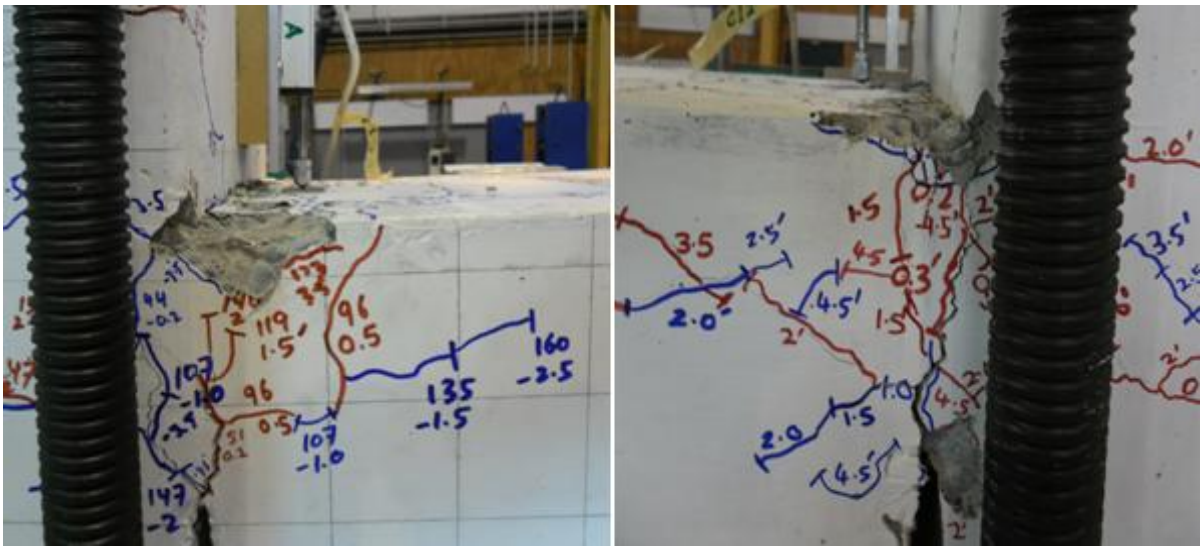

(a) Specimen A (b) Specimen B

Figure 5-30: *Hinge damage at 4.5% drift*

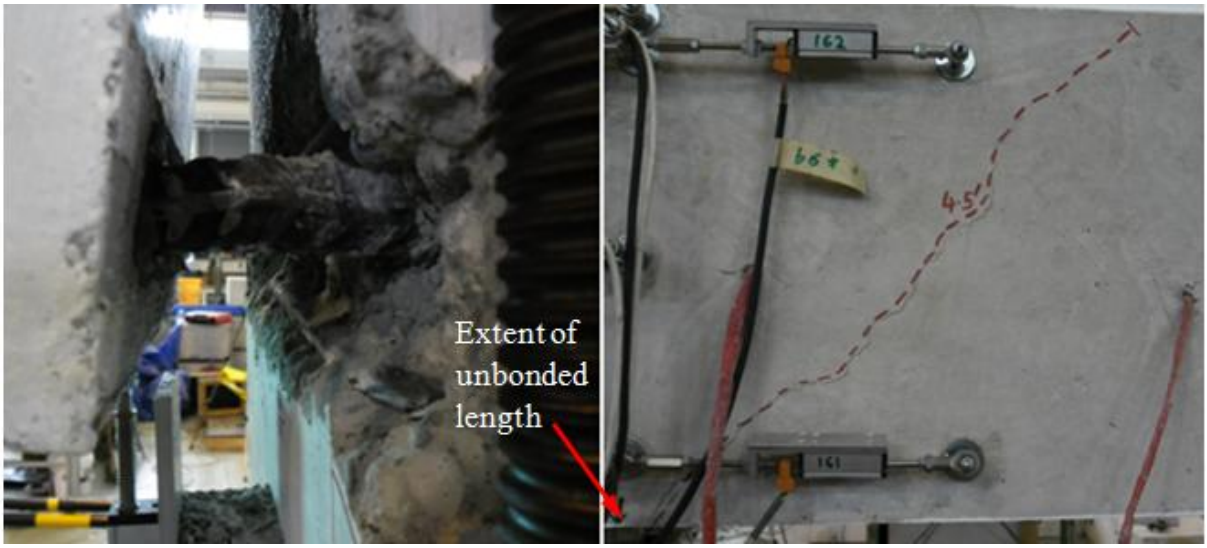

(a) Bar buckling across slot (b) ‘S’ crack in Specimen B beam

Figure 5-31: *New damage observations at 4.5% drift*

The other major development during loading at 4.5% drift was the significant increase in damage to the beam soffit unbonded regions on both specimens. For the first time, cracks formed on the joint end of the beam soffits in both specimens, suggesting buckling of the bars was placing significant demands on the unbonding tubes. At the other end of the unbonded

length on specimen B, a vertical drop was evident over the cracks which had widened to approximately 0.3 mm. Typical cracking within this region is illustrated in Figure 5-32(a).

(a) Typical beam soffit damage at 4.5% drift (b) Bar fracture at 5.5% drift

Figure 5-32: *Beam soffit damage and bar fracture*

A single loading cycle was carried out for each specimen at 5.5% drift. Initial bar fracture occurred on both specimens during the first cycle to +5.5% drift; an example is shown in Figure 5-32(b). This was followed by a second fracture during loading to the second +5.5% drift peak after which testing was stopped due to excessive beam twisting and concerns over system capacity in the event of another fracture. In three of the four bar fractures, the fracture occurred immediately adjacent to the end of the unbonding tube. This suggests the lug bearing mechanism described in Section 5.4.1 may have lead to localised bar weakness in this area thus making it fracture in this location preferentially. Further damage was also observed in the hinges and beam soffits in the vicinity of the unbonded length. The ‘S’ crack in specimen B widened to 1 mm, coinciding with further diagonal cracking on the east hinge as illustrated in Figure 5-33. This crack reached 2.1 mm in width with dropping of the beam clearly evident over the hinge.

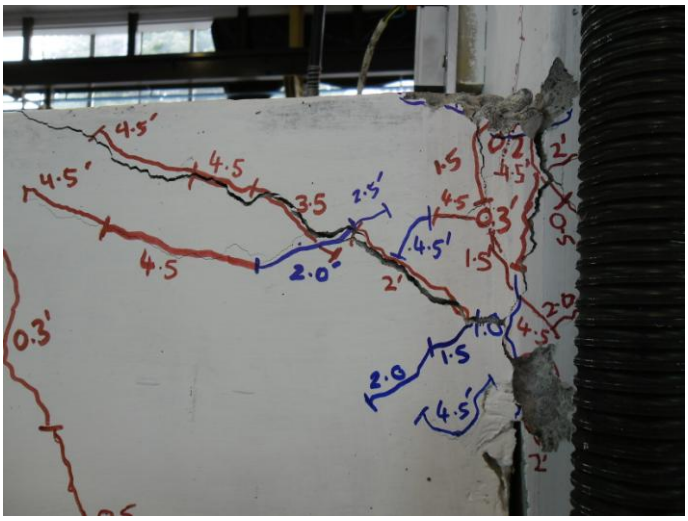

Figure 5-33: *Beam dropping over diagonal hinge crack in specimen B at 5.5% drift*

5.4.3 Beam Elongation

Measured beam elongation is shown for specimens A and B in Figure 5-34 and Figure 5-35, respectively. These measurements were taken at the beam centreline across the slotted region using linear potentiometers. Table 5-6 gives the measured beam elongation for the entire subassembly at various drifts compared with values found by Au (2010). Comparisons with monolithic beams are also given based on research by Fenwick and Megget (1993).

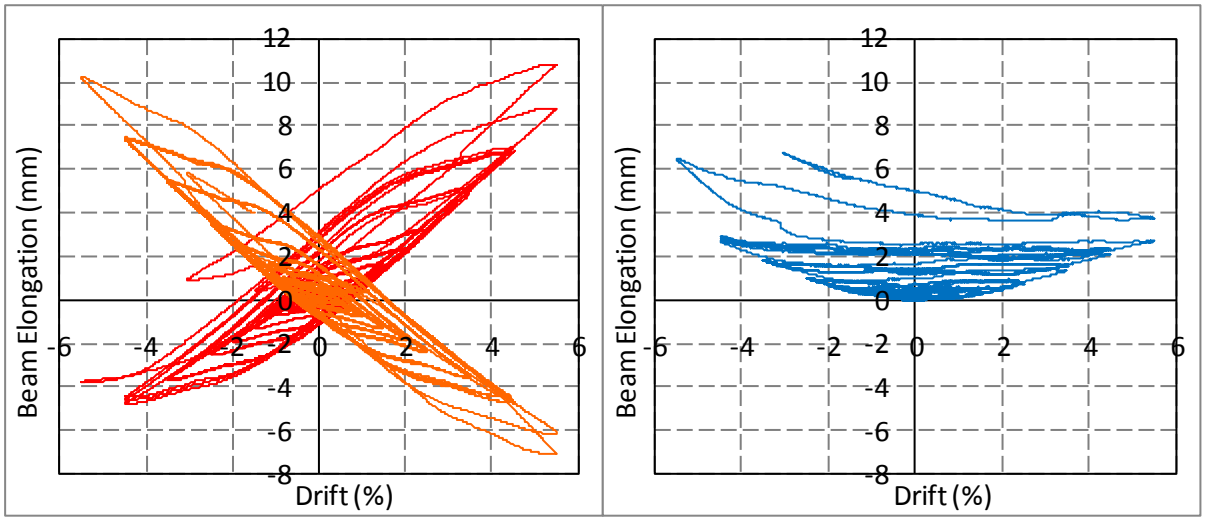

(a) Elongation within each beam (b) Total specimen elongation

Figure 5-34: *Components of beam elongation specimen A*

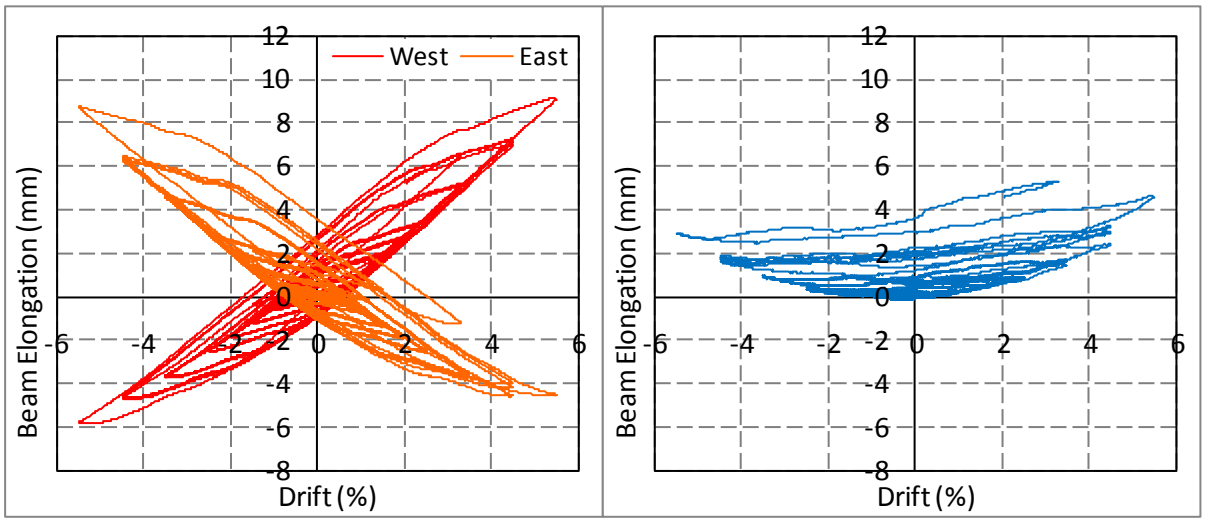

(a) Elongation within each beam (b) Total specimen elongation

Figure 5-35: *Components of beam elongation specimen B*

Good agreement in beam elongation values exists between all the slotted beam specimens with the values consistently below the lower bound for monolithic specimens as shown in Table 5-6. The primary reason for this is the geometric effect of simultaneous gap opening and closing on alternate sides of the joint which act to cancel one another out. As discussed in Section 5.5.3, the top longitudinal beam reinforcement remains nominally elastic throughout

the testing of both specimens. This also contributes to the low observed beam elongation by keeping material elongation to a minimum.

Table 5-6: *Specimen beam elongation with comparisons*

	Total Beam Elongation (%h_b)		
Drift Level	1.0% Drift (SLS)	2.5% Drift (ULS)	4.5% Drift (LS)
Specimen A	0.07%	0.21%	0.67%
Specimen B	0.07%	0.21%	0.76%
Au SB2	0.05%	0.21%	0.67%
Au SB3	0.05%	0.19%	0.53%
Lower Bound Monolithic	2.0%		
Upper Bound Monolithic	5.0%		

Residual beam elongation is also negligible for both specimens as shown in Table 5-7. These measurements correspond to the elongation of each individual beam as the specimen passes through 0% drift after completing all cycles at the stated drift level. As expected, the maximum readings were consistently observed during gap opening rotations. Combined with comparisons to Au (2010) specimens, it can be concluded that the use of Grade 500 top beam reinforcement or hangers does not result in significant reductions in residual beam elongation. As such, Grade 300 reinforcement appears suitable in these applications. However, the use of Grade 500 reinforcement for hangers is still preferable in order to keep the bar size down.

Table 5-7: *Specimen residual beam elongations with comparisons*

	Top Beam Reinforcement Grade (MPa)	Hanger Reinforcement Grade (MP(a)	Residual Beam Elongation (% h_b)		
			1.0% Drift (SLS)	2.5% Drift (ULS)	4.5% Drift (LS)
Specimen A	300	500	0.12%	0.38%	0.71%
Specimen B	300	500	0.10%	0.30%	0.64%
Au SB2	300	500/300	0.04%/0.09%	0.3%/0.48%	0.43%/0.56%
Au SB3	500	500	0.06%	0.28%	0.49%

5.4.4 System Energy Dissipation and Stiffness

Energy dissipation per cycle is plotted as equivalent viscous damping for specimens A and B in Figure 5-36. Average values are also shown as solid lines on the figure. While a small discrepancy exists around the level of drift corresponding to first cracking, the hysteretic energy dissipation is very similar between the two specimens. No degradation in energy dissipating capacity is evident throughout the entire drift sequence. These results clearly show that properly detailed slotted beams can provide a good degree of energy dissipation capacity with a high reliability.

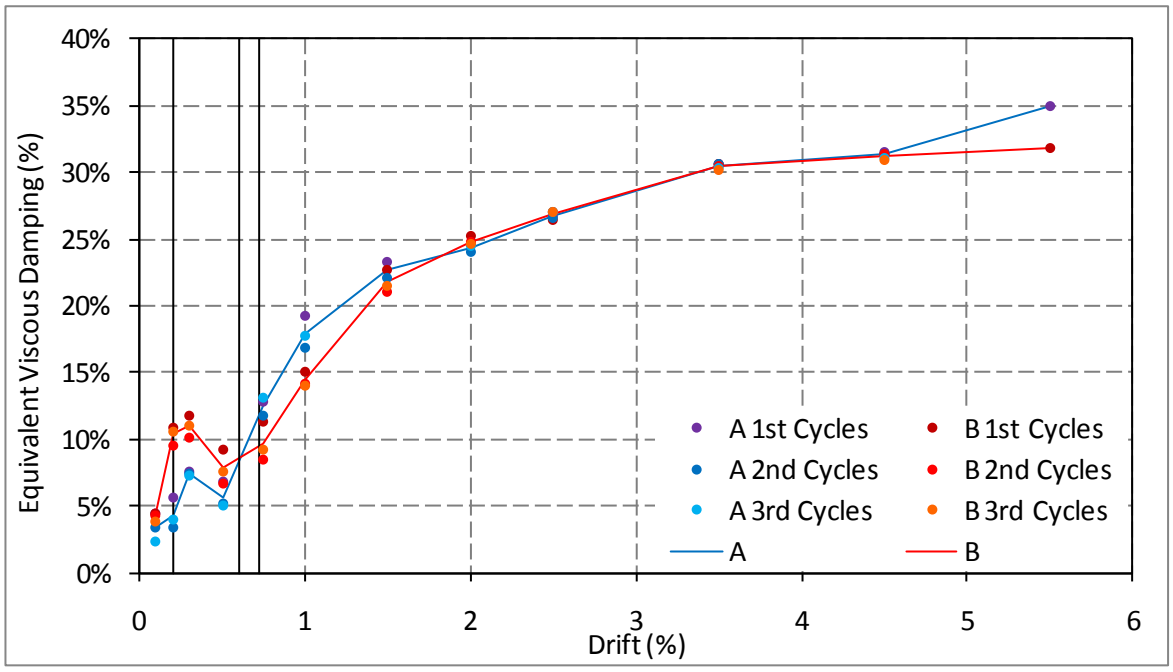

Figure 5-36: *Hysteretic energy dissipation for specimens A and B*

Figure 5-37 gives a comparison in average energy dissipation capacities between specimens A and B and those tested by Au (2010). The monolithic specimen tested by Au (2010) is also included as a benchmark. Energy dissipation is relatively constant across all the specimens, with SB2 dropping away after 3.5% drift due to excessive bar slip through the joint. From these results it can be concluded that well detailed slotted beams have a comparable energy dissipation capacity to monolithic beams. While the energy dissipating capacities are similar between the two systems, it is important to note that those achieved by the slotted beams are achieved with considerably less damage.

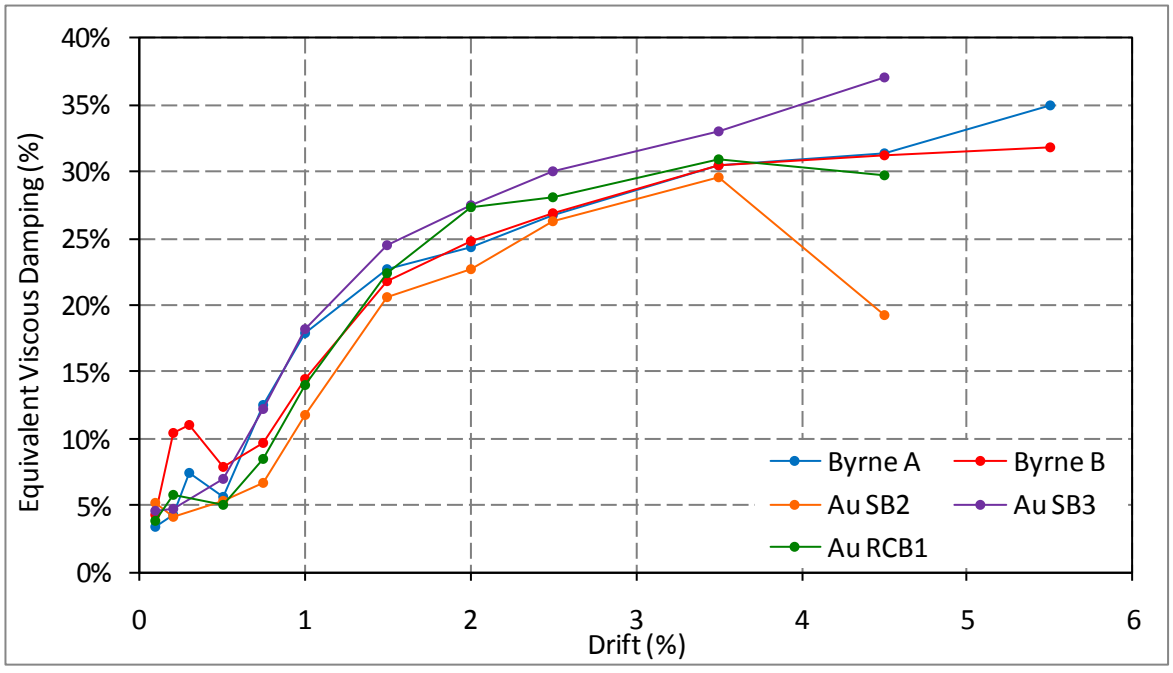

Figure 5-37: *Average hysteretic energy dissipation comparisons*

The average peak to peak stiffness at each drift level for specimens A and B is shown in Figure 5-38. This figure is calculated by dividing the change in force to displace the specimen from peak negative to peak positive drift during any given cycle by the corresponding displacement. As expected, clear stiffness degradations are evident at first cracking and through the yield range of both specimens. The loss of stiffness in both specimens is steady up to 4.5% drift after which a small drop off is evident. This corresponds to bar fracture in both cases. The response of specimen A is slightly stiffer than that of specimen B, most likely due to the increased joint reinforcement area and concrete strength. However, the difference is negligible and indicates that specimen B was still adequately detailed.

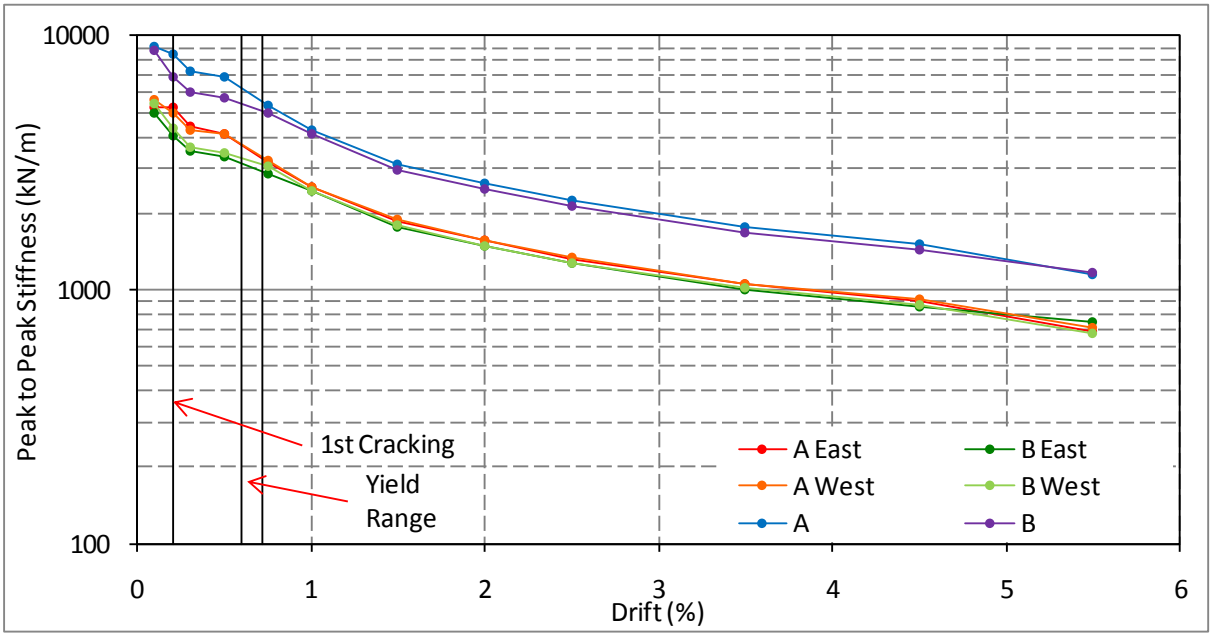

Figure 5-38: *Average peak to peak stiffness for specimens A and B*

Figure 5-39 gives a comparison in the rate of peak to peak stiffness degradation between the same specimens as listed previously. It is clear from the figure that the slotted beam specimens do not have the same rapid initial stiffness degradation apparent in the monolithic specimen. This is due to the fact that the stiffness in a slotted beam is driven primarily by the unbonded bottom reinforcement which responds linearly up until yield. In a monolithic beam, however, stiffness is linked to initial cracking resulting in a notable drop after this event. The stiffness of the monolithic system then falls away faster due to the higher degree of damage incurred. Like the energy dissipation capacity, the stiffness of SB2 drops away rapidly due to significant bar slip. From these results, it can be concluded that well detailed slotted beams have a lower rate of stiffness degradation than monolithic beams.

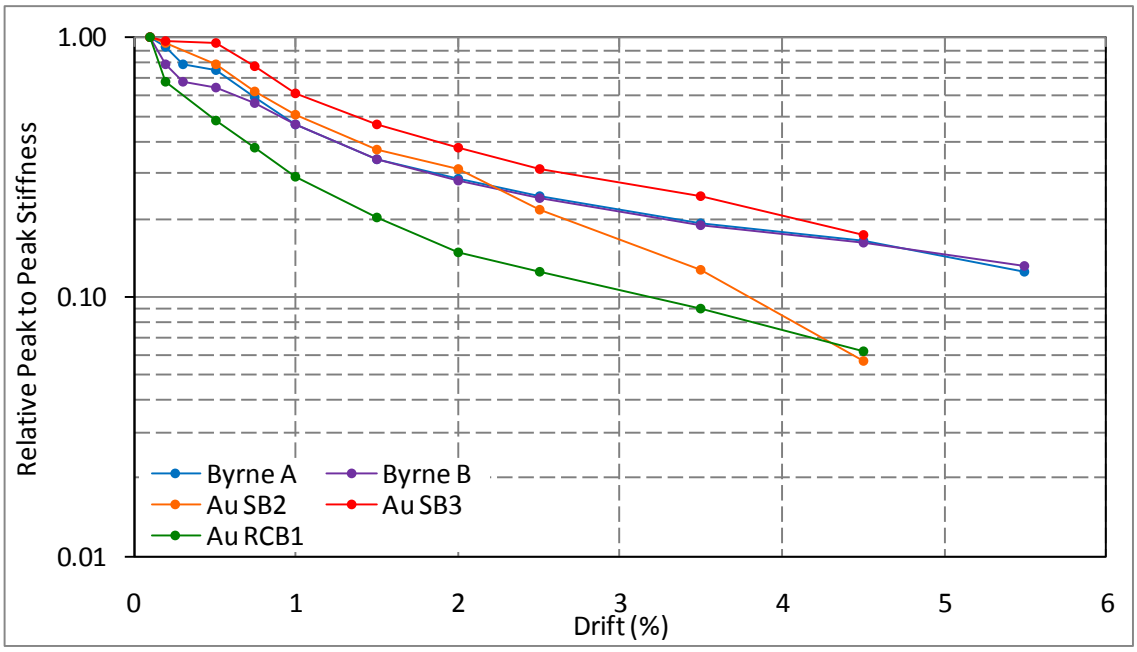

Figure 5-39: *Average peak to peak stiffness degradation comparisons*

5.4.5 Vertical Sliding Across Joint

Vertical sliding across the beam-column interface is an important aspect of slotted beam behaviour. Excessive sliding can lead to displacement incompatibility between the frame and floor slab. Figure 5-40 shows the vertical sliding for each drift level as measured across the beam slots. These values are averages of those calculated during each individual cycle at a given drift level. Spring potentiometers on the beam soffits were used as those on the top were affected by concrete crushing during larger drift cycles.

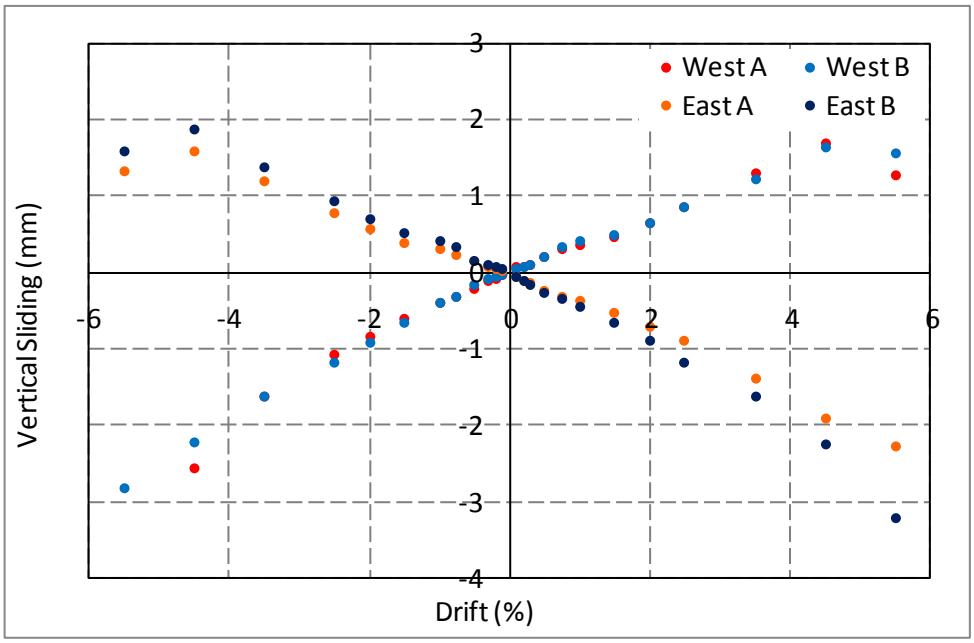

Figure 5-40: *Average vertical sliding across hinge for specimens A and B*

It is clear from Figure 5-40 that vertical sliding increases linearly with drift. This is in slight contrast to the results of Au (2010) where the amount of sliding was found to plateau

somewhat after specimen yield. The results are very similar between specimens with vertical sliding observed during gap closing rotations on average 1.3 times larger than those observed during gap opening rotations. As shown in Table 5-8, this is opposite to the trend observed by Au (2010) where vertical sliding during gap opening rotations was the most significant. Note that data is reported up to 3.5% to allow comparison with the results of Au (2010).

Table 5-8: *Specimen vertical sliding with comparisons*

	Absolute Average Vertical Sliding (% h_b)			
	Gap Opening Rotations		Gap Closing Rotations	
	2.5% Drift (ULS)	3.5% Drift	2.5% Drift (ULS)	3.5% Drift
Specimen A	0.20%	0.30%	0.24%	0.36%
Specimen B	0.21%	0.31%	0.27%	0.39%
Au SB1	0.06%	0.18%	0.09%	0.08%
Au SB2	0.19%	n/a	0.09%	n/a

This discrepancy is explained by diagonal cracks observed on the hinge as illustrated in Figure 5-33. Such cracking was first noticed at 3.5% drift in conjunction with inclination of the bottom beam bars entering the unbonding tubes. These cracks suggest insufficient shear hanger capacity was provided for gap closing rotations as a result of the overstrength moment capacity being far greater than anticipated. Perhaps more importantly, lower overstrength values during compression inducing rotations would cause differential hanger activation which could lead to elongation of the hangers over a number of cycles. These observations are supported by the hanger strain profiles as reported in Section 5.6.2. Despite observing differential hanger strains, such cracking did not occur during testing by Au (2010). However, the beam overstrength values were not as variable as in specimen A and B – most likely due to a combination of PVC tubes being used for the unbonded length and bar slip failure/bar fracture occurring before the overstrength mechanism discussed in Section 5.4.1 could be mobilised. Given these results, it is recommended that the shear hangers be designed for the gap closing beam overstrength ratio as opposed to the system overstrength ratio.

5.4.6 Component Drift Relative Contributions

Figure 5-41 and Figure 5-42 show the relative contribution of each component to specimen drift throughout the testing sequence. Only the primary components contributing to specimen drift were considered; namely joint shear deformation, column and beam elastic flexure, and beam fixed-end rotation. Beam and column shear contributions were considered to be negligible. Except for beam fixed-end rotation, all results were calculated using the corresponding average peak readings at each drift level for positive and negative drifts. This enabled consistent comparisons between results for gap opening and closing beam fixed-end

rotations which were calculated using the results of each beam individually. This approach was used as opposed to plotting the combined specimen response because the latter would mask the difference in drift contributions between gap opening and closing rotations. Beam and column flexural stiffness was taken as 0.46 and 0.56I_g, respectively, based on analyses in both Excel and Response 2000 (Bentz, 2000).

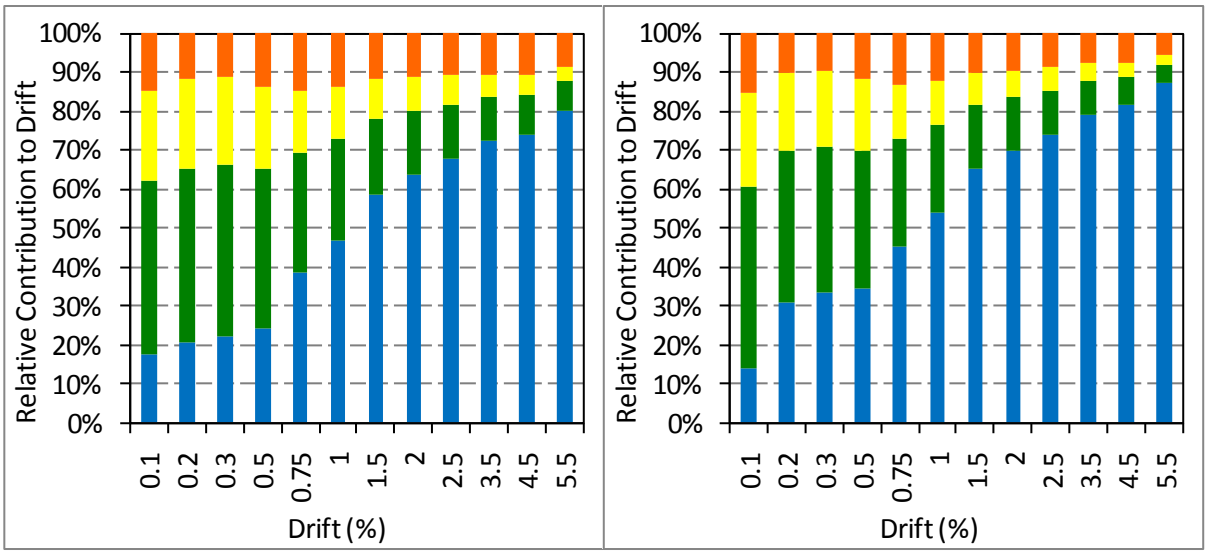

(a) Gap closing rotations (b) Gap opening rotations

Figure 5-41: *Relative contributions of drift components in specimen A*

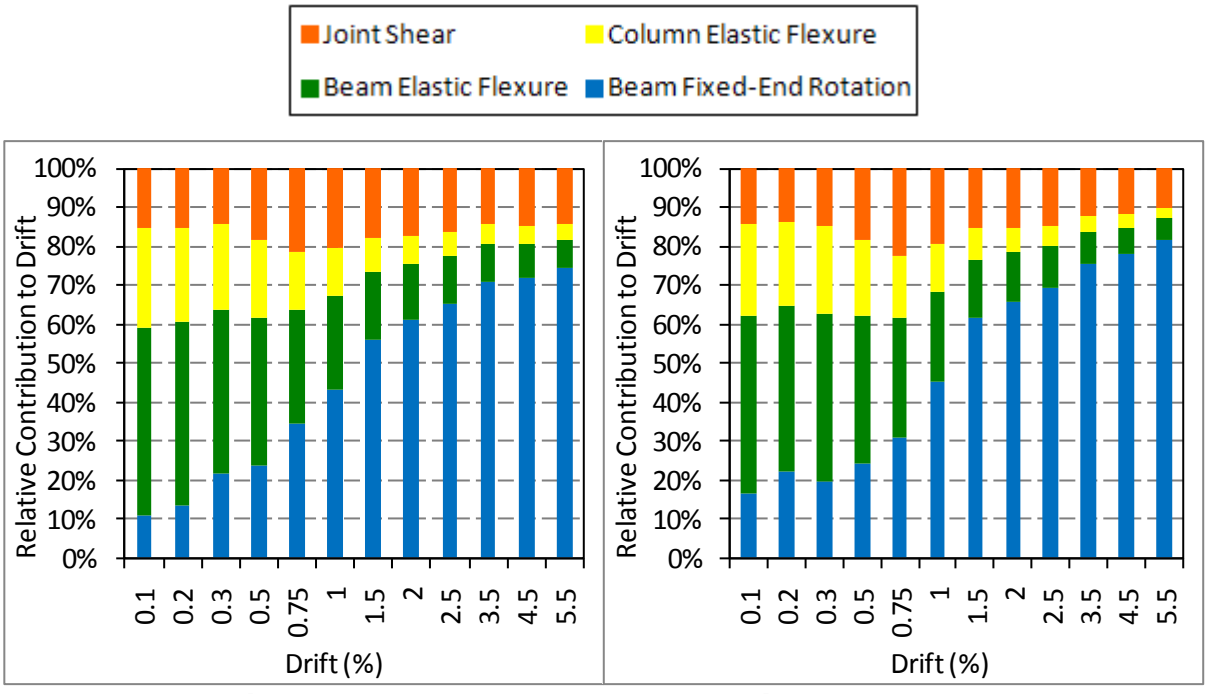

(a) Gap closing rotations (b) Gap opening rotations

Figure 5-42: *Relative contributions of drift components in specimen B*

As expected, the relative drift contributions from column flexure are similar both between specimens and gap opening/closing rotations. This is due to the columns being significantly stronger than the beams; the column yield to beam overstrength at the column face moment

ratio, $M_{y,col}/M_{o,b}$, was approximately 1.8. As a result, the columns remained within the elastic range where performance is more consistent and reliable. Beam flexure relative contributions are also reasonably constant across both beam opening and closing rotations, although not to the same extent as the column contributions. Both the beam and column relative contributions are found to decrease for drift levels beyond specimen yield (> 0.75%). This is due to the beam fixed-end rotation component becoming inelastic and overwhelming the elastic response of these members. This is an important result as it confirms the majority of the damage and energy dissipation within the system is occurring within this region through tension/compression yielding of the bottom beam reinforcement.

Unlike the beam and column components, the relative contribution from joint shear deformations does not change significantly throughout the entire drift sequence. As expected, the joint response is the same for gap opening and closing because these occur simultaneously on either side of the joint. Maximum joint deformation contributions of 15 and 22% were observed for specimens A and B, respectively. This small discrepancy probably reflects the greater level of joint reinforcement and higher concrete strength present in specimen A. Nonetheless, these figures are consistent with the 20% value typical of monolithic frames (Paulay & Priestley, 1992) and indicate a satisfactory joint response in both cases.

The beam fixed-end rotation contribution is consistently larger for gap opening contributions. This observation is true for both specimens across the entire drift sequence and suggests that gap opening stiffness is less than that for gap closing. Considering the concrete prying mechanism is active during gap closing rotations, this would appear logical. However, the corresponding figures calculated directly from force displacement data as per Section 5.4.4 suggest the opposite is true as do tentative suggestions by Au (2010).

5.4.7 Variation of Neutral Axis Depth within the Hinge

The variation in neutral axis depth within the hinge for each specimen throughout the drift sequence is illustrated in Figure 5-43. During gap opening rotations, neutral axis depth was found to decrease linearly with drift. This is similar to the trend observed by Au (2010) and replicates the behaviour within monolithic beams. However, during gap closing drifts, the neutral axis remained within the bottom 20% of the hinge depth throughout testing. While similar to the findings of Au (2010), the monolithic analogy is not applicable in this case. Neutral axis depth data is used in the discussion of shear hanger activation (Section 5.6.2)

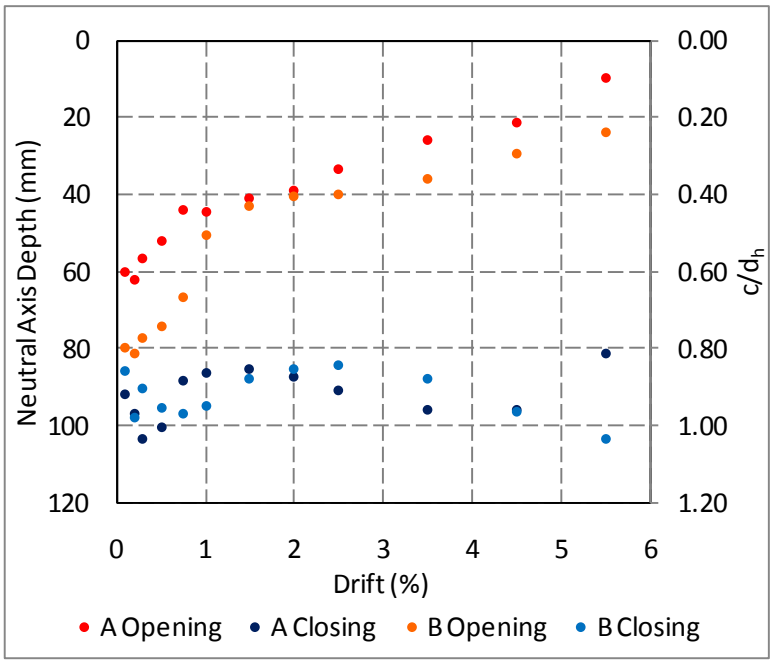

Figure 5-43: *Variation of neutral axis depth within the hinge for specimens A and B*

5.5 Longitudinal Beam Reinforcement and Bond Performance

5.5.1 Bottom Longitudinal Reinforcement Strain Profiles

The bottom longitudinal reinforcement strain profiles at peak drifts for specimens A and B are shown in Figure 5-44 and Figure 5-45, respectively. In some cases at higher drift, the strain gauges failed due to overextension – this generally occurred at a strain of 2.07%. Strain gauge readings after any gauge first reached this value were disregarded resulting in omitted data points in the corresponding figures.

It is clear that the longitudinal reinforcement is subject to inelastic strains in both compression and tension from a very early stage in both specimens. This inelasticity is generally confined to the unbonded region where multiple gauges failed due to the high strains reached. Yielding is only observed to reach the outer column strain gauge – located 100 mm from the column face – during post-ULS drifts indicating very little strain penetration into the joint. Furthermore, negligible strains were observed at the column centreline meaning the degree of bar slip was insignificant.

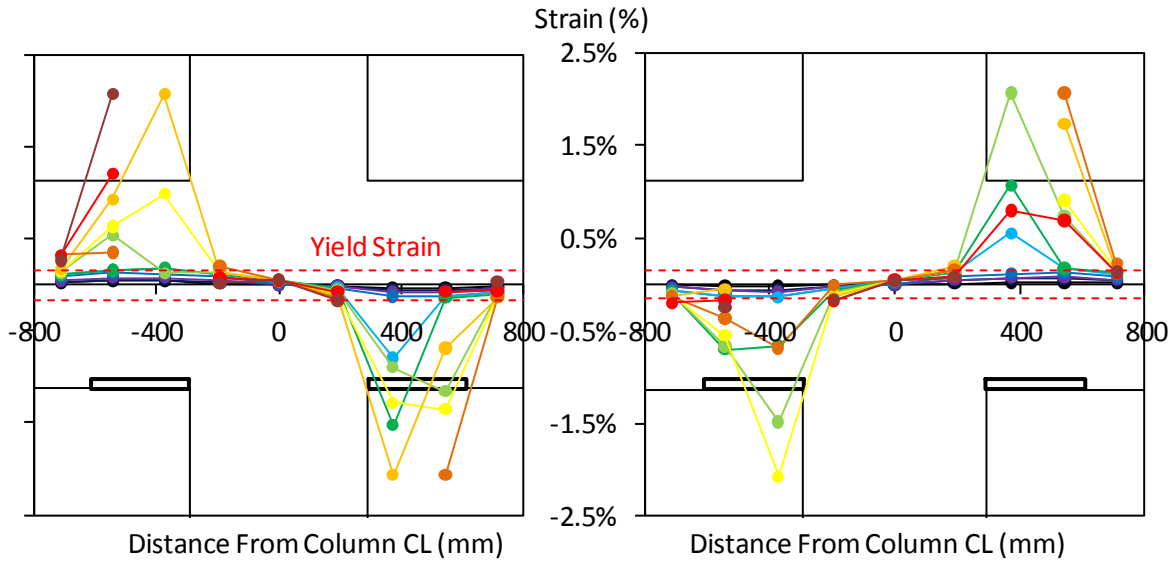

(a) Positive drifts (b) Negative drifts

Figure 5-44: *Bottom beam reinforcement strain profiles for specimen A*

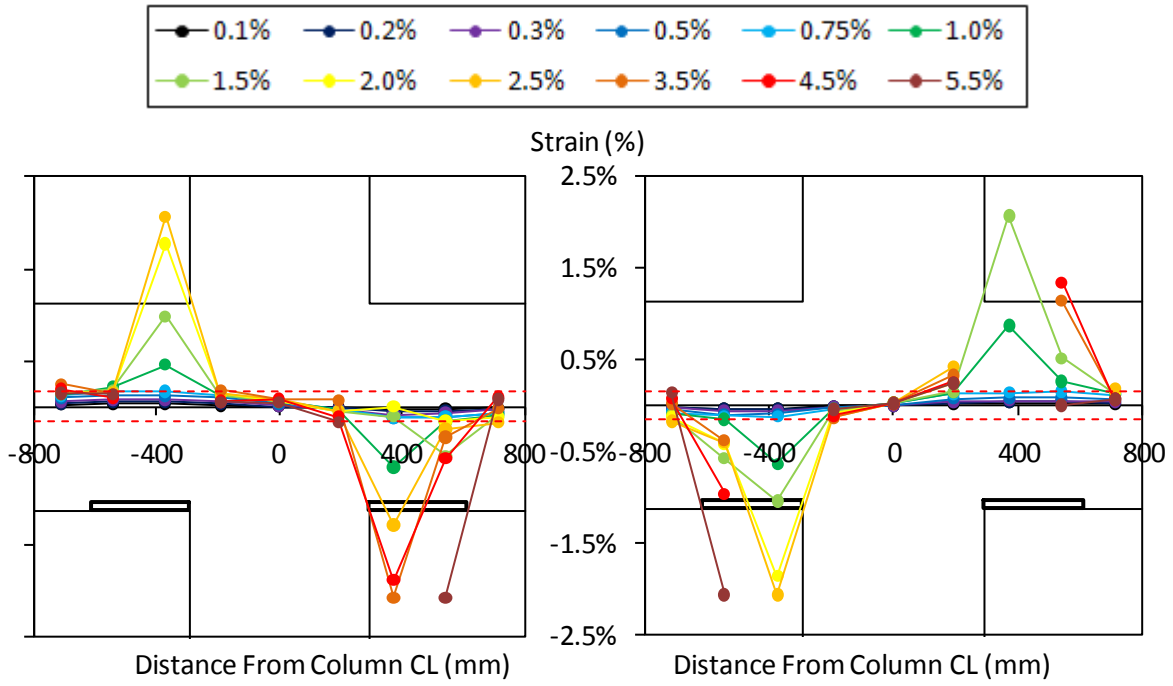

(a) Positive drifts (b) Negative drifts

Figure 5-45: *Bottom beam reinforcement strain profiles for specimen B*

It is clear that the longitudinal reinforcement is subject to inelastic strains in both compression and tension from very early in the testing sequence for both specimens. This inelasticity is generally confined to the unbonded region where multiple gauges failed due to the high strains reached. Yielding is only observed to reach the outer column strain gauge – located 100 mm from the column face – during post-ULS drifts indicating very little strain penetration into the joint. Furthermore, negligible strains were observed at the column centreline meaning the degree of bar slip was insignificant.

Strain penetration lengths of the bottom longitudinal reinforcement were calculated by numerically integrating the strain profiles between 0.5 and 3.5% drift to obtain the bar deformation and equating this with the corresponding theoretical value. Note that while these values were only recorded into the column, it is likely that the majority of strain penetration occurred here anyway as discussed below. The theoretical value was taken as the average strain within the unbonded length times the strain penetration length. The resulting inequality was then solved in Excel using the 'Goal-seek' function. Using this process, strain penetration length, L_{sp}, was found to be 0.0085 and $0.0079 f_y d_b$ for specimens A and B, respectively. This is significantly lower than the values reported by Au (2010) for slotted beams and the monolithic benchmark value of $0.022 f_y d_b$ (Paulay & Priestley, 1992). However, these figures are backed up by experimental observations of minimal strain penetration into the joint as reported in Section 5.4.2.

The low strain penetration observed and calculated is likely due to the unbonded bottom reinforcement acting as a fuse and concentrating inelastic behaviour within this region. As a result, the joint and beam beyond the unbonded tubes are relatively well protected against strain penetration. The majority of strain penetration that does occur should be assigned to the joint region. This recommendation is based on observations of cone formation on the column faces as reported in Section 5.4.2. Furthermore, due to the high level of confinement and cover around the embedded end of the unbonded tube, it is difficult to imagine much strain penetration occurring here. In summary, a value of $0.01 f_y d_b$ is suggested for determining strain penetration in design situations which should be assigned entirely to the joint end of the unbonded length.

5.5.2 Anchorage of Bottom Longitudinal Reinforcement

Anchorage of the bottom longitudinal reinforcement was found to be sufficient with no discernable bar slip occurring in either specimen. As the primary focus of this research, this is a very satisfactory result. This section uses experimental measurements to derive key variables relating to reinforcement bond in order to refine the design recommendations discussed in Chapter 4.

Due to the limited strain that can be recorded by the strain gauges, stresses in the bottom longitudinal reinforcement must be inferred from the measured beam shears and specimen geometry. Using the resulting stresses in conjunction with the nominal material properties, the corresponding overstrength factors can be determined as illustrated in Figure 5-46.

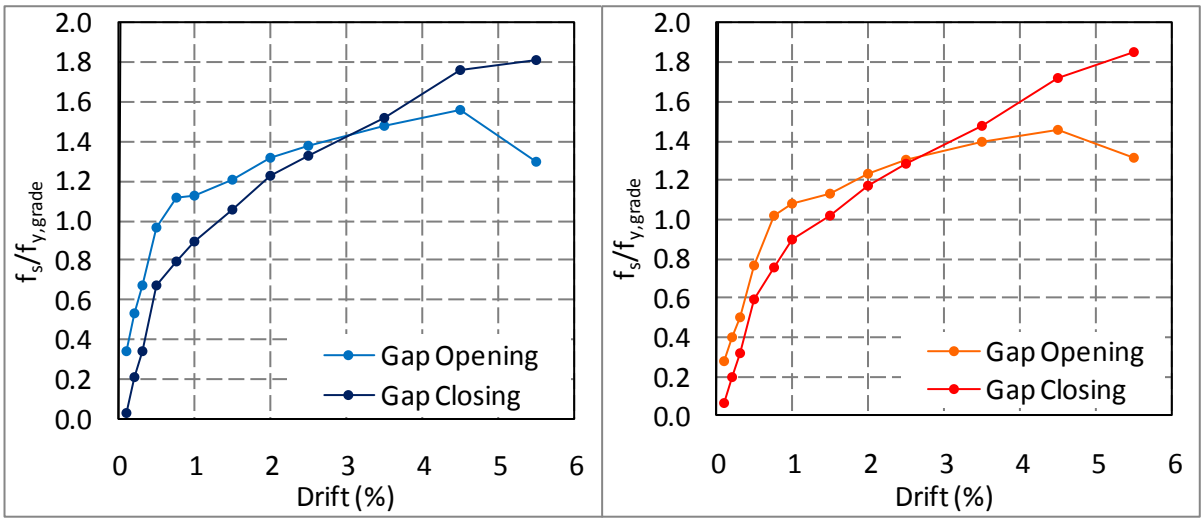

(a) Specimen A (b) Specimen B

Figure 5-46: *Bottom longitudinal reinforcement overstrength factors for specimens A and B*

As expected, the overstrength factors for gap opening are very similar to the beam overstrength factors reported in Section 5.4.1. This is because the bottom reinforcement alone governs the behaviour for such rotations. These overstrength factors reach approximately 1.5 at 4.5% drift before dropping sharply due to subsequent bar fracture. However, there is a small discrepancy between the two factors for gap closing rotations. This is primarily due to the inability of the global estimation method to account for prying within the hinge. Gap closing overstrength factors became dominant between 2.5 and 3% drift, corresponding to initiation of buckling restraint provided by the unbonding tubes as discussed in Section 5.4.1. Based on the results in Figure 5-46, the bottom reinforcement overstrength factor, λ_{ob}, is on the order of 1.35 at ULS drift. This is in agreement with the factor adopted for design as discussed in Section 4.2.4.

As a result of design decisions, not enough strain gauges were installed to provide sufficient data resolution to calculate meaningful bond stress profiles over the column depth. This approach was taken to ensure bond disruption due to strain gauges was kept to a minimum. However, the inferred stresses discussed above are easily converted into average bond stresses, u_a. These are reported in Figure 5-47 below with u_a reaching approximately 1.35 and $1.48\sqrt{f_c'}$ for specimens A and B, respectively. To allow comparison with design values, this corresponds to maximum bond stress ratios, u_{max}/u_a, of 0.54 and 0.49, respectively – recall from Sections 4.1.1 and 4.2.4 that u_{max} is assumed to be $2.5\sqrt{f_c'}$ within both slotted and monolithic joints. Average bond stress is higher in specimen B because of the lower concrete strength yet similar degree of reinforcement activation.

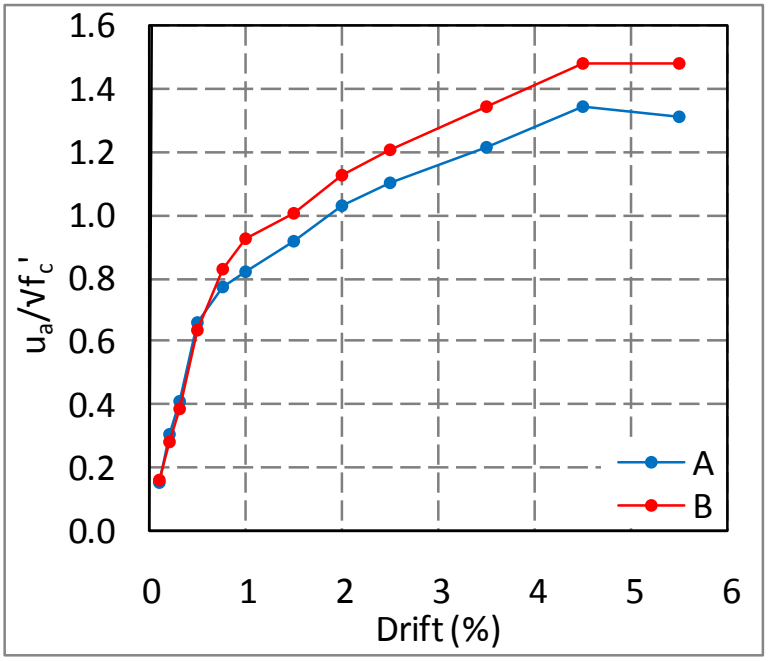

Figure 5-47: *Bottom longitudinal reinforcement average bond stress for specimens A and B*

While the observed bond stress values are already relatively high – monolithic joints assume a design value of $0.67u_{max}$ – it is possible that even higher values may have been observed had the beams been able to introduce more force across the joint. Figure 5-47 shows that bond stress increases with drift throughout the entire test, suggesting that the maximum possible value may not have been mobilised. This idea is supported by the lack of joint damage and strain penetration as reported in Sections 5.4.2 and 5.5.1. Note that the plateau for specimen A and small decrease for specimen B is due to a drop off in shear demand through the joint due to bar fracture as opposed to bond degradation. As such, data recorded beyond 4.5% drift has been excluded from subsequent graphs where it is found to induce the same effect. Nonetheless, the fact that this potentially higher average bond stress was not observed means the design value can only be increased marginally to $0.59u_{max}$.

Figure 5-48(a) shows the strain penetration into the joint for specimens A and B expressed as a portion of the column neutral axis depth, c_{col}. The same quantity is graphed in Figure 5-48(b), except this time cover concrete – also assumed ineffective at providing bond – is included. The strain penetration lengths are those determined in Section 5.5.1 while c_{col} was calculated using moment-curvature analysis. Relative strain penetration, L_{sp}/c_{col}, was found to reach values of approximately 0.09 and 0.08 at ULS drift for specimens A and B, respectively. The values are higher in specimen A for two reasons. Firstly, a greater strain penetration length was calculated for this specimen and, secondly, neutral axis depths within specimen B were larger to account for the decreased concrete strength. The values show more agreement when cover concrete is included because this is constant between specimens.

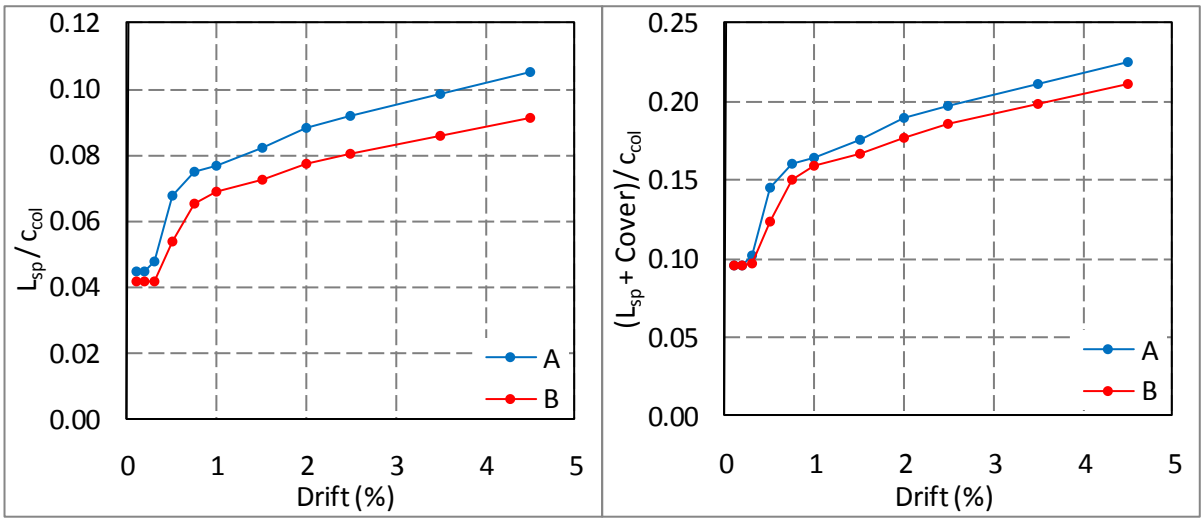

(a) Strain penetration only (b) Strain penetration and cover

Figure 5-48: *Relative strain penetration into the joint for specimens A and B*

The value of $(L_{sp} + cover)/c_{col}$ can be used to determine an appropriate design value for the portion of the neutral axis depth effective in transferring force from the reinforcement into the concrete strut mechanism through bond, k. Increased k values result in more bond length which leads to lower local bond stress demands. Based on Figure 5-48(b), an appropriate design value for k at ULS can be calculated as per Equation 5-2:

$$k = 1 - \frac{(L_{sp} + cover)}{c_{col}}$$

$$= 1 - 0.2$$

$$= 0.8 \qquad \text{Equation 5-2}$$

This is the same as the value adopted for monolithic joints. Using this value in conjunction with other experimentally determined quantities, it is possible to back calculate the bond uniformity factor, ξ_b, as discussed in Section 4.5.3, at different drift levels by rearranging Equation 4-59. This approach was used as opposed to directly calculating ξ_b from the bottom longitudinal reinforcement stresses due to the inaccuracy of these readings as discussed above. The resulting variation of ξ_b with drift is shown in Figure 5-49. After an initial spike in values, ξ_b was found to be consistently on the order of 2.0 for both specimens. The initial spike was due to the concrete strut mechanism taking the majority of the joint shear demand, as illustrated in Figure 5-65(b), while the consistency indicates a lack of bond degradation throughout testing. Such consistency was not observed in the testing of Au (2010), suggesting the supplementary vertical joint stirrups have improved the bond performance.

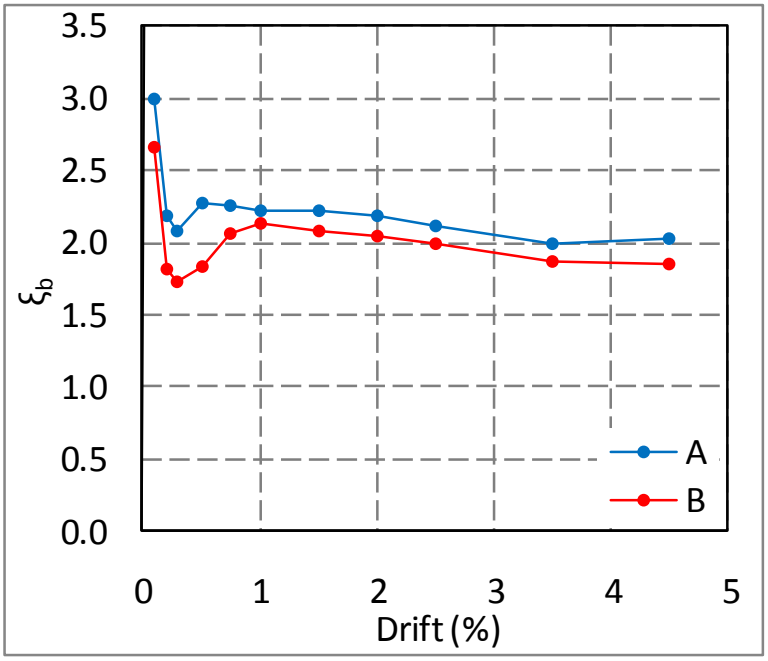

Figure 5-49: *Bond stress uniformity factor for specimens A and B*

It is also evident that ξ_b is relatively high throughout the test – monolithic joints assume a value of 1.25. This indicates a significant local bond demand within the column compression zone. While this is expected due to the lack of concrete compression from the beam soffit as discussed in Section 4.2.1, the fact that such high values are able to be sustained indicates very satisfactory bond performance. In terms of peak maximum bond stress, u_{max}, within the column compression zone, this corresponds to values on the order of 2.7 and $3\sqrt{f_c'}$. These values are greater than the assumed maximum bond stress of $2.5\sqrt{f_c'}$ indicating very well confined concrete and reduced strain penetration in this region.

In addition to the more technical analyses above, it is important to note the overall effect of the concrete strength in specimen B at testing being 25% lower than specified. This reduction in concrete strength corresponds to a provided column depth 86% of that required by design using Equation 4-22. The fact that specimen B still exhibited excellent performance with no obvious bar slip indicates this equation is likely to be overly conservative. This point is discussed further in Section 4.2.4.

5.5.3 Top Longitudinal Reinforcement Strain Profiles

The top longitudinal reinforcement strain profiles at peak drifts for specimens A and B are shown in Figure 5-50 and Figure 5-51, respectively. As expected, the reinforcement remained nominally elastic throughout testing with minor inelastic excursions during post-ULS gap closing rotations. The low degree of reinforcement activation in compression is a testament to the lack of damage observed in this region as the concrete remains effective throughout the

entire drift sequence. Combined with the observations in Section 5.4.3, it can be concluded that Grade 300 reinforcement is suitable for use in this application.

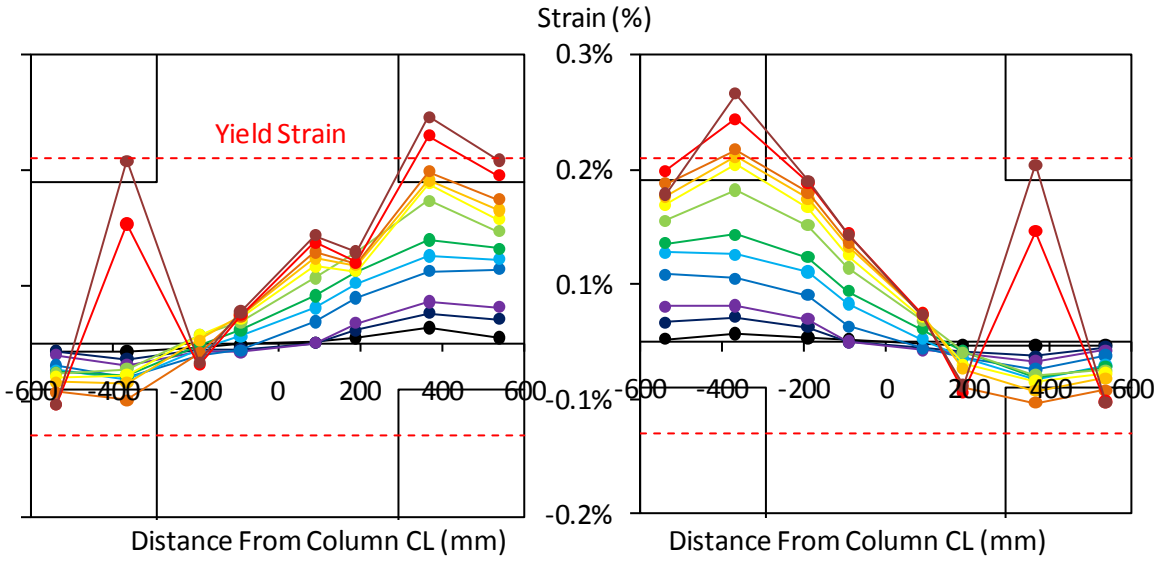

(a) Positive drifts (b) Negative drifts

Figure 5-50: *Top beam reinforcement strain profiles for specimen A*

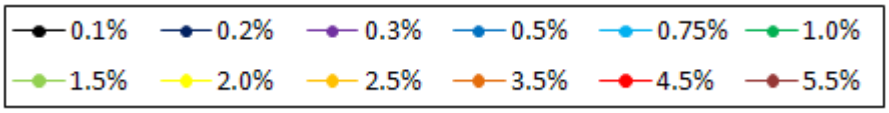

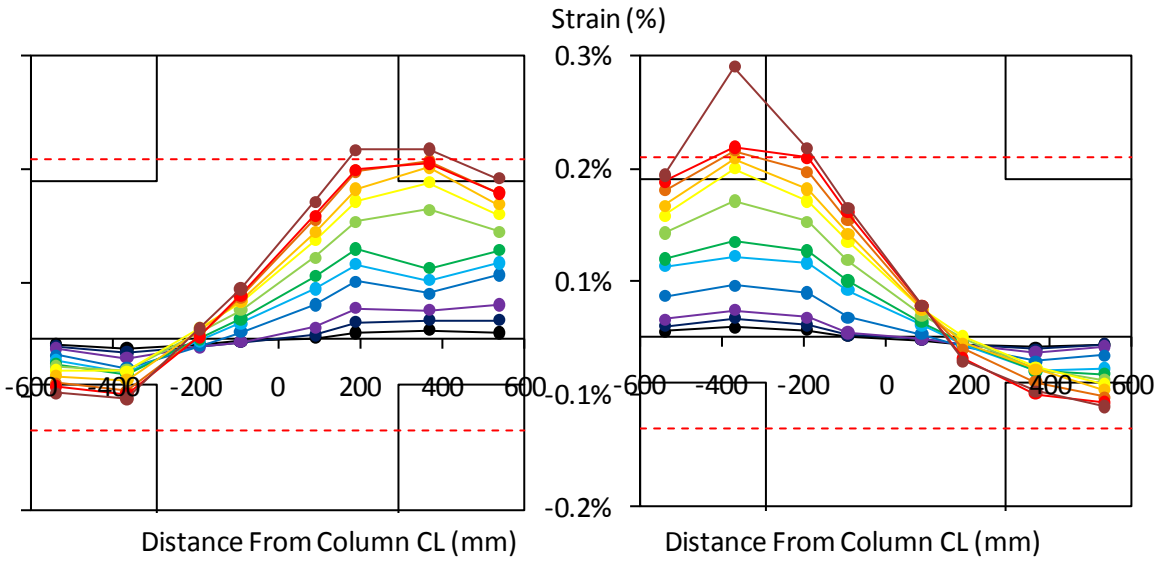

(a) Positive drifts (b) Negative drifts

Figure 5-51: *Top beam reinforcement strain profiles for specimen B*

During what should have been compression inducing rotations in specimen A, high elastic tensile strains occurred in isolated strain gauges on either side of the joint. Given the symmetry of these spikes, they cannot simply be dismissed as erroneous readings. Instead, it is likely localised tension was induced in the bars due to opening of the diagonal hinge cracks observed during the later drift levels.

Strain penetration lengths within the top longitudinal reinforcement of 0.026 and 0.027$f_y d_b$ were calculated for specimens A and B, respectively, using a similar process to that described in Section 5.5.1. This time however, the theoretical value of 4/3L_{sp} was adopted for reinforcement in the elastic range as recommended by Palermo (2004). Just as for the bottom longitudinal reinforcement, it would be expected that the vertical joint stirrups would reduce the strain penetration length of the top reinforcement. However, the values were greater than those observed by Au (2010), suggesting inaccuracies in the data. The most likely source of error is the location of the strain gauges used in the calculations; these should be located within the hinge region where maximum strain is expected. Regrettably, the nearest gauge was approximately 80 mm from the column face. Thus the recorded strains would be less than the actual maximum and the resulting strain penetration length higher. Given this oversight, the likely reduction in strain penetration length due to the vertical joint stirrups cannot be confirmed. The value of 0.022$f_y d_b$ adopted by Au (2010) should be assumed until further research is undertaken.

5.5.4 Anchorage of Top Longitudinal Reinforcement

Figure 5-52 shows the overstrength factors for the top longitudinal reinforcement of both specimens as determined directly from strain gauge data. As discussed in Section 5.5.3, this reinforcement remains nominally elastic throughout testing with the larger demands occurring during gap closing rotations. This is in accordance with the design assumptions of Section 4.2.5. However, the degree of activation during gap closing rotations is much lower – on the order of 0.3f_y at ULS and never reaching above 0.4. Thus the design assumptions for the degree of compression activation were overly conservative at 0.5.

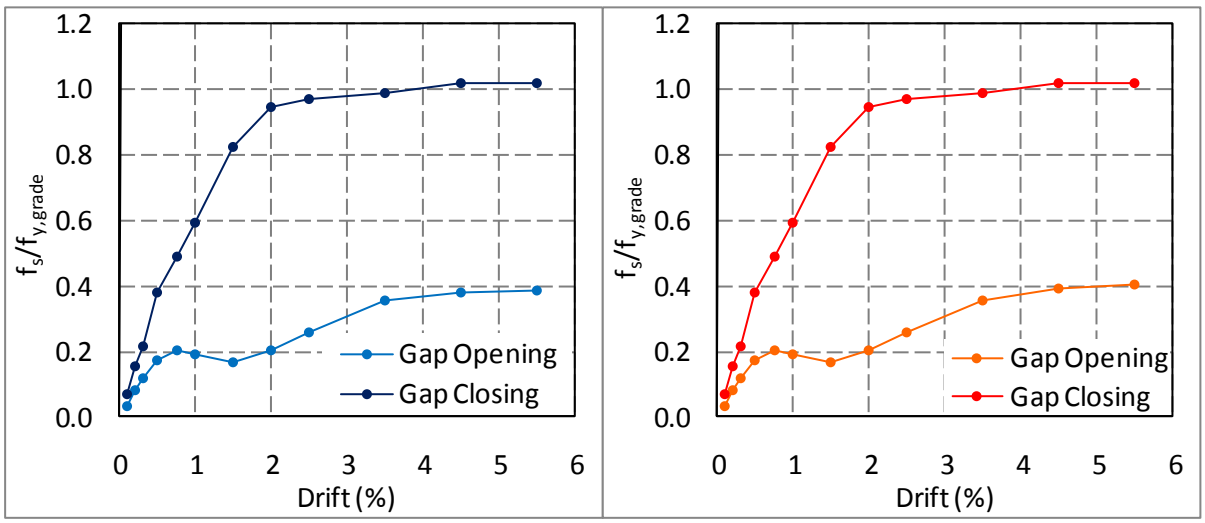

(a) Specimen A (b) Specimen B

Figure 5-52: *Top longitudinal reinforcement overstrength factors for specimens A and B*

Average bond stress, u_a, along the top longitudinal reinforcement is illustrated in Figure 5-53. As with the bottom longitudinal reinforcement, u_a was found to increase throughout the test with specimen B exhibiting marginally higher values. The average bond stress remains below $1.5\sqrt{f_c'}$ as required by NZS3101:2006 for bond of nominally elastic reinforcement. Given the ratio of provided to required column depth was 2.3 and 2 to 1 for specimens A and B, respectively, few further conclusions can be drawn.

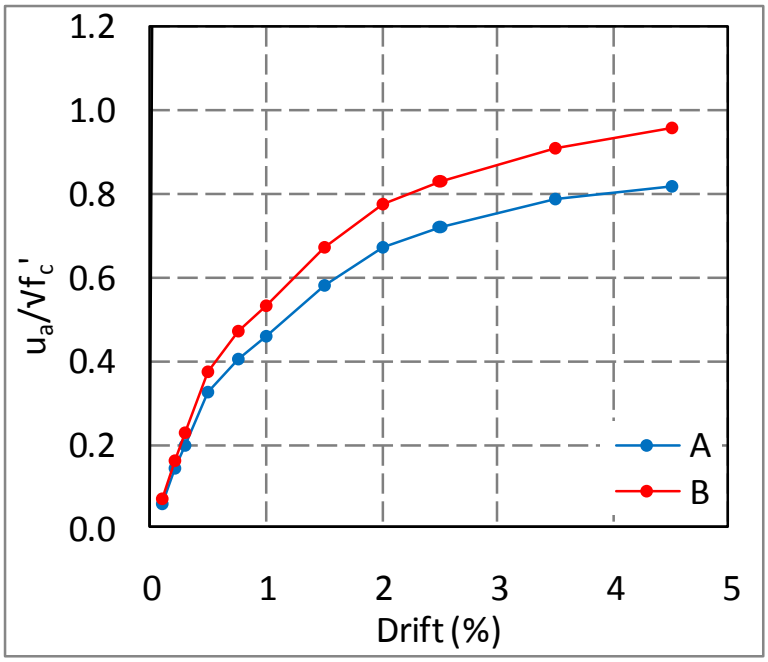

Figure 5-53: *Top longitudinal reinforcement average bond stress for specimens A and B*

5.5.5 Bar Fracture Analysis

As discussed in Section 5.4.1, both specimens failed through bar fracture before completing the second cycle at 5.5% drift. The occurrence of bar fracture can be estimated from the total plastic strain applied to the bar throughout its loading history using empirical relationships. These empirical relationships are based on the Coffin-Manson equation given below:

$$\varepsilon_{ap} = \varepsilon_f'(2N_f)^c \qquad \text{Equation 5-3}$$

Where ε_f' and c are experimentally determined constants. Using Equation 5-3, Mander, Panthaki, and Kasalanati (1994), and Brown and Kunnath (2004) developed the relationships in Equation 5-4 for fatigue life of reinforcing steel:

$$19.1\ mm\ bar: \varepsilon_{ap} = 0.16(2N_f)^{-0.57}$$

$$22.2\ mm\ bar: \varepsilon_{ap} = 0.13(2N_f)^{-0.51} \qquad \text{Equation 5-4}$$

Where N_f is the number of cycles until failure and ε_{ap} is the peak plastic strain amplitude that occurs during each cycle. These relationships can be combined with Miner's rule (1945) to produce the following equation for predicting the occurrence of failure due to low cycle fatigue:

$$D_{total} = \sum_{i=1}^{n} D_i = \sum_{i=1}^{n} \frac{1}{N_{f,i}} = \sum_{i=1}^{n} 2\left(\frac{\varepsilon_f'}{\varepsilon_{ap}}\right)^{1/c} \qquad \text{Equation 5-5}$$

Using Equation 5-5 in conjunction with peak plastic strain amplitudes during each cycle, it is possible to predict theoretically when bar fracture will occur. Peak plastic strain amplitudes are estimated using the loading history combined with moment-rotation relationships. Unbonded length was taken as L_{ub} + L_{sp} using the appropriate value from Section 5.5.1. Failure was deemed to occur when D_{total} reached a value of 1.0. The results of this theoretical estimation of bar fracture are presented in Figure 5-54.

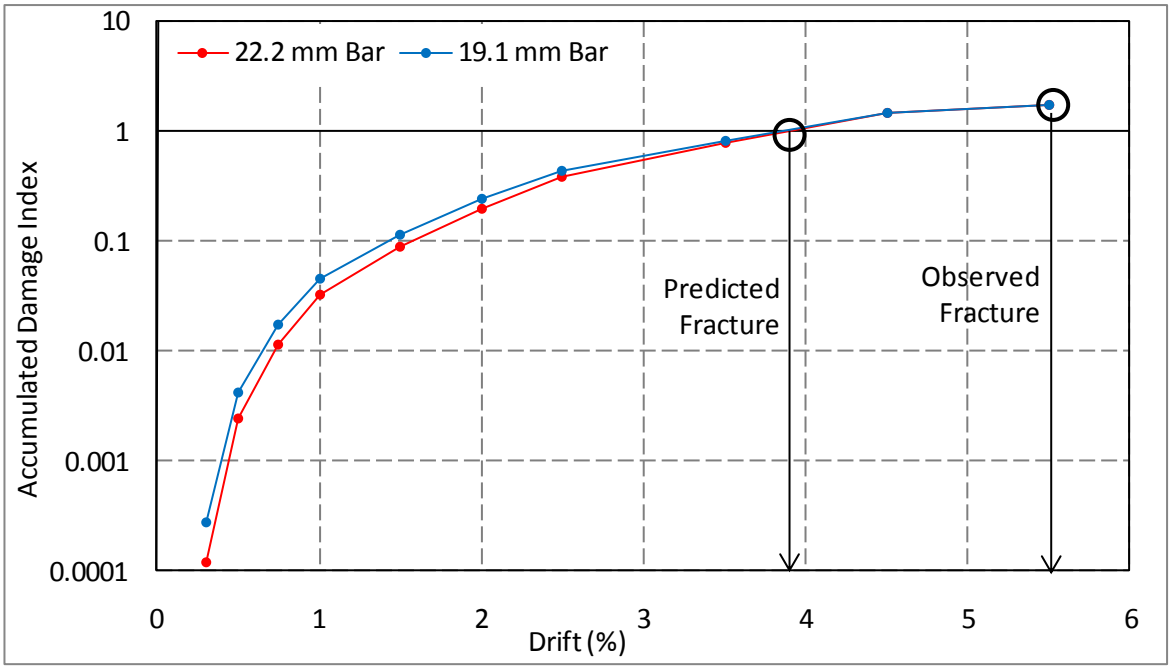

Figure 5-54: *Predicted versus observed bar fracture*

It is clear from Figure 5-54 that the theoretical method underestimates the drift at which bar fracture occurs. Note that although no equation calibrated to D20 bars was available, the convergence of the predictions using equations calibrated to both larger and smaller bar sizes suggests this is not a significant source of error. However, there are a number of other possible reasons for the difference between experimental and theoretical results. Firstly, and probably the most significant, is the difference in conditions under which the theoretical relationships were developed compared with those prevalent during the experimental testing. These differences include strain rate during testing, strain amplitude, and unrestrained bar

length. It is also possible that some conservatism was built into the above equations given scatter in the results. Material properties could vary between typical NZ reinforcing steel and the samples used in the above studies. Given the difference in results, it is recommended that further research be undertaken to calibrate these relationships for use in predicting bar fracture within slotted beams.

5.6 Beam and Joint Shear Reinforcement and Joint Performance

5.6.1 Supplementary Vertical Joint Reinforcement Strain Profiles

Figure 5-55 through Figure 5-58 illustrate the peak drift strain profiles of the supplementary vertical joint stirrups for specimens A and B. Omitted data in Figure 5-57(a) is due to strain gauge failure prior to the start of testing. As expected, vertical stirrup activation is in tension only and generally in the elastic range for both specimens. Furthermore, the degree of activation is relatively uniform across the joint. These observations confirm that the stirrup response has been effectively isolated from column flexural actions on the joint as higher, possibly inelastic stirrup activation towards the outside of the joint would otherwise have been observed. This confirms the success of the hook detail used for anchorage of the vertical stirrups.

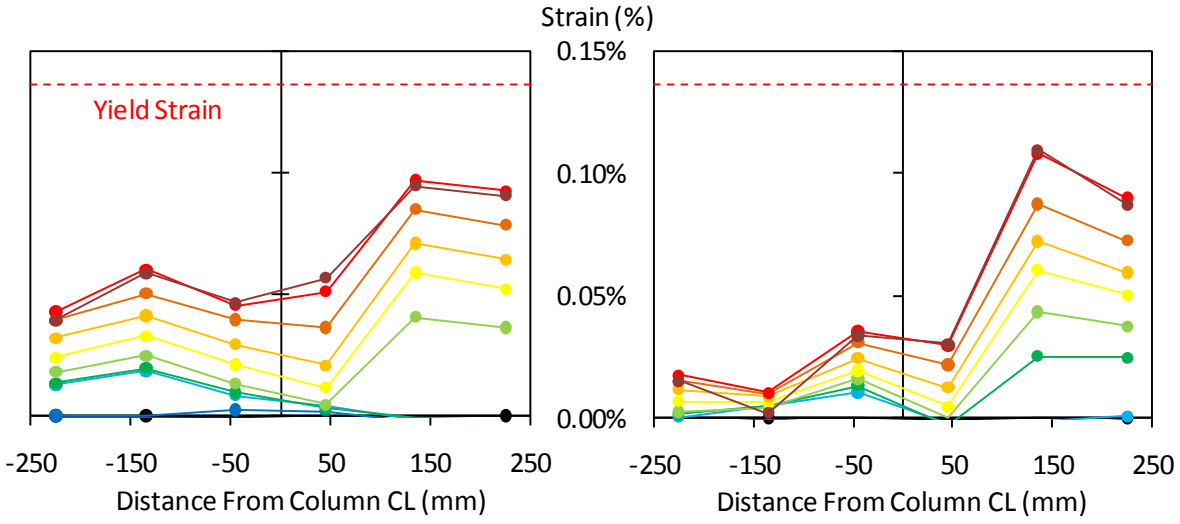

(a) Positive drifts (b) Negative drifts

Figure 5-55: *Exterior vertical joint stirrup strain profiles for specimen A*

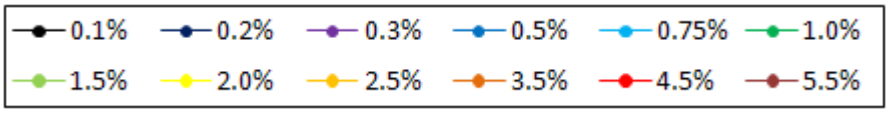

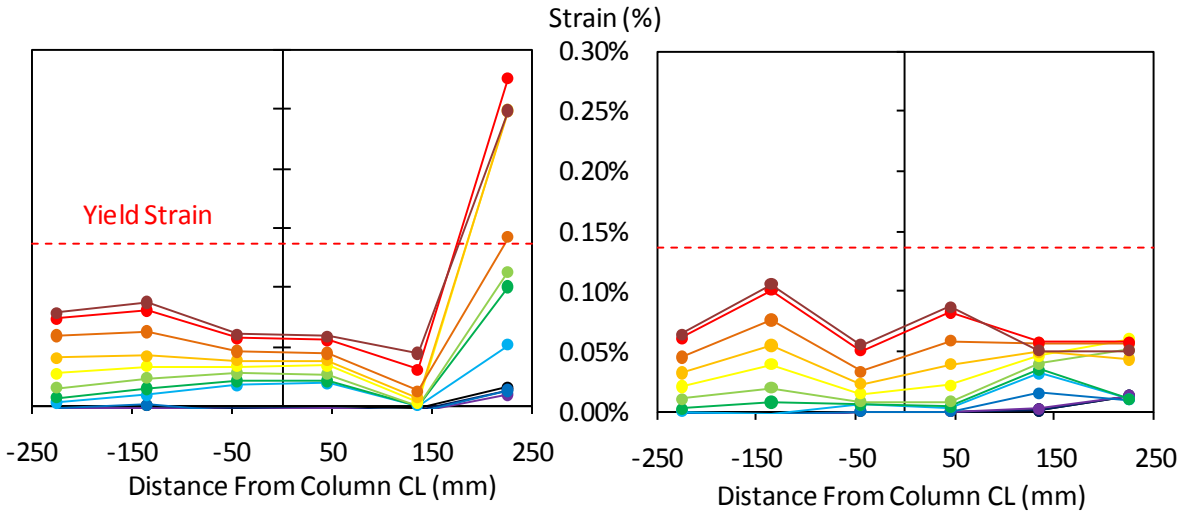

(a) Positive drifts (b) Negative drifts

Figure 5-56: *Interior vertical joint stirrup strain profiles for specimen A*

The degree of activation is also similar between the exterior and interior sets suggesting the column reinforcement, that would, if anything, reduce the demand on the exterior sets, is relatively ineffective at providing clamping action to the beam bars. Given the vertical stirrups do not reach yield in the majority of cases, the required density could perhaps be relaxed for ease of construction.

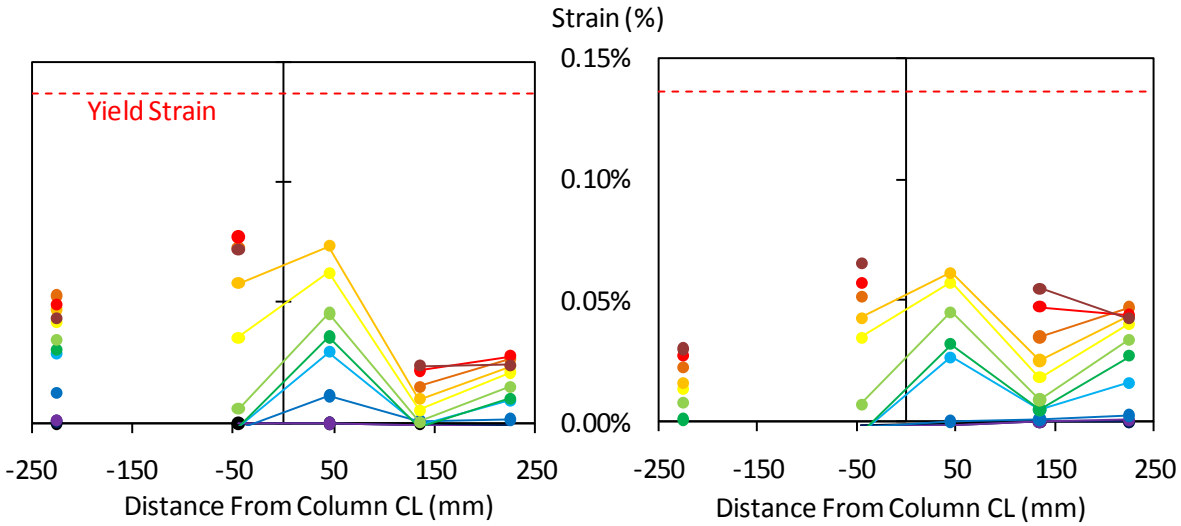

(a) Positive drifts (b) Negative drifts

Figure 5-57: *Exterior vertical joint stirrup strain profiles for specimen B*

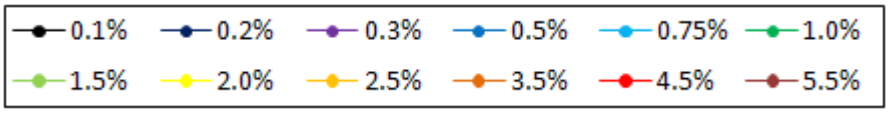

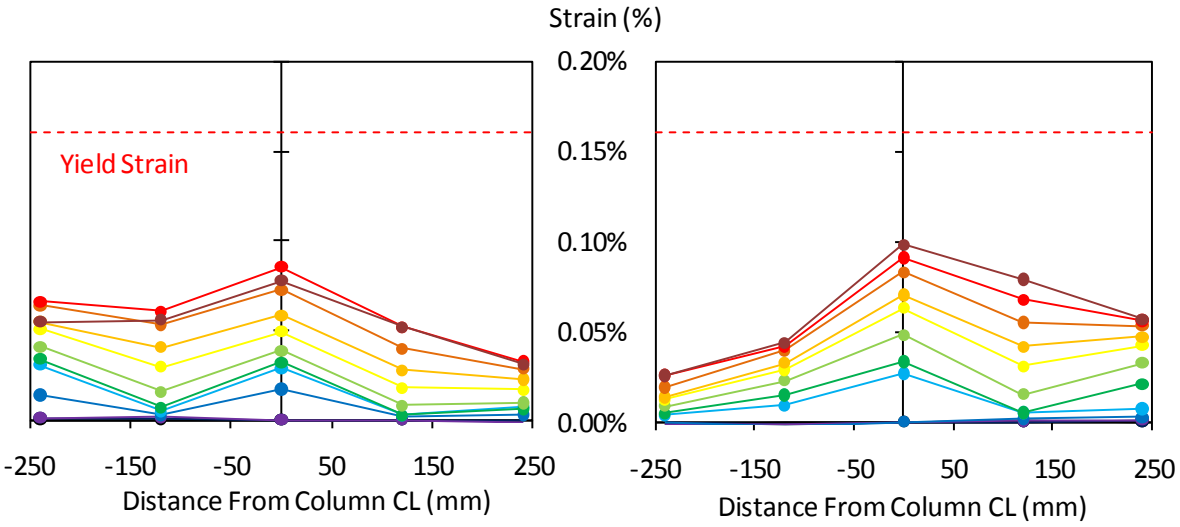

(a) Positive drifts (b) Negative drifts

Figure 5-58: *Interior vertical joint stirrup strain profiles for specimen B*

5.6.2 Hanger Reinforcement Strain Profiles and Shear Transfer Mechanism

Figure 5-59 and Figure 5-60 show the shear hanger strain profiles at peak drifts for Specimens A and B, respectively. The localised inelastic tensile strains in the hinge regions during gap closing rotations are due to a combination of flexural and shear activation. Corresponding downwards beam shear activates the hangers in tension while a difference between the hanger depth and neutral axis induces further tension through flexural actions. These strains are found to increase with drift due to increasing beam shear and elongation demand over this region. Visual evidence of increasing elongation is provided by the large primary crack along the beam-column interface as discussed in Section 5.4.2. The neutral axis depth does not have a significant bearing on the magnitude of the flexural component given this remains between 80 – 100 mm as reported in Section 5.4.7. With the hangers in both specimens installed at a depth of 60 mm, or $0.6d_h$, the resulting lever arms are on the order of 20 – 40 mm.

A reduced degree of tensile activation generally occurs in the hinge region during gap opening rotations as explained below. According to Section 5.4.7, the neutral axis is initially located at around the same depth as the hangers and is then found to increase linearly to approximately 20 mm at 5.5% drift. This means that flexural actions induce tension in the hanger at all drift levels with a maximum lever arm similar to that during gap closing rotations. However, given upwards beam shear induces compression within the hangers during such rotations, the flexural and shear components act to cancel one another out. Because the hanger is activated in net tension, it can be deduced that hanger flexural demands are significantly larger than those induced by shear. Unfortunately, because only one strain gauge was used in each location, the flexural and shear components cannot be separated.

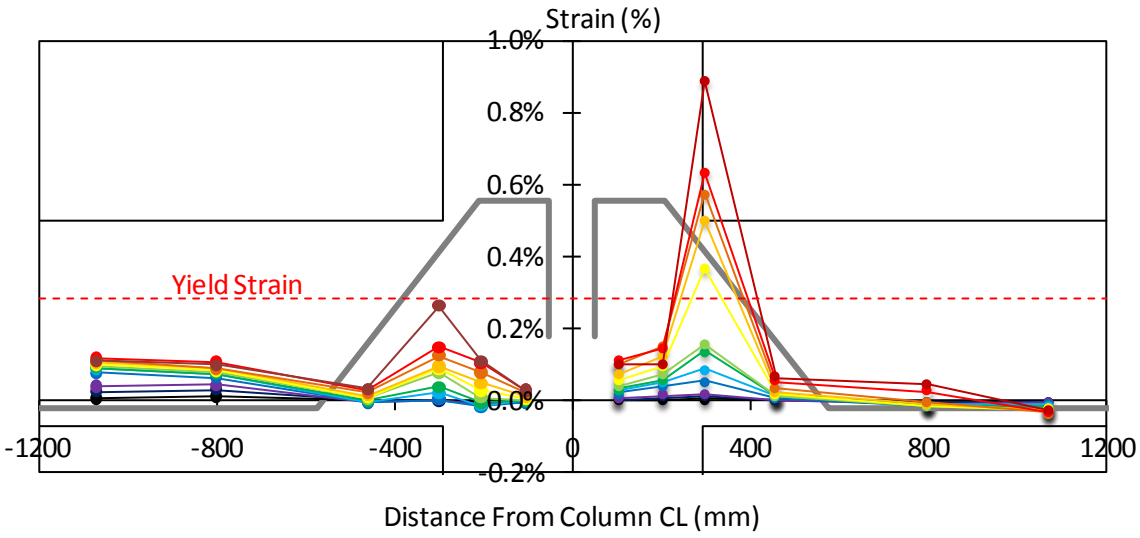

(a) Positive drifts

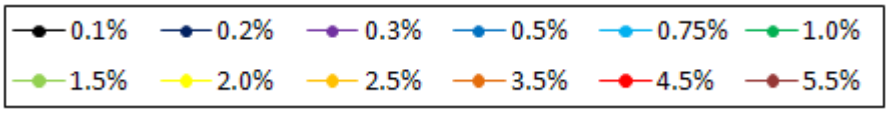

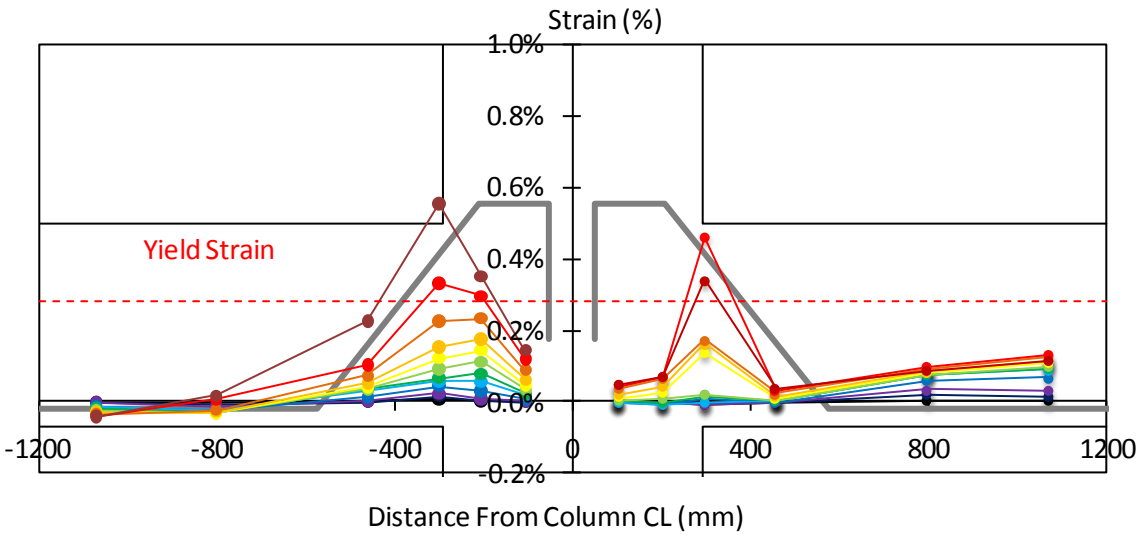

(b) Negative drifts

Figure 5-59: *Shear hanger strain profiles for specimen A*

Based on the above observations, hanger activation is critical during gap closing rotations when both flexural and shear actions induce tension demands. Furthermore, given shear contributions are not able to be easily influenced, the goal when determining an appropriate hanger depth should be focussed on limiting flexural strains. At the ULS drift, relative neutral axis depths are found to be 0.37 and $0.87d_h$ for gap opening and closing, respectively. Thus, if designing purely for flexure, one would adopt a hanger depth of $0.62d_h$ to ensure equal tension activation in each case. However, shear contributions would act to decrease the tension activation for gap opening rotations while doing the opposite for gap closing rotations.

Adjusting the hanger location to account for these contrasting influences, a depth on the order of 0.65 to 0.75d_h seems appropriate. This is similar to the recommendations of Au (2010).

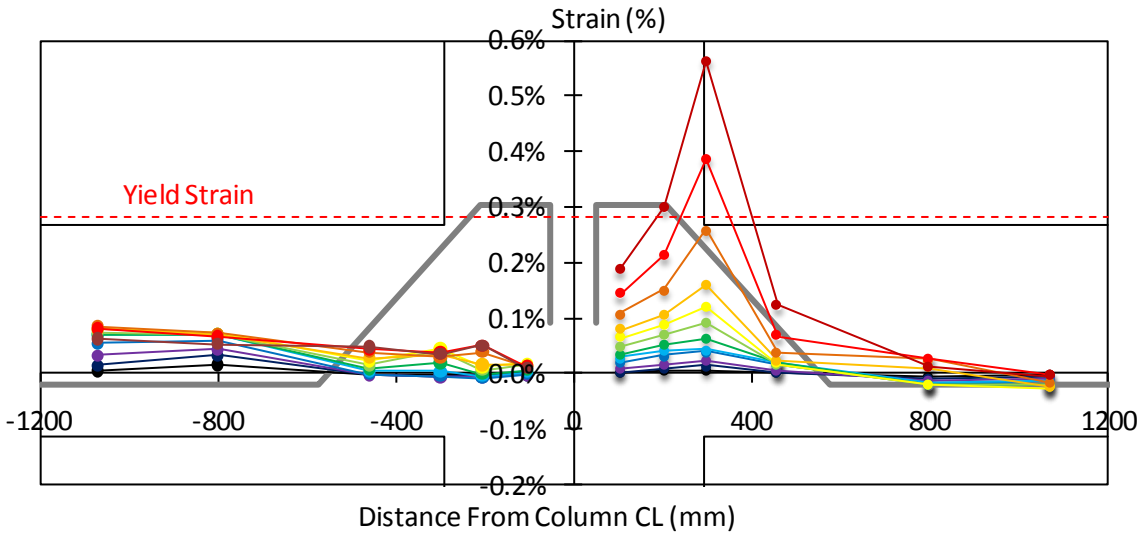

(a) Positive drifts

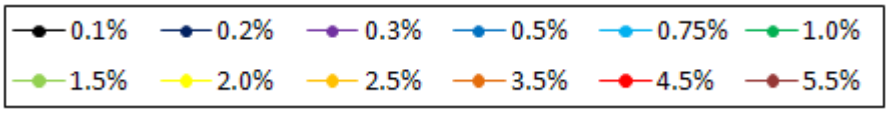

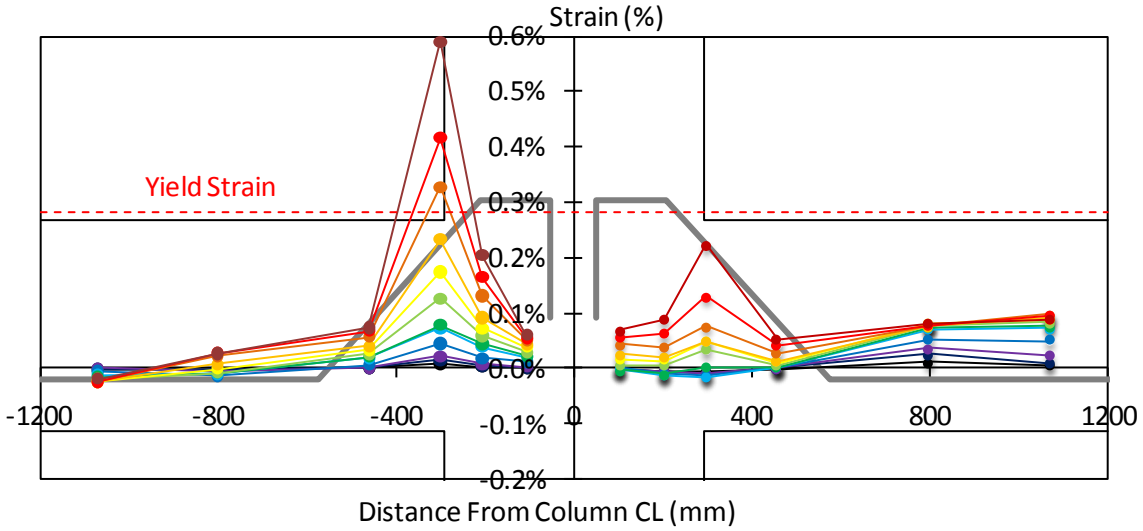

(b) Negative drifts

Figure 5-60: *Shear hanger strain profiles for specimen B*

Shear transfer between the beam and joint is facilitated through a combination of shear hanger activation, aggregate interlock within the hinge, and dowel action of top longitudinal reinforcement. Given the numerous contributing mechanisms, accurately quantifying each one is not possible with the instrumentation employed here. While Au (2010) attempted to do so by considering the former two mechanisms only, this approach neglected dowel action in the beam reinforcement which, due to the relatively large area of steel involved, seems misguided. Furthermore, given the flexural/shear interaction discussed above and the inability

to separate these components, the portion of hanger activation resisting shear cannot be determined accurately enough to draw any meaningful conclusions. The reliability of a concrete aggregate interlock mechanism within the hinge is questionable regardless given the wide, full-depth cracks that open vertically along the hinge/column interface as discussed in Section 5.4.2. As such, the Author recommends shear hanger reinforcement is detailed to resist the entire beam shear demand until further research indicates otherwise.

5.6.3 Beam Stirrup Strain Profiles

The beam stirrup strain profiles for specimens A and B are illustrated in Figure 5-61 and Figure 5-62, respectively. Stirrup strains generally remained below $0.5\varepsilon_y$ throughout the testing regime, indicating sufficient shear reinforcement was provided. As expected, compression activation during normal response is negligible. The isolated compression readings at higher drifts within the east beam of specimen A are likely due to a strain gauge error as buckling of the longitudinal reinforcement in this region would cause tensile activation. Increased localised tensile strains were consistently observed in the beam stirrups adjacent to the end of the unbonding tubes. This is due to the hangers being ineffective at carrying shear beyond their inclined portion thus requiring the stirrups to pick up the demand through the usual beam shear mechanism.

During gap closing cycles at higher drift levels, the stirrup sets closest to the joint were activated in tension to a greater extent than the other sets also encompassed by the inclined hanger section. Because the beam stirrups are unable to facilitate shear transfer across the hinge, this must be due to some other mechanism. Dropping of the beam over the hinge region during higher drifts as discussed in Section 5.4.2 is the most likely explanation. Given the stiffness of the top longitudinal reinforcement, there is likely to be a differential drop between these bars and the rest of the beam over the hinge. Because the stirrups are restrained by this reinforcement, these are subject to this differential movement and thus activated in tension. That this mechanism is reliant on beam dropping would also explain why the effect is worst in specimen B where the most damage of this type was observed. Nonetheless, these results clearly show that a stirrup spacing of $4d_b$ is sufficient within the unbonded region when used in conjunction with steel unbonding tubes.

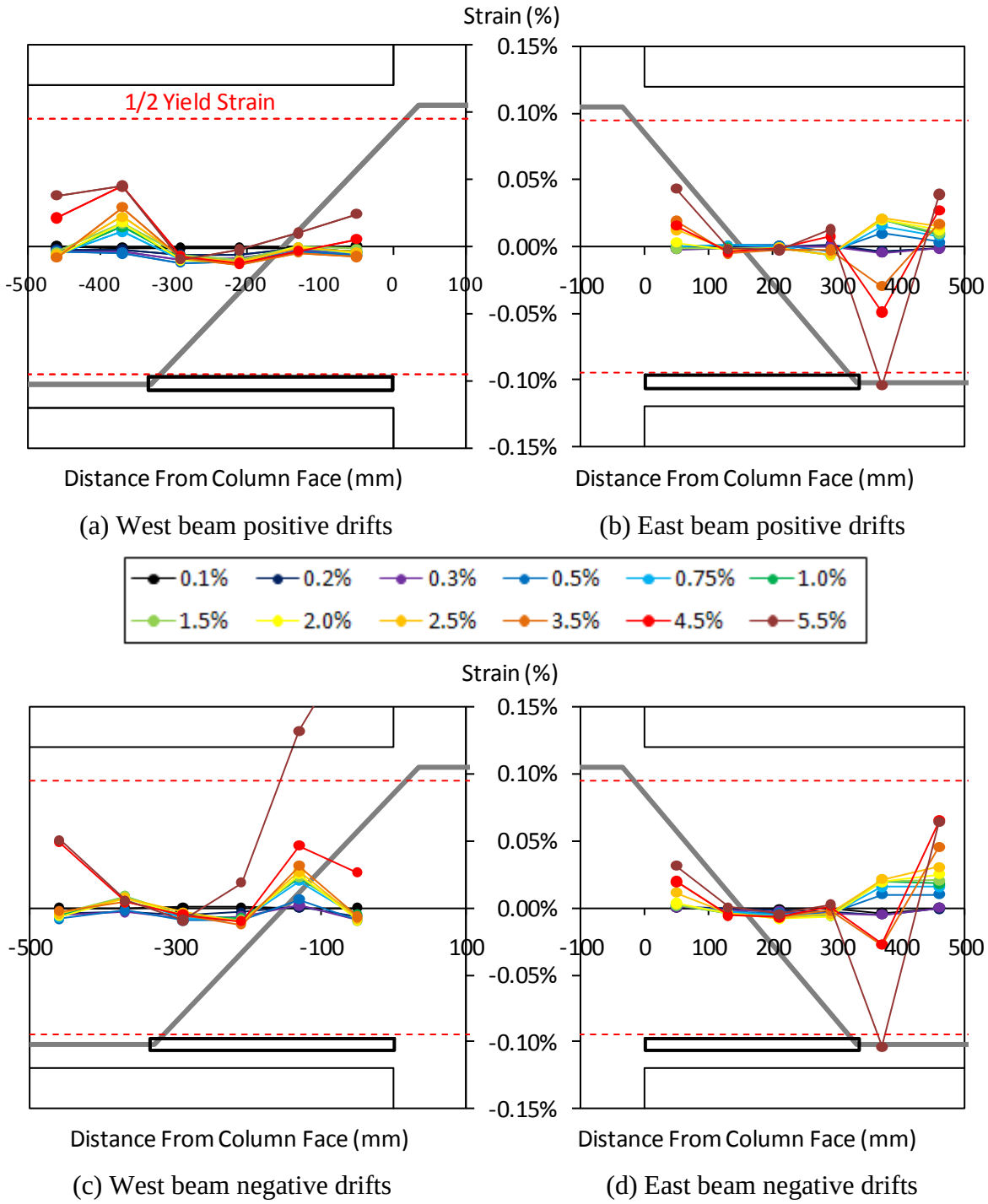

(a) West beam positive drifts (b) East beam positive drifts

(c) West beam negative drifts (d) East beam negative drifts

Figure 5-61: *Beam stirrup strain profiles for specimen A*

Individual catcher stirrups were installed in specimen B to prevent the shear hangers from bursting out of the beam soffit during gap opening rotations. These are illustrated in Figure 5-62 and were located at the shear hanger bend. It is clear that these dedicated stirrups were not activated to a significant enough level to justify the inclusion. From this it is inferred that the adjacent stirrup sets were able to provide sufficient restraint to the shear hangers in this case. However, it is recommended that a catcher stirrup be used in practice given the larger shear demands, and thus larger hangers required, when floor slabs are present. Furthermore, torsional behaviour of the beam-floor system during an earthquake can result in even greater

hanger forces that must be resisted by the beam stirrups. Finally, in practice D25 bars would generally be used for the bottom longitudinal reinforcement. Assuming the standard stirrup spacing of $4d_b$, this could, in the worst case, result in no restraint being provided for 50 mm either side of the hanger bend.

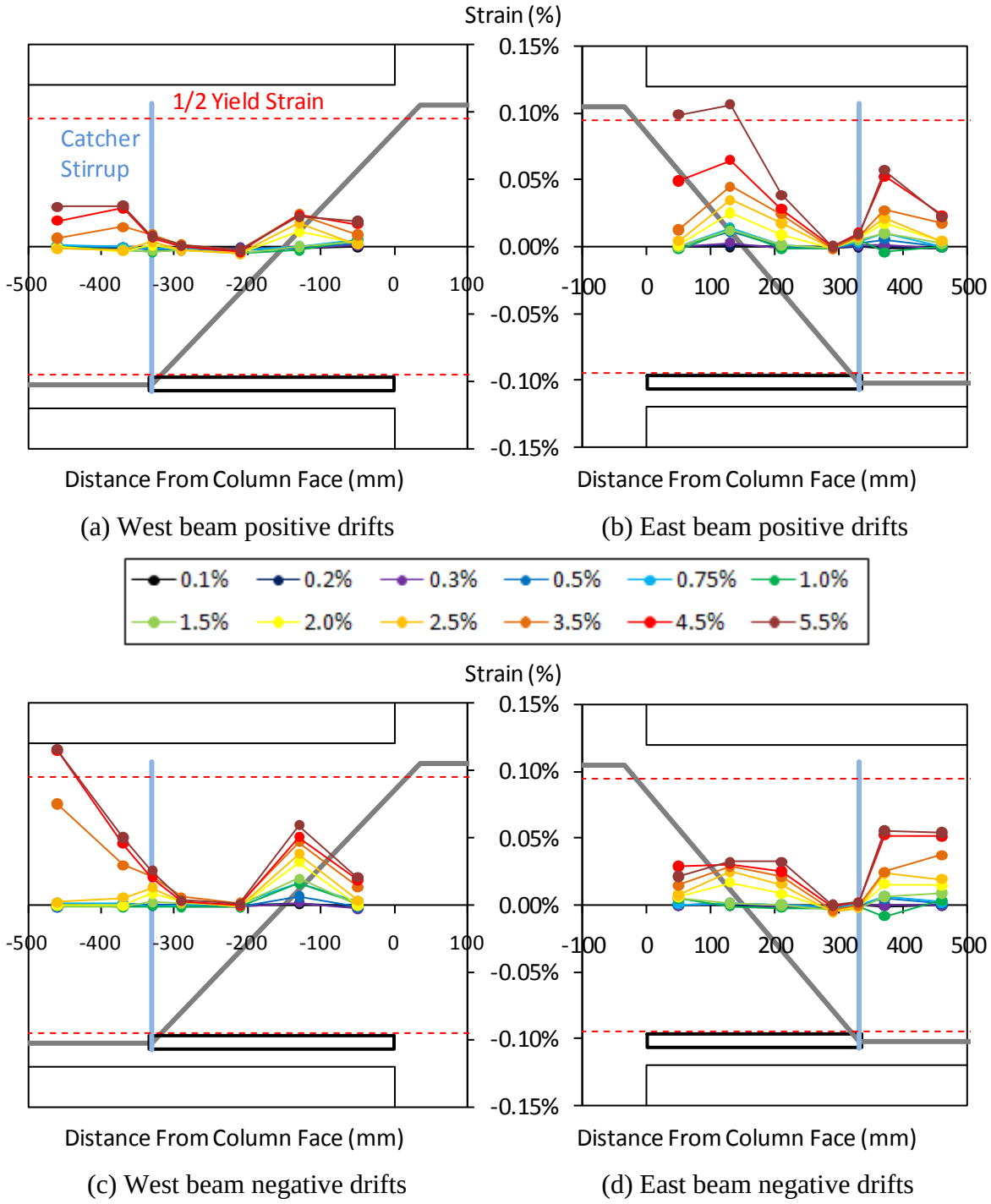

(a) West beam positive drifts (b) East beam positive drifts

(c) West beam negative drifts (d) East beam negative drifts

Figure 5-62: *Beam stirrup strain profiles for specimen B*

5.6.4 Horizontal Joint Reinforcement Strain Profiles

Horizontal joint shear reinforcement strain profiles for specimens A and B are illustrated in Figure 5-63 and Figure 5-64 below. In both cases the joint remained well within the elastic

range with maximum stirrup activation on the order of 0.26 and 0.33ε_y at ULS drift for specimens A and B, respectively. Maximum activation was below 0.5ε_y throughout the test in both specimens. This indicates that both joints were significantly over-reinforced. The overall response envelope was also relatively symmetrical, with no significant bias towards the bottom of the joint or kink in the vicinity of the bottom longitudinal beam reinforcement. Note that the upper and lower strain gauge pairs correspond to the first two sets of column stirrups adjacent to the joint as opposed to stirrups within the joint itself; i.e. a total of 4 column stirrup sets have been strain gauged. Differential joint stirrup activation was the driving factor behind the joint shear mechanism proposed by Au (2010) and presented in Section 4.5.1. In particular, increased localised stirrup activation immediately adjacent to the bottom beam bars was indicative of bar slip. A lack of such activation suggests the revised joint shear mechanism discussed in Section 4.5.2 is governing the joint behaviour.

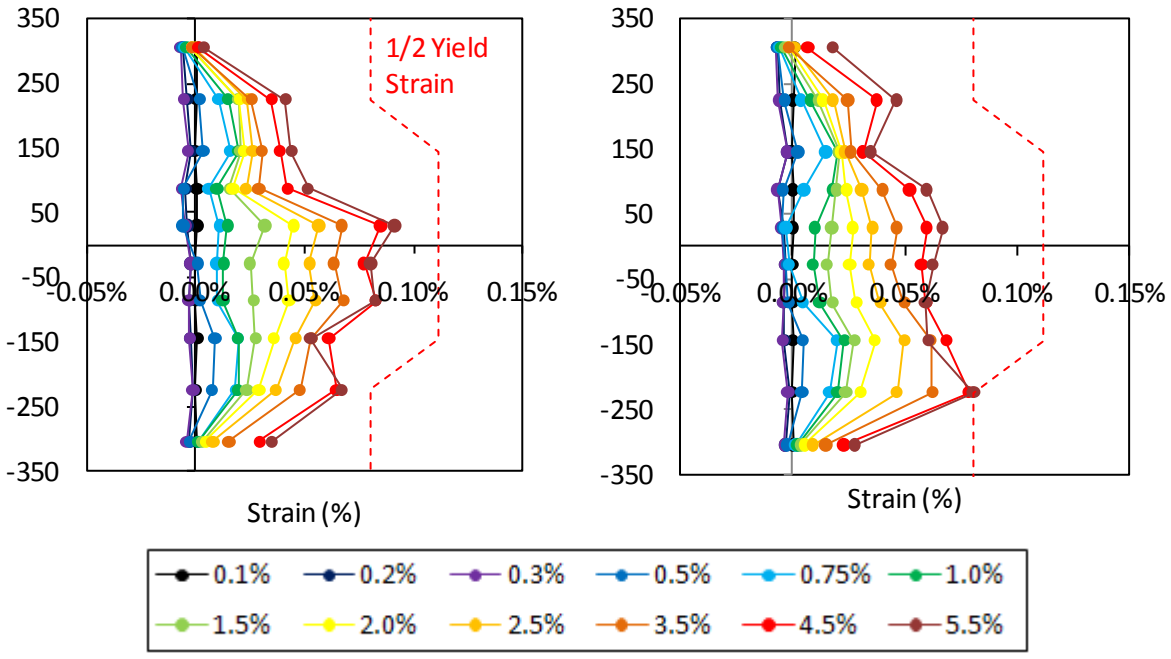

(a) Positive drifts (b) Negative drifts

Figure 5-63: *Horizontal joint reinforcement strain profiles for specimen A*

While the joint stirrup response was relatively symmetric, the column stirrup response was not. The first column stirrup set below the joint is consistently activated to a higher degree than the corresponding set above the joint. The average magnitude of this difference is 10 and 18% in specimens A and B, respectively, and can be explained as follows. In a monolithic joint, a portion of the horizontal joint shear is resisted directly through compression of adjacent beam soffits. The remainder is transferred to the column stirrups through concrete struts coming off the longitudinal beam reinforcement. However, in the bottom part of a slotted joint, the entire shear demand must be resisted by the latter method. As a result, the

column stirrups immediately adjacent to the joint are activated to a higher level. Fortunately, given the larger column depths required for use of slotted beams, the current NZS3101:2006 provisions for column shear reinforcement appear sufficient.

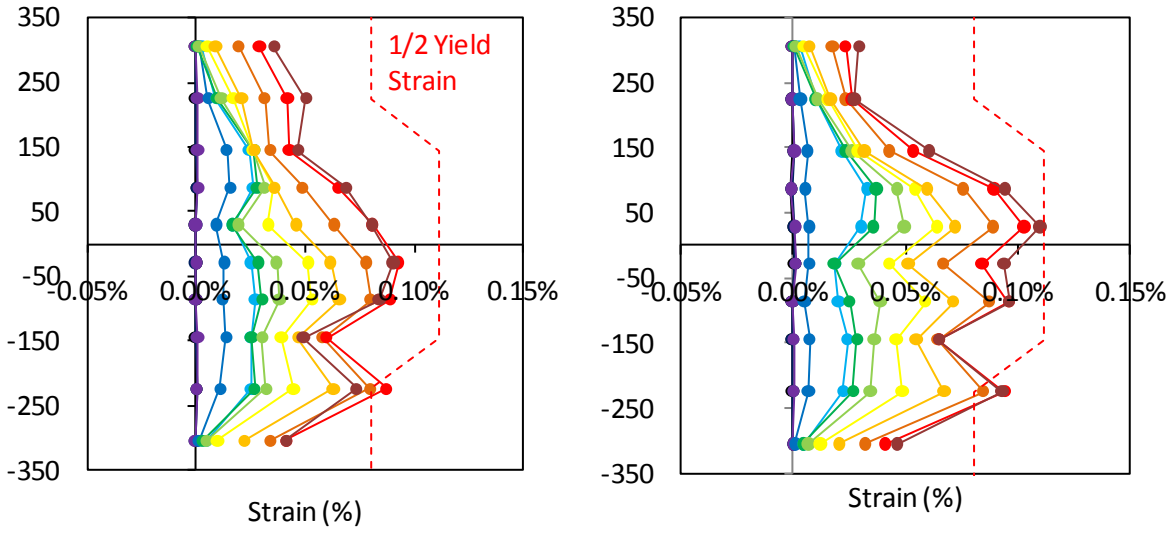

(a) Positive drifts (b) Negative drifts

Figure 5-64: *Horizontal joint reinforcement strain profiles for specimen B*

Using the proposed joint shear reinforcement provisions from Section 4.5.5, horizontal joint shear activation can be estimated in the case this amount of reinforcement had been provided. Because the joint remains elastic, this can be done on a pro-rata basis, and the corresponding maximum activation at ULS drift is found to be 0.45 and $0.50\varepsilon_y$ for specimens A and B, respectively. Similarly, revised maximum activation throughout the test is found to be approximately 0.70 and $0.75\varepsilon_y$. Thus even using the less stringent joint reinforcement requirements proposed in Section 4.5.5, the designer can be satisfied that the joint will remain elastic during seismic loading.

5.6.5 Contribution of Joint Shear Mechanisms

The relative contributions of the strut and truss mechanisms to horizontal joint shear demand are quantified in this section. Figure 5-65 shows the relative contribution of the truss and strut mechanisms to the overall joint shear demand in specimens A and B. These figures were calculated from the measured joint reinforcement activation and load cell readings. It can be seen that the strut contribution remains high throughout the testing of both specimens, consistently above $0.65V_{jh}$. As discussed in Section 4.5.1, this is typical of joints incorporating large column depths. The lack of joint damage as reported in Section 5.4.2 provides visual evidence as to the effectiveness of the strut mechanism.

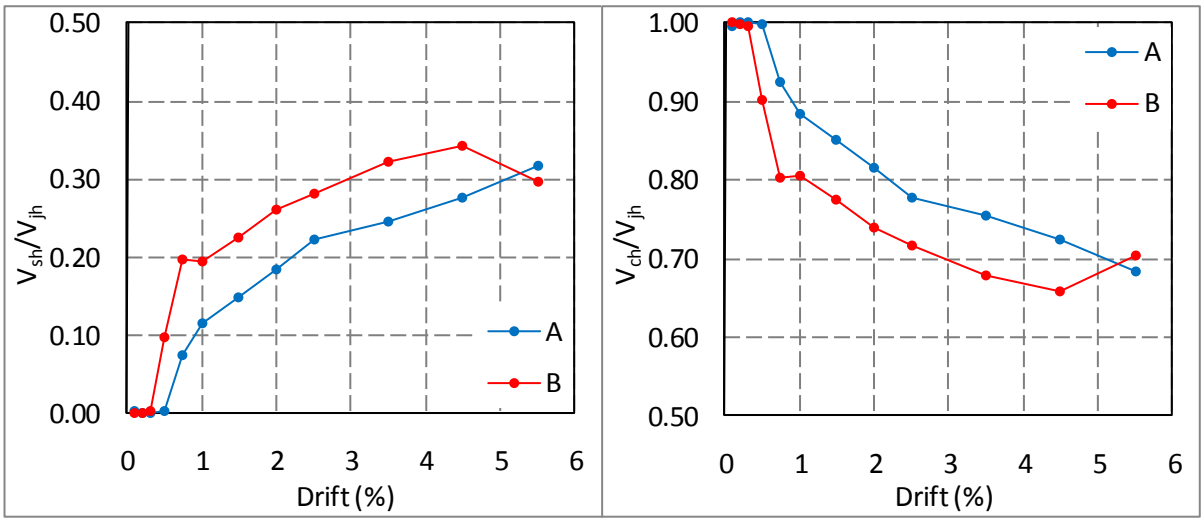

(a) V_{sh}/V_{jh} (b) V_{ch}/V_{jh}

Figure 5-65: *Relative contribution of truss and strut mechanisms to joint shear demand for specimens A and B*

It should be noted that any assistance to joint shear capacity from the vertical joint stirrups is inherently included as part of V_{ch}. This is because V_{ch} is calculated simply as joint shear demand minus observed horizontal joint reinforcement activation. Given the vertical joint reinforcement is consistently activated in tension it is likely to be contributing to the overall truss mechanism and strut confinement to some extent. Unfortunately, activation through these mechanisms is not readily isolated from the intended clamping response. However, an overall allowance should be made to account for this interaction when determining required horizontal joint reinforcement.

Figure 5-66 shows the variation of horizontal joint shear stress throughout the testing of each specimen. It can be seen that v_{jh} reaches values of 0.11 and $0.14f_c'$ at ULS drift (2.5%) in specimens A and B, respectively. This is less than the $0.2f_c'$ limit in NZS3101:2006 to ensure crushing of the joint does not occur and, comparing these values, it follows that the strut mechanism was possibly acting at approximately 65% of its capacity. The true level of strut mobilisation is probably lower due to the unknown contribution of the vertical joint stirrups to V_{ch} as discussed above. This reinforces the observation from Section 5.6.4 that the joints of both specimens were significantly over-reinforced.

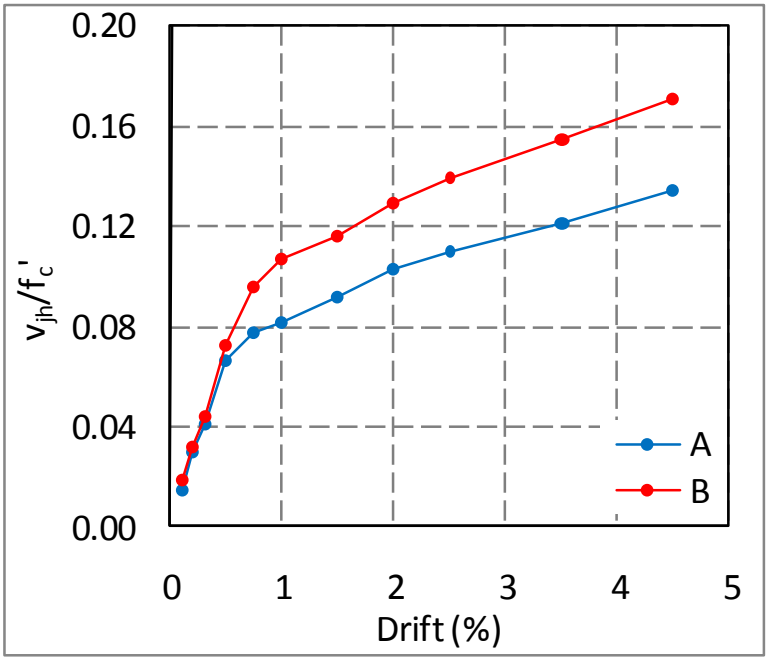

Figure 5-66: *Horizontal joint shear stress*

Chapter 6 - CONCLUSIONS

6.1 Concluding Remarks

The following conclusions can be drawn from the research undertaken:

- Bond performance within interior joints incorporating slotted beams can be significantly improved through the use of supplementary vertical joint stirrups. These represent a cheap, simple method of improving bond performance that can readily be adopted in practice.

- With the use of supplementary vertical joint stirrups, prevention of bar slip can be achieved with column depths between 22 – 24d_b for f_c' = 40 MPa. Practically, this corresponds to column depths between 550 – 600 mm when D25 beam bars are used. This is approximately 40% more conservative than current NZS3101:2006 provisions for fully ductile frames with asymmetric beam reinforcement.

- When supplementary vertical joint stirrups are not provided, prevention of bar slip is expected to be achieved with column depths between 27 – 30d_b for f_c' = 40 MPa. Practically, this corresponds to column depths between 675 – 750 mm when D25 beam bars are used.

- Overstrength factors for Grade 300 bottom longitudinal beam reinforcement were found to be 1.43 and 1.57 at the Ultimate Limit State (2.5% drift) and Maximum Credible Event (3.5% drift) earthquakes, respectably.

- The mechanism governing joint shear behaviour was found to be similar to that within a monolithic joint when sufficient bond is provided to the bottom longitudinal reinforcement. As expected for the relatively large column depths used, the concrete strut contributions to joint shear were dominant on the order of 75% at ULS drift.

- As a direct result of the above point, no additional horizontal joint reinforcement is required in the bottom half of the joint. It is possible that, horizontal joint reinforcement requirements can be relaxed when slotted beams are used. The recommendations developed in this thesis are approximately 20% less stringent than those in NZS3101:2006 for typical axial stress ratios on the order of 0.05 – 0.2. Axial stress ratios above 0.3 should not be used as a justification for reducing the area of horizontal joint reinforcement as joint crushing occurs beyond this level.

- Reduction in the required area of horizontal joint reinforcement is due to the increased effectiveness of the strut mechanism with larger column depths, and assistance to joint equilibrium provided by the vertical joint stirrups. Practically, this translates to less congested beam-column joints. Should designers wish to use them, current NZS3101:2006 provisions for joint shear reinforcement are more than adequate for slotted beams.

- Grade 300 top longitudinal reinforcement was found to perform satisfactorily in both specimens. This reinforcement remained nominally elastic and resulted in minimal beam elongation on the order of 0.7% and 0.2% of beam depth at the Life Safety (4.5% drift) and Ultimate Limit states, respectively. As a result, floor slab participation in flexural strength of beams is expected to be minimal and floor gravity support can be maintained through large earthquakes.

- As a result of the top longitudinal reinforcement remaining elastic, current NZS3101:2006 provisions for bond of nominally elastic reinforcement are applicable. This means fewer, larger diameter bars can be used here to reduce hinge and joint congestion.

- By ensuring prevention of bar slip failure through the use of larger columns and provision of vertical joint reinforcement, joint shear failure is also excluded as a failure mechanism. A stable hysteretic response was observed through 4.5% drift for both specimens after which time bar fracture occurred. While a corresponding loss of energy dissipation ensued, the overall hysteresis loop shape – and thus the system energy dissipation capacity – was not compromised.

- The shear hangers should be designed to the gap closing beam overstrength as opposed to the system overstrength ratio. Due to cracking observed within the hinge region, the aggregate interlock mechanism cannot be relied upon for shear transfer across this region. As such, the shear hangers should be designed to resist the entire beam overstrength shear demand. Furthermore, the shear hangers should be located at a depth of between $0.65 – 0.75d_h$ to minimise strains within the hanger.

- Strain penetration of the bottom longitudinal reinforcement was found to be approximately $0.01f_y d_b$ with the majority of this being assigned to the joint. This reduction compared with the typical value of $0.022f_y d_b$ (Paulay and Priestley, 1992) is

primarily due to the unbonded beam bars acting as a fuse and concentrating damage within this region.

- Au (2010) detailing recommendations of $4d_b$ stirrup spacing within the unbonded length and the use of steel unbonding tubes were found to prevent damage within the unbonding region up to 4.5% drift.

- Au (2010) longitudinal beam reinforcement asymmetry recommendations were found to produce a suitable response. The ratio of top to bottom longitudinal beam reinforcement, A'_s/A_s, should be on the order of 2.0.

- A catcher stirrup should be used in practice at the bottom shear hanger bend even though it was not explicitly required in the testing undertaken as part of this research. This detailing is recommended due to the increased beam shear demands expected when floor slabs are present and to prevent the situation where adjacent stirrup sets are spaced far from the hanger bend; this spacing could be up to 50 mm either side when D25 beam bars are used.

6.2 Future Research

During the course of this research, a number of areas requiring further research were identified. These are presented below:

- Bar fracture due to low cycle fatigue needs to be examined in further detail. While such failures only occurred during large interstorey drifts in the testing presented here, these tests only covered a single loading regime. Dedicated sub-assembly tests, preferably exposed to a variety of dynamic loading regimes are recommended. Such a study should also encompass the effects of varying unbonding tube configurations including clearance and wall thickness.

- An interaction exists between supplementary vertical joint stirrups and the truss mechanism for carrying shear within the joint. This needs to be investigated further as it is likely to reduce the amount of horizontal joint shear reinforcement required for use with slotted beams.

- Further testing should be carried out on beam-column specimens with reduced horizontal joint reinforcement and column depths to determine the lower bound values applicable for design.

- Replacement of the bottom longitudinal reinforcement with energy dissipating devices should be investigated. This would negate the issue of bond through interior beam-column joints and facilitate practical, economic repair options following a moderate earthquake.

- The relative contribution of supplementary vertical joint stirrups to the various mechanisms of bond improvement needs to be determined such that all of these mechanisms can be accounted for in design.

- Shear transfer contributions across the hinge from dowel action in the top longitudinal reinforcement and aggregate interlock should be determined. This will enable more economic sizing of the shear hangers which are currently detailed to take the entire beam shear demand.

- The required column depth for prevention of bar slip when supplementary vertical joint stirrups are not used should be confirmed experimentally. Recommendations presented in Section 4.2.4 should be used as the basis for further investigation. This research is not a priority given the prohibitively large column depths expected to be required.

Chapter 7 - REFERENCES

ACI Committee 352 (2002); *Recommendations for design of beam-column connections in monolithic reinforced concrete structures*, ACI Report 352R-02 (Draft)

ACI Committee 374 (2005); *Acceptance criteria for moment frames based on structural testing and commentary*: ACI Technical Document 374.1-05

ACI Committee 408 (1992); *State-of-the-art report on bond under cyclic loads*, ACI Report 408.2R-92

Amaris, A. , Pampanin, S., Bull, D. K., Carr, A. J. (2008); *Experimental investigation on a hybrid jointed precast frame with non-tearing floor connections*: New Zealand Society of Earthquake Engineering Conference, Wairakei, Pg: 1-16, Paper 26

Arioglu, N., Arioglu, E., Girgin, Z. (2006); *Evaluation of ratio between splitting tensile strength and compressive strength for concretes up to 120 MPa and its application in strength criterion*: ACI Materials Journal, Vol: 103, No: 1, Pg: 18-24

Au, E. (2010); *The mechanics and design of a non-tearing floor connection using slotted reinforced concrete beams*: Masters thesis; Department of Civil and Natural Resources Engineering, University of Canterbury, Christchurch.

Beckingsale, C. W. (1980); *Post-elastic behaviour of reinforced concete beam-column joints*: PhD thesis; Department of Civil Engineering, University of Canterbury, Christchurch.

Bentz, E. C. (2000); *Sectional analysis of reinforced concrete members*: PhD Thesis; Department of Civil Engineering, University of Toronto.

Birss, G. R. (1978); *The elastic behaviour of earthquake resistant reinforced concrete interior beam-column joints*: Masters thesis; Department of Civil Engineering, University of Canterbury, Christchurch.

Blakeley, R. W. G., Megget, L. M., Priestley, M. J. N. (1975); *Seismic performance of two full sized reinforced concrete beam-column joint units*: Bulletin of the New Zealand National Society for Earthquake Engineering, Vol: 8, No: 1, Pg: 38-69

Brooke, N., Megget, L. M., Ingham, J. (2005); *Design of ductile reinforced concrete moment resisting frames using grade 500E reinforcement*: School of Engineering Report 617, Department of Civil and Environmental Engineering, University of Auckland

Brown, J., Kunnath, S. K. (2004); *Low-cycle fatigue failure of reinforcing steel bars*: ACI Materials Journal, Vol: 101, No: 6, Pg: 457 - 466

CAE (1991); *Guidelines for the use of Structural Precast Concrete in Buildings*: Ed. 1. Christchurch; Centre for Advanced Engineering

CAE (1999); *Guidelines for the use of Structural Precast Concrete in Buildings*: Ed. 2. Christchurch; Centre for Advanced Engineering

Canbay, E., Frosch, R. J. (2005); *Bond strength of lap-spliced bars*: ACI Structural Journal, Vol: 102, No: 4, Pg: 605

Carr, A. J. (2005); *Ruaumoko Manual Volume 2: User Manual for the 2-Dimensional Version Ruaumoko 2D*: Department of Civil Engineering, University of Canterbury, Christchurch

Cheng, M. L., Restrepo, J. I., Park, R. (2000); *Seismic behaviour and design of reinforced concrete interior beam column joints*: Research Report, Department of Civil Engineering, University of Canterbury

Cheung, P. C., Paulay, T., Park, R. (1991); *Seismic design of reinforced concrete beam-column joints with floor slab*: Research Report 91-4, Department of Civil Engineering, University of Canterbury

Choi, O. C., Lee, W. S. (2002); *Interfacial bond analysis of deformed bars to concrete*: ACI Structural Journal, Vol: 99, No: 6, Pg: 750-756

Ciampi, V., Eligehausen, R., Bertero, V. V., Popov, E. P. (1982); *Hysteretic behavior of deformed reinforcing bars under seismic excitations*: 7th European Conference on Earthquake Engineering, Athens, Greece, Pg: 179 - 187

Dancygier, A. N., Katz, A. (2009); *Bond between deformed reinforcement and normal and high-strength concrete with and without fibers*: Materials and Structures, Vol: 43, No: 6, Pg: 839-856

Durrani, A., J., Wight, J. K. (1982); *Experimental and analytical study of internal beam to column connections subjected to reversed cyclic loading*: Reporta UMEE82R3, Department of Civil Engineering, The University of Michigan

Eligehausen, R., Popov, E. P., Bertero, V. V. (1982); *Local bond stress-slip relationships of deformed bars under generalized excitations*: Proceedings of the 7th European conference on earthquake engineering, Athens, Greece, Pg: 69-80

Eligehausen, R., Popov, E. P., Bertero, V. V. (1983); *Local bond stress-slip relationships of deformed bars under generalized excitations*: Report UCB/EERC-83/23, Earthquake Engineering Research Centre, Unversity of California, Berkeley

Engstrom, B., Magnusson, J., Huang, Z. 1998. Pull-out bond behavior of ribbed bars in normal and high-strength concrete with various confinements. In *Bond and Development of Reinforcement: A Tribute to Dr. Peter Gergely*, edited by R. T. Leon.

Esfahani, M. R., Rangan, B. V. (1996); *Studies on bond between concrete and reinforcing bars*, Research Report 1/96; School of Civil Engineering, Curtin University of Technology, Perth, Western Australia

Esfahani, M. R., Rangan, B. V. (1998); *Local bond strength of reinforcing bars in normal strength and high-strength concrete*: ACI Structural Journal, Vol: 95, No: 2, Pg: 96-106

Federation internationale du beton (2000); *Bond of reinforcement in concrete: State of the art report*: CEB-FIB Bulletin 10, International Federation for Structural Concrete, Lausanne, Switzerland

Fenwick, R. C. (2010): *Personal Communication*.

Fenwick, R. C. , Megget, L. M. (1993); *Elongation and load deflection characteristics of reinforced concrete members containing plastic hinges*: Bulletin of the New Zealand National Society for Earthquake Engineering, Vol: 26, No: 1, Pg: 28-41

Gambarova, P. G., Rosati, G. P. (1997); *Bond splitting in bar pull-out: behavioural laws and concrete cover role*: Magazine of Concrete Research, Vol: 49, No: 179, Pg: 99-110

Hakuto, S., Park, R., Tanaka, H. (1995); *Retrofitting of reinforced concrete moment resisting frames*: Research Report 95-4, Department of Civil Engineering, University of Canterbury

Hakuto, S., Park, R., Tanaka, H. (1999); *Effect of deterioration of bond of beam bars passing through interior beam-column joints on flexural strength and ductility*: ACI Structural Journal, Vol: 96, No: 5, Pg: 858-864

Hall, J. F. (1994); *Northridge earthquake January 17, 1994 - Preliminary reconnaissance report*, Earthquake Engineering Research Institute

Hamad, B. S. (1995); *Bond strength improvement of reinforcing bars with specially designed rib geometries*: ACI Structural Journal, Vol: 92, No: 1, Pg: 3-13

Harajli, M., Hamad, B., Karam, K. (2002); *Bond-slip response of reinforcing bars embedded in plain and fiber concrete*: Journal of Materials in Civil Engineering, Vol: 14, No: 6, Pg: 503-511

Harries, K. A., Kharel, G. (2003); *Experimental investigation of the behavior of variably confined concrete*: Cement and Concrete Research, Vol: 33, No, Pg: 873-880

Holmes, W. T., Somers, P. (1995); *Northridge earthquake of January 17, 1994 reconnaissance report - Reinforced concrete buildings*: Earthquake Spectra, Vol: 11 (Supp. 2), No, Pg: 49-98

Ichinose, T., Kanayama, Y., Inoue, Y., Bolander, J. E. (2004); *Size effect on bond strength of deformed bars*: Construction and Building Materials, Vol: 18, No, Pg: 549-558

Lau, D. B. N. (2001); *The influence of precast-prestressed flooring on the seismic performance of concrete perimeter frame buildings*: Masters thesis; Department of Civil and Resources Engineering, University of Auckland, Auckland.

Lau, D. B. N., Fenwick, R. C., Davidson, B. J. (2007); *Influence of Precast Prestressed Flooring on the Seismic Performance of Reinforced Concrete Perimeter Frame Buildings*: School of Engineering Report 653, Department of Civil and Environmental Engineering, University of Auckland

Leon, R. T. (1989); *Interior joints with variable anchorage lengths*: Journal of Structural Engineering, Vol: 115, No: 9, Pg: 2261-2275

Leslie, B. J. (2010); *The development and validation of a non-tearing floor precast concrete structural system for seismic regions*: Masters thesis; Department of Civil and Natural Resources Engineering, University of Canterbury, Christchurch.

Lindsay, R. (2004); *Experiments on the seismic performance of hollow-core floor systems in precast concrete buildings*: Masters thesis; Department of Civil and Natural Resources Engineering, University of Canterbury, Christchurch.

MacGregor, J. G., Wight, J. K. (2005); *Reinforced Concrete: Mechanics and Design*: Upper Saddle River, New Jersey; Pearson Prentice Hall

Malvar, L. J. (1992); *Bond of reinforcement under controlled confinement*: ACI Materials Journal, Vol: 89, No: 6, Pg: 593-601

Mander, J. B., Panthaki, F. D., Kasalanati, A. (1994); *Low-cycle fatigue behaviour of reinforcing steel*: Journal of Materials in Civil Engineering, Vol: 6, No: 4, Pg: 453-468

Matthews, J. G. (2004); *Hollowcore floor slab performance following a severe earthquake*: PhD thesis; Department of Civil and Natural Resources Engineering, University of Canterbury, Christchurch.

Mehta, P., Kumar, M. , Paulo, J. M. (2005); *Concrete: Microstructure, Properties, and Materials*; McGraw - Hill Professional

Milburn, J. R., Park, R. (1982); *Behaviour of reinforced concrete beam-column joints designed to NZS3101*: Research Report 82-7, Department of Civil Engineering, University of Canterbury

Miner, M. A. (1945); *Cumulative damage in fatigue*: American Society of Mechanical Engineers - Journal of Applied Mechanics, Vol: 12, No: 3, Pg: 159 - 164

Mitchell, D., DeVall, R. H., Kobayashi, K., Tinawi, R., Tso, W. K. (1996); *Damage to concrete structures due to the January 17, 1995, Hyogo-ken Nanbu (Kobe) earthquake*: Canadian Journal of Civil Engineering, Vol: 23, No: 3, Pg: 757-770

Muir, C. A. (2011): *Personal Communication*.

Muir, C. A., Bull, D. K., Au, E., Pampanin, S. (2010); *Comparison of strain hardening behaviour of non-tearing and traditional reinforced concrete beams*: Undergraduate research project report, Department of Civil and Natural Resources Engineering, University of Canterbury

Norton, J. A., King, A. B., Bull, D. K., Chapman, H. E., McVerry, G. H., Larkin, T. J., Spring, K. C. (1994); *Northridge earthquake reconnaissance report*: Bulletin of the New Zealand National Society for Earthquake Engineering, Vol: 27, No: 4, Pg: 235-344

Ogura, N., Bolander, J. E., Ichinose, T. (2008); *Analysis of bond splitting failure of deformed bars within structural concrete*: Engineering Structures, Vol: 30, No, Pg: 428-435

Ohkubo, M. , Matsuoka, T., Yoshioka, T., Anderson, D. L. (1999); *Shear transfer mechanism of reinforced concrete beams with a slot at the beam end*: Procession of Japan Concrete Institute, Vol: 21, No: 3, Pg: 523-528

Ohkubo, M., Hamamoto, T. (2004); *Developing reinforced concrete slotted beam structures to reduce earthquake damage and to enhance seismic structural performance*: 13th World Conference on Earthquake Engineering, Vancouver, Pg:

Palermo, A (2004); *The use of controlled rocking in the seismic design of bridges*: PhD; Technical University of Milan, Italy.

Pampanin, S., Pagani, C., Zambelli, S. (2004); *Cable-stayed and suspended post-tensioned solution for precast concrete frames*: Procession of NZ Concrete Industry Conference, Queenstown, New Zealand, Pg:

Park, R., Paulay, T. (1975); *Reinforced Concrete Structures*: New York; John Wiley & Sons Inc.

Paulay, T., Priestley, M. J. N. (1992); *Seismic Design of Reinforced Concrete and Masonry Structures*: New York; John Wiley & Sons Inc.

Peng, B. H. H. (2009); *Seismic performance assessment of reinforced concrete buildings with precast concrete floor systems*: PhD thesis; Department of Civil and Natural Resources Engineering, University of Canterbury, Christchurch.

Plizzari, G. A., Deldossi, M. A., Massimo, S. (1998); *Transverse reinforcement effects on anchored deformed bars*: Magazine of Concrete Research, Vol: 50, No: 2, Pg: 161-177

Popov, E. P. (1980); *Seismic behavior of reinforced concrete moment-resisting frames*: Proceedings of the 7th World Conference on Earthquake Engineering, Istanbul, Turkey, Pg: 355-362

Priestley, M. J. N. (1991); *Overview of the PRESSS research program*: PCI Journal, Vol: 36, No: 4, Pg: 50 - 57

Priestley, M. J. N., Sritharan, S., Conley, J. R., Pampanin, S. (1999); *Preliminary results and conclusions from the PRESSS five-storey precast concrete test building*: PCI Journal, Vol: 44, No: 6, Pg: 42 - 67

Restrepo, J. I. (1992); *The seismic behaviour of connections between precast concrete elements*: PhD thesis; Department of Civil Engineering, University of Canterbury, Christchurch.

Ruitong, D., Park, R. (1987); *A comparison of the behaviour of reinforced concrete beam-column joints designed for ductility and limited ductility*: Research Report 87-4, Department of Civil Engineering, University of Canterbury

Scott, R. H. (1996); *Intrinsic mechanisms in reinforced concrete beam-column connection behaviour*: ACI Structural Journal, Vol: 93, No: 3, Pg: 336-346

Soylev, T. A. (2011); *The effect of fibers on the variation of bond between steel reinforcement and concrete with casting position*: Construction and Building Materials, Vol: 25, No, Pg: 1736-1746

Soylev, T. A., Francois, R. (2006); *Effects of bar-placement conditions on steel-concrete bond*: Materials and Structures, Vol: 39, No, Pg: 211-220

Standards Association of New Zealand (2004); *Structural Design Actions: Earthquake Actions NZS1170.5*: Wellington, New Zealand

Standards Association of New Zealand (2006); *Concrete Structures Standard NZS 3101*: Wellington, New Zealand

Tastani, S. P., Pantazopoulou, S. J. (2010); *Direct tension pullout bond test: Experimental results*: Journal of Structural Engineering, Vol: 136, No: 6, Pg: 731-743

Thrane, L. N., Pade, C., Idzerda, C., Kaasgaard, M. 2010. Effect of rheology of SCC on bond strength of ribbed reinforcement bars. In *Design, Production and Placement of Self-Consolidating Concrete*, edited by K. H. Khayat and D. Feys.

Viwathanatepa, S., Popov, E. P., Bertero, V. V. (1979); *Effects of generalized loadings on bond of reinforcing bars embedded in confined concrete blocks*: Report UCB/EERC-79/22, Earthquake Engineering Research Centre, University of California, Berkeley

Yasar, E., Erdogan, Y., Kilic, A. (2004); *Effect of limestone aggregate type and water-cement ratio on concrete strength*: Materials Letters, Vol: 58, No: 5, Pg: 772-777

Zuo, J., Darwin, D. (2000); *Splice strength of conventional and high relative rib area bars in normal and high-strength concrete*: ACI Structural Journal, Vol: 97, No: 4, Pg: 630-641

APPENDIX A – DATABASE SPECIMENS

A.1 Database Notes

Geometric and mechanical properties of the database specimens are reported as per Figure A1 below:

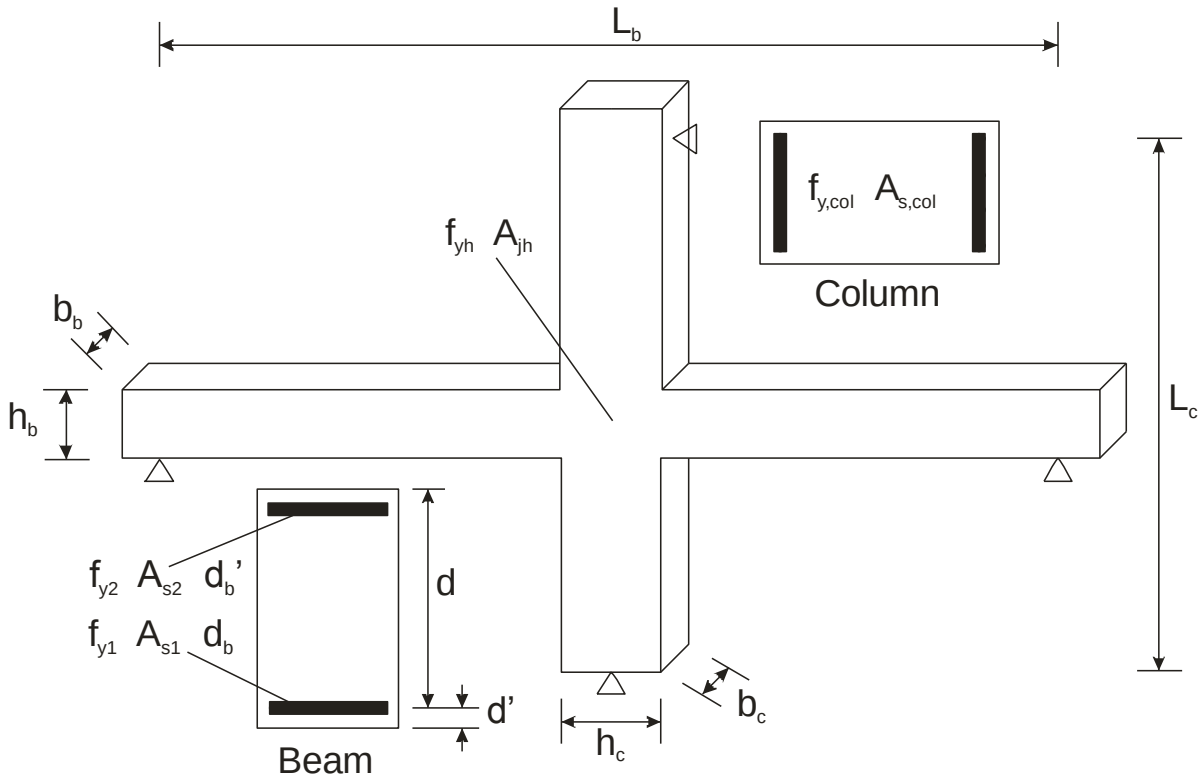

Figure A1: *Database specimen properties*

The following general notes correspond to the database summary tables presented in the following section:

1) Excludes column bars on the face of the joint as these are activated in flexure
2) Excludes dummy sets within s/2 of the longitudinal reinforcement
3) According to NZS3101:2006
4) Normalised to f_c' = 30 MPa & f_y = 300 MPa
5) Normalised by α_s from NZS3101:2006 to account for reinforcement asymmetry
6) Normalised by α_p from NZS3101:2006 to account for axial pressure
7) Deemed to have occurred when the measured slip exceeds the bar lug spacing

Quantities not reported in the database summaries such as maximum bond stress and reinforcement activation were taken directly from available strain gauge profiles.

A.2 Database Specimen Summaries

Researcher:	Beckingsale
Year:	1980
Test I.D:	B11

Specimen Geometry		
L_b	4877	mm
h_b	610	mm
b_b	356	mm
d'	41	mm
d	569	mm
L_c	3354	mm
h_c	457	mm
b_c	457	mm

Mechanical Properties		
f_{y1}	298	MPa
A_{s1}	1134	mm^2
f_{y2}	298	MPa
A_{s2}	2268	mm^2
$f_{y,col}$	380	MPa
$A_{s,col}$	4646	mm^2
[1]$A_{jv,prvd}$	1548	mm^2
f_{yh}	336	MPa
[2]$A_{jh,prvd}$	3040	mm^2
f_c'	35.9	MPa
$N^*/A_g f_c'$	0.04	-

Joint Reinforcement		
M_{ob}^+	251	kNm
M_{ob}^-	447	kNm
[3]V^*_{ojh}	1133	kN
[3]α_j	1.33	-
[3]$6V^*_{ojh}/f_c' b_j h_c$	0.92	-
[3]$A_{jh,req}$	2433	mm^2
$A_{jh,prvd}/A_{jh,req}$	124	%
[3]α_v	0.67	-
[3]$A_{jv,req}$	1930	mm^2
$A_{jv,prvd}/A_{jv,req}$	80	%

Effective Column Depths		
[4]$(h_c/d_b)_{material}$	28.7	-
[4]$(h_c/d_b')_{material}$	28.7	-
β	0.50	-
[3]$\alpha_{s,bottom}$	1.80	-
[5]$(h_c/d_b)_{\alpha s}$	24.7	-
[3]α_p	1.00	-
[6]$(h_c/d_b)_{axial}$	28.7	-
[6]$(h_c/d_b')_{axial}$	28.7	-
[7]Bar slip?	Bottom	-

Researcher:	Beckingsale
Year:	1980
Test I.D:	B12

Specimen Geometry		
L_b	4877	mm
h_b	610	mm
b_b	356	mm
d'	41	mm
d	569	mm
L_c	3354	mm
h_c	457	mm
b_c	457	mm

Mechanical Properties		
f_{y1}	298	MPa
A_{s1}	1701	mm^2
f_{y2}	298	MPa
A_{s2}	1701	mm^2
$f_{y,col}$	380	MPa
$A_{s,col}$	4646	mm^2
$^{1}A_{jv,prvd}$	1548	mm^2
f_{yh}	336	MPa
$^{2}A_{jh,prvd}$	3040	mm^2
f_c'	34.6	MPa
$N^*/A_g f_c'$	0.04	-

Joint Reinforcement		
M_{ob}^+	348	kNm
M_{ob}^-	348	kNm
$^{3}V^*_{ojh}$	1148	kN
$^{3}\alpha_i$	1.33	-
$^{3}6V^*_{ojh}/f_c' b_j h_c$	0.97	-
$^{3}A_{jh,req}$	1915	mm^2
$A_{jh,prvd}/A_{jh,req}$	158	%
$^{3}\alpha_v$	0.67	-
$^{3}A_{jv,req}$	1517	mm^2
$A_{jv,prvd}/A_{jv,req}$	101	%

Effective Column Depths		
$^{4}(h_c/d_b)_{material}$	28.2	-
$^{4}(h_c/d_b')_{material}$	28.2	-
β	1.00	-
$^{3}\alpha_{s,bottom}$	1.55	-
$^{5}(h_c/d_b)_{\alpha s}$	28.2	-
$^{3}\alpha_p$	1.00	-
$^{6}(h_c/d_b)_{axial}$	28.2	-
$^{6}(h_c/d_b')_{axial}$	28.2	-
^{7}Bar slip?	Top/Bottom	-

Researcher:	Beckingsale
Year:	1980
Test I.D:	B13

Specimen Geometry		
L_b	4877	mm
h_b	610	mm
b_b	356	mm
d'	41	mm
d	569	mm
L_c	3354	mm
h_c	457	mm
b_c	457	mm

Mechanical Properties		
f_{y1}	298	MPa
A_{s1}	1701	mm^2
f_{y2}	298	MPa
A_{s2}	1701	mm^2
$f_{y,col}$	380	MPa
$A_{s,col}$	4646	mm^2
$^1A_{jv,prvd}$	1548	mm^2
f_{yh}	336	MPa
$^2A_{jh,prvd}$	2027	mm^2
f_c'	31.4	MPa
$N^*/A_g f_c'$	0.44	-

Joint Reinforcement		
M_{ob}^+	347	kNm
M_{ob}^-	347	kNm
$^3V^*_{ojh}$	1144	kN
$^3\alpha_i$	0.69	-
$^3 6V^*_{ojh}/f_c' b_j h_c$	1.06	-
$^3A_{jh,req}$	1098	mm^2
$A_{jh,prvd}/A_{jh,req}$	183	%
$^3\alpha_v$	0.49	-
$^3A_{jv,req}$	630	mm^2
$A_{jv,prvd}/A_{jv,req}$	244	%

Effective Column Depths		
$^4(h_c/d_b)_{material}$	26.8	-
$^4(h_c/d_b')_{material}$	26.8	-
β	1.00	-
$^3\alpha_{s,bottom}$	1.55	-
$^5(h_c/d_b)_{\alpha s}$	26.8	-
$^3\alpha_p$	1.17	-
$^6(h_c/d_b)_{axial}$	31.4	-
$^6(h_c/d_b')_{axial}$	31.4	-
^{7}Bar slip?	No	-

Researcher:	Birss
Year:	1978
Test I.D:	B1

Specimen Geometry		
L_b	4877	mm
h_b	610	mm
b_b	356	mm
d'	40	mm
d	570	mm
L_c	3490	mm
h_c	457	mm
b_c	457	mm

Mechanical Properties		
f_{y1}	288	MPa
A_{s1}	2514	mm^2
f_{y2}	288	MPa
A_{s2}	2514	mm^2
$f_{y,col}$	380	MPa
$A_{s,col}$	5423	mm^2
$^1A_{jv,prvd}$	1810	mm^2
f_{yh}	346	MPa
$^2A_{jh,prvd}$	1013	mm^2
f_c'	27.9	MPa
$N^*/A_g f_c'$	0.05	-

Joint Reinforcement		
M_{ob}^+	459	kNm
M_{ob}^-	459	kNm
$^3V^*_{ojh}$	1165	kN
$^3\alpha_i$	1.31	-
$^36V^*_{ojh}/f_c'b_jh_c$	1.20	-
$^3A_{jh,req}$	3300	mm^2
$A_{jh,prvd}/A_{jh,req}$	31	%
$^3\alpha_v$	0.66	-
$^3A_{jv,req}$	2655	mm^2
$A_{jv,prvd}/A_{jv,req}$	68	%

Effective Column Depths		
$^4(h_c/d_b)_{material}$	24.0	-
$^4(h_c/d_b')_{material}$	24.0	-
β	1.00	-
$^3\alpha_{s,bottom}$	1.55	-
$^5(h_c/d_b)_{\alpha s}$	24.0	-
$^3\alpha_p$	1.00	-
$^6(h_c/d_b)_{axial}$	24.0	-
$^6(h_c/d_b')_{axial}$	24.0	-
^{7}Bar slip?	No	-

Researcher:	Birss
Year:	1978
Test I.D:	B2

Specimen Geometry		
L_b	4877	mm
h_b	610	mm
b_b	356	mm
d'	40	mm
d	570	mm
L_c	3490	mm
h_c	457	mm
b_c	457	mm

Mechanical Properties		
f_{y1}	288	MPa
A_{s1}	2514	mm^2
f_{y2}	288	MPa
A_{s2}	2514	mm^2
$f_{y,col}$	380	MPa
$A_{s,col}$	5423	mm^2
$^{1}A_{jv,prvd}$	1810	mm^2
f_{yh}	398	MPa
$^{2}A_{jh,prvd}$	265	mm^2
f_c'	31.5	MPa
$N^*/A_g f_c'$	0.44	-

Joint Reinforcement		
M_{ob}^+	462	kNm
M_{ob}^-	462	kNm
$^{3}V^*_{ojh}$	1316	kN
$^{3}\alpha_i$	0.70	-
$^{3}6V^*_{ojh}/f_c' b_j h_c$	1.20	-
$^{3}A_{jh,req}$	1521	mm^2
$A_{jh,prvd}/A_{jh,req}$	17	%
$^{3}\alpha_v$	0.49	-
$^{3}A_{jv,req}$	1034	mm^2
$A_{jv,prvd}/A_{jv,req}$	175	%

Effective Column Depths		
$^{4}(h_c/d_b)_{material}$	25.5	-
$^{4}(h_c/d_b')_{material}$	25.5	-
β	1.00	-
$^{3}\alpha_{s,bottom}$	1.55	-
$^{5}(h_c/d_b)_{\alpha s}$	25.5	-
$^{3}\alpha_p$	1.17	-
$^{6}(h_c/d_b)_{axial}$	29.9	-
$^{6}(h_c/d_b')_{axial}$	29.9	-
^{7}Bar slip?	No	-

Researcher:	Blakeley et al
Year:	1975
Test I.D:	Unit 1

Specimen Geometry		
L_b	8840	mm
h_b	889	mm
b_b	457	mm
d'	90	mm
d	799	mm
L_c	4242	mm
h_c	686	mm
b_c	686	mm

Mechanical Properties		
f_{y1}	299	MPa
A_{s1}	2570	mm^2
f_{y2}	282	MPa
A_{s2}	4225	mm^2
$f_{y,col}$	289	MPa
$A_{s,col}$	15885	mm^2
$^{1}A_{jv,prvd}$	6354	mm^2
f_{yh}	297	MPa
$^{2}A_{jh,prvd}$	9169	mm^2
f_c'	48.5	MPa
$N^*/A_g f_c'$	0.03	-

Joint Reinforcement		
M_{ob}^+	774	kNm
M_{ob}^-	1268	kNm
$^{3}V^*_{ojh}$	2268	kN
$^{3}\alpha_i$	1.36	-
$^{3}6V^*_{ojh}/f_c'b_jh_c$	0.85	-
$^{3}A_{jh,req}$	4584	mm^2
$A_{jh,prvd}/A_{jh,req}$	200	%
$^{3}\alpha_v$	0.68	-
$^{3}A_{jv,req}$	4160	mm^2
$A_{jv,prvd}/A_{jv,req}$	153	%

Effective Column Depths		
$^{4}(h_c/d_b)_{material}$	33.3	-
$^{4}(h_c/d_b')_{material}$	33.3	-
β	0.61	-
$^{3}\alpha_{s,bottom}$	1.80	-
$^{5}(h_c/d_b)_{\alpha s}$	28.6	-
$^{3}\alpha_p$	1.00	-
$^{6}(h_c/d_b)_{axial}$	33.3	-
$^{6}(h_c/d_b')_{axial}$	33.3	-
^{7}Bar slip?	No	-

Researcher:	Cheng
Year:	2000
Test I.D:	Unit 1

Specimen Geometry		
L_b	3190	mm
h_b	550	mm
b_b	300	mm
d'	32	mm
d	518	mm
L_c	2450	mm
h_c	390	mm
b_c	390	mm

Mechanical Properties		
f_{y1}	525	MPa
A_{s1}	904	mm^2
f_{y2}	525	MPa
A_{s2}	904	mm^2
$f_{y,col}$	518	MPa
$A_{s,col}$	1709	mm^2
[1]$A_{jv,prvd}$	452	mm^2
f_{yh}	353	MPa
[2]$A_{jh,prvd}$	855	mm^2
f_c'	33.3	MPa
$N^*/A_g f_c'$	0.43	-

Joint Reinforcement		
M_{ob}^+	269	kNm
M_{ob}^-	269	kNm
[3]V^*_{ojh}	928	kN
[3]α_i	0.71	-
[3]$6V^*_{ojh}/f_c' b_j h_c$	1.10	-
[3]$A_{jh,req}$	1051	mm^2
$A_{jh,prvd}/A_{jh,req}$	81	%
[3]α_v	0.49	-
[3]$A_{jv,req}$	489	mm^2
$A_{jv,prvd}/A_{jv,req}$	93	%

Effective Column Depths		
[4]$(h_c/d_b)_{material}$	20.5	-
[4]$(h_c/d_b')_{material}$	20.5	-
β	1.00	-
[3]$\alpha_{s,bottom}$	1.55	-
[5]$(h_c/d_b)_{\alpha s}$	20.5	-
[3]α_p	1.17	-
[6]$(h_c/d_b)_{axial}$	23.9	-
[6]$(h_c/d_b')_{axial}$	23.9	-
[7]Bar slip?	No	-

Researcher:	Cheng
Year:	2000
Test I.D:	Unit 2

Specimen Geometry		
L_b	3190	mm
h_b	550	mm
b_b	300	mm
d'	32	mm
d	518	mm
L_c	2450	mm
h_c	390	mm
b_c	390	mm

Mechanical Properties		
f_{y1}	525	MPa
A_{s1}	904	mm^2
f_{y2}	525	MPa
A_{s2}	904	mm^2
$f_{y,col}$	518	MPa
$A_{s,col}$	1709	mm^2
[1]$A_{jv,prvd}$	452	mm^2
f_{yh}	353	MPa
[2]$A_{jh,prvd}$	1495	mm^2
f_c'	33.3	MPa
$N^*/A_g f_c'$	0.43	-

Joint Reinforcement		
M_{ob}^+	269	kNm
M_{ob}^-	269	kNm
[3]V^*_{ojh}	928	kN
[3]α_i	0.71	-
[3]$6V^*_{ojh}/f_c'b_jh_c$	1.10	-
[3]$A_{jh,req}$	1051	mm^2
$A_{jh,prvd}/A_{jh,req}$	142	%
[3]α_v	0.49	-
[3]$A_{jv,req}$	489	mm^2
$A_{jv,prvd}/A_{jv,req}$	93	%

Effective Column Depths		
[4]$(h_c/d_b)_{material}$	20.5	-
[4]$(h_c/d_b')_{material}$	20.5	-
β	1.00	-
[3]$\alpha_{s,bottom}$	1.55	-
[5]$(h_c/d_b)_{\alpha s}$	20.5	-
[3]α_p	1.17	-
[6]$(h_c/d_b)_{axial}$	23.9	-
[6]$(h_c/d_b')_{axial}$	23.9	-
[7]Bar slip?	Top	-

Researcher:	Cheng
Year:	2000
Test I.D:	Unit 3

Specimen Geometry		
L_b	3190	mm
h_b	550	mm
b_b	300	mm
d'	32	mm
d	518	mm
L_c	2450	mm
h_c	390	mm
b_c	390	mm

Mechanical Properties		
f_{y1}	525	MPa
A_{s1}	678	mm^2
f_{y2}	525	MPa
A_{s2}	678	mm^2
$f_{y,col}$	518	MPa
$A_{s,col}$	1709	mm^2
$^1A_{jv,prvd}$	452	mm^2
f_{yh}	353	MPa
$^2A_{jh,prvd}$	855	mm^2
f_c'	37	MPa
$N^*/A_g f_c'$	0.10	-

Joint Reinforcement		
M_{ob}^+	208	kNm
M_{ob}^-	208	kNm
$^3V^*_{ojh}$	696	kN
$^3\alpha_i$	1.25	-
$^36V^*_{ojh}/f_c'b_jh_c$	0.85	-
$^3A_{jh,req}$	1062	mm^2
$A_{jh,prvd}/A_{jh,req}$	80	%
$^3\alpha_v$	0.64	-
$^3A_{jv,req}$	642	mm^2
$A_{jv,prvd}/A_{jv,req}$	70	%

Effective Column Depths		
$^4(h_c/d_b)_{material}$	21.7	-
$^4(h_c/d_b')_{material}$	21.7	-
β	1.00	-
$^3\alpha_{s,bottom}$	1.55	-
$^5(h_c/d_b)_{\alpha s}$	21.7	-
$^3\alpha_p$	1.00	-
$^6(h_c/d_b)_{axial}$	21.7	-
$^6(h_c/d_b')_{axial}$	21.7	-
^{7}Bar slip?	Top	-

Researcher:	Cheng
Year:	2000
Test I.D:	Unit 4

Specimen Geometry		
L_b	3190	mm
h_b	550	mm
b_b	300	mm
d'	32	mm
d	518	mm
L_c	2450	mm
h_c	390	mm
b_c	390	mm

Mechanical Properties		
f_{y1}	525	MPa
A_{s1}	452	mm^2
f_{y2}	525	MPa
A_{s2}	904	mm^2
$f_{y,col}$	518	MPa
$A_{s,col}$	1709	mm^2
$^1A_{jv,prvd}$	452	mm^2
f_{yh}	353	MPa
$^2A_{jh,prvd}$	855	mm^2
f_c'	37	MPa
$N^*/A_g f_c'$	0.10	-

Joint Reinforcement		
M_{ob}^+	147	kNm
M_{ob}^-	269	kNm
$^3V^*_{ojh}$	688	kN
$^3\alpha_i$	1.24	-
$^3 6V^*_{ojh}/f_c' b_j h_c$	0.85	-
$^3A_{jh,req}$	1416	mm^2
$A_{jh,prvd}/A_{jh,req}$	60	%
$^3\alpha_v$	0.64	-
$^3A_{jv,req}$	856	mm^2
$A_{jv,prvd}/A_{jv,req}$	53	%

Effective Column Depths		
$^4(h_c/d_b)_{material}$	21.7	-
$^4(h_c/d_b')_{material}$	21.7	-
β	0.50	-
$^3\alpha_{s,bottom}$	1.80	-
$^5(h_c/d_b)_{\alpha s}$	18.6	-
$^3\alpha_p$	1.00	-
$^6(h_c/d_b)_{axial}$	21.7	-
$^6(h_c/d_b')_{axial}$	21.7	-
^{7}Bar slip?	Top/Bottom	-

Researcher:	Cheng
Year:	2000
Test I.D:	Unit 8

Specimen Geometry		
L_b	3190	mm
h_b	550	mm
b_b	300	mm
d'	32	mm
d	518	mm
L_c	2450	mm
h_c	390	mm
b_c	390	mm

Mechanical Properties		
f_{y1}	525	MPa
A_{s1}	904	mm^2
f_{y2}	525	MPa
A_{s2}	904	mm^2
$f_{y,col}$	518	MPa
$A_{s,col}$	2413	mm^2
$^{1}A_{jv,prvd}$	804	mm^2
f_{yh}	354	MPa
$^{2}A_{jh,prvd}$	1571	mm^2
f_c'	33.2	MPa
$N^*/A_g f_c'$	0.10	-

Joint Reinforcement		
M_{ob}^+	269	kNm
M_{ob}^-	269	kNm
$^{3}V^*_{ojh}$	928	kN
$^{3}\alpha_i$	1.24	-
$^{3}6V^*_{ojh}/f_c' b_j h_c$	1.10	-
$^{3}A_{jh,req}$	1835	mm^2
$A_{jh,prvd}/A_{jh,req}$	86	%
$^{3}\alpha_v$	0.64	-
$^{3}A_{jv,req}$	1111	mm^2
$A_{jv,prvd}/A_{jv,req}$	72	%

Effective Column Depths		
$^{4}(h_c/d_b)_{material}$	20.5	-
$^{4}(h_c/d_b')_{material}$	20.5	-
β	1.00	-
$^{3}\alpha_{s,bottom}$	1.55	-
$^{5}(h_c/d_b)_{\alpha s}$	20.5	-
$^{3}\alpha_p$	1.00	-
$^{6}(h_c/d_b)_{axial}$	20.5	-
$^{6}(h_c/d_b')_{axial}$	20.5	-
^{7}Bar slip?	Top/Bottom	-

Researcher:	Durrani & Wight
Year:	1982
Test I.D:	X1

Specimen Geometry		
L_b	2496	mm
h_b	419	mm
b_b	279	mm
d'	38	mm
d	381	mm
L_c	2248	mm
h_c	362	mm
b_c	362	mm

Mechanical Properties		
f_{y1}	345	MPa
A_{s1}	1134	mm^2
f_{y2}	331	MPa
A_{s2}	1548	mm^2
$f_{y,col}$	420	MPa
$A_{s,col}$	4054	mm^2
$^1A_{jv,prvd}$	1013	mm^2
f_{yh}	352	MPa
$^2A_{jh,prvd}$	865	mm^2
f_c'	34.3	MPa
$N^*/A_g f_c'$	0.05	-

Joint Reinforcement		
M_{ob}^+	181	kNm
M_{ob}^-	234	kNm
$^3V^*_{ojh}$	900	kN
$^3\alpha_i$	1.31	-
$^3 6V^*_{ojh}/f_c' b_j h_c$	1.20	-
$^3A_{jh,req}$	2336	mm^2
$A_{jh,prvd}/A_{jh,req}$	37	%
$^3\alpha_v$	0.66	-
$^3A_{jv,req}$	1504	mm^2
$A_{jv,prvd}/A_{jv,req}$	67	%

Effective Column Depths		
$^4(h_c/d_b)_{material}$	22.2	-
$^4(h_c/d_b')_{material}$	19.0	-
β	0.73	-
$^3\alpha_{s,bottom}$	1.80	-
$^5(h_c/d_b)_{\alpha s}$	19.1	-
$^3\alpha_p$	1.00	-
$^6(h_c/d_b)_{axial}$	22.2	-
$^6(h_c/d_b')_{axial}$	19.0	-
^{7}Bar slip?	Top/Bottom	-

Researcher:	Durrani & Wight
Year:	1982
Test I.D:	X2

Specimen Geometry		
L_b	2496	mm
h_b	419	mm
b_b	279	mm
d'	38	mm
d	381	mm
L_c	2248	mm
h_c	362	mm
b_c	362	mm

Mechanical Properties		
f_{y1}	345	MPa
A_{s1}	1134	mm^2
f_{y2}	331	MPa
A_{s2}	1548	mm^2
$f_{y,col}$	420	MPa
$A_{s,col}$	4054	mm^2
$^{1}A_{jv,prvd}$	1013	mm^2
f_{yh}	352	MPa
$^{2}A_{jh,prvd}$	1298	mm^2
f_c'	33.6	MPa
$N^*/A_g f_c'$	0.06	-

Joint Reinforcement		
M_{ob}^{+}	181	kNm
M_{ob}^{-}	234	kNm
$^{3}V^*_{ojh}$	882	kN
$^{3}\alpha_i$	1.31	-
$^{3}6V^*_{ojh}/f_c' b_j h_c$	1.20	-
$^{3}A_{jh,req}$	2333	mm^2
$A_{jh,prvd}/A_{jh,req}$	56	%
$^{3}\alpha_v$	0.66	-
$^{3}A_{jv,req}$	1500	mm^2
$A_{jv,prvd}/A_{jv,req}$	67	%

Effective Column Depths		
$^{4}(h_c/d_b)_{material}$	22.0	-
$^{4}(h_c/d_b')_{material}$	18.8	-
β	0.73	-
$^{3}\alpha_{s,bottom}$	1.80	-
$^{5}(h_c/d_b)_{\alpha s}$	19.0	-
$^{3}\alpha_p$	1.00	-
$^{6}(h_c/d_b)_{axial}$	22.0	-
$^{6}(h_c/d_b')_{axial}$	18.8	-
^{7}Bar slip?	No	-

Researcher:	Durrani & Wight
Year:	1982
Test I.D:	X3

Specimen Geometry		
L_b	2496	mm
h_b	419	mm
b_b	279	mm
d'	38	mm
d	381	mm
L_c	2248	mm
h_c	362	mm
b_c	362	mm

Mechanical Properties		
f_{y1}	345	MPa
A_{s1}	851	mm^2
f_{y2}	331	MPa
A_{s2}	1161	mm^2
$f_{y,col}$	420	MPa
$A_{s,col}$	2692	mm^2
[1]$A_{jv,prvd}$	567	mm^2
f_{yh}	352	MPa
[2]$A_{jh,prvd}$	865	mm^2
f_c'	31.0	MPa
$N^*/A_g f_c'$	0.05	-

Joint Reinforcement		
M_{ob}^+	137	kNm
M_{ob}^-	177	kNm
[3]V^*_{ojh}	752	kN
[3]α_i	1.32	-
[3]$6V^*_{ojh}/f_c'b_jh_c$	1.11	-
[3]$A_{jh,req}$	1624	mm^2
$A_{jh,prvd}/A_{jh,req}$	53	%
[3]α_v	0.66	-
[3]$A_{jv,req}$	1047	mm^2
$A_{jv,prvd}/A_{jv,req}$	54	%

Effective Column Depths		
[4]$(h_c/d_b)_{material}$	21.1	-
[4]$(h_c/d_b')_{material}$	18.1	-
β	0.73	-
[3]$\alpha_{s,bottom}$	1.80	-
[5]$(h_c/d_b)_{\alpha s}$	18.2	-
[3]α_p	1.00	-
[6]$(h_c/d_b)_{axial}$	21.1	-
[6]$(h_c/d_b')_{axial}$	18.1	-
[7]Bar slip?	Top/Bottom	-

Researcher:	Hakuto et al
Year:	1995
Test I.D:	O4

Specimen Geometry		
L_b	3510	mm
h_b	500	mm
b_b	300	mm
d'	52	mm
d	448	mm
L_c	2900	mm
h_c	600	mm
b_c	460	mm

Mechanical Properties		
f_{y1}	308	MPa
A_{s1}	1810	mm^2
f_{y2}	308	MPa
A_{s2}	1810	mm^2
$f_{y,col}$	300	MPa
$A_{s,col}$	0.0	mm^2
$^{1}A_{jv,prvd}$	0.0	mm^2
f_{yh}	300	MPa
$^{2}A_{jh,prvd}$	0	mm^2
f_c'	52.9	MPa
$N^*/A_g f_c'$	0.0	-

Joint Reinforcement		
M_{ob}^+	292	kNm
M_{ob}^-	292	kNm
$^{3}V^*_{ojh}$	1322	kN
$^{3}\alpha_i$	1.40	-
$^{3}6V^*_{ojh}/f_c'b_jh_c$	0.85	-
$^{3}A_{jh,req}$	2211	mm^2
$A_{jh,prvd}/A_{jh,req}$	0.0	%
$^{3}\alpha_v$	0.70	-
$^{3}A_{jv,req}$	1290	mm^2
$A_{jv,prvd}/A_{jv,req}$	0.0	%

Effective Column Depths		
$^{4}(h_c/d_b)_{material}$	33.2	-
$^{4}(h_c/d_b')_{material}$	33.2	-
β	1.00	-
$^{3}\alpha_{s,bottom}$	1.55	-
$^{5}(h_c/d_b)_{\alpha s}$	33.2	-
$^{3}\alpha_p$	1.00	-
$^{6}(h_c/d_b)_{axial}$	33.2	-
$^{6}(h_c/d_b')_{axial}$	33.2	-
^{7}Bar slip?	No	-

Researcher:	Hakuto et al
Year:	1995
Test I.D:	O5

Specimen Geometry		
L_b	3510	mm
h_b	500	mm
b_b	300	mm
d'	52	mm
d	448	mm
L_c	2900	mm
h_c	600	mm
b_c	460	mm

Mechanical Properties		
f_{y1}	306	MPa
A_{s1}	1608	mm^2
f_{y2}	306	MPa
A_{s2}	1608	mm^2
$f_{y,col}$	300	MPa
$A_{s,col}$	0.0	mm^2
$^1A_{jv,prvd}$	0.0	mm^2
f_{yh}	300	MPa
$^2A_{jh,prvd}$	0	mm^2
f_c'	35.1	MPa
$N^*/A_g f_c'$	0.0	-

Joint Reinforcement		
M_{ob}^+	259	kNm
M_{ob}^-	259	kNm
$^3V^*_{ojh}$	1091	kN
$^3\alpha_i$	1.40	-
$^3 6V^*_{ojh}/f_c' b_j h_c$	0.85	-
$^3A_{jh,req}$	1952	mm^2
$A_{jh,prvd}/A_{jh,req}$	0.0	%
$^3\alpha_v$	0.70	-
$^3A_{jv,req}$	1290	mm^2
$A_{jv,prvd}/A_{jv,req}$	0.0	%

Effective Column Depths		
$^4(h_c/d_b)_{material}$	20.3	-
$^4(h_c/d_b')_{material}$	20.3	-
β	1.00	-
$^3\alpha_{s,bottom}$	1.55	-
$^5(h_c/d_b)_{\alpha s}$	20.3	-
$^3\alpha_p$	1.00	-
$^6(h_c/d_b)_{axial}$	20.3	-
$^6(h_c/d_b')_{axial}$	20.3	-
^{7}Bar slip?	No	-

Researcher:	Leon
Year:	1989
Test I.D:	BCJ1

Note: Test material strengths not published

Specimen Geometry		
L_b	2032	mm
h_b	305	mm
b_b	203	mm
d'	30	mm
d	275	mm
L_c	2464	mm
h_c	203	mm
b_c	254	mm

Mechanical Properties		
f_{y1}	420	MPa
A_{s1}	254	mm^2
f_{y2}	420	MPa
A_{s2}	531	mm^2
$f_{y,col}$	420	MPa
$A_{s,col}$	2389	mm^2
$^{1}A_{jv,prvd}$	760	mm^2
f_{yh}	420	MPa
$^{2}A_{jh,prvd}$	253	mm^2
f_c'	30	MPa
$N^*/A_g f_c'$	0.0	-

Joint Reinforcement		
M_{ob}^+	39	kNm
M_{ob}^-	79	kNm
$^{3}V^*_{ojh}$	309	kN
$^{3}\alpha_i$	1.4	-
$^{3}6V^*_{ojh}/f_c'b_jh_c$	1.20	-
$^{3}A_{jh,req}$	892	mm^2
$A_{jh,prvd}/A_{jh,req}$	28	%
$^{3}\alpha_v$	0.7	-
$^{3}A_{jv,req}$	4160	mm^2
$A_{jv,prvd}/A_{jv,req}$	81	%

Effective Column Depths		
$^{4}(h_c/d_b)_{material}$	16.1	-
$^{4}(h_c/d_b')_{material}$	11.2	-
β	0.48	-
$^{3}\alpha_{s,bottom}$	1.80	-
$^{5}(h_c/d_b)_{\alpha s}$	13.9	-
$^{3}\alpha_p$	1.00	-
$^{6}(h_c/d_b)_{axial}$	16.1	-
$^{6}(h_c/d_b')_{axial}$	11.2	-
^{7}Bar slip?	Top/Bottom	-

Researcher:	Leon
Year:	1989
Test I.D:	BCJ2

Note: Test material strengths not published

Specimen Geometry		
L_b	2032	mm
h_b	305	mm
b_b	203	mm
d'	30	mm
d	275	mm
L_c	2464	mm
h_c	254	mm
b_c	254	mm

Mechanical Properties		
f_{y1}	420	MPa
A_{s1}	254	mm^2
f_{y2}	420	MPa
A_{s2}	531	mm^2
$f_{y,col}$	420	MPa
$A_{s,col}$	1773	mm^2
$^1A_{jv,prvd}$	760	mm^2
f_{yh}	420	MPa
$^2A_{jh,prvd}$	253	mm^2
f_c'	30	MPa
$N^*/A_g f_c'$	0.0	-

Joint Reinforcement		
M_{ob}^+	39	kNm
M_{ob}^-	79	kNm
$^3V^*_{ojh}$	387	kN
$^3\alpha_j$	1.4	-
$^3 6V^*_{ojh}/f_c' b_j h_c$	1.20	-
$^3A_{jh,req}$	892	mm^2
$A_{jh,prvd}/A_{jh,req}$	28	%
$^3\alpha_v$	0.7	-
$^3A_{jv,req}$	749	mm^2
$A_{jv,prvd}/A_{jv,req}$	101	%

Effective Column Depths		
$^4(h_c/d_b)_{material}$	20.2	-
$^4(h_c/d_b')_{material}$	14.0	-
β	0.48	-
$^3\alpha_{s,bottom}$	1.80	-
$^5(h_c/d_b)_{\alpha s}$	17.4	-
$^3\alpha_p$	1.00	-
$^6(h_c/d_b)_{axial}$	20.2	-
$^6(h_c/d_b')_{axial}$	14.0	-
^{7}Bar slip?	Top/Bottom	-

Researcher:	Leon
Year:	1989
Test I.D:	BCJ3

Note: Test material strengths not published

Specimen Geometry		
L_b	2032	mm
h_b	305	mm
b_b	203	mm
d'	30	mm
d	275	mm
L_c	2464	mm
h_c	305	mm
b_c	254	mm

Mechanical Properties		
f_{y1}	420	MPa
A_{s1}	254	mm^2
f_{y2}	420	MPa
A_{s2}	531	mm^2
$f_{y,col}$	420	MPa
$A_{s,col}$	1773	mm^2
$^{1}A_{jv,prvd}$	760	mm^2
f_{yh}	420	MPa
$^{2}A_{jh,prvd}$	253	mm^2
f_c'	30	MPa
$N^*/A_g f_c'$	0.0	-

Joint Reinforcement		
M_{ob}^+	39	kNm
M_{ob}^-	79	kNm
$^{3}V^*_{ojh}$	426	kN
$^{3}\alpha_i$	1.4	-
$^{3}6V^*_{ojh}/f_c' b_j h_c$	1.10	-
$^{3}A_{jh,req}$	818	mm^2
$A_{jh,prvd}/A_{jh,req}$	31	%
$^{3}\alpha_v$	0.7	-
$^{3}A_{jv,req}$	572	mm^2
$A_{jv,prvd}/A_{jv,req}$	133	%

Effective Column Depths		
$^{4}(h_c/d_b)_{material}$	24.2	-
$^{4}(h_c/d_b')_{material}$	16.8	-
β	0.48	-
$^{3}\alpha_{s,bottom}$	1.80	-
$^{5}(h_c/d_b)_{\alpha s}$	20.8	-
$^{3}\alpha_p$	1.00	-
$^{6}(h_c/d_b)_{axial}$	24.2	-
$^{6}(h_c/d_b')_{axial}$	16.8	-
^{7}Bar slip?	Top/Bottom	-

Researcher:	Leon
Year:	1989
Test I.D:	BCJ3

Note: Test material strengths not published

Specimen Geometry		
L_b	2032	mm
h_b	305	mm
b_b	203	mm
d'	30	mm
d	275	mm
L_c	2464	mm
h_c	356	mm
b_c	254	mm

Mechanical Properties		
f_{y1}	420	MPa
A_{s1}	254	mm^2
f_{y2}	420	MPa
A_{s2}	531	mm^2
$f_{y,col}$	420	MPa
$A_{s,col}$	1520	mm^2
[1]$A_{jv,prvd}$	507	mm^2
f_{yh}	420	MPa
[2]$A_{jh,prvd}$	253	mm^2
f_c'	30	MPa
$N^*/A_g f_c'$	0.0	-

Joint Reinforcement		
M_{ob}^+	39	kNm
M_{ob}^-	79	kNm
[3]V^*_{ojh}	425	kN
[3]α_j	1.4	-
[3]$6V^*_{ojh}/f_c' b_j h_c$	0.94	-
[3]$A_{jh,req}$	698	mm^2
$A_{jh,prvd}/A_{jh,req}$	36	%
[3]α_v	0.7	-
[3]$A_{jv,req}$	418	mm^2
$A_{jv,prvd}/A_{jv,req}$	121	%

Effective Column Depths		
[4]$(h_c/d_b)_{material}$	28.3	-
[4]$(h_c/d_b')_{material}$	19.6	-
β	0.48	-
[3]$\alpha_{s,bottom}$	1.80	-
[5]$(h_c/d_b)_{\alpha s}$	24.3	-
[3]α_p	1.00	-
[6]$(h_c/d_b)_{axial}$	28.3	-
[6]$(h_c/d_b')_{axial}$	19.6	-
[7]Bar slip?	No	-

Researcher:	Milburn & Park
Year:	1982
Test I.D:	Unit 1

Note: No longitudinal reinforcement strain gauge data within joint

Specimen Geometry		
L_b	5740	mm
h_b	457	mm
b_b	229	mm
d'	30	mm
d	427	mm
L_c	3350	mm
h_c	406	mm
b_c	305	mm

Mechanical Properties		
f_{y1}	315	MPa
A_{s1}	1608	mm^2
f_{y2}	315	MPa
A_{s2}	1608	mm^2
$f_{y,col}$	303	MPa
$A_{s,col}$	2714	mm^2
$^{1}A_{jv,prvd}$	905	mm^2
f_{yh}	320	MPa
$^{2}A_{jh,prvd}$	2413	mm^2
f_c'	41.3	MPa
$N^*/A_g f_c'$	0.08	-

Joint Reinforcement		
M_{ob}^{+}	226	kNm
M_{ob}^{-}	226	kNm
$^{3}V^*_{ojh}$	1023	kN
$^{3}\alpha_i$	1.26	-
$^{3}6V^*_{ojh}/f_c' b_j h_c$	1.20	-
$^{3}A_{jh,req}$	2403	mm^2
$A_{jh,prvd}/A_{jh,req}$	100	%
$^{3}\alpha_v$	0.65	-
$^{3}A_{jv,req}$	1470	mm^2
$A_{jv,prvd}/A_{jv,req}$	49	%

Effective Column Depths		
$^{4}(h_c/d_b)_{material}$	32.5	-
$^{4}(h_c/d_b')_{material}$	32.5	-
β	1.00	-
$^{3}\alpha_{s,bottom}$	1.55	-
$^{5}(h_c/d_b)_{\alpha s}$	32.5	-
$^{3}\alpha_p$	1.00	-
$^{6}(h_c/d_b)_{axial}$	32.5	-
$^{6}(h_c/d_b')_{axial}$	32.5	-
^{7}Bar slip?	No	-

Researcher:	Milburn & Park
Year:	1982
Test I.D:	Unit 2

Note: PHZ in beam

Specimen Geometry		
L_b	5740	mm
h_b	457	mm
b_b	229	mm
d'	30	mm
d	427	mm
L_c	3350	mm
h_c	406	mm
b_c	305	mm

Mechanical Properties		
f_{y1}	307	MPa
A_{s1}	1885	mm^2
f_{y2}	307	MPa
A_{s2}	1885	mm^2
$f_{y,col}$	303	MPa
$A_{s,col}$	2714	mm^2
$^1A_{jv,prvd}$	905	mm^2
f_{yh}	286	MPa
$^2A_{jh,prvd}$	905	mm^2
f_c'	0.07	MPa
$N^*/A_g f_c'$	0.08	-

Joint Reinforcement		
M_{ub}^+	227	kNm
M_{ub}^-	227	kNm
$^3V^*_{ojh}$	1073	kN
$^3\alpha_j$	1.28	-
$^3 6V^*_{ojh}/f_c' b_j h_c$	1.11	-
$^3A_{jh,req}$	2873	mm^2
$A_{jh,prvd}/A_{jh,req}$	31	%
$^3\alpha_v$	1988	-
$^3A_{jv,req}$	1470	mm^2
$A_{jv,prvd}/A_{jv,req}$	46	%

Effective Column Depths		
$^4(h_c/d_b)_{material}$	27.2	-
$^4(h_c/d_b')_{material}$	27.7	-
β	1.00	-
$^3\alpha_{s,bottom}$	1.55	-
$^5(h_c/d_b)_{\alpha s}$	27.2	-
$^3\alpha_p$	1.00	-
$^6(h_c/d_b)_{axial}$	27.2	-
$^6(h_c/d_b')_{axial}$	27.7	-
^{7}Bar slip?	No	-

Researcher:	Restrepo
Year:	1992
Test I.D:	Unit 6

Specimen Geometry		
L_b	3810	mm
h_b	700	mm
b_b	300	mm
d'	43	mm
d	657	mm
L_c	2800	mm
h_c	600	mm
b_c	450	mm

Mechanical Properties		
f_{y1}	285	MPa
A_{s1}	1810	mm^2
f_{y2}	285	MPa
A_{s2}	1810	mm^2
$f_{y,col}$	456	MPa
$A_{s,col}$	4523	mm^2
$^{1}A_{jv,prvd}$	1810	mm^2
f_{yh}	301	MPa
$^{2}A_{jh,prvd}$	3581	mm^2
f_c'	44.0	MPa
$N^*/A_g f_c'$	0.0	-

Joint Reinforcement		
M_{ob}^+	400	kNm
M_{ob}^-	400	kNm
$^{3}V^*_{ojh}$	965	kN
$^{3}\alpha_i$	1.40	-
$^{3}6V^*_{ojh}/f_c' b_j h_c$	0.85	-
$^{3}A_{jh,req}$	2039	mm^2
$A_{jh,prvd}/A_{jh,req}$	176	%
$^{3}\alpha_v$	0.70	-
$^{3}A_{jv,req}$	1099	mm^2
$A_{jv,prvd}/A_{jv,req}$	165	%

Effective Column Depths		
$^{4}(h_c/d_b)_{material}$	30.3	-
$^{4}(h_c/d_b')_{material}$	30.3	-
β	1.00	-
$^{3}\alpha_{s,bottom}$	1.55	-
$^{5}(h_c/d_b)_{\alpha s}$	30.3	-
$^{3}\alpha_p$	1.00	-
$^{6}(h_c/d_b)_{axial}$	30.3	-
$^{6}(h_c/d_b')_{axial}$	30.3	-
^{7}Bar slip?	No	-

Researcher:	Ruitong & Park	Note: PHZs in beams
Year:	1987	
Test I.D:	Unit 1	

Specimen Geometry		
L_b	4238	mm
h_b	457	mm
b_b	229	mm
d'	42	mm
d	415	mm
L_c	2473	mm
h_c	406	mm
b_c	305	mm

Mechanical Properties		
f_{y1}	294	MPa
A_{s1}	402	mm^2
f_{y2}	294	MPa
A_{s2}	1005	mm^2
$f_{y,col}$	498	MPa
$A_{s,col}$	1608	mm^2
$^1A_{jv,prvd}$	402	mm^2
f_{yh}	303	MPa
$^2A_{jh,prvd}$	915	mm^2
f_c'	45.9	MPa
$N^*/A_g f_c'$	0.0	-

Joint Reinforcement		
M_{ub}^+	53	kNm
M_{ub}^-	112	kNm
$^3V^*_{ojh}$	386	kN
$^3\alpha_j$	1.40	-
$^36V^*_{ojh}/f_c'b_jh_c$	0.85	-
$^3A_{jh,req}$	1161	mm^2
$A_{jh,prvd}/A_{jh,req}$	79	%
$^3\alpha_v$	0.70	-
$^3A_{jv,req}$	556	mm^2
$A_{jv,prvd}/A_{jv,req}$	72	%

Effective Column Depths		
$^4(h_c/d_b)_{material}$	34.2	-
$^4(h_c/d_b')_{material}$	34.2	-
β	0.40	-
$^3\alpha_{s,bottom}$	1.80	-
$^5(h_c/d_b)_{\alpha s}$	29.5	-
$^3\alpha_p$	1.00	-
$^6(h_c/d_b)_{axial}$	34.2	-
$^6(h_c/d_b')_{axial}$	34.2	-
^{7}Bar slip?	No	-

Researcher:	Ruitong & Park
Year:	1987
Test I.D:	Unit 2

Note: PHZs in beams

Specimen Geometry		
L_b	4238	mm
h_b	457	mm
b_b	229	mm
d'	42	mm
d	415	mm
L_c	2473	mm
h_c	406	mm
b_c	305	mm

Mechanical Properties		
f_{y1}	300	MPa
A_{s1}	628	mm^2
f_{y2}	314	MPa
A_{s2}	1232	mm^2
$f_{y,col}$	476	MPa
$A_{s,col}$	2513	mm^2
$^1A_{jv,prvd}$	628	mm^2
f_{yh}	283	MPa
$^2A_{jh,prvd}$	834	mm^2
f_c'	36.0	MPa
$N^*/A_g f_c'$	0.0	-

Joint Reinforcement		
M_{ub}^+	76	kNm
M_{ub}^-	146	kNm
$^3V^*_{ojh}$	507	kN
$^3\alpha_i$	1.40	-
$^36V^*_{ojh}/f_c'b_jh_c$	0.85	-
$^3A_{jh,req}$	1602	mm^2
$A_{jh,prvd}/A_{jh,req}$	52	%
$^3\alpha_v$	0.70	-
$^3A_{jv,req}$	750	mm^2
$A_{jv,prvd}/A_{jv,req}$	84	%

Effective Column Depths		
$^4(h_c/d_b)_{material}$	24.3	-
$^4(h_c/d_b')_{material}$	17.3	-
β	0.51	-
$^3\alpha_{s,bottom}$	1.80	-
$^5(h_c/d_b)_{\alpha s}$	20.9	-
$^3\alpha_p$	1.00	-
$^6(h_c/d_b)_{axial}$	24.3	-
$^6(h_c/d_b')_{axial}$	17.3	-
^{7}Bar slip?	Top	-

Researcher:	Ruitong & Park
Year:	1987
Test I.D:	Unit 3

Note: PHZs in beams

Specimen Geometry		
L_b	4238	mm
h_b	457	mm
b_b	229	mm
d'	42	mm
d	415	mm
L_c	2473	mm
h_c	406	mm
b_c	305	mm

Mechanical Properties		
f_{y1}	294	MPa
A_{s1}	402	mm^2
f_{y2}	294	MPa
A_{s2}	603	mm^2
$f_{y,col}$	530	MPa
$A_{s,col}$	1433	mm^2
$^1A_{jv,prvd}$	226	mm^2
f_{yh}	327	MPa
$^2A_{jh,prvd}$	406	mm^2
f_c'	36.2	MPa
$N^*/A_g f_c'$	0.0	-

Joint Reinforcement		
M_{ub}^+	52	kNm
M_{ub}^-	111	kNm
$^3V^*_{ojh}$	381	kN
$^3\alpha_j$	1.40	-
$^36V^*_{ojh}/f_c'b_jh_c$	0.85	-
$^3A_{jh,req}$	1074	mm^2
$A_{jh,prvd}/A_{jh,req}$	38	%
$^3\alpha_v$	0.70	-
$^3A_{jv,req}$	523	mm^2
$A_{jv,prvd}/A_{jv,req}$	43	%

Effective Column Depths		
$^4(h_c/d_b)_{material}$	30.4	-
$^4(h_c/d_b')_{material}$	30.4	-
β	0.40	-
$^3\alpha_{s,bottom}$	1.80	-
$^5(h_c/d_b)_{\alpha s}$	26.2	-
$^3\alpha_p$	1.00	-
$^6(h_c/d_b)_{axial}$	30.4	-
$^6(h_c/d_b')_{axial}$	30.4	-
^{7}Bar slip?	No	-

Researcher:	Ruitong & Park
Year:	1987
Test I.D:	Unit 4

Note: PHZs in beams

Specimen Geometry		
L_b	4238	mm
h_b	457	mm
b_b	229	mm
d'	42	mm
d	415	mm
L_c	2473	mm
h_c	406	mm
b_c	305	mm

Mechanical Properties		
f_{y1}	300	MPa
A_{s1}	628	mm^2
f_{y2}	314	MPa
A_{s2}	1232	mm^2
$f_{y,col}$	498	MPa
$A_{s,col}$	2287	mm^2
$^1A_{jv,prvd}$	402	mm^2
f_{yh}	312	MPa
$^2A_{jh,prvd}$	604	mm^2
f_c'	40.1	MPa
$N^*/A_g f_c'$	0.0	-

Joint Reinforcement		
M_{ub}^+	76	kNm
M_{ub}^-	97	kNm
$^3V^*_{ojh}$	509	kN
$^3\alpha_i$	1.40	-
$^36V^*_{ojh}/f_c'b_jh_c$	0.85	-
$^3A_{jh,req}$	1454	mm^2
$A_{jh,prvd}/A_{jh,req}$	42	%
$^3\alpha_v$	0.70	-
$^3A_{jv,req}$	717	mm^2
$A_{jv,prvd}/A_{jv,req}$	56	%

Effective Column Depths		
$^4(h_c/d_b)_{material}$	25.6	-
$^4(h_c/d_b')_{material}$	18.3	-
β	0.51	-
$^3\alpha_{s,bottom}$	1.80	-
$^5(h_c/d_b)_{\alpha s}$	22.0	-
$^3\alpha_p$	1.00	-
$^6(h_c/d_b)_{axial}$	25.6	-
$^6(h_c/d_b')_{axial}$	18.3	-
^{7}Bar slip?	Top	-